AN EXAMINATION OF METAL HYDRIDES AND PHASE-CHANGE MATERIALS FOR YEAR-ROUND VARIABLE-TEMPERATURE ENERGY STORAGE IN BUILDING HEATING AND COOLING SYSTEMS

by

Patrick Edward Krane

A Dissertation

Submitted to the Faculty of Purdue University

In Partial Fulfillment of the Requirements for the degree of

Doctor of Philosophy

Department of Mechanical Engineering

West Lafayette, Indiana

May 2022

THE PURDUE UNIVERSITY GRADUATE SCHOOL
STATEMENT OF COMMITTEE APPROVAL

Dr. Amy Marconnet, Chair

School of Mechanical Engineering

Dr. James Braun

School of Mechanical Engineering

Dr. Neera Jain

School of Mechanical Engineering

Dr. Davide Ziviani

School of Mechanical Engineering

Dr. Timothee Pourpoint

School of Aeronautics and Astronautics

Approved by:

Dr. Nicole Key

Ad Maiorem Dei Gloriam

ACKNOWLEDGMENTS

First of all, special thanks are due to my advisor, Prof. Amy Marconnet. Her advice, feedback, support, and guidance throughout my time in graduate school have been invaluable, and she has been consistently kind and patient throughout the time that I have worked for her. I would also like to thank the other PIs for the projects that have gone into this dissertation, Profs. James Braun, Neera Jain, and Davide Ziviani, whose feedback has played an important role in my work on this project. All three of them have made many important suggestions and corrections to my work over the last few years. Prof. Ziviani was an enormous help in getting me to know what I needed for this project about the modeling of thermal systems, and Prof. Jain was a similar help about systems and controls.

The idea for this project grew out of previous work on residential ice storge by Aaron Tam, and the model he used for that system was used as a starting point for designing both the metal-hydride and the variable-temperature storage models, so I would like to thank him for his work on that. The multi-parametric controller used to combine the dynamic and static models in the metal hydride system was designed by Dr. Austin Nash, so I thank him for his work on that and for all his advice and help in using that controller and integrating into the rest of the model. I also thank Prof. Timothee Pourpoint and Dr. Tyler Voskuilen for their work on the Metal Hydride Toolbox, which was used in the metal hydride system model in this project. I would like to thank Trevor Bird as well for his advice on linearizing the dynamic model

Funding for this project was provided by the Center for High Performance Buildings, and other work of mine in graduate school has been funded by Intel, SpaceX, and the Laura Winkelman Davidson Endowment. I thank all of them for their financial support. I also thank Emerson for providing Herrick Laboratories with data on its YH compressors that was used in this dissertation.

I would like to thank all members of the Marconnet Thermal and Energy Conversion Lab (both current members and former members I overlapped with) for all of their advice and support throughout my time working with them. Particular thanks are due to Dr. David Gonzalez Cuadrado for his help and advice as I was considering graduate school and beginning my graduate research work. Other members of the MTEC Lab whom I would like to thank by name since I have worked with them the longest are Albraa Alsaati, Meghavin Bhatasana, Dr. Aaditya Candadai, and Dr.

Rajath Kantharaj. I would also like to thank Francisco Lozano and Louis Villa, each of whom I have worked with on a research project separate from the work presented here. For their advice and support when I was considering and applying for graduate school, I would like to thank Profs. Timothy Fisher and Guillermo Paniagua.

Finally, I would like to thank in a special way my father, Prof. Matthew Krane, for all of his advice and support on career decisions throughout my time as an undergraduate and a graduate student.

TABLE OF CONTENTS

LIST OF TABLES

LIST OF FIGURES

NOMENCLATURE

Variable	Meaning	Variable	Meaning
A	Phase Interaction Energy	$\dot{g}$	Internal Heat Generation
A	Linear State-Space Matrix	GHI	Global Horizontal Irradiance
A_c	Cross-Sectional Area	h	Specific Enthalpy
A_s	Surface Area	h_{conv}	Convection Heat Transfer Coefficient
a_n	Correlation Coefficient	I_β	Irradiance on a Sloped Surface
B	Linear State-Space Matrix	J	Objective Function
C	Cost	k	Time Step
C	Linear State-Space Matrix	K_{loss}	Head Loss Coefficient
c	Specific Heat	k_r	Heat Ratio
C_A	Arrhenius Rate Pre-Exponential Constant	L	Latent Heat
C^*	Heat Capacity Ratio	l	Length
COP	Coefficient of Performance	m	Mass
$costfnc$	Optimization Cost Function	$\dot{m}$	Mass Flow Rate
c_P	Constant-Pressure Specific Heat	n	Number
D	Diameter	NTU	Number of Transfer Units
D	Linear State-Space Matrix	P	Pressure
d	Width	Pr	Prandtl Number
DHI	Direct Horizontal Irradiance	**Q**	Input Weighting Matrix
DNI	Direct Normal Irradiance	q	Quality
E_A	Reaction Activation Energy	$\dot{Q}$	Heat Transfer Rate
f	State Variable Rate of Change	R	Gas Constant
g	Output Variable Rate of Change	**R**	Output Weighting Matrix

Variable	Meaning	Variable	Meaning
r	Reaction Rate	Δ	Change
R_B	Ratio of Radiation on a Tilted Surface to a Horizontal Surface	ΔH	Enthalpy of Reaction
Re	Reynolds Number	ΔS	Entropy of Reaction
$SEER$	Seasonal Energy Efficiency Ratio	δ	Declination
T	Temperature	ε	Effectiveness
t	Time	η	Efficiency
u	Input Variable Vector	θ	Angle Of Incidence
UA	Overall Heat Transfer Coefficient Times Surface Area	θ_b	Solar Cooling Factor
V	Volume	μ	Chemical Potential
w	Weight Fraction	ρ	Density
$\dot{W}$	Work	ρ_g	Ground Reflectance
w_{PCM}	Specific Energy to Change Phase-Change Temperature	τ	Index Variable
x	State Variable Vector	ϕ	Latitude
x_{stor}	State of Charge	φ	Porosity
β	Slope	ω	Hour Angle
γ	Surface Azimuth Angle		

Subscript	Meaning	Subscript	Meaning
$1P$	One-Phase	c	Critical
$2P$	Two-Phase	cf	Circulating Fluid
A	$MmNi_{4.5}Cr_{0.5}$ reactor	ch	Channel
atm	Atmospheric	$charge$	Charge Mode
B	$LaNi_5$ reactor	$comp$	Compressor

Subscript	Meaning	Subscript	Meaning
$cond$	Condenser/ Condensation	$load$	Load
$conv$	Conventional	m	Melting
$cool$	Cold Storage	max	Maximum
day	Day	mid	Middle Point
$demand$	Demand Charges	min	Minimum
des	Desired	new	New
$design\ load$	Design Load	$non-HVAC$	Loads not from the HVAC System
$discharge$	Discharge Mode	$off-peak$	Off-Peak
$elec$	Electric Heating	old	Old
eq	Equilibrium	$on-peak$	On-Peak
est	Estimated	$operating$	Operating
$evap$	Evaporator/Evaporation	out	Outlet
G	Gas	$outdoor$	Outdoor Loop
$ground$	Ground heat exchanger	PCM	Phase change material
H	Hydrogen	pen	Penalty
$heat$	Heat Storage	$plates$	Heat Exchanger Plates
$hour$	Hour	$prev$	Previous
$house$	House	$pump$	Pump
hp	Heat Pump	$pumps$	Pumps
HX	Heat Exchanger	PV	Solar photovoltaic array
hyd	Hydride	r	Reactor
in	Inlet	$rated$	Rated
$indoor$	Indoor Loop	ref	Refrigerant
$initial$	Initial	$rem\ charge$	Remaining Charging
L	Liquid	s	Isentropic
lat	Latent	$samp$	Sampling

Subscript	Meaning	Subscript	Meaning
$sens$	Sensible	tot	Total
setpoint	Setpoint	wg	Water Glycol
shell	Shell	$wg\ loop$	Water Glycol Loop
$shift$	Shift	z	Zenith
$solar$	Solar	$\alpha, 0$	α-phase boundary
$stor$	Stored	$\beta,0$	β-phase boundary
storage	System with Energy Storage	∞	Ambient
$tank$	Storage Tank		

Superscript	Meaning	Superscript	Meaning
°	Molar	~	Augmented

Acronym	Meaning	Acronym	Meaning
A/C	Air Conditioning	RMSE	Root Mean Square Error
COP	Coefficient of Performance	SAEWME	Summer Afternoon and Evening, Winter Morning and Evening
CSP	Concentrated Solar Power	SAWA	Summer Afternoon, Winter Afternoon
HVAC	Heating, Ventilation, and Air Conditioning	SAWM	Summer Afternoon, Winter Morning
MPC	Multi-Parametric Controller	SEER	Seasonal Energy Efficiency Ratio
NRMSE	Normalized Root Mean Square Error	TCES	Thermochemical Energy Storage
PCM	Phase-Change Material	TES	Thermal Energy Storage
PCT	Phase-Change Temperature	TOU	Time-of-Use
PV	Photovoltaics		

ABSTRACT

Thermal energy storage (TES) is used to reduce the operating costs of heating, ventilation, and air conditioning (HVAC) systems by shifting loads away from on-peak periods, to reduce the maximum heating or cooling capacity needed from the HVAC system, and to store excess energy generated by on-site solar power. The most commonly-used form of TES is ice storage with air conditioning (A/C) systems in commercial buildings. There has been extensive research into many other forms of TES for use with HVAC systems, both in commercial and residential buildings. However, this research is often limited to use with either heating or cooling systems.

Year-round, high-density storage for both heating and cooling would yield significantly larger cost savings than existing TES systems, particularly for residential buildings, where heating loads are often larger than cooling loads. This dissertation examines the feasibility of using metal hydrides for year-round storage, as well as analyzing the potential of variable-temperature energy storage for optimizing system performance beyond allowing for year-round use.

Metal hydrides are metals that exothermically absorb and endothermically desorb hydrogen. Since the temperature this reaction occurs at depends on the hydrogen pressure, hydrides can be used for energy storage at varying temperatures. System architecture for using metal hydrides with an HVAC system is developed. A thermodynamic model which combines a dynamic model of the hydride reactors with a static model of the HVAC system is used to calculate operating costs, compared to a conventional HVAC system, for different utility rates and locations. The payback period of the system is unacceptably high, due to the high initial cost of metal hydrides and the operating costs of compressing hydrogen to move it between hydride reactors.

In addition to the metal hydride system model, a generalized model of a variable-temperature TES system is used to determine the potential cost savings from dynamically altering the storage temperature to achieve optimal cost savings. Dynamic tuning does result in cost savings but is most effective for storage tank sizes significantly smaller than the optimal tank size. An alternate system design where the storage tank is charged with the outlet flow from the house achieves larger cost savings even for the optimally-sized tanks. Payback periods calculated for optimal sizing show that year-round storage has a lower payback period than separate cold and heat storage if the year-round storage system is not more expensive than two separate storage tanks.

1. INTRODUCTION

1.1 Motivation for Energy Storage in Building Heating and Cooling

Building energy usage accounts for around 76% of the electricity and 40% of the energy used in the United States, and this share of electricity usage has increased over time [1]. As shown in Figure 1-1 around 72% of energy usage in buildings in the United States occurs in residential and commercial buildings, and around 35% of building energy usage is used to provide heating, cooling, and ventilation [1]. Thus, any improvement to the efficiency, operating cost, or environmental impact of heating, ventilation, and air-conditioning (HVAC) systems in residential and commercial buildings would have large effects. One area of research into improving HVAC systems is the integration of thermal energy storage (TES) with an HVAC system.

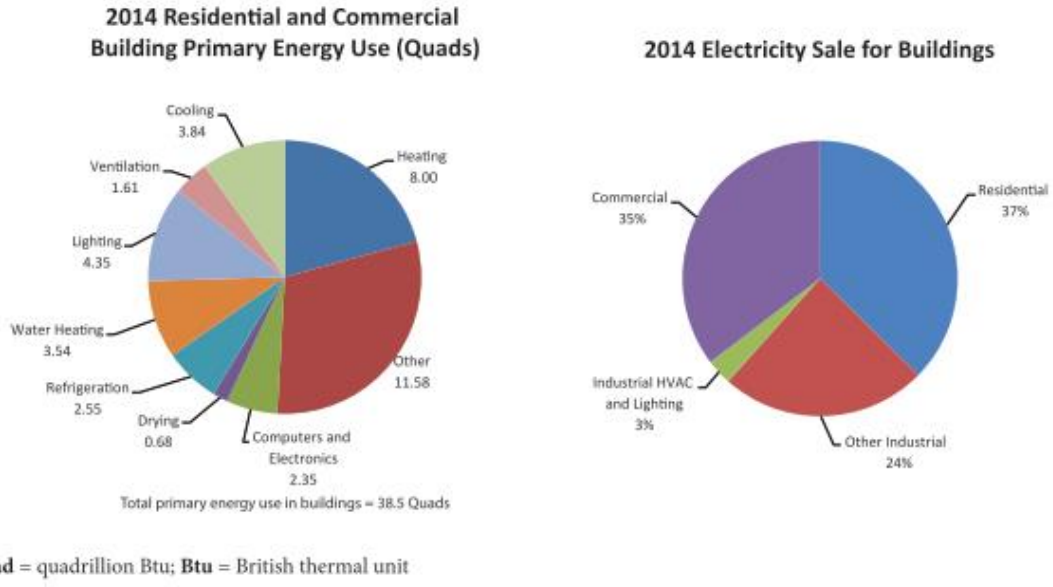

Figure 1-1. Breakdown of energy consumption in buildings by use and type of building. Image reproduced from US Department of Energy [1].

TES systems integrated into buildings are classified as either active systems, where the storage system is charged and discharged by the HVAC system, or passive systems, which are charged and discharged by changes in the outside temperature [2,3]. Passive TES reduces the overall heating and cooling loads at the building by increasing the thermal capacitance of the building [4]. Active TES, which will be the focus of this dissertation, is used in buildings for three

reasons: (1) to reduce operating costs if time-of-use (TOU) rates are in place, (2) to reduce initial costs from downsizing other components of the HVAC system, and (3) to store excess energy generated by on-site renewable energy sources- generally, solar photovoltaics (PV)- for later use. These motivators are described in more detail below.

1.1.1 Time-of-Use Utility Rates

The demand for electricity from the electric grid is not constant over time. This can increase the cost of providing electricity, since the methods used to produce extra electricity at peak hours are generally less efficient than those used to provide the base electric load throughout the day, and transmission losses are higher at times when more electricity is being transmitted [5]. One study found that the energy required to generate and transmit energy at off-peak hours was 10-30% less than that required to generate and transmit the same amount of energy during on-peak hours [5]. In addition to being less efficient, the power generation used to meet the marginal load at peak hours often also has a larger negative effect on the environment [5].

These factors incentivize energy companies to look for ways to minimize the variation in electricity demand over the course of a day. This incentive leads to demand-side management, which tries to incentivize electricity consumers to modify their consumption in a way that would reduce variation in electrical demand [6–8]. One of the main ways this is done is through the use of TOU utility rates, where electricity is more expensive during peak hours, and demand charges, where consumers are charged based on their peak electricity consumption [9–11]. These rate structures are commonly used for commercial buildings, and are becoming more common for residential buildings [11]. Thermal energy storage can be used to take advantage of TOU rates by charging the energy storage system during off-peak hours and discharging it during on-peak hours, thereby reducing operating costs by shifting some of the electricity demand from more expensive on-peak hours to cheaper off-peak hours [8,12,13]. This load-shifting will also reduce the maximum electricity consumption during the on-peak periods, thereby also reducing any on-peak demand charges [8,14].

1.1.2 Component Downsizing

When using energy storage with a building cooling system, some of the initial cost of installing the TES system can be offset by reducing the costs of other components. Without TES, the chiller in a cooling system must be sized to be able to meet the highest cooling load the building experiences. With TES, the chiller can instead be sized to the average load for the operating period with the highest loads, since the TES system can be charged at times with lower or no cooling loads and discharged at times of peak load [15]. This reduction in required chiller capacity can be maximized by sizing the chiller and the storage system so that the chiller runs at capacity for the entirety of the design day [15,16]. Furthermore, the installation cost of fans and ductwork inside the building can be reduced if the TES system is used to lower the air temperature to a lower value than a conventional system during peak hours, which reduces the maximum flow rate of air [16]. For heating, the benefits from component downsizing will depend on the method used to provide heating loads to the building, and the benefits from it may be less than they are for cooling. For instance, the cost savings from reducing the capacity of an electric resistance heater will be less than those from reducing the capacity of a heat pump.

1.1.3 On-Site Solar Power Generation

Thermal energy storage can also be incorporated with on-site solar power generation. In this case, energy storage is used because the power generated by a solar PV array varies over the course of the day. Thermal energy storage can store excess energy at times when solar power generation exceeds the electricity demand of the building, and then release that energy at other times when demand exceeds generation [13,17]. This can be done as part of a zero-energy or low-energy home that seeks to minimize use of the electric grid by storing energy during the day when generation is highest and releasing it to meet heating or cooling loads at night, when there is not solar generation available [13,18]. In buildings which use both grid electricity and solar power, TES may be used for the purpose of load-shifting as described in Section 1.1.1. In this case, the control logic for charging and discharging is modified to reflect the fact that on-peak and off-peak rates are only applied to grid electricity. Because of this, the system should be charged with excess solar power even at times when it would normally not be charged, and should be discharged to reduce the on-peak load only if that load cannot be fully met by the solar power generation [18,19].

1.2 Existing Technologies for Thermal Energy Storage in Buildings

The most common form of TES used with building HVAC systems is ice storage, used with air conditioning (A/C) systems [7,13,20,21]. During off-peak hours, an ice storage system is charged using a cooling load produced by the chiller to cool water until it freezes into ice [8,21]. It is discharged by melting the ice by exchanging heat between it and a warmer fluid, which is cooled by this heat transfer and then used to deliver the cooling load to the building [8,21]. The cooling provided by melting the ice reduces the load on the chiller. The next most common TES method is sensible heat storage using water, where energy is stored by heating or cooling water, and this stored energy is then used to meet a portion of the heating or cooling load in the building [18,21,22]. Water is used as a storage material in both cases due to its low cost, minimal safety or reliability issues, and high energy density for both sensible and latent heat storage [13,21]. However, ice storage is more commonly used because it has a much higher energy density and is easier to build modular storage tanks for [21]. Ice storage is used primarily in commercial buildings; it has been shown to be economically viable across a range of conditions for this, but is currently less viable for residential use [7,23,24].

A variety of other methods of energy storage for building heating and cooling have been studied and, in some cases, implemented to a limited degree in practice. These have included the use of phase change materials (PCMs) other than ice (such as eutectic salts and paraffin wax) for cooling [13,21,25], sensible heat storage in rocks and fluids other than water for heating [22], the use of PCMs for storage with heating [22,26,27], and thermochemical energy storage for both heating and cooling [17,28].

1.3 Variable-Temperature Energy Storage

Conventional latent-heat TES systems are limited to a fixed melting point, which limits their use either to cooling or heating applications. Sensible heat storage is not limited to a fixed operating temperature, but its lower energy density makes it less economically viable than latent heat energy storage [13,18,21]. Furthermore, since energy is stored by changing the temperature of the material, the storage temperature cannot be freely changed since doing so would also affect the state of charge of the system. For latent-heat TES systems to be used year-round, it would be useful to have a storage medium with a controllable storage temperature. The advantages of such

a system are discussed in Section 1.3.1, and the current feasibility of developing such a system is discussed in Section 1.3.2.

1.3.1 Advantages

Variable-temperature TES would have the advantage of being usable year-round, thereby reducing the payback period of the system by increasing the frequency with which it is used during the year. In addition, there is the potential to increase cost savings by dynamically tuning the phase-change temperature in both cooling and heating modes in order to increase the energy efficiency of the system.

Year-round, high-density storage, for both heating and cooling that could be integrated with a standard vapor-compression heat pump could yield significantly larger cost savings than existing systems through more frequent use. This would be particularly true for residential buildings, where heating loads are larger than cooling loads in most climates (for commercial buildings, cooling loads are generally higher due to the larger internal gain inside the building). This increase in cost savings could make the difference between the system being economically viable or not, since ice storage was found to be close to cost-effective for residential buildings under some conditions [24].

The potential benefits from dynamically tuning the storage temperature of a TES system are less established. Given the difficulties in achieving variable-temperature storage, there has not been much study of how to maximize cost savings by charging and discharging the storage system at optimal temperatures (from the perspective of minimizing the power needed for the chiller or heat pump) or what the potential cost savings would be. There has been some study recently of the benefits that variable-temperature passive TES might bring [29], but there has not been comparable study for active TES. Higher phase-change temperatures than ice have generally been found desirable for cold storage (as long as they are not too high for the material to be used for cold storage at all), since they result in a higher coefficient of performance (COP) for the chiller [13,21,25]. While using the highest possible temperature for cold storage and the lowest possible for heat storage would serve as a baseline for optimizing the storage temperature of a system, further improvement may be possible by seeking to optimize heat exchanger flow rates to improve heat pump performance or reduce pump work and duct size. Furthermore, the ability to charge a

storage system at a significantly different temperature from the temperature it is discharged at might allow the system to be charged with a cooling fluid after it has been used to cool the house, thereby further increasing the operating temperatures of the chiller (or decreasing the operating temperature of a heat pump in heating mode).

1.3.2 Feasibility

Year-round latent heat storage, where the same system stores latent heat for both heating and cooling, is not currently possible. This is because a PCM used for heat storage must have a phase-change temperature above room temperature, while a PCM for cool storage must have one below room temperature. Since presently the phase-change temperature of a PCM can only be varied a few degrees (requiring substantial energy costs) [29,30], it is not feasible to use the same material for both heat storage and cold storage. Systems using 2 PCMs, one for heating and one for cooling, have been studied [27], but the use of two separate PCM storage tank means the system has substantially higher installation and material costs.

As an alternative to latent heat storage, thermochemical energy storage could potentially be used for variable-temperature storage (as reaction temperatures can be tuned with pressure, for instance), but this has not received much attention for applications in building heating and cooling. Most thermochemical TES systems previously considered have been intended specifically for either heating or cooling [28]. Existing systems that are used for both heating and cooling have used district heating with a desiccant cooling system rather than a vapor-compression heat pump, so the storage system is used for heat storage continually even if it is part of a larger system that provides both heating and cooling loads [31]. Nonetheless, thermochemical storage has the potential to be used for variable-temperature storage since the reactions used to store and release energy depend not only on the temperature of the storage material but also on the presence and concentration of the material with which it reacts.

The potential of thermochemical energy storage and active research into tunable PCMs motivate the examination of the performance of a TES system with variable-temperature storage to assess the potential benefits should such a system become viable and to quantify the temperature variation and control strategy required to achieve these benefits. Furthermore, this study would provide insights into the optimal design and operation that could be used in other studies into year-

round storage, including storage using 2 PCMs or thermochemical storage. In addition to examining the maximum potential of variable-temperature storage, this work designs and evaluates the efficacy of a particular method of thermochemical energy storage by examining year-round TES leveraging metal hydrides as a storage medium.

1.4 Metal Hydrides

While tunable PCMs are an active area of research, currently the most feasible way of achieving year-round variable-temperature TES with a single storage system is thermochemical energy storage (TCES). One form of TCES that has not previously been examined for energy storage in buildings is metal hydrides. Metal hydrides are metals that exothermically absorb and endothermically desorb hydrogen. Metal hydrides can be used for energy storage- and have been studied for energy storage in concentrated solar power (CSP) plants- where heat is stored when hydrogen is released and released when hydrogen is absorbed [32–35]. These reactions generally have a high enthalpy of reaction, and thus a high energy density for storage [36].

Metal hydrides can be used for energy storage at different temperatures because the hydriding and dehydriding reactions are functions of both temperature and pressure, so the temperature at which the reaction occurs is not fixed. Since hydrides can potentially be used for year-round energy storage with a high energy density, one thrust of this project will be to determine a design for such a storage system and to build a model of this system and use it to examine its performance.

1.5 Project Goals

This dissertation evaluates the potential of variable-temperature thermal energy storage systems for building HVAC systems and of metal hydrides as a material for variable-temperature storage. This analysis primarily focuses on residential buildings. To analyze the potential of metal hydrides, a dynamic model of a pair of metal hydride reactors is constructed and integrated into a larger model of a building HVAC system. This model is used to estimate the operating costs of the system with and without metal hydride energy storage, and from these the payback period of the metal hydrides. A similar HVAC system model, in which the dynamic model of the metal hydrides is replaced with a simpler, more abstract model of a PCM storage tank with a variable phase-

change temperature, is used to examine the maximum potential cost savings from variable-temperature storage. This model is used to find the operating temperatures that will minimize operating costs, and the resulting costs are compared to those for operating at a single, fixed optimal temperature for each of heating and cooling, as well as those for a system using real PCMs for storage. Key contributions of this work include understanding the feasibility of the metal hydride energy storage for year-round energy storage and analyzing the potential improvements to system performance from variable-temperature energy storage systems integrated with HVAC systems.

Specific tasks to accomplish these goals include:

1. Determining a working system architecture for incorporating metal hydrides into a building HVAC system
2. Building a dynamic model of a 2-reactor metal hydride system and a controller that can be used to connect it to a larger system model
3. Building a static model of a building HVAC system, including the load-shifting control logic for an energy storage system
4. Sizing the hydride system and heat pump for relevant locations and calculate the initial cost of the system, compared to a conventional system, based on this sizing
5. Examining system performance for residential and commercial buildings
6. Determining alternate control logic for the hydrides if coupled with on-site solar PV, and examine system performance for a residential building with on-site solar PV
7. Building a model of an HVAC system with energy storage that can be used to examine the optimal storage temperature of a variable-temperature TES system
8. Examining the cost savings from varying the storage temperature, how they change with the frequency with which the temperature is changed, and what control logic for changing the storage temperature can achieve close to maximum cost savings
9. Examining whether cost savings from variable-temperature storage can be increased by charging the system with the outlet flow from the house (rather than delivering the cooling load to the house with the outlet flow from the storage tank)

10. Calculating the operating costs for variable-temperature over a year of operation and compare these results to a system using two separate PCMs for cold storage and heat storage.

1.6 Outline of This Dissertation

This document describes the model for a metal hydride energy storage system that is integrated with a building HVAC system, as well as analyzing the optimal strategy for varying the storage temperature in an abstracted variable-temperature storage system.

Chapter 2 provides a review of relevant literature, including the use of ice storage with A/C systems, other forms of energy storage that have been considered for use with building HVAC systems, work on varying the phase-change temperature of PCMs, the use of metal hydrides for energy storage, and the effect of increased solar PV usage on TOU utility rates.

Chapter 3 describes the model used for the two-reactor metal hydride system, and how a linearized form of this model is used by a model-predictive controller to achieve the target heat rates in these reactors.

Chapter 4 describes the system architecture used to integrate metal hydride energy storage with a building HVAC system, and how this system architecture is modelled.

Chapter 5 describes the results of using the model described in Chapters 3 and 4 to determine the potential cost savings and payback period for this system for residential and commercial buildings, including residential buildings with on-site solar PV.

Chapter 6 describes the model, control logic, and optimization problem used to determine the potential cost savings and optimal control logic for a variable-temperature TES system.

Chapter 7 describes the results obtained from using the model described in Chapter 6 to determine how to obtain cost savings from dynamic tuning of a variable-temperature storage system, and how these results change for different locations and rate structures.

Chapter 8 examines the optimal sizing of a variable-temperature storage system, and how the results from dynamic tuning differ for an optimally-sized system.

Chapter 9 provides a summary of the work contained in this dissertation and discusses future lines of research suggested by this work.

2. LITERATURE REVIEW[1]

Before designing the variable-temperature energy storage system, it is important to understand the state of the art for TES. This chapter summarizes the current state of TES for building heating and cooling, starting with ice storage (Section 2.1) and other forms of cold storage (Section 2.2), then heat storage (Section 2.3) and thermochemical energy storage (Section 2.4). The potential of tunable PCMs (Section 2.5) and metal hydrides (Section 2.6) for variable-temperature storage is discussed. Previous research on metal hydride systems is discussed, including both system design for TES (Section 2.7) and the modeling of hydride systems (Section 2.8). Finally, since one part of this project examines how the performance of metal hydride TES changes with on-site solar PV, the effect of solar PV on TOU rates is briefly discussed (Section 2.9).

2.1 Ice Storage with Building Air Conditioning

Ice storage is a widely-used technology for load shifting in commercial buildings. Around 1500 ice storage systems were in use in the United States in 1993 [7], and this number has greatly increased since then, especially since 2014 [20]. In 2017, one of the largest manufacturers of ice storage systems had installed energy storage systems in over 4000 buildings around the world [37], including 3422 MWh of energy storage in the United States [38]. Ice storage is the most commonly-used thermal storage technology for load shifting in buildings [7,20,39]. The use of ice storage for load shifting in commercial buildings has led to significant cost savings in practice for a variety of locations [7,12,21,23], and modelling results have shown the potential for these systems to significantly reduce peak demand for weather conditions in every climate zone in the contiguous United States [23].

Ice storage systems can be classified as static or dynamic, direct or indirect, and internal or external. In static systems, ice builds up on the cooling coils or plates, while in a dynamic system it is removed to a separate storage tank as it is produced [21]. This has the advantage of improving

[1] Portions of this chapter are taken from the papers Krane et al. 2021 [124], Krane et al. 2021 (2) [125], and Krane et al. 2022 [126].

the heat transfer between the coolant and the tank, but it requires a more complex system and many dynamic systems lose some of the ice they freeze to defrosting [21].

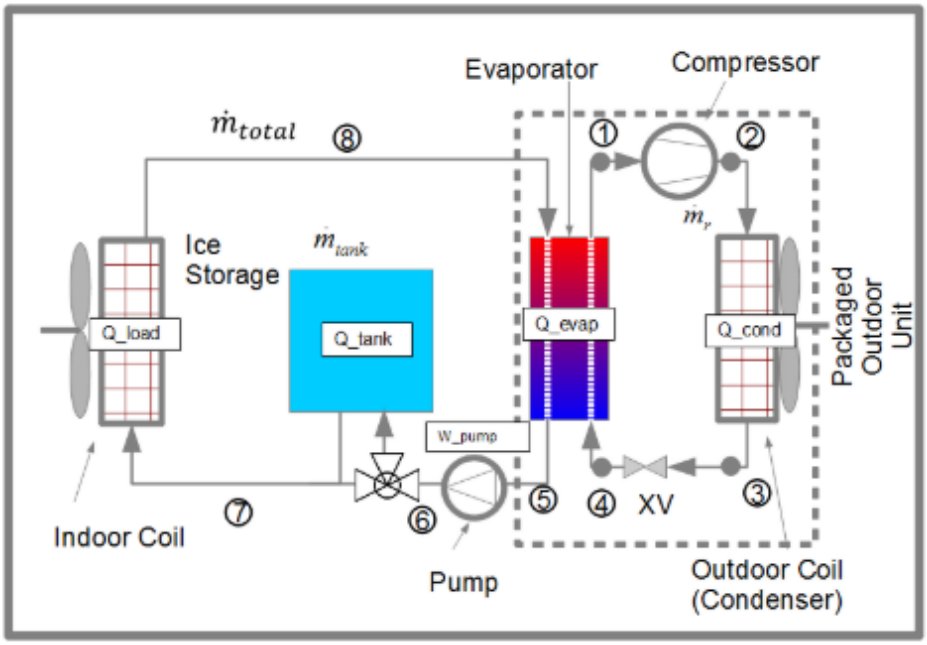

Figure 2-1. Diagram of a static indirect internal ice storage system, where a secondary loop delivers cooling loads from the chiller to the storage tank and the house, and from the storage tank to the house. Image reprinted from Tam *et al.* with permission from Elsevier [24].

Direct systems are systems where ice is made directly on the evaporator, whereas in indirect systems, the cooling load is delivered from the evaporator to the ice by a secondary fluid [40,41]. In an internal system, the water used to make ice never leaves the storage tank, while in an external system, the melted water delivers the cooling load in discharge mode to the house [15,41]. Indirect internal systems are the most commonly used [15,41]. A diagram of a static indirect internal ice storage system is shown in Figure 2-1 [24].

Ice storage is commonly used because its high energy density (and thus smaller system volume for the same storage capacity) gives it a significant advantage over sensible heat storage systems, while its low cost and lack of safety concerns give it an advantage over other PCMs [13,21,25]. The main disadvantage of ice storage is its low melting temperature (compared to the desired temperature for delivering the load to the house), which means that the chiller must operate at a lower temperature when charging, thereby significantly reducing its COP [12,13,21,23,25]. The energy consumption of an HVAC system with ice storage is reduced by the chiller operating

at more favorable ambient temperatures when charging than it would if meeting the cooling load during the on-peak period. However, this effect is generally outweighed by the effect of the lower COP at the temperatures required to charge the system, increased pump work, and thermal losses in the storage tank, resulting in increased energy consumption at the building [12,23,42]. Even so, this increased energy consumption can still yield reduced operating costs since the cost savings from shifting the load away from on-peak hours outweigh the effect of increased off-peak consumption [42]. Furthermore, since on-peak energy generation is less efficient and environmentally-friendly than base-load generation, the total energy consumption and environmental effect (including power plant generation and transmission) of a building with ice storage can, in some conditions, be favorable compared to a building without storage [5,23]. A study of the effect of TES on energy usage that included losses in the production and transmission of electricity found that both ice storage and chilled water storage resulted in higher on-site energy consumption, but lower energy consumption and emissions once the source was considered [43].

Different control strategies have been examined to divide the cooling load in a commercial building between the chiller and the ice storage system. In a chiller-priority control scheme, the ice storage system is only discharged to meet cooling loads in excess of what the chiller can meet [8,11,14,16,40]. This is simple to implement, and allows for downsizing the chiller, but loses out on much of the potential cost savings from shifting loads away from on-peak hours [8,16,40]. Constant-proportion control increases these cost savings by having the ice storage system always take a certain percentage of the on-peak load [16,40]. Storage-priority control tries to maximize these cost savings by fully discharging the storage system at on-peak hours [8,14,16,40]. However, this requires more complicated controls to ensure that the system does not finish discharging too soon [8,16,40]. These can include predictive controls, setting the discharge rate based on predicted weather, and reactive controls, adjusting the discharge rate based on the secondary fluid return temperature and remaining ice available [16]. For systems with predictive control, a load-limiting strategy can be used where the storage system is fully discharged with its load distributed so that the chiller operates at a constant load throughout the on-peak period, thereby minimizing demand charges [8,14]. For all of these control schemes, the storage system is charged by the chiller operating at capacity during off-peak hours when the building is unoccupied, and thus does not require a cooling load [8,14]. A diagram showing how ice storage changes the load profile of a cooling system when using load-limiting storage is shown in Figure 2-2.

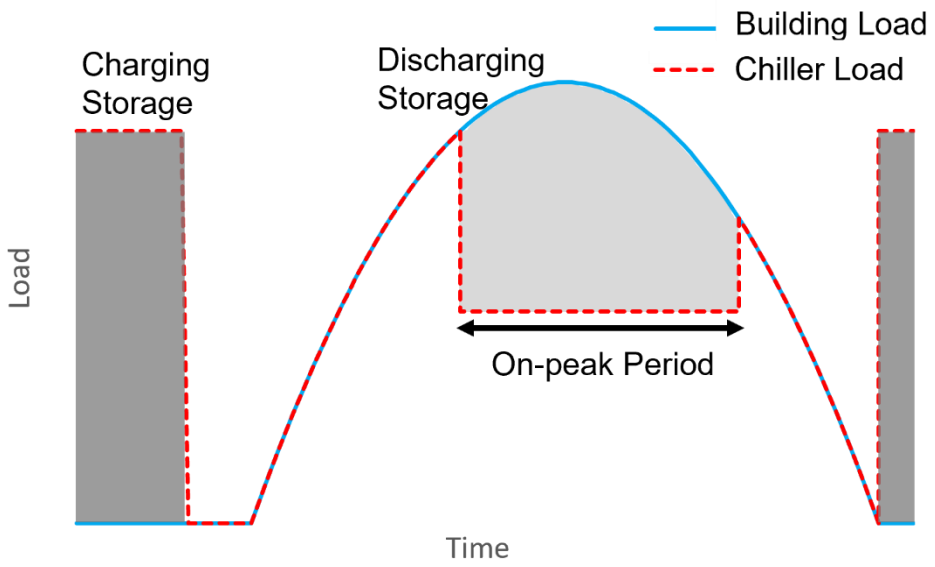

Figure 2-2. Diagram showing the cooling load of a building and the cooling load provided by the chiller over the course of a day when using load-limiting storage with an ice storage system. The shaded regions illustrate the shifting of cooling load from the on-peak to off peak periods and the reduction in the peak chiller load through the use of TES.

Optimal controllers that seek to minimize the system operating costs have also been studied; these can achieve significantly larger cost savings but are harder to implement and require longer-term weather forecasting [8,40]. A load-limiting control scheme has been found to achieve results close to optimal control [8], and a rules-based controller that includes target values for on-peak demand charges based on previous days has been found to be even closer [14].

A common method for sizing ice storage systems is to size the system based on a design day so that the chiller runs at capacity throughout the day, with storage being charged when this exceeds the building load, and discharged when building load exceeds chiller capacity [8,14,40]. On this design day, both chiller-priority and storage-priority control produce the same load distribution [40].

While ice storage is primarily used in commercial buildings, the increasing availability of TOU rates in residential buildings has led to investigation of whether ice storage should be used in them as well [11,24,44]. One significant difference between residential and commercial buildings is that residential buildings have more significant cooling loads at night (when commercial buildings are often unoccupied). Ice storage systems for commercial buildings are typically designed to charge at night when the chiller does not have to provide a load to the building, since it is unoccupied [39]. Since this is not the case for residential buildings, the system is more

likely to operate with the chiller providing a cooling load to both the storage system and the house [11]. This can affect load-shifting strategies since charging during the night at full capacity may drive up off-peak or anytime demand charges. Ice storage can achieve significant cost savings for residential buildings, particularly in hot climates, but generally not enough to achieve an economically viable payback period [24]. Residential ice storage systems have been produced commercially, but are much less common and widely available than systems for commercial buildings [44].

2.2 Other Methods of Energy Storage for Building Cooling

2.2.1 Chilled Water Storage

After ice storage, the most commonly used form of energy storage in building cooling is sensible heat storage in chilled water [7,21]. Water is commonly used for this purpose for its low cost, compatibility with conventional refrigeration system components, and high energy density compared to other forms of sensible heat storage [13,21]. Chilled water storage has the further advantage of operating within a temperature range that does not require the chiller to be designed for lower temperatures or to operate at a lower COP. The main downside of chilled water compared to ice storage is its lower energy density, which means it requires a much larger storage volume to store the same amount of energy [13,21]. Chilled water storage is more economically competitive with ice storage for larger buildings, since the marginal cost of increasing the system size decreases as system size increases, if there is sufficient storage space for a larger system [13,21]. Nonetheless, ice storage has been found to be more economic for the majority of buildings [21]. Since the energy density of chilled water storage is a function of the temperature difference the water goes through in charging and discharging, one important design consideration is maximizing this temperature difference and ensuring a consistent value across different operating conditions [45].

One difference in operation between chilled water and ice storage is that most ice storage systems are internal systems, where the ice never leaves the storage tank, while it is more common in chilled water systems to use the chilled water to deliver the cooling load when discharging [18,21,46]. Another important design consideration for chilled water systems is minimizing efficiency losses due to the mixing of water at different temperatures. Mixing losses are the most important cause of loss of storage efficiency in water sensible heat TES systems [21,47,48].

Methods of reducing mixing losses include storing water in multiple tanks or in thermally-stratified tanks, where water at different temperatures is separated into layers by the temperature-dependence of its density [21,47,49].

2.2.2 Other Phase Change Materials

Because the low melting temperature of ice means that heat pump performance is reduced when charging ice storage systems, other PCMs have been considered for cold storage in buildings. These materials usually have melting temperatures in the range of 5-10°C [25]. The most commonly considered alternative materials are eutectic salts, which are mixtures of water and inorganic salts designed to freeze at a specific temperature, in this case usually around 8°C [7,13,21,50]. While much less commonly-used than ice storage, eutectic salts have been used in practice in some commercial buildings [7,21,50]. Their main advantage over ice storage is their higher melting temperature, which means they can be charged at normal operating temperatures for a chiller used in an A/C system. Thus, performance is not reduced in charging and the chiller used in the system does not have to be designed for lower-temperature operation [13]. However, their latent heat is lower than that of water, meaning they have a lower energy density for storage (although they still have a significantly higher energy density than sensible heat storage) [21,50]. Furthermore, there are significant issues with corrosion and subcooling that make eutectic salts generally less attractive as a storage material than ice [50,51].

In addition to eutectic salts, there has been some research into the use of paraffin waxes as PCMs for TES with building cooling [25,51,52]. Waxes considered for this application generally have melting temperatures in the desired 5-10°C range [25,50]. Their latent heat is lower than that of water, and usually also lower than that of eutectic salts [50,51]. However, they avoid the issues with subcooling and corrosion that arise with eutectic salts [51]. Flammability is a concern for waxes, as well as low thermal conductivity, although the latter can be overcome by using a composite of wax with a graphite matrix [25,51]. While they remain an active area of research, wax PCMs for building TES have so far not had much commercial success [25].

While other PCMs studied for building TES have significantly different properties and involve different challenges than ice storage, in general the methods used for sizing and the control

logic for charging and discharging an ice storage system are still applicable to them as well [13,25,51].

2.3 Energy Storage for Building Heating

2.3.1 Sensible Heat Storage

Sensible heat storage is more commonly used for heating than for cooling, due to the larger potential temperature difference used to store energy [53]. For instance, hot water can be stored at temperatures in the range of 20-95°C, a much greater range than is available for cooling [22]. Sensible heat storage in water is used for heating as well as for cooling [18,22,54,55]. Hot water storage can be used to meet the demand for both space heating and hot water in a building [18]. As in cooling mode, thermal stratification in the storage tanks is important and charged water can be used to deliver the load to the building [18]. Using salt water for energy storage, with thermal stratification achieved through the use of the density gradient created by increasing salt concentration, can mitigate mixing losses in hot water [22]. The use of existing ground water in aquifers for thermal storage has been examined [22,53,54]. This allows for a larger storage volume and better potential for long-term storage, but is only viable for locations with large heating loads [22]. Sensible heat storage in water, including aquifer storage, and solid sensible heat storage in materials such as feolite are used in practice in heating and cooling systems [53]. While water is generally used for storage at temperatures below 100°C, other fluids, such as oils and molten salts, as well as solid storage in rock beds, may be used for higher-temperature storage [22].

2.3.2 Latent Heat Storage

The use of PCMs for energy storage has been considered for building heating systems as well as for cooling [22,26,27,52,55]. Such systems are not common in commercial applications [27], but have been studied at the laboratory scale [26,27] and modelling work has shown a potential for cost savings in commercial buildings [56]. Eutectic salts, salt hydrates, and paraffins are common material types considered for this application [22]. The materials considered for this application generally have melting temperatures in the range of 20-60°C [22,55]. The melting temperature should be high enough that the PCM can provide a heating load when solidifying, but

low enough for it to be melted by being heated by a heat pump operating at typical temperatures for building heating [22,55].

As with the use of similar materials for TES with cooling, the low thermal conductivity of many of these materials (particularly paraffin waxes) means that one important area of research is heat transfer enhancements for the PCM tank [26,27,52]. Without these enhancements, charging the system can fail to fully melt the PCM, thereby reducing the effective energy density of the system [26]. The addition of fins and of carbon fiber brushes has been studied to address this problem [26,27].

In general, the use of PCMs for storage in heating has received less attention than their use for storage in cooling, partially due to the lack of a storage material as convenient and affordable as ice, and partially due to heating loads in commercial buildings usually being lower than cooling loads due to higher internal gain. However, one area of research has examined the possibility of using PCMs to store heating loads but be used to reduce the cooling demand on the building. This can be done by using a PCM with a building cooling, heating, and power system where waste heat from electrical power generation supplies the heat that drives an absorption chiller that provides cooling loads to the building [57,58]. In this system, a PCM can be used to store heat from the waste heat and release it to the chiller later [57,58]. Thus, while the PCM stores energy in order to deliver a cooling load, the PCM is actually storing heat, and therefore has a melt temperature above room temperature [57,58]. Since the exhaust gas can be at temperatures around 300°C, the melting temperature will be much higher than it is for other systems described here; one study found an optimal value to be 183°C [57].

2.4 Thermochemical Energy Storage in Buildings

In recent years, there has been increasing study into the use of thermochemical energy storage in buildings. These studies have primarily focused on using TCES for energy storage in buildings with solar heating, which charges the TCES system [17,31,54,59–62]. These systems store energy through a reversible reaction where one material (the sorbent) adsorbs another (the sorbate) [17]. In a TCES system, heat is used to charge the system by causing the sorbent to desorb the sorbate [17]. The sorbent and sorbate are then separated until the system is discharged, when the sorbent adsorbs the sorbate, releasing heat [17]. TCES systems are classified as either closed

systems, where the sorbate is stored in a separate tank after being desorbed, and open systems, where the sorbate is released to the atmosphere [17]. Water vapor is commonly used as a sorbate, with Zeolite [17,31,61] and silica gel [17,31,62] being two commonly-used sorbents. Other sorbents that have been considered include strontium boride [54] and vermiculite-calcium chloride [59]. The two chief advantages of TCES are its capacity for long-term energy storage and its high energy density (per-volume energy storage is generally higher than that of latent heat storage) [17,28,59].

Because of the long-term storage capacity of TCES, much research has focused on seasonal energy storage, where excess solar heating is stored in the summer for future use providing heating during the winter [17,31,59,60,62]. Long-term storage is most viable in high-latitude locations, which have a greater mismatch between solar availability in the summer and winter as well as significant building heating loads in the winter [59]. TCES systems have also been examined for short-term storage in the winter in locations with higher solar availability, where solar heating charges the system during the day and the system is discharged to meet the heating load during the night [17,31,59]. While most TCES systems built so far have been laboratory prototypes [28], one system was built in Germany to provide short-term heat storage for heating a school building in winter and cooling a jazz club in summer [31]. This study used a district heating system instead of solar heating to charge the system, and used the system as a desiccant cooling system powered by district heat in cooling mode [31].

Thermochemical energy storage has the potential to allow for the same storage system to operate at different temperatures in different climates, to adjust the operating temperature if needed during operation, and potentially to use the same storage system for both heating and cooling. However, this potential of TCES has not received much attention, with most systems previously considered being intended specifically for heating or cooling [28], except those that are used with district heating (and thus used only for heat storage, even if they this is used for both heating and cooling loads) as described above [31].

2.5 Varying the Phase Change Temperature of Phase Change Materials

While sensible heat storage and thermochemical storage can be used to store heat for both cooling and heating [18,31], this is harder to do with latent heat storage since energy must be stored

at a specific melting temperature (or temperature range, for eutectics) [21,22]. Systems using different PCMs for heating and cooling have been examined [27,56], but these are more expensive and complex since they are essentially using two different storage systems rather than a single system that stores energy for both applications. If the phase change temperature of a material could be significantly altered so that the material could be used to store energy for heating at one temperature and for cooling at another temperature, this would allow for year-round energy storage using only a single PCM.

Finding ways to significantly alter the phase-change temperature of a PCM is an active area of research [29,30,63,64]. However, none of the proposed methods are ready for practical deployment. The main focus of much of this research has been on the creation of energy barriers that would prevent the loss of stored energy in between charging and discharging [30,63]. This can be done for solid-solid phase transitions in certain ceramics [63] and plastic crystals [64], through pressure-induced phase transitions. However, for ceramics, this process requires the creation of the material through high-temperature sintering and the phase transition has a low energy density [63]. Phase transitions in plastic crystals have a higher energy density, but still require a large change in pressure to achieve the desired change in transition temperature [64].

More recent research has found ways to adjust the temperature of a solid-liquid phase change. Han et al. [30] achieved this for an organic PCM by doping it with azobenzene photoswitches and activating these with UV light. This was found to allow for the melt temperature to be altered by 3-10°C [30]. However, the process is highly inefficient, with an energy efficiency of 2.7-3%, due to the high energy requirements for activating the photoswitches [30]. A more energy-efficient method was recently developed by Lau et al. [29]. This method uses a PCM with a high salt concentration as a dual-ion battery: as the salt cations and anions are stored in the electrodes, the phase-change temperature of the PCM increases due to the change in the ionic concentration [29]. Using polyethylene glycol as the PCM and lithium oxalatodifluoroborate as the salt, they were able to achieve a change in the melt temperature of around 6°C with ~50% energy efficiency and a phase-change enthalpy in the range of 100-150 kJ/kg [29]. This is currently the most promising research into variable phase-change temperatures; however, further research, in particular studying larger-scale application (the results given are for a system with only 16 mg of PCM [29]) will be needed before it can be used in practical applications. Furthermore,

significantly larger changes in phase-change temperature (~20°C) will be needed before it would allow the same PCM to be used for TES for building heating and cooling.

2.6 Metal Hydrides

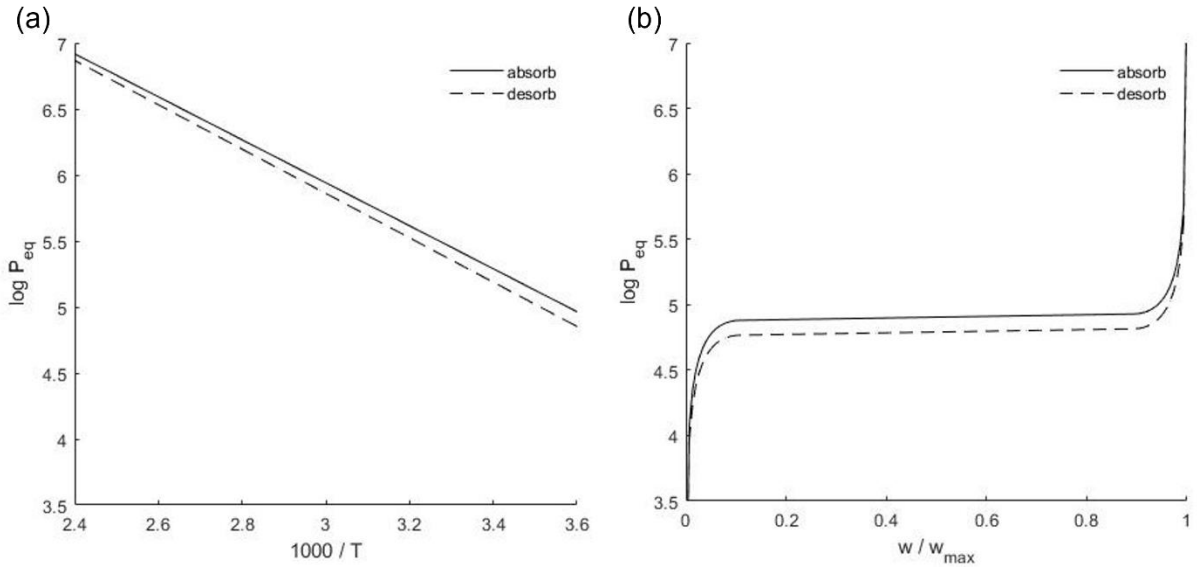

Figure 2-3. (a) Van't Hoff diagram showing relationship between temperature and equilibrium pressure for $LaNi_5$. (b) Relationship between hydrogen fraction stored and equilibrium pressure for a $LaNi_5$. These images were created using data from the Metal Hydride Toolbox developed by Voskuilen et al. [36].

Metal hydrides are metals that absorb and desorb hydrogen. In the adsorption reaction, the hydride stores hydrogen inside the metal lattice; this is an exothermic reaction. The desorption of hydrogen, where stored hydrogen is released, is an endothermic reaction. The material property that determines whether these reactions occur is the equilibrium pressure. If the hydrogen pressure surrounding the hydride is lower than the equilibrium pressure, hydrogen is desorbed; if the pressure is greater than the equilibrium pressure, hydrogen is absorbed [36]. There are different values for the equilibrium pressure for absorption and desorption; no reaction occurs if the pressure is in between these values [36]. Equilibrium pressure is a function of temperature; it increases as temperature increases [36,65]. Thus, for both absorption and desorption reactions in a hydride, the temperature and pressure will both move towards equilibrium if not altered by an external source. When hydrogen is being absorbed, the pressure decreases as the amount of gaseous hydrogen decreases, and the release of heat increases the hydride temperature and thus the equilibrium

pressure; the pressure decreases and the equilibrium pressure increases, thus bringing them closer together until the reaction ceases. In a desorption reaction, the pressure increases and the equilibrium pressure decreases, again bringing them closer together (since desorption occurs when pressure is less than equilibrium).

A Van't Hoff diagram of the relationship between the reaction temperature and pressure can be seen in Figure 2-3a. Since the equilibrium pressure increases with increasing temperature, altering the pressure in the system can alter the temperature at which adsorption/desorption occurs. Thus, since the temperature at which the reaction occurs can be altered, metal hydrides can be used for variable-temperature energy storage.

The equilibrium pressure also depends on the weight percentage of hydrogen absorbed by the metal hydride [36,65]. This relationship is shown in Figure 2-3b. Away from the minimum or maximum weight percentages, there is a plateau where there is only a small increase in equilibrium pressure as the weight percentage increases, but on either side of the plateau, the pressure increases rapidly with small changes in weight percent. As a result, a metal hydride will have a maximum weight percent where the slope of the pressure curve becomes approximately vertical.

Metal hydrides have been considered for both hydrogen storage and energy storage applications, often for use with renewable energy sources. This has included using hydrides for compact hydrogen storage for fuel cells [66–72] and for energy storage with CSP [32–35,73–78]. Systems with multiple metal hydride reactors have also been evaluated for heating and cooling applications, where the hydride reactors are used in place of a heat pump [79–85].

2.7 Metal Hydride System Design

A common design for metal hydride systems, used for energy storage and for heating and cooling systems, is to have a pair of metal hydride reactors connected so that hydrogen can flow between them. In other words, as hydrogen is desorbed in one reactor, it flows to the other reactor, which absorbs it. Experimental work has been done with this system design [34,81,82] and models of this system have been developed [35,73,79]. A diagram of such a system is shown in Figure 2-4. In the first operating mode, one reactor desorbs hydrogen that then flows to the other reactor, which absorbs it. In the second operating mode, the hydrogen previously stored in the second

reactor is desorbed and flows back to the first reactor, where it is absorbed until the system is in the same state as it was at the beginning of the first operating mode.

When used for heating and cooling applications, the system runs continuously back-and-forth between these two operating modes. For cases where this system is used for energy storage, the two-reactor system does not run continuously but instead absorbs heat from an external source at one time and releases it later [32,33,73,75,86]. In this kind of energy storage system, only one reactor is directly used for energy storage while the other reactor stores the hydrogen released by that reactor [33]. In general, two hydride reactors are not required for energy storage systems, since hydrogen released by one metal hydride can be compressed, stored, and released from a pressure vessel instead of a second hydride reactor [32,34,35]. However, a two-reactor design is commonly studied since it allows for more compact hydrogen storage without the need to compress hydrogen to high pressures and can avoid the costs from compressing hydrogen [32].

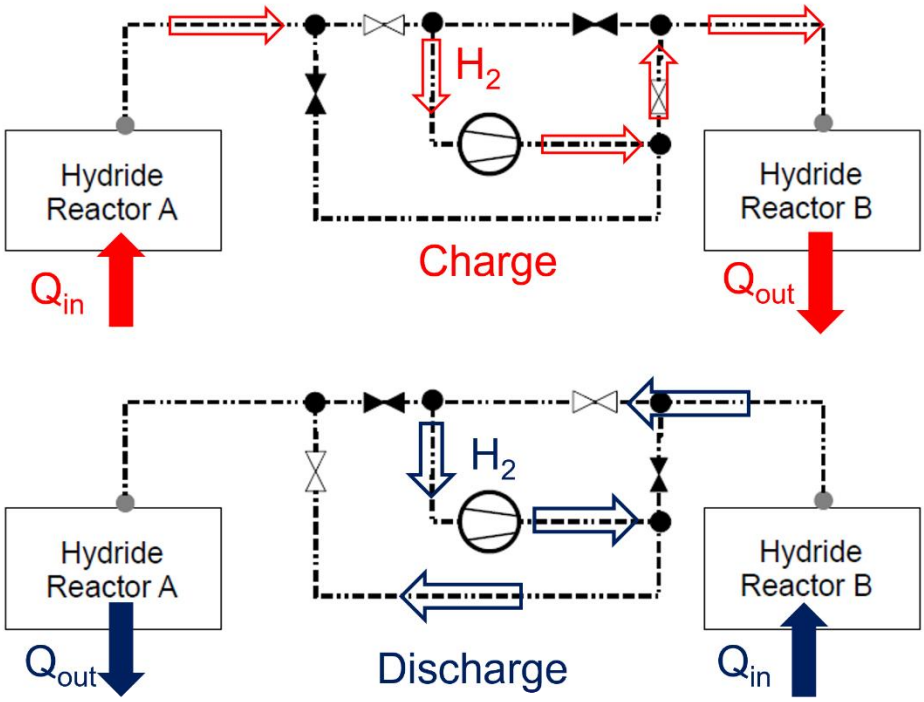

Figure 2-4. Schematic of a pressure-driven two-reactor metal hydride system. In charging mode (a), the compressor drives flow from Reactor 1 to Reactor 2, resulting in Reactor 1 desorbing hydrogen and absorbing heat, while Reactor 2 absorbs hydrogen and releases heat. In discharging mode (b), the compressor drives flow in the opposite direction, resulting in absorption in Reactor 1 and desorption in Reactor 2.

Two-reactor metal hydride systems can be characterized as temperature-driven or pressure-

driven systems. In a temperature-driven system, the flow between hydride reactors is driven by a difference in the equilibrium pressures of the reactors that depends on their temperatures, which are controlled through heat transfer to and from the reactors [32,33,76,79–81,85,87]. To understand how such a system works, we can examine the Van't Hoff plot for one such system shown in Figure 2-5. For the first operating mode, the system is charged using a heat flow, Q_{in}, to raise the temperature in one reactor, where its equilibrium pressure is higher than that of the second reactor at its current operating temperature. This means that hydrogen flows from the first reactor to the second, causing the pressure in the first to go below equilibrium (resulting in a desorption reaction) and the pressure in the second to go above equilibrium (resulting in an absorption reaction).

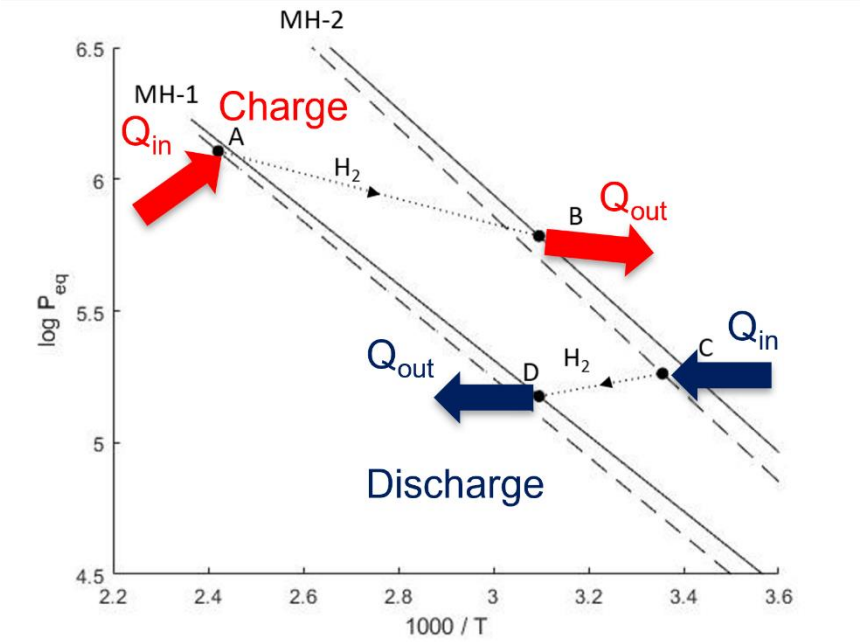

Figure 2-5. Van't Hoff plot of the two metal hydrides in a two-reactor system. The system is charged by adding heat to a reactor at position A, driving the desorption of hydrogen that flows to the other reactor, at position B, where it is absorbed, releasing heat. The system is discharged by changing the temperatures of the reactors, so that the second reactor, now at position C, desorbs hydrogen (absorbing heat) that flows to and is absorbed (releasing heat) by the first reactor, now at position D.

These reactions will continue since there is not a stable state where both the reactors are at equilibrium pressure and there is not a pressure gradient driving hydrogen flow between them. The reaction continues until the change in the equilibrium pressures with weight fraction is sufficient that there is no longer a pressure difference between the reactors when both of them are at

equilibrium. Then, to discharge the system, the first reactor is no longer heated, reducing its temperature, while the second reactor also has its temperature reduced to the temperature at which it provides the cooling load. At this new condition, there is a pressure difference in the opposite direction when both reactors at equilibrium. Thus, the reverse of the previous process occurs: the second reactor desorbs hydrogen, causing it to absorb heat, and the hydrogen moves to the first reactor, where it is absorbed, causing the reactor to release heat to a heat sink. This system design can be used to deliver a cooling load with the second reactor or a heating load with the first reactor when discharged.

A pressure-driven system uses a compressor to drive hydrogen flow between reactors, as shown in Figure 2-4, thereby moving the pressures in the reactors away from equilibrium and driving the reactions [80,82]. This removes the need for a heat source to drive the reaction and allows for greater freedom in selecting metal hydrides since a temperature-driven system requires the materials to have appropriate equilibrium pressures at the operating temperatures for the reactions to occur. For cooling applications, pressure-driven systems have been found to achieve higher COPs than temperature-driven systems [80], but require the increased cost of installing and running the compressor, while temperature-driven systems have the advantage of allowing the use of waste heat. A second hydride reactor is still used in pressure-driven cooling systems [82]. However, for a pressure-driven energy storage system, a pressure vessel can store hydrogen instead of a second hydride reactor [32,35]. This has the advantage of reducing the initial cost of the system, but the disadvantages of requiring a larger storage volume and requiring increased operating costs for hydrogen compression [32].

This use of the metal hydride system design described here for energy storage has previously been considered primarily for use with CSP. These systems use two metal hydrides reactors at different temperatures, with the high-temperature reactor at temperatures from 500-700°C, while the low-temperature reactor is close to room temperature [32,74]. However, the low-temperature reactor is sometimes heated to temperatures of 100°C or even 160°C in order to accommodate the use of cheaper metal hydrides [32]. These systems are usually temperature-driven [32,33,73,74], since the large changes in temperature in the high-temperature reactor make it easier to change the equilibrium pressure enough between charging and discharging that the reaction can be driven entirely by the temperature change. However, pressure-driven systems, using only a single hydride reactor with a pressure vessel, have also been considered [35], since

the cost of the low-temperature metal hydride is typically the dominant cost in the system [32]. Most room-temperature hydrides are alloys of titanium or rare earth elements [36], which are much more expensive than other hydrides [75]. This high cost is why it is considered worthwhile to heat the low-temperature reactor to temperatures over 100°C to use the cheaper alanate hydrides [32]. It is also likely a major reason why CSP is the primary application for which metal hydrides are considered for energy storage, since the high temperatures involved in this application allow for the use of more affordable hydrides.

2.8 Modelling and Control of Metal Hydride Systems

Numerous models of the heat and mass transfer in metal hydride reactors have been developed. The majority of these focus on a single metal hydride reactor. A 1-D radial model of a single reactor was first developed by Choi and Mills [88]. A similar 1-D model was found to obtain results that generally have good agreement with experimental values, outside of initial transients [89]. Axisymmetric 2-D models have been used to examine the system with more fidelity [78,90–93]. More computationally-intensive 3-D models of a hydride reactor, first developed by Aldas et al. [94], have been used to analyze the performance benefits of complicated system geometries, such as the addition of fins [95,96] or a tapered bed structure [35] to improve heat transfer.

With respect to two-reactor systems, modeling has been more limited. Kang [79] used a 1-D model to examine a metal hydride air conditioning system. More recently, Bhouri and Bürger [97] developed a 2-D model of an energy storage system for use with CSP that used a magnesium hydride reactor with a magnesium hydroxide reactor, although this model only examined hydrogen absorption. Bhogilla [77] used a 2-D model for a similar energy storage system that used metal hydrides in both reactors and modelled both charging and discharging of the system, and Nyamsi et al. [73] used a 3-D model to examine a pair of hydride reactors used for energy storage. Notably, none of these models considered a pair of hydride reactors with an auxiliary hydrogen compressor.

Similarly, control strategies for metal hydride reactors have focused on single-reactor systems used for hydrogen storage; relevant literature is summarized in Table 2-1. All of these papers focused on a single-reactor system for hydrogen storage, with Chabane et al. [72] also examining the control of the fuel cell the hydride reactor is being used to supply hydrogen to. Because of this, the output variable of these controllers is either the hydrogen flow rate or the

temperature or pressure of the reactor, with the latter generally being used because of its influence on the reaction rate in the reactor. For instance, while Georgiadis et al. [71] and Panos et al. [70] use outlet temperature as the output variable of the controller, they do so in order to achieve the outlet temperature that will result in the optimal hydrogen release rate. For the input variables, Cho et al. [69] and Dunikov et al. [98] open and close a valve that allows for hydrogen flow in and out of the reactor in order to control the hydrogen flow rate. The rest of the controller papers control the heat source used to drive the desorption in the reactor, either by using the flow rate [70–72] or temperature [68] of a heating fluid, or the voltage of a thermoelectric heater [99]. While similar inputs would be considered for a case where the hydride reactor was being used for energy storage or air conditioning, the output variable for such cases would be the heat transfer to or from the reactor, which is not considered by any of these controllers.

Table 2-1. Summary of the controller types and input and output variables that have previously been considered for single reactor metal hydride systems.

Authors	**Controller**	**Control Variable**	**Output Variable**
Georgiadis et al. (2009) [71]	Multi-parametric (mp) MPC	Heating Fluid Flow Rate	Outlet Temperature
Panos et al. (2010) [70]	mp-MPC	Heating Fluid Flow Rate	Outlet Temperature
Cho et al. (2013) [69]	PID	Discharge Valve Opening	Hydrogen Flow Rate
Nuchkrua and Leephakpreeda (2013) [99]	Neuro-fuzzy PID	Thermoelectric Voltage	Reactor Temperature
Aruna and Jays Christa (2020) [68]	Fuzzy PID	Heating Temperature	Reactor Pressure
Chabane et al. (2021) [72]	PI	Heating Fluid Flow Rate	Reactor Pressure
Dunikov et al. (2021) [98]	PID	Hydrogen Valve Opening	Hydrogen Flow Rate

Different models of the hydride system are also used for controller design. Dunikov et al. [98] uses a 3-D model of the temperature and pressure within the reactor, while Georgiadis et al. [71] and Panos et al. [70] both use a 2-D model for this. In contrast, Cho et al. [69], Chabane et al. [72], and Aruna and Jays Christa [68] all use a lumped model that neglects the effect of these variations. The linear models used for control synthesis are obtained using model identification techniques and simulation data from the system model [68,70,71]. Aruna and Jays Christa [68] examine different methods of converting their nonlinear model into a linear model for use in a controller, and find the best results when using a Box-Jenkins model. All of the methods compared

are black-box methods [68]; that is, they develop the linear model using only input and output data rather than deriving such a model from first principles. This poses a disadvantage from the perspective of control design because it limits the operation of the controller to a small region around the linearization point.

With respect to two-reactor systems, experimental demonstrations [81,82] used logic-based controllers to operate the system but did not involve the design of real-time controllers that could achieve specific heat transfer rates at specific times, as would be desired for an energy storage system which is charged and discharged over a longer period of time and may not be charged or discharged continuously. These experimental systems have also used either heat transfer from a fluid or a compressor to drive the system operation but have not examined how to control a system that uses both. In summary, previous work on control strategies for metal hydride reactors has not considered real-time control for a two-reactor system using both temperature and pressure to drive operation, nor control using a linear model derived from the system dynamics rather than from a black-box model.

2.9 Effect of Solar PV on Time-of-Use Rate Structures

The increasing use of solar photovoltaics (PV) for on-site energy generation provides additional benefits for the use of energy storage in load shifting for both cooling and heating. Available solar power in the afternoon significantly reduces demand from the grid during on-peak hours [100]. With sufficient solar penetration, peak electricity demand from the grid would no longer occur in the afternoon but in the morning and evening [101]. However, there is a significant mismatch between peak solar generation (around noon) and peak power demand (around 5 PM). A study of solar power in Wisconsin found that this results in diminishing returns for solar penetration once it accounts for 15-20% of power generation, but that solar penetration could be significantly increased if the demand curve were shifted to be closer to the solar generation curve [102]. Energy storage could be used to accomplish this, and the shifting of peak demand from the grid to the morning and evening would incentivize utility companies to charge TOU rates that would encourage shifting loads away from these times.

Rate structures for locations that have significant on-site generation typically include an avoided cost rate (ACR), which is a credit given for times when on-site generation exceeds

consumption. The ACR is generally significantly lower than the rate charged for electricity usage [10], which provides an incentive for using on-site PV to charge a storage system when generation exceeds consumption. Previous studies have adjusted discharge rates for storage during on-peak hours based on whether solar generation exceeds demand [19].

2.10 Summary

Ice storage is a mature technology for energy storage for building cooling, and load-shifting control schemes have been developed for it that are applicable to other forms of energy storage. A variety of other forms of TES have been considered for use with building HVAC systems. Each of these has its own advantages and disadvantages, and some have been put into practical use. However, most of these forms are only usable for either heating or cooling mode, and not both. Sensible heat storage in water can be used for both but has a lower energy density than latent heat or thermochemical storage, and other forms of energy storage can be used with district heating systems if a cooling system that is powered by the heat input (such as an absorption chiller or desiccant cooling system). However, high-density year-round storage for a building with a vapor-compression heat pump is not currently achievable.

If variable-temperature PCM storage becomes feasible, it could be used for year-round storage, as well as to improve performance by operating at optimal temperatures. This is not currently viable but is an active area of research where several methods have been examined in recent years. Alternatively, TCES using metal hydrides could also be used for year-round energy storage. Metal hydrides allow for variable-temperature storage since the reaction temperature is also a function of hydrogen pressure. Metal hydrides have been studied for other energy storage applications, primarily for use with CSP, but not for energy storage with a building HVAC system. Both one-reactor and two-reactor systems have been studied for metal hydrides; in two-reactor systems, the second reactor stores hydrogen released by the first reactor. Modelling work has been done on both one-reactor and two-reactor systems, but controllers for metal hydride systems have primarily been studied for single reactors.

In addition to shifting loads from on-peak to off-peak periods, energy storage is also used in buildings with on-site solar PV to store excess solar power generation. Increased use of solar

PV will also affect the use of energy storage by changing when the most power is needed from the grid, and thus when the on-peak hours in TOU rates are applied.

Thus, a variable-temperature energy storage system with high energy density which could be used with a typical building HVAC system has not currently been developed. Metal hydrides could be used for this purpose but have not been studied for it. Furthermore, while there is potential for such systems from thermochemical energy storage and the potential development of variable-temperature PCMs, there has not been a study of how to get optimal cost savings out of a variable-temperature energy storage system for TES in buildings.

3. METAL HYDRIDE SUBSYSTEM MODEL[2]

The first step in building a model of an HVAC system with metal hydride energy storage is to build a model of the energy storage system itself. A two-reactor system, such as is described in Section 2.7, is used for reasons explained in Section 4.1.1. The dynamic model of the two-reactor system is described in Section 3.1. A linearized version of this model, described in Section 3.2, is used by a model-predictive controller, described in Section 3.3, to set the heat rates out of the hydride reactors in the dynamic model to desired values set by the static model of the HVAC system. The controller is shown to successfully achieve its target values for test cases in Section 3.4.

3.1 Metal Hydride Reactor Model

A subsystem model (coded in Matlab) of the metal hydride reactors determines the operating temperatures and pressures of the reactors, the rate of change of the hydrogen in each reactor, and the heat transfer with the circulating fluid flowing through a given secondary loop. This subsystem model consists of two metal hydride reactors connected by a line through which hydrogen flows, with a compressor to help move the hydrogen (see Figure 3-1). Each reactor is a shell-and-tube heat exchanger, with the metal hydride bed in the shell and the circulating fluid flowing through the tubes. The porous metal hydride bed is filled with hydrogen, which can flow in and out of the reactor; however, since the hydrogen is not circulating through the reactor, the heat exchange is modelled as occurring between the circulating fluid and a solid wall (the metal hydride) rather than between two circulating fluids.

Table 3-1. Maximum weight fraction (w_{max}) and enthalpy of reaction (ΔH) for the metal hydrides selected as the preliminary materials for the system [36]. In the units, 'M' is metal, 'H' hydrogen.

Material	w_{max}	ΔH **(absorption)**	ΔH **(desorption)**
$MmNi_{4.5}Cr_{0.5}$	0.0121 kg H/ kg M	11.67 MJ/kg M	12.65 MJ/kg M
$LaNi_5$	0.0151 kg H/ kg M	15.46 MJ/kg M	15.95 MJ/kg M

[2] Portions of this chapter are taken from the papers Krane et al. 2021 [124] and Krane et al. 2022 [126].

The heat exchanger model considers a single circulating fluid tube and the surrounding metal hydride as a representative unit cell control volume and assumes by symmetry that these unit cell results can be used for the reactor as a whole. As shown in Figure 3-1, in each unit cell there is hydrogen flow into or out of the shell, water glycol flow in the tube, and heat transfer between the water glycol and the metal hydride. The materials selected for use as the hydrides in the reactors are $LaNi_5$ in the high-temperature reactor and $MmNi_{4.5}Cr_{0.5}$ ('Mm' here is mischmetal, an alloy of rare-earth elements) in the low-temperature reactor. These materials are selected to minimize compressor work by choosing materials where as much hydrogen flow as possible in both heating and cooling modes can be driven by the difference in equilibrium pressures at their operating temperatures rather than by compressor work. Key properties of these materials are described in Table 3-1. The material properties of these metal hydrides, as well as equations for equilibrium pressure and reaction rate, are taken from a Matlab Toolbox developed by Voskuilen, Waters, and Pourpoint [36].

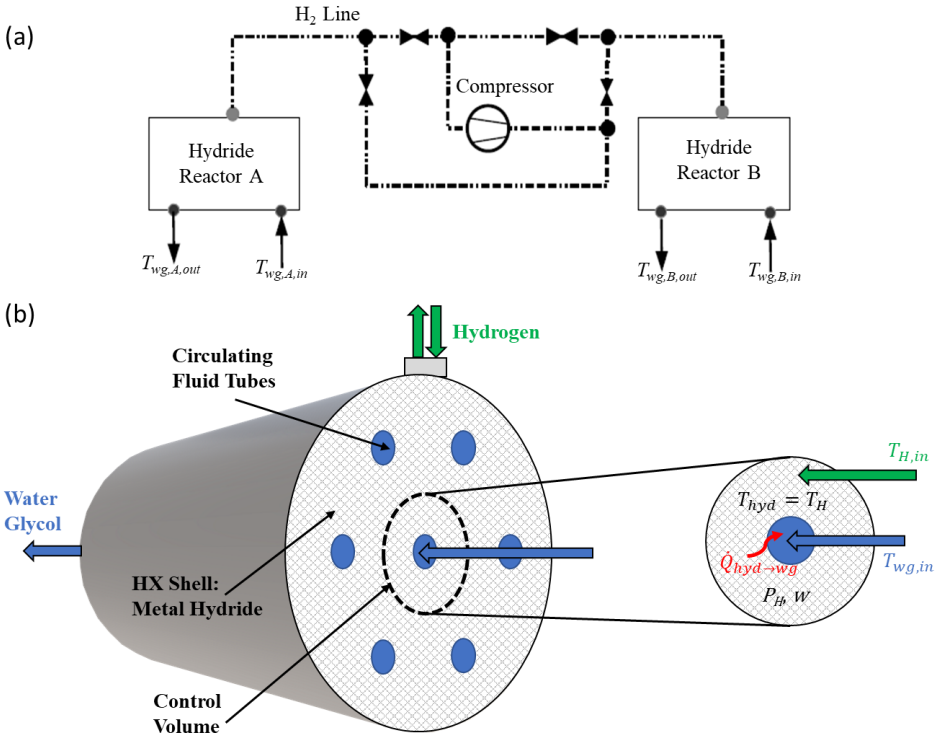

Figure 3-1. (a) Diagram of the metal hydride subsystem model showing the overall system considered by the model and (b) the control volume in each shell-and-tube reactor. Seven tubes are shown for clarity, while the actual system has a much higher number.

Within the control volume, it is assumed that the hydrogen in the reactors is an ideal gas, that the hydrogen and hydride in the reactor are in thermal equilibrium ($T_{hyd} = T_H$), and that all spatial variation in temperature and pressure are negligible (thus, the model is 0-D). Neglecting these temperature and pressure variations allows for a linear state-space model to more easily be derived from this model, which is helpful when designing the controller, and also helps reduce the computation time required by the model. Given these assumptions, the energy balance for a single control volume is given by

$$\left(m_{hyd}c_{hyd} + m_H c_{p,H}\right)\frac{dT_{hyd}}{dt} = rm_{hyd}\Delta H + \varepsilon\dot{m}c_{wg}\left(T_{sf,in} - T_{hyd}\right) + \dot{m}_{H,in}c_{p,H}\left(T_{H,in} - T_{hyd}\right), \tag{1}$$

which couples with the heat exchanger calculations, where the Dittus-Boelter correlation for fully-developed turbulent flow in a circular tube [103] is used to find the Nusselt number:

$$Nu = \frac{h_{conv}D_{tube}}{k_{sf}} = \begin{cases} 0.023Re^{0.8}\mathrm{Pr}^{0.4}, & T_{hyd} > T_{cf} \\ 0.023Re^{0.8}\mathrm{Pr}^{0.3}, & T_{hyd} < T_{cf} \end{cases} \tag{2}$$

$$T_{cf,out} = T_{sf,in} + \varepsilon\left(T_{hyd} - T_{cf,in}\right), \tag{3}$$

$$\varepsilon = 1 - e^{-NTU} \tag{4}$$

$$NTU = \frac{h_{conv}A_s}{\dot{m}c_{wg}} \tag{5}$$

$$\dot{Q}_{hyd\to wg} = \varepsilon\dot{m}c_{wg}\left(T_{hyd} - T_{cf,in}\right). \tag{6}$$

In these equations, h_{conv} is the convection heat transfer coefficient, Re the Reynolds number, Pr the Prandtl number, m_H the hydrogen mass, m_{hyd} the hydride mass, $c_{p,H}$ the hydrogen specific heat, c_{hyd} the hydride specific heat, r the reaction rate, ΔH the enthalpy of reaction, ε is the effectiveness of the heat exchanger, $\dot{m}$ the water glycol mass flow rate through the reactor, T_{hyd} the temperature in the hydride bed, $T_{cf,in}$ and $T_{cf,out}$ the inlet and outlet circulating fluid temperature, $\dot{m}_{H,in}$ the hydrogen flow rate into the reactor, $T_{H,in}$ the hydrogen inlet temperature, NTU the number of transfer units, and A_s the surface area of a tube.

The mass balance equation relates the evolution of the hydrogen mass to the reaction rate and the mass flow rate of hydrogen, $\dot{m}_H$ (note that unlike $\dot{m}_{H,in}$, $\dot{m}_H$ is used for both flow into and

out of the reactor):

$$\frac{dm_H}{dt} = rm_{hyd} + \dot{m}_H. \tag{7}$$

The hydrogen pressure in the reactor, *P*, is found using the ideal gas law:

$$P_H = \frac{m_H R_H T_{hyd}}{V_H}. \tag{8}$$

The volume of hydrogen (V_H) can be found using the porosity of the metal hydride bed (φ) and the total volume of the hydride section of the heat exchanger (V_{shell}) according to:

$$V_H = \varphi V_{shell}. \tag{9}$$

Thus, the mass balance can be re-written in terms of pressure as

$$\frac{dP_H}{dt} = \frac{R_H T_{hyd}}{\varphi V_{shell}}\left(rm_{hyd} + \dot{m}_H\right). \tag{10}$$

The reaction rate, *r*, which appears in both the energy and pressure balance, is the rate of change of the weight fraction of hydrogen stored in the hydride. It is a function of the pressure, *P*, and weight fraction, *w*, of the hydride, as well as the equilibrium pressure, P_{eq}, of the hydride, which is itself a function of the temperature, T_{hyd}, and weight fraction, *w*, of the hydride. The reaction rate is calculated using Eq. 11:

$$r = \frac{dw}{dt} = \begin{cases} C_A e^{-\frac{E_a}{RT_{hyd}}} ln\left(\frac{P_H}{P_{eq}}\right) w, & P_H < P_{eq,des} \\ 0, & P_{eq,des} \leq P_H \leq P_{eq,abs}. \\ C_A e^{-\frac{E_a}{RT_{hyd}}} ln\left(\frac{P_H}{P_{eq}}\right)(w_{max} - w) & P_H > P_{eq,abs} \end{cases} \tag{11}$$

In these equations, C_A and E_A are constant material properties of the metal hydride, w_{max} is the maximum weight fraction of the metal hydride, and the equilibrium pressures are given by

$$P_{eq} = P_{atm} e^{\frac{\mu(x,T_{hyd})}{RT_{hyd}}}, \tag{12}$$

where the chemical potential, $\mu(x,T)$, is defined as

$$\mu = \begin{cases} \mu_{\alpha,0} + 2RT_c\left(1 - \frac{2w}{w_{max}}\right) + RT\,ln\frac{w}{w_{max}-w}, & w < w_{\alpha,0} \\ \Delta H° - T\Delta S° + A\left(\frac{w}{w_{max}} - 0.5\right) & w_{\alpha,0} \le w \le w_{\beta,0} \\ \mu_{\beta,0} + 2RT_c\left(1 - \frac{2w}{w_{max}}\right) + RT\,ln\frac{w}{w_{max}-w}, & w_{\beta,0} < w \end{cases}. \quad (13)$$

In this equation, α and β are different phases of the metal hydride. The α-phase ($w < w_{\alpha,0}$) is a solid solution, while the β-phase ($w > w_{\beta,0}$) is the metal hydride phase, with a high concentration of hydrogen absorbed [104]. The system can also be in a two-phase region ($w_{\alpha,0} < w < w_{\beta,0}$); here, there is a much weaker dependence of the chemical potential on weight fraction [104]. The material properties $\Delta H°$ and $\Delta S°$ have different values for absorption and desorption, resulting in different equilibrium pressures for absorption and desorption. Together, Eqs. 1 through 13 are used to solve for the state of each reactor. The reactors are coupled through the mass flow rate of hydrogen into the reactor, which is calculated for each reactor as

$$\dot{m}_{H,A} = \begin{cases} A_{c,H\ line}\sqrt{\frac{2\rho_H\left(P_{H,B}+\Delta P_{comp}-P_{H,A}\right)}{K_{loss}}}, & flow\ from\ B\ to\ A \\ -A_{c,H\ line}\sqrt{\frac{2\rho_H\left(P_{H,A}+\Delta P_{comp}-P_{H,B}\right)}{K_{loss}}}, & flow\ from\ A\ to\ B \end{cases}, \quad (14)$$

where

$$\dot{m}_{H,B} = -\dot{m}_{H,A}. \quad (15)$$

The work $\dot{W}$ done by the compressor on the hydrogen is calculated, and the enthalpy, h, at the compressor inlet and outlet, using Eqs. 16-19:

$$\eta_{comp} = \frac{h_{comp\ out,s}-h_{comp\ in}}{h_{comp\ out}-h_{comp\ in}} = \frac{c_P\left(T_{comp\ out,s}-T_{comp\ in}\right)}{c_P\left(T_{comp\ out}-T_{comp\ in}\right)} \quad (16)$$

$$h_{comp\ out,s} = c_P T_{comp\ in}\left(\frac{P_{comp\ out}}{P_{comp\ in}}\right)^{\frac{R}{c_P}} \quad (17)$$

$$h_{comp\ out} = h_{comp\ in} + \frac{\left(h_{comp\ out,s}-h_{comp\ in}\right)}{\eta_{comp}} \quad (18)$$

$$\dot{W} = \dot{m}_{H,in}\left(h_{comp\ out} - h_{comp\ in}\right). \quad (19)$$

A compressor efficiency (η_{comp}) of 0.6 is used for the results in Sections 3.4 and 5.3.1-5.3.2, and an efficiency of 0.8 for all other results.

3.2 Linear State-Space Model

3.2.1 State-Space Model Description

While the governing dynamics of the two-reactor hydride system are nonlinear, the derived model is not well suited for control algorithm synthesis. In order to design a controller for the metal hydride model, we first created a linear version of the governing equations for the metal-hydride subsystem using a standard state-space representation. This linear model takes the form

$$f(x,u) = \frac{dx}{dt} = \boldsymbol{A}(x - x_0) + \boldsymbol{B}(u - u_0) + f(x_0, u_0)\,. \tag{20}$$

In this equation, *x* is the standard state-space notation for the dynamic state vector of the system:

$$x = \begin{bmatrix} T_{hyd,m} \\ P_{\mathrm{H},m} \\ w_m \\ T_{hyd,n} \\ P_{\mathrm{H},n} \\ w_n \end{bmatrix}. \tag{21}$$

Here, $m = A$ and $n = B$ when the system is in charging mode, while $m = B$ and $n = A$ in discharge mode. In other words, the reactor where *absorption* occurs is always referred to as reactor *m*, and the reactor where *desorption* occurs as reactor *n*, even though these are different reactors depending on the operating mode of the system. The linearization is conducted this way because the reaction rate equations are different depending on whether the hydride is absorbing or desorbing. In other words, the equations stay the same for both charging and discharging modes, with only the values of constants that are material-dependent changing.

The vector *u* is the control input vector that includes both control inputs and disturbance inputs:

$$u = \begin{bmatrix} \dot{m}_{wg,m} \\ \dot{m}_{wg,n} \\ \Delta P_{comp} \\ T_{wg,m} \\ T_{wg,n} \end{bmatrix}. \tag{22}$$

Note, disturbance inputs are variables that are not necessarily constant, but which cannot be directly controlled.

The matrices *A* and *B* are calculated at the linearization point (x_0, u_0) by calculating the Jacobian for each of the state equations with respect to *x* for *A*, and with respect to *u* for *B*:

$$\boldsymbol{A} = \begin{bmatrix} \frac{\partial f_1}{\partial x_1} & \cdots & \frac{\partial f_1}{\partial x_6} \\ \cdots & \cdots & \cdots \\ \frac{\partial f_6}{\partial x_1} & \cdots & \frac{\partial f_6}{\partial x_6} \end{bmatrix} \tag{23}$$

$$\boldsymbol{B} = \begin{bmatrix} \frac{\partial f_1}{\partial u_1} & \cdots & \frac{\partial f_1}{\partial u_5} \\ \cdots & \cdots & \cdots \\ \frac{\partial f_6}{\partial u_1} & \cdots & \frac{\partial f_6}{\partial u_5} \end{bmatrix}. \tag{24}$$

When solved at the linearization point, using the values x_0 and u_0 for *x* and *u*, *A* and *B* become arrays of constants, making Eq. 20 a linear equation.

When linearizing a system of equations, it is typical to choose the point (x_0, u_0) to be one where the system is in equilibrium, so that $f(x_0, u_0) = 0$. However, for the hydride reactors, equilibrium is only reached at the end of a reaction, whereas we need the linear model to be reasonably accurate at operating conditions that are reached during the reaction itself. Since we have an analytical formulation for the linear model, we can update the linear model based on the current operating condition and resynthesize the controller as needed to ensure that the linear model reasonably approximates the nonlinear dynamics of the hydride reactors.

In addition to using a linear form of the governing equations, the controller also needs a linear equation for the output variables which it is trying to control—in this case the heat transfer rates out of the reactors—as shown in Eq. 25.

$$g(x,u) = \begin{bmatrix} \dot{Q}_{out,m} \\ \dot{Q}_{out,n} \end{bmatrix} = \boldsymbol{C}(x - x_0) + \boldsymbol{D}(u - u_0) + g(x_0, u_0)\,. \tag{25}$$

The arrays *C* and *D* are determined using the Jacobian, similar to Eqs. 23 and 24:

$$\boldsymbol{C} = \begin{bmatrix} \frac{\partial g_1}{\partial x_1} & \cdots & \frac{\partial g_1}{\partial x_6} \\ \frac{\partial g_2}{\partial x_1} & \cdots & \frac{\partial g_6}{\partial x_6} \end{bmatrix} \tag{26}$$

$$\boldsymbol{D} = \begin{bmatrix} \frac{\partial g_1}{\partial u_1} & \cdots & \frac{\partial g_1}{\partial u_5} \\ \frac{\partial g_2}{\partial u_1} & \cdots & \frac{\partial g_2}{\partial u_5} \end{bmatrix}. \tag{27}$$

3.2.2 State-Space Model Validation

In this section, we validate the linearized model against the nonlinear one. We first describe the specific parameterization of the model based on chosen material properties and system dimensions, followed by a comparison of the linearized and nonlinear models through numerical simulations.

Here we consider $MmNi_{4.5}Cr_{0.5}$ as the material in reactor A and $LaNi_5$ as the material in reactor B. These materials are selected to operate within a pressure range of 1-10 bar for the temperatures at which the HVAC system operates. These materials are selected based on the operating temperatures of an air conditioning system with which this storage system could ultimately be integrated. The properties of these materials are taken from the toolbox developed by Voskuilen et al. [36] and are summarized in Table 3-2. By deriving the nonlinear model, and its linearization, from first principles, the model can easily be parameterized for any choice of metal hydrides. Each hydride reactor, modeled as a shell-and-tube heat exchanger, has the dimensions described in Table 3-3. The different lengths of each hydride reactor are due to their different storage capacities and thus different volumes of hydride required.

Table 3-2. Material properties of MmNi4.5Cr0.5 (Reactor A) and LaNi5 (Reactor B). All values are taken from the Toolbox developed by Voskuilen et al. [36]. Values used in this Toolbox are taken from previous literature where available; when not available (density and specific heat of MmNi4.5Cr0.5), values are based on values in literature for other metal hydrides of the same class.

Property	**Symbol**	**Units**	**$LaNi_5$**	**$MmNi_{4.5}Cr_{0.5}$**
Density	ρ	kg/m^3	8300	8200
Specific Heat	c	J/(kg K)	355	419
Enthalpy of Reaction (abs.)	ΔH_a	MJ / kg M	15.46	11.67
Enthalpy of Reaction (des.)	ΔH_d	MJ / kg M	15.95	12.65
Maximum Weight Fraction	w_{max}	kg H / kg M	0.0151	0.0121

Table 3-3. Dimensions of the shell-and-tube heat exchangers for the hydride reactors. Only the length varies between the two reactors. Each tube and its surrounding shell represent 1 control volume within the system shown in Figure 3-1.

Property	**Value**	**Units**
Tube Diameter	4	mm
Shell Diameter	7	mm
Number of Tubes	400	-
Length of Reactor A	1.77	m
Length of Reactor B	1.54	m

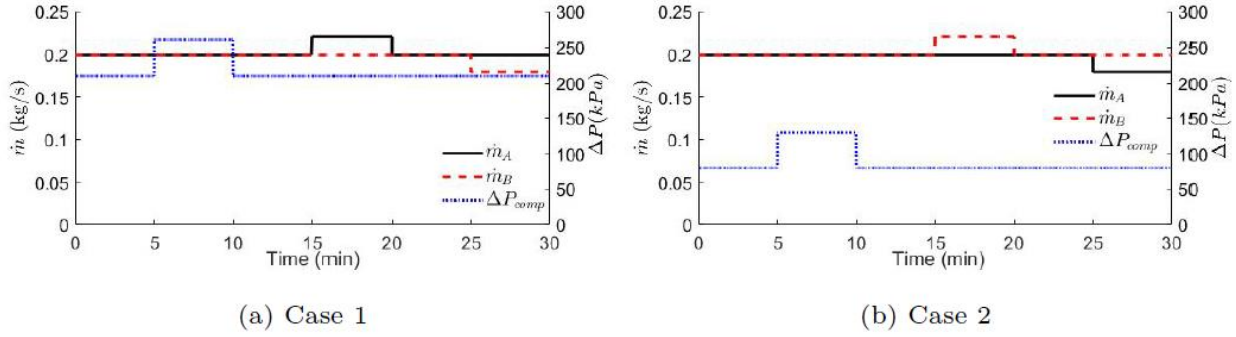

(a) Case 1 (b) Case 2

Figure 3-2. Input circulating fluid mass flow rate and compressor pressure difference for the test cases studied. In (a) Case 1, hydrogen is desorbed in reactor B and flows to reactor A, while in (b) Case 2, hydrogen desorbs in in reactor A and flows to reactor B.

The pipe for transferring hydrogen between the reactors has a diameter of 1 cm and an assumed overall loss coefficient (K_{loss}) of 40. These properties and dimensions are used in all calculations for the metal hydride system, both in this section and in Chapter 5, except for the number of tubes in the shell-and-tube heat exchanger, which is changed as a way of scaling the energy storage system for the results in Chapter 5.

To determine the suitability of the linear state-space model for use in controller design, the dynamics predicted by the linear model are compared to those predicted by the nonlinear model for a given set of input conditions. To compare the models, the linear and nonlinear governing equations are simulated in MATLAB using a variable-step solver that uses fifth-order numerical differentiation with a relative error tolerance of 10^{-3} and an absolute error tolerance of 10^{-6}.

We consider two cases. In Case 1, the initial conditions are defined so that hydrogen is desorbed in reactor B and flows to reactor A, where it is absorbed, as shown in Figure 3-3 and Figure 3-4. In Case 2, the initial conditions are defined such that hydrogen is desorbed in reactor A and flows to reactor B where it is absorbed, as shown in Figure 3-6 and Figure 3-7.

Table 3-4. Initial values for the state and input variables for Case 1 and Case 2. Note that kg H indicates mass of hydrogen and kg M indicates mass of the metal hydride.

Variable	Case 1	Case 2	Units	Variable	Case 1	Case 2	Units
$T_{hyd,A}$	6.89	6.89	°C	$T_{hyd,B}$	36.9	34.9	°C
$P_{h,A}$	480	290	kPa	$P_{h,B}$	290	360	kPa
w_A	0.006	0.007	kg H / kg M	w_B	0.006	0.007	kg H / kg M
$\dot{m}_A$	0.2	0.2	kg/s	$\dot{m}_B$	0.2	0.2	kg/s
$T_{wg,in,A}$	1.89	11.9	°C	$T_{wg,in,B}$	42.9	30.9	°C
ΔP_{comp}	210	80	kPa				

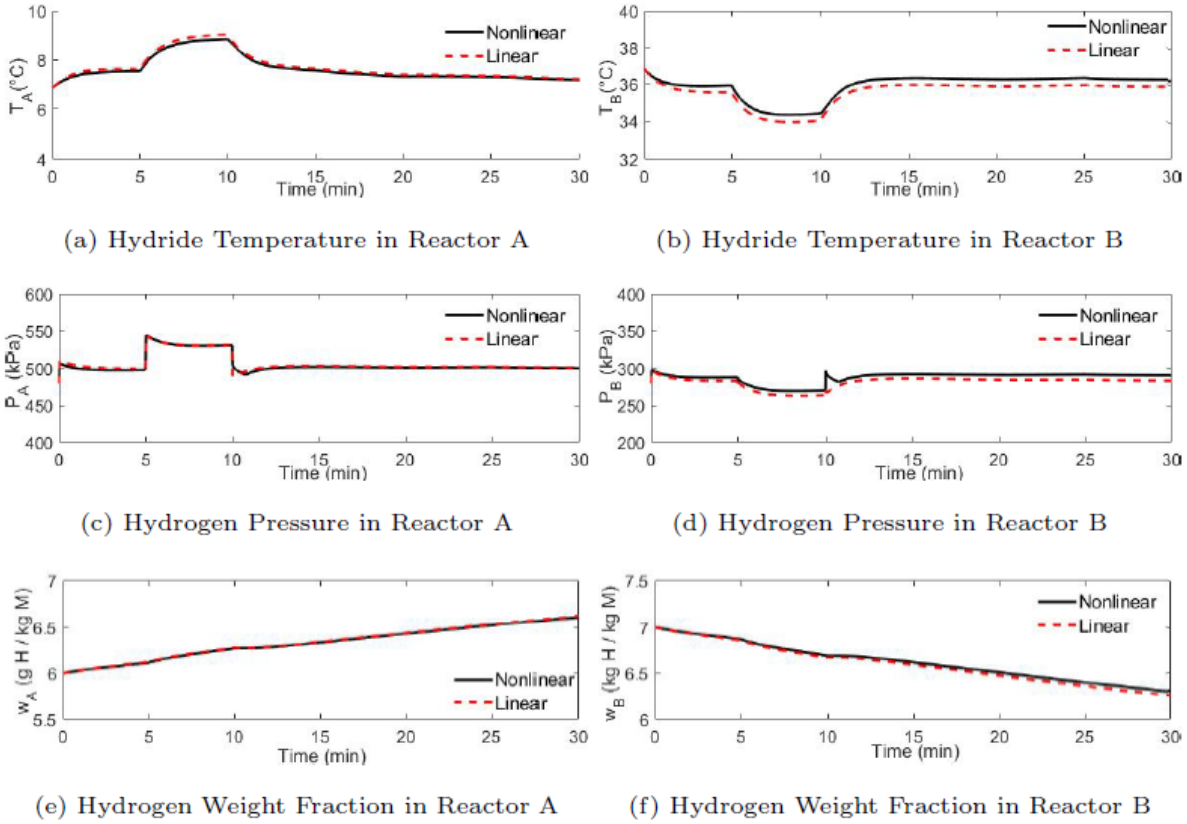

Figure 3-3. Comparison of the dynamic state variables for Reactors A and B between the linear model (dashed lines) and the nonlinear model (solid lines) for Case 1 (hydrogen is flowing from reactor B to reactor A).

These two cases, respectively, represent the charging and discharging modes of the energy storage system. In both cases, each of the three control input variables is perturbed for a five-minute period, and the dynamic response of each model is observed. These perturbations to the input variables are shown for both cases in Figure 3-2. The initial values of the state variables (x_0), as well as the input and disturbance variables (u_0) are listed in Table 3-4 and the simulation is initialized at the linearization point (x_0, u_0).

The linear model matches the nonlinear model closely. This is quantified using the root mean square error (RMSE) between the state variables predicted by the linear model and the nonlinear model, as shown in Table 3-5. The normalized RMSE (NRMSE) values are calculated using Eq. 28. All variables of the same type (e.g., temperature, pressure, or weight fraction) are normalized against the same value, determined by finding the maximum range over which each variable varies in either reactor (A or B):

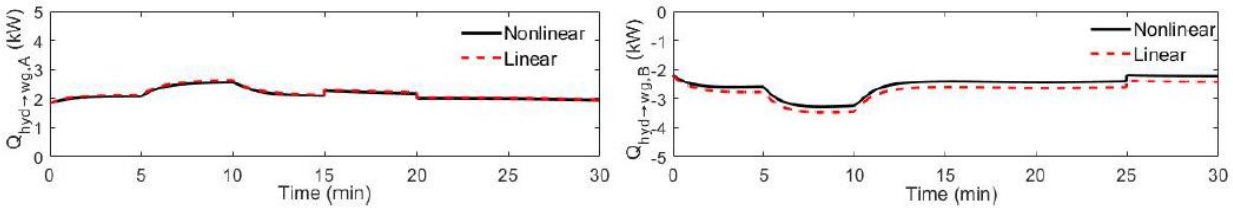

(a) Reactor A (b) Reactor B

Figure 3-4. Comparison of the heat transfer rates associated with Reactors A and B between the linear model (dashed lines) and the nonlinear model (solid lines) for Case 1 (hydrogen is flowing from reactor B to reactor A).

$$NRMSE = \frac{RMSE}{\max(\Delta x_A, \Delta x_B)} \tag{28}$$

$$\Delta x_A = max\left(max\left(x_A - x_{A,i}\right)_{Case\ 1}, max\left(x_A - x_{A,i}\right)_{Case\ 2}\right) - min\left(\min\left(x_A - x_{A,i}\right)_{Case\ 1}, \min\left(x_A - x_{A,i}\right)_{Case\ 2}\right) \tag{29}$$

$$\Delta x_B = max\left(max\left(x_B - x_{B,i}\right)_{Case\ 1}, max\left(x_B - x_{B,i}\right)_{Case\ 2}\right) - min\left(\min\left(x_B - x_{B,i}\right)_{Case\ 1}, \min\left(x_B - x_{B,i}\right)_{Case\ 2}\right). \tag{30}$$

The fastest response in the system is that of the hydrogen pressure (seen in Figure 3-3c and Figure 3-3d) to the change in the pressure difference created by the compressor (ΔP_{comp}) at t=5 min and at t=10 min. At t=5 min, increasing ΔP_{comp} results in an almost immediate change in the hydrogen pressure of reactor A ($P_{H,A}$) approximately equal to the change in ΔP_{comp}, as seen in Figure 3-3c. To understand why $P_{H,A}$ changes more than $P_{H,B,}$ we can revisit the two terms of the pressure balance (recall Eq. 10: $\frac{dP_H}{dt} = \frac{R_H T_{hyd}}{\varphi V_{shell}}\left(rm_{hyd} + \dot{m}_H\right)$): (1) the absorption or desorption rate (depending on the direction of the reaction), rm_{hyd}, and (2) the hydrogen mass flow rate into the reactor, $\dot{m}_{H,in}$.

At this operating condition, r_B (the reaction rate on a per unit mass of hydride basis) is more sensitive to changes in pressure than r_A. When ΔP_{comp} increases, the magnitude of $\dot{m}_{H\ in}$ increases in each reactor. This term becomes much larger than the absorption rate in reactor A or the desorption rate in reactor B. However, the desorption rate in reactor B increases enough to balance the mass flow rate after only a small change in $P_{H,B}$, while it takes a much larger change in $P_{H,A}$ before the absorption rate in reactor A balances the mass flow rate.

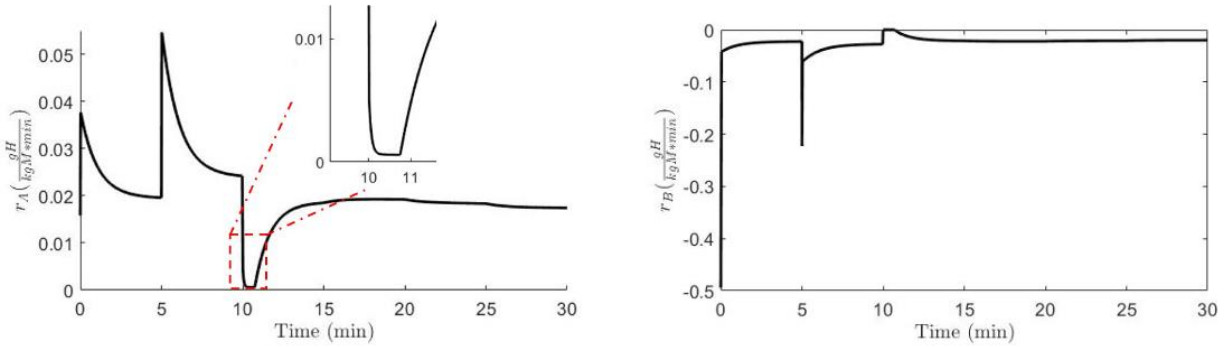

(a) Reactor A (b) Reactor B

Figure 3-5. Reaction rates in Reactor A and B for Case 1.

Thus, $P_{H,A}$ increases much more than $P_{H,B}$ decreases. This process occurs very quickly; in the initial second after ΔP_{comp} increases, the driving pressure difference $P_{H,B} + \Delta P_{comp} - P_{H,A}$ decreases by 94.8%. Thus, it appears as a step change when plotted over a 30-minute time span in Figure 3-3. The linear state-space model successfully captures this response, as seen in Figure 3-3c and Figure 3-3d.

At t = 10 min, when ΔP_{comp} returns to its original value, there is a significant step change in both pressures. The change in ΔP_{comp} causes hydrogen to flow from reactor A to reactor B, whereas it otherwise flows from reactor B to reactor A in Case 1. Therefore, in both reactors, rm_{hyd} and $\dot{m}_{H,in}$ have the same sign, so $r_B m_{hyd,B}$ cannot balance $\dot{m}_{H\,in,B}$ as it did before. Once the initial pressure difference has been reduced, the mass flow is reduced to a small value, so the changes in pressure are primarily due to the reaction rates. However, the response of r_B to the change in the pressure causes r_B to go to zero, as shown in Figure 3-5b. As shown in Figure 3-5a, however, r_A decreases but does not go to zero. This means that for approximately 45 seconds, hydrogen is being absorbed in one reactor but not desorbed in the other. Thus, the pressure in both reactors slowly decreases, since hydrogen is flowing out of reactor B, but the absorption rate in reactor A is larger than the flow rate in. After ~45 seconds, the increasing temperature seen in Figure 3-3b causes the absorption rate for reactor B to grow larger than $\dot{m}_{H\,in,B}$, so $P_{H,B}$ starts increasing. This increase leads to an increased mass flow rate to reactor A, which is larger than the absorption rate in reactor A, resulting in $P_{H,A}$ increasing as well.

The most significant difference between the linear and nonlinear models can be seen in Figure 3-3d, where the linear model does not capture the initial spike in $P_{H,B}$ and the decay that follows it, but accurately captures the behavior of the pressure after that time. This is because the reaction

rate equation (Eq. 11) is discontinuous when it goes to zero. Since the linear model does not include this discontinuity, it fails to capture the behavior of the pressure while the reaction rate is equal to zero. However, once the reaction rate is again nonzero, the linear model again follows the nonlinear model.

The response of the hydride temperature in each reactor to the change in ΔP_{comp} is shown in Figure 3-3a and Figure 3-3b. Here, the increased reaction rate after the increase in ΔP_{comp} results in an increase in the heat released or absorbed by the reaction, pushing the temperature of the hydrides in both reactors away from the temperature of the circulating fluid in their reactors.

This causes the heat transfer rate between the hydride in each reactor and the circulating fluid to increase, as shown in Figure 3-4. Once these heat transfer rates are approximately equal to the heat transfer from absorption and desorption, the temperatures become close to steady. While the linear model underestimates $T_{hyd,B}$ after the step change, as shown in Figure 3-3b at t = 5 min, it stays within 10% of the nonlinear model, and $T_{hyd,A}$ stays within 5% throughout the simulation.

Table 3-5. RMSE and NRMSE for all state variables for Case 1.

RMSE						
t (min)	$T_{hyd,A}$ (°C)	$P_{H,A}$ (kPa)	w_A ($\frac{kg\ H}{kg\ M}$)	$T_{hyd,B}$ (°C)	$P_{H,B}$ (kPa)	w_B ($\frac{kg\ H}{kg\ M}$)
0-5	0.095	3.08	0.0047	0.248	3.70	0.0074
5-10	0.156	0.477	0.0060	0.384	6.06	0.017
10-15	0.094	2.66	0.0034	0.354	7.23	0.022
15-20	0.077	1.24	0.0061	0.376	6.26	0.029
20-25	0.057	0.847	0.0082	0.388	6.70	0.036
25-30	0.041	0.622	0.010	0.389	7.04	0.042
NRMSE						
t (min)	$T_{hyd,A}$ (°C)	$P_{H,A}$ (kPa)	w_A ($\frac{kg\ H}{kg\ M}$)	$T_{hyd,B}$ (°C)	$P_{H,B}$ (kPa)	w_B ($\frac{kg\ H}{kg\ M}$)
0-5	2.40%	2.26%	0.356%	6.27%	2.71%	0.561%
5-10	3.93%	0.357%	0.455%	9.71%	4.43%	1.26%
10-15	2.36%	1.94%	0.258%	8.99%	5.30%	1.69%
15-20	1.93%	0.910%	0.470%	9.57%	4.59%	2.20%
20-25	1.42%	0.612%	0.621%	9.86%	4.92%	2.69%
25-30	1.02%	0.446%	0.780%	9.90%	5.17%	3.20%

In contrast to the visible changes in pressure and temperature that occur when ΔP_{comp} changes, there is not a significant change in these variables when either of the mass flow rates are changed. However, as shown in Figure 3-4, there is a step change in the heat transfer rate in each reactor

when there is a change in the mass flow rate in that reactor. This is because the heat transfer rate is a linear function of the mass flow rate. This change is accurately captured by the linear model, as seen in Figure 3-4a and Figure 3-4b. All variables stay within 10% of the nonlinear model throughout the simulation.

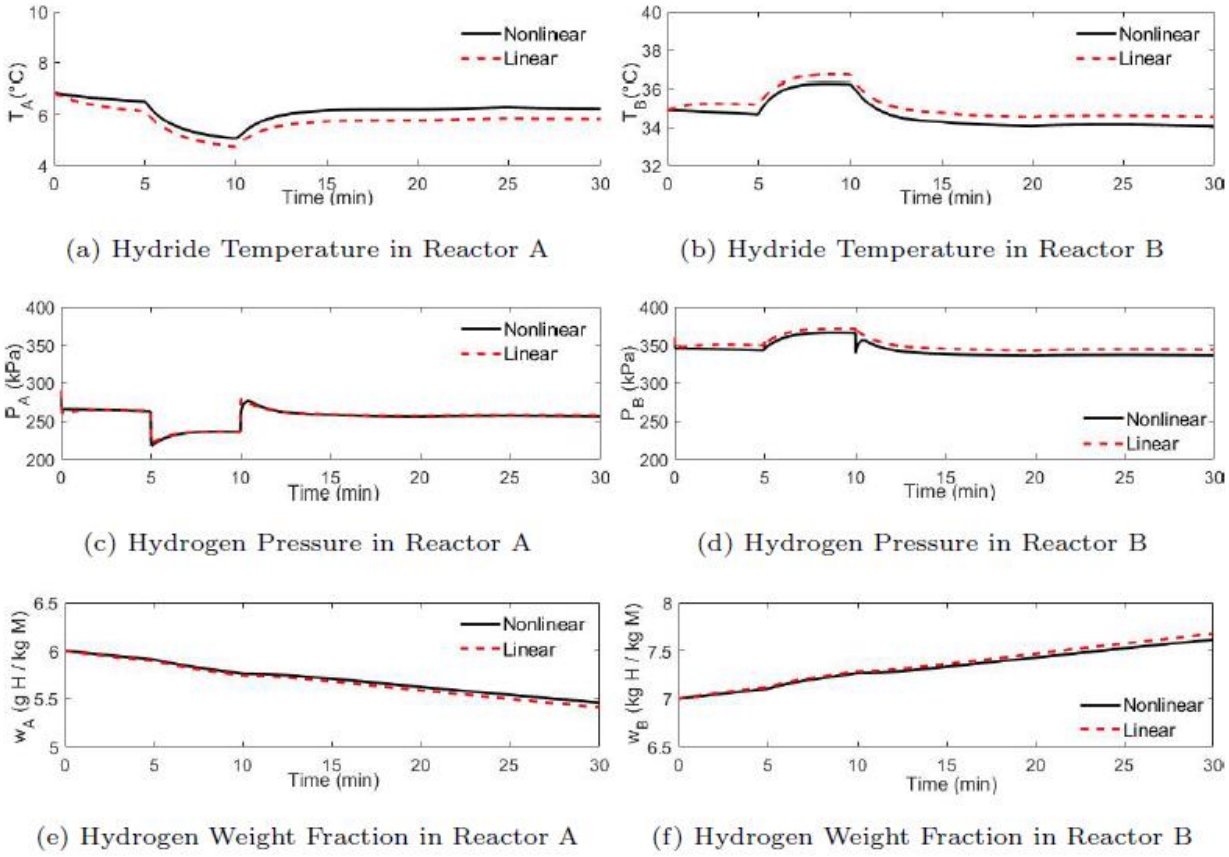

Figure 3-6. Comparison of the dynamic state variables for Reactors A and B between the linear model (dashed lines) and the nonlinear model (solid lines) for Case 2 (hydrogen is flowing from reactor A to reactor B).

Finally, the change in the weight fraction over time is different from that of the hydride temperature and pressure because the weight fraction changes continually (except for w_B while r_B is equal to zero) and does not enter a near-equilibrium state. The dynamics of the weight fraction are controlled by the reaction rate, which is the derivative of the weight fraction. As discussed in regard to the pressure dynamics, the reaction rate in both reactors changes quickly in the seconds after the change in ΔP_{comp} until $r_A m_{hyd,A}$, $r_B m_{hyd,B}$, and $\dot{m}_{H\,in}$ have approximately equal magnitudes. This quick change in the reaction rate, combined with the very slow change for the rest of the

simulation period, results in the weight fraction in each reactor resembling a linear function with a different slope after t = 5 min, as seen in Figure 3-3e and Figure 3-3f.

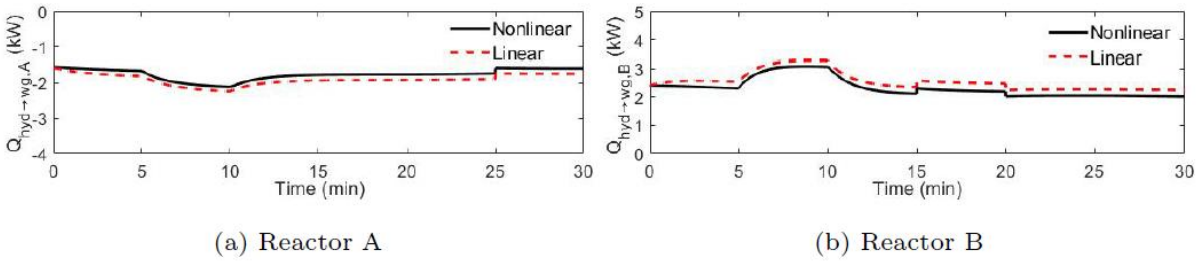

(a) Reactor A (b) Reactor B

Figure 3-7. Comparison of the heat transfer rates associated with Reactors A and B between the linear model (dashed lines) and the nonlinear model (solid lines) for Case 2 (hydrogen flowing from reactor A to reactor B).

After ΔP_{comp} returns to its original value at t = 10 min, the rate of change of the weight fraction also returns to approximately its original value. For the weight fraction, the error of the linear models stays below 4% for both reactors as shown in Table 3-5. Like the pressure, the weight fraction does not respond significantly to changes in the mass flow rates.

For Case 2, despite hydrogen flow in the system moving in the opposite direction, the same trends can be seen as discussed for Case 1. The pressure dynamics are similar, including r_B going to zero for some time after t = 10 min. However, because reactor A is desorbing hydrogen here rather than absorbing it as in Case 1, the pressure in both reactors increases while r_B equals zero, and then decreases once absorption starts in reactor B, as seen in Figure 3-6c and Figure 3-6d. The same general trends can also be seen in the temperature and weight fraction dynamics, with the only differences being due to the reversal of which reactor is absorbing hydrogen and releasing heat to the circulating fluid, and which is desorbing hydrogen and being heated by the circulating fluid.

Overall, the linear model predictions match those of the nonlinear model well in Case 2. As seen in Table 3-6, there is a larger error for the hydride temperature states in this case than for Case 1, but the linear model is still accurate within 12.5% across the entire simulation period. The error for $P_{H,A}$ is lower for this case, remaining within 1% of the nonlinear model, while the highest error for $P_{H,B}$ is still less than 6% different from the nonlinear model. The error between the linear and nonlinear model predictions for the weight fraction states follows a similar pattern to Case 1,

continually increasing over time while never exceeding 5%, without any of the changes to the inputs noticeably affecting the rate at which the error increases.

Table 3-6. RMSE and NRMSE for all state variables for Case 2.

RMSE						
t (min)	$T_{hyd,A}$ (°C)	$P_{H,A}$ (kPa)	w_A ($\frac{kg\ H}{kg\ M}$)	$T_{hyd,B}$ (°C)	$P_{H,B}$ (kPa)	w_B ($\frac{kg\ H}{kg\ M}$)
0-5	0.272	1.01	0.011	0.380	5.22	0.012
5-10	0.317	0.818	0.017	0.399	5.54	0.017
10-15	0.391	1.16	0.025	0.455	7.46	0.023
15-20	0.428	0.790	0.033	0.474	7.02	0.034
20-25	0.424	0.978	0.039	0.476	7.29	0.045
25-30	0.407	1.17	0.045	0.479	7.58	0.056
NRMSE						
t (min)	$T_{hyd,A}$ (°C)	$P_{H,A}$ (kPa)	w_A ($\frac{kg\ H}{kg\ M}$)	$T_{hyd,B}$ (°C)	$P_{H,B}$ (kPa)	w_B ($\frac{kg\ H}{kg\ M}$)
0-5	6.92%	0.743%	0.811%	9.66%	3.83%	0.886%
5-10	8.05%	0.608%	1.30%	10.2%	4.07%	1.27%
10-15	9.93%	0.851%	1.89%	11.6%	5.47%	1.75%
15-20	10.9%	0.577%	2.46%	12.0%	5.14%	2.61%
20-25	10.8%	0.718%	2.95%	12.1%	5.34%	3.43%
25-30	10.3%	0.858%	3.42%	12.1%	5.55%	4.23%

3.3 Model-Predictive Controller

The linearized form of the system model is used in a multi-input, multi-output model-predictive controller (MPC) that controls the heat transfer rates from the hydride reactors, $g(x,u)$. The MPC uses the linearized model to predict the response of the system over an N-step time horizon and uses this prediction to find the optimal values of the control variables, $[u(k), u(k+1), \cdots u(k+N)]$, for the time period. The control variables for that time step are then set to the values $u(k)$. The MPC used for this project was designed by Dr. Austin Nash.

For the MPC, the input variables u are divided into control variables u and disturbance inputs d, where d represents the inputs not set by the controller- in this case, the temperatures $T_{wg,in,m}$ and $T_{wg,in,n}$. Similarly, the matrices **B** and **D** are broken up into **B** and $\mathbf{B_d}$, **D** and $\mathbf{D_d}$. The discretized equations for the state and output variables are then written as:

$$x(k+1) = \boldsymbol{A}x(k) + \boldsymbol{B}u(k) + \boldsymbol{B_d}d(k) \tag{31}$$

$$\boldsymbol{y}(k) = \boldsymbol{C}x(k) + \boldsymbol{D}u(k) + \boldsymbol{D_d}d(k). \tag{32}$$

In Eq. 31, $x(k)$ is the state of the system at time step k, and $x(k+1)$ the state at the time step $t(k+1)$, defined as

$$t(k+1) = t(k) + t_{samp}. \tag{33}$$

In Eq. 33, t_{samp} is the sampling time used by the MPC. It is important to note that is not the same as the time step used to solve the nonlinear model. To drive the output variables to their desired values, we add an error tracking state, $x_i(k)$, to the control model, where the error tracking state is defined as

$$x_i(k+1) = \dot{Q}(k) - r(k). \tag{34}$$

In this equation, $r(k)$ is the reference tracking state (the desired output values). This gives us the updated control model

$$\tilde{x}(k+1) = \widetilde{\boldsymbol{A}}\tilde{x}(k) + \widetilde{\boldsymbol{B}}u(k) + \widetilde{\boldsymbol{B}}_{\boldsymbol{d}}\tilde{d}(k) \tag{35}$$

$$\tilde{y}(k) = \widetilde{\boldsymbol{C}}\tilde{x}(k) \tag{36}$$

where

$$\widetilde{\boldsymbol{A}} = \begin{bmatrix} \boldsymbol{A} & \boldsymbol{0} \\ \boldsymbol{C} & \boldsymbol{0} \end{bmatrix}, \quad \widetilde{\boldsymbol{B}} = \begin{bmatrix} \boldsymbol{B} \\ \boldsymbol{D} \end{bmatrix}, \widetilde{\boldsymbol{B}}_{\boldsymbol{d}} = \begin{bmatrix} \boldsymbol{B}_{\boldsymbol{d}} & \boldsymbol{0} \\ \boldsymbol{D}_{\boldsymbol{d}} & -\boldsymbol{I} \end{bmatrix}, \widetilde{\boldsymbol{C}} = [\boldsymbol{0}, \quad \boldsymbol{I}] \tag{37}$$

$$\tilde{x}(k) = [x(k), \quad x_i(k)]^T, \quad \tilde{d}(k) = [d(k), \quad r(k)]^T. \tag{38}$$

The output of the augmented model is thus $\tilde{y}(k) = x_i(k)$. Therefore, to drive the heat transfer rates to their desired values, the controller drives $\tilde{y}(k)$ to zero. Thus, the MPC solves the optimization problem given in Equation 39:

$$\begin{gathered} \min \quad J(u(k), \cdots, u(k+N), \tilde{y}(k), \cdots, \tilde{y}(k+N)) \\ s.t. \, \tilde{y}(\tau+1) = \tilde{C}\tilde{x}(\tau+1) \; \forall \, \tau \in [1, N-1] \\ u_{min} \leq u(\tau) \leq u_{max}, \forall \, \tau \in [1, N] \\ |u(k) - u(k-1)| \leq \delta u_{max} \end{gathered} \tag{39}$$

where

$$J = \sum_{\tau=k}^{k+N} \tilde{y}\,(\tau)^T \boldsymbol{Q}\tilde{y}(\tau) + u(\tau)^T \boldsymbol{R}u(\tau) \tag{40}$$

$$\tilde{x}(\tau+1) = \widetilde{\boldsymbol{A}}\tilde{x}(\tau) + \widetilde{\boldsymbol{B}}u(\tau) + \widetilde{\boldsymbol{B}}_{\boldsymbol{d}}\tilde{d}(\tau). \tag{41}$$

This problem is constrained by minimum and maximum values of the control variables, u_{min} and u_{max}, and by a maximum step by which they can be changed at one time step, δu_{max}. The values used in the weighting matrices **Q** and **R** are selected by running the model for different values and finding which resulted in the best performance. Based on these tests, the values used are **Q** = [3×10^{11}, 3×10^{11},1] and **R** = [100,100]. The high values for q_1 and q_2 are due in part to the

difference in scale between the mass flow rates and the compressor pressure difference- the latter is approximately 10^6 times larger than the former- and also due to the heat transfer rates being directly dependent on the mass flow rates. This direct dependence means that high values for q_1 and q_2 are needed for the compressor pressure difference to be used at all if it is possible for the controller to use the mass flow rates. Comparing performance to cases with lower values of q_1 and q_2 showed that this use of the compressor did improve the performance of the controller.

3.4 Controller Performance for Test Cases

To test the controller, we examine its performance for the system modelled in Section 3.2.2, with the material properties described in Table 3-2 and the dimensions described in Table 3-3. The controller is tested for two test cases, with the initial conditions previously given in Table 3-4. The first case, which represents the system charging, is used to test the ability of the system to respond to changing target heat rates. The second case, which represents the system discharging, is used to test the ability of the controller to respond to changes in the disturbance inputs (the water glycol inlet temperatures).

3.4.1 Varying Target Heat Rates

The MPC is designed primarily for referencing tracking, so we first verify its performance in the context of tracking variable heat transfer rates in each reactor. The model is simulated using the initial conditions for the charge case (Case 1 in Table 3-4). Moreover, the control input variables are bounded based on the values shown in Table 3-7.

The model is simulated for a two-hour period with the desired heat transfer rate setpoints changing every 30 minutes and the controller re-linearizing around the current operating point when the setpoint changes. The control input variables are updated at a frequency of 1 Hz. The reference value for the heat transfer rate in Reactor A increases over a series of three step changes which are mirrored by step *decreases* in the heat transfer rate in Reactor B. The closed-loop simulation results for this case are shown in Figure 3-8.

Considering this case, Figure 3-8 shows that the controller successfully tracks the step changes in the heat transfer rates in each reactor, doing so primarily through adjustments of each of the circulating fluid mass flow rates of (see Figure 3-8a and Figure 3-8c). This is consistent with

the linear relationship between mass flow rate and heat transfer rate in each reactor. In addition, the mass flow rates slowly increase over time in between step changes, adjusting to maintain a fixed heat transfer rate while the temperature differential between each reactor and the associated circulating fluid decreases. As shown in Figure 3-8e, the controller makes less use of the compressor pressure difference to achieve its objectives. While its value does change over time, the difference between the minimum and maximum values of ΔP_{comp} is only around 1% of the range of values the controller can set it to, while the difference between the minimum and maximum values of $\dot{m}_A$ is approximately 50% of its range.

For these results, the ratio of the heat rates in the two reactors is held constant even when the magnitude of the target heat rate changes. Specifically, the heat rate in reactor A has the opposite sign and 85% of the magnitude of the heat rate in reactor B. To see how the controller performance changes for a different ratio between the heat rates, we consider a case with the same initial conditions and target values for $\dot{Q}_{hyd\rightarrow wg,B}$, but with the ratio of the magnitudes of the heat rates set to 100%. The control input signals and resulting heat rates, compared to the reference values, are shown in Figure 3-9.

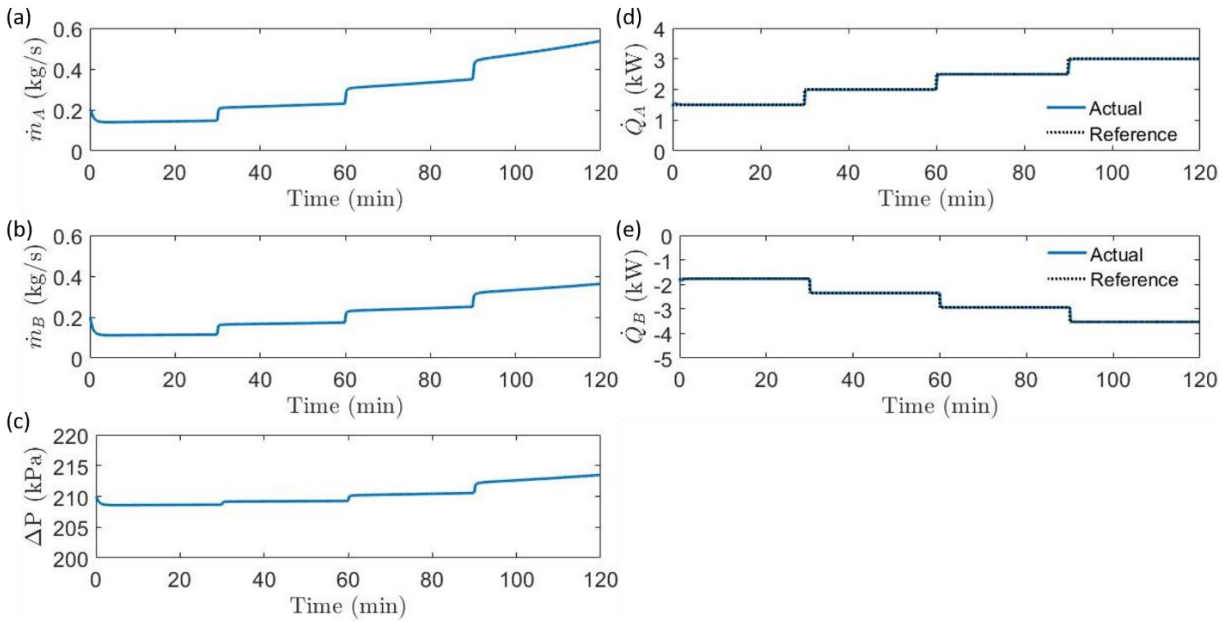

Figure 3-8. (a-c) Input values set by the controller and (d-e) output heat rates in the hydride reactors compared to the target value for the charging case with varying heat rates. The model is re-linearized and the target value changed every 30 minutes.

Table 3-7. Upper and lower bounds on the control input variables

Variable	Units	Minimum	Maximum
$\dot{m}_A$	kg/s	0	0.8
$\dot{m}_B$	kg/s	0	0.8
ΔP_{comp}	kPa	0	500

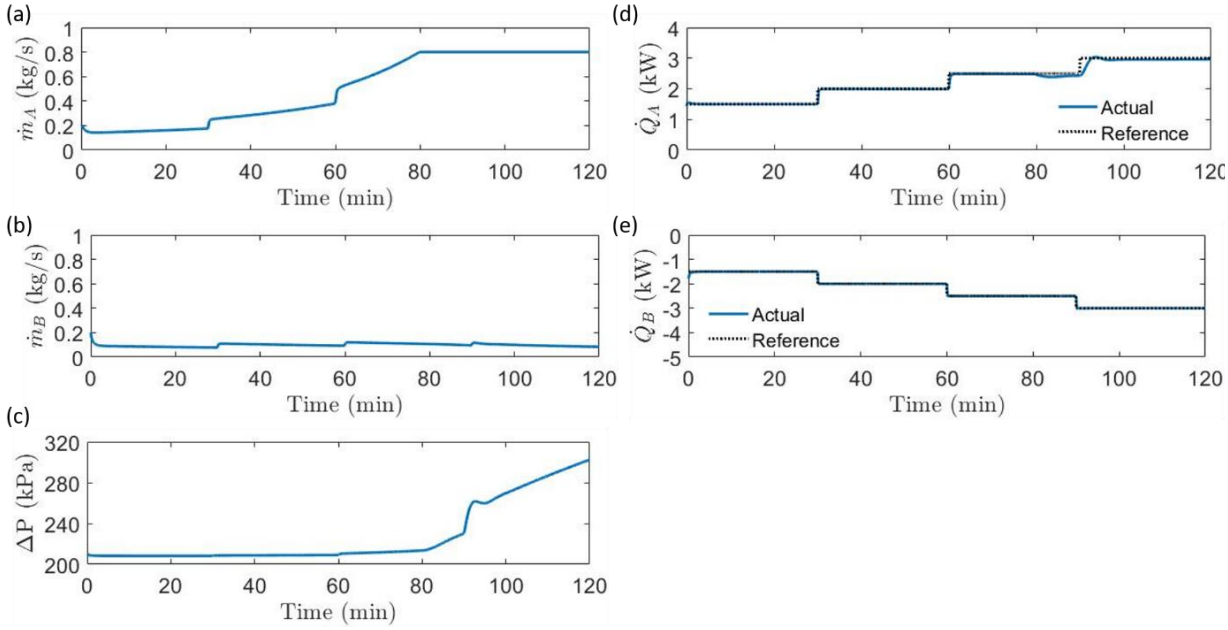

Figure 3-9. (a-c) Input values set by the controller and (d-e) output heat rates in the hydride reactors compared to the target value for the charging case with varying heat rates, where the ratio of heat rates is increased to 100%. The model is re-linearized and the target value changed every 30 minutes.

A major departure in these results, as compared to those shown in Figure 3-8, is the response of the controller when the circulating fluid mass flow rate through reactor A saturates at its upper bound of 0.8 kg/s as shown at t = 80 min in Figure 3-9a. The model predictive controller, recognizing this constraint, begins to increase the pressure differential across the compressor, since this is now the best variable to use to control the heat rate in Reactor A (see Figure 3-9c). Looking at Figure 3-9d, we can see that the compressor is able to keep the heat rate close to the target value using the compressor pressure difference, and that it can adjust to a change in the target value, but that there is now a noticeable delay after the target value changes before the actual heat is brought up to it. While Reactor A requires a larger mass flow rate over time because the reactor temperature

is moving towards the circulating fluid temperature, in Reactor B the reactor temperature moves away from the circulating fluid temperature. Thus, as seen in Figure 3-9b the mass flow rate required to meet the target heat rate decreases over time, so much so that that the values used to meet the final target heat rate are similar to the values used to meet the initial target value, even though the final target value is much larger.

For the controller to stay on target for a full cycle, the system should spend most of the time in a near-equilibrium state. This will avoid a situation where the compressor pressure difference and the mass flow rate in one reactor are saturated. In this state, the absorption or desorption rate in each reactor balances out the mass flow rate between them, and the energy transfer from the reaction balances out the heat transfer to the circulating fluid in each reactor. It is therefore important to select a ratio between the target heat rates that allows for near-equilibrium operation if the controller is being used for a full charging or discharging cycle.

3.4.2 Varying Disturbance Inputs

To test the ability of the controller to mitigate exogenous disturbances, we consider constant target heat rates in each reactor for the discharge case (Case 2 in Table 3-4), but now change the circulating fluid temperatures every 10 minutes as shown in Figure 3-10f. For this case, the model is still re-linearized every 30 minutes. The control input signals and resulting heat rates are compared to their target values in Figure 3-10.

As shown in Figure 3-10, the controller achieves the target values with only very brief initial spikes in the error whenever the heat rate changes. These results are achieved primarily by using the mass flow rates, with only slight use of the compressor. Even with these significant changes to the disturbance inputs (each temperature changes by a total of 10 °C over the course of the case study), the controller has no problems successfully adjusting the input variables in order to deliver the target heat rates. The controller can adjust to the changes in the disturbance inputs successfully without re-linearizing.

The success of the controller demonstrated here means that the dynamic model of the metal hydride reactors described in Section 3.1 can be integrated into a static model of a building HVAC system. In this integration, the dynamic model calculates the state of the reactors and the controller ensures that the heat transfer between them and the water glycol loops in the dynamic model

matches the values set in the static model. The static model into which the dynamic model is integrated is described in Chapter 4.

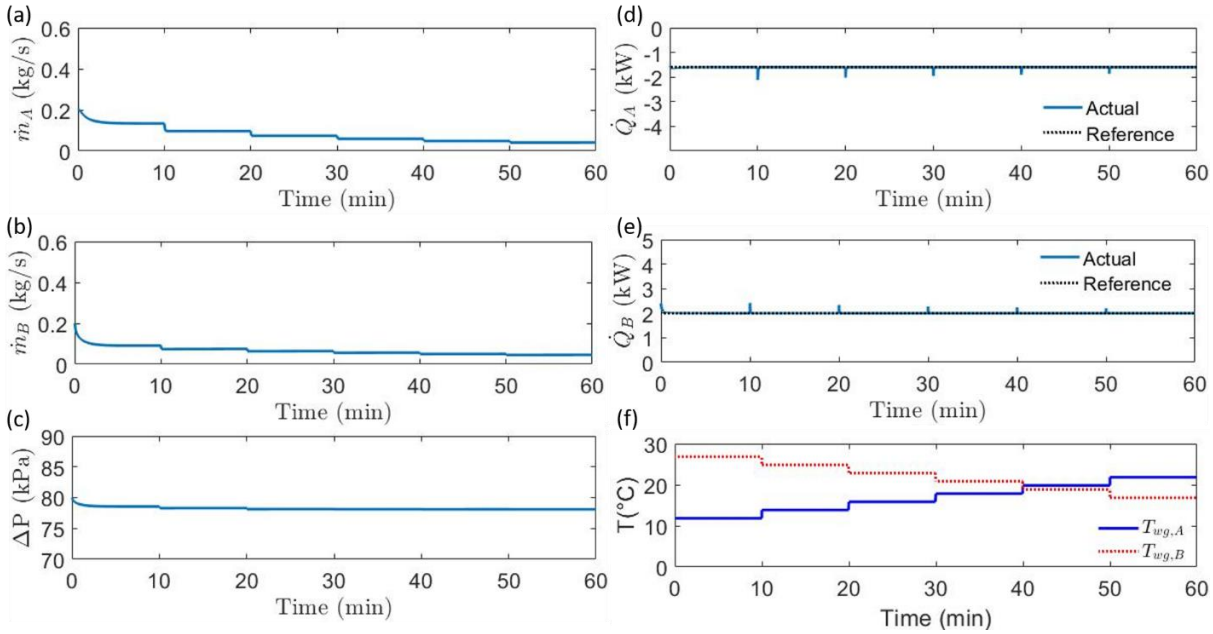

Figure 3-10. (a-c) Input values set by the controller, (d-e) output heat rates in the hydride reactors, and (f) changing disturbance inputs for the discharging case. The circulating fluid temperature changes every 10 minutes, and the model is re-linearized every 30 minutes.

4. BUILDING HEATING AND COOLING SYSTEM MODEL[3]

The metal hydride subsystem model described in Chapter 3 is integrated into a larger model of a heating and cooling system that uses metal hydrides for thermal energy storage. The system architecture is described in Section 4.1. The static model of this system (which the dynamic model of the metal hydride storage system is incorporated into) is described in Section 4.2.

4.1 System Architecture

4.1.1 Feasibility of a Hydrogen Storage Tank

One major question in designing the system architecture is whether to use a pressure vessel or a second metal hydride reactor to store the hydrogen released by the metal hydride reactor used for energy storage. A one-reactor design with a hydrogen tank would be the simplest system architecture and would significantly reduce the initial cost of the system. However, it would require the storage of hydrogen at high pressures, which would be a safety concern for a residential system.

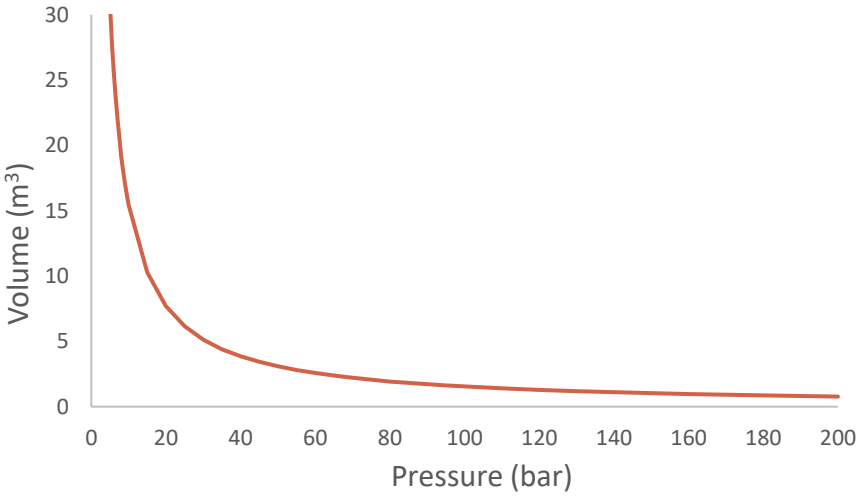

Figure 4-1. Storage volume and pressure required for a pressure vessel to store the hydrogen released by a metal hydride energy storage system with the cold storage capacity of the ice storage system modeled by Tam et al. [24]

[3] Portions of this chapter are taken from the paper Krane et al. 2022 [126].

The feasibility of this design is examined by an initial analysis of the required volume and pressure of the tank needed if the metal hydride reactor had the cold storage capacity of the residential ice storage system modeled by Tam et al. [24]. The results of this analysis can be seen in Figure 4-1, which shows the volume of tank required as a function of storage pressure. From these results, it is concluded that this design is not feasible, as using a pressure vessel with a volume less than 1 m^3 would require storage at pressures greater than 100 bar. Since either the volume or the pressure would be prohibitively large if a hydrogen storage tank were used, a two-reactor system design is used instead.

4.1.2 Two-Reactor System Architecture

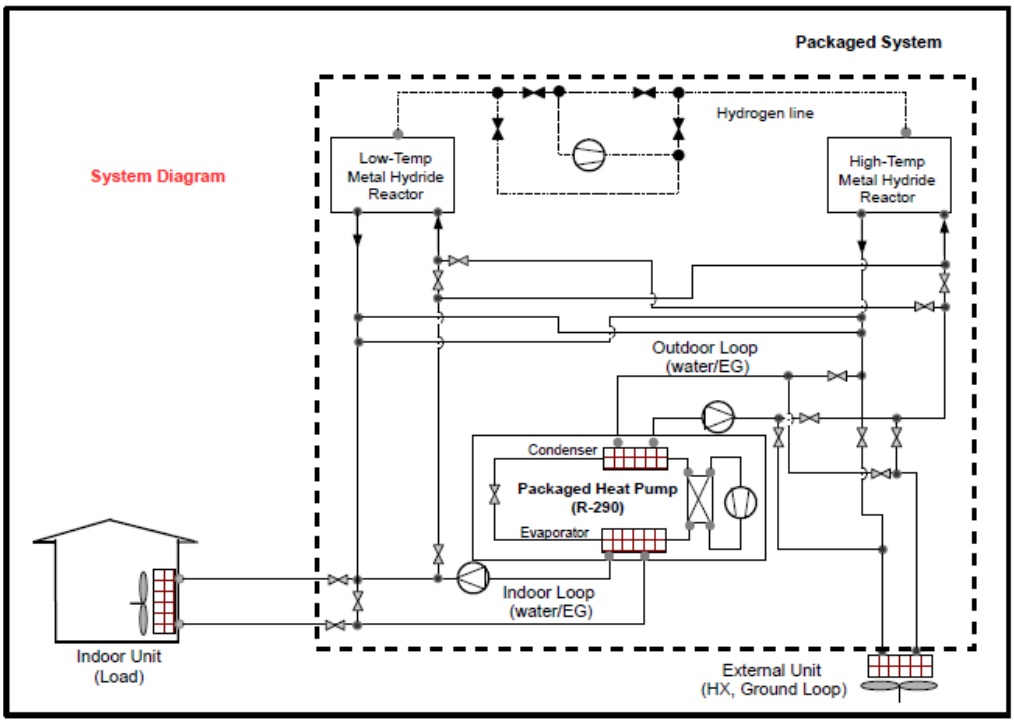

Figure 4-2. Diagram of the complete system, including packaged heat pump, secondary loops, house, external unit, hydride reactors, and hydrogen line between the reactors.

The focus of this study is a two-reactor metal hydride system. Each reactor is assumed to be a shell-and-tube heat exchanger, as described in Section 3.1. When operating, the two hydride reactors are connected, and one metal hydride reactor stores the hydrogen released by the other. A diagram of the complete system is shown in Figure 4-2. This system can be used for either

residential or commercial buildings. At the center of the system is a packaged propane heat pump with a 4-way valve that is connected to two water-glycol loops. Note that in Figure 4-2 the heat exchangers are labeled for cooling mode, where the heat pump is removing heat from the indoor loop. These two water-glycol loops are an *indoor loop*, which exchanges heat with an indoor heat exchanger in the house as well as the heat pump, and an *outdoor loop*, which exchanges heat with an external heat exchanger as well as the heat pump. The 4-way valve within the heat pump cycle is employed to switch between heating and cooling modes by reversing which loop the heat pump transfers heat to and which it removes heat from.

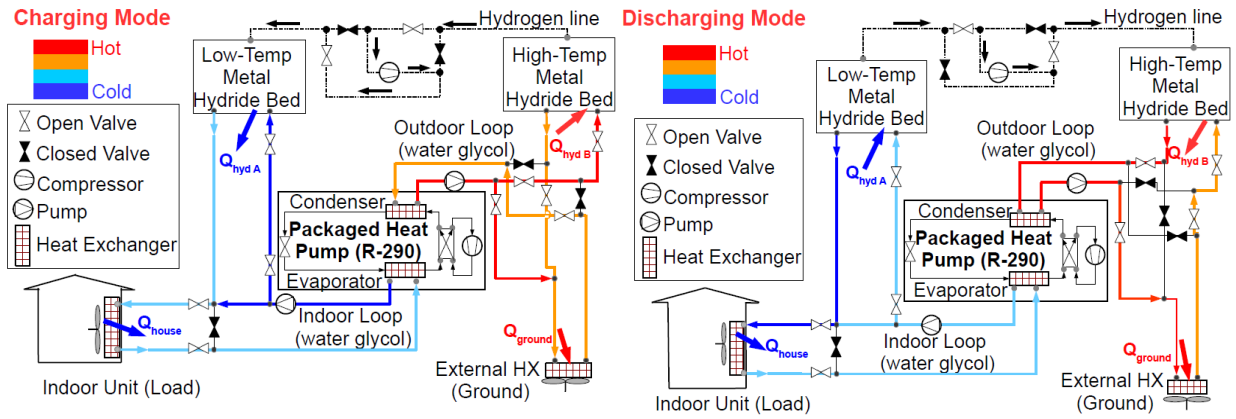

Figure 4-3. (a) Cooling system in charging mode. Flow is split off the outdoor loop to heat one hydride reactor; this, as well as the compressor if needed, drives the hydride to release hydrogen that flows to the other reactor, which absorbs the hydrogen and releases heat to the indoor loop. (b) Cooling system in discharge mode. Flow from the outdoor loop to the hydride reactor is now at a lower temperature. This, and the compressor if needed, results in flow now moving from the low-temperature reactor back to the high-temperature reactor. As the low-temperature reactor releases hydrogen, it absorbs heat from the indoor loop, cooling the water glycol before it goes to the house and thus reducing the load on the heat pump.

In addition to these components, there are the two metal hydride reactors which are connected to allow hydrogen to flow between them. A compressor on the hydrogen line can be used to drive hydrogen flow between these reactors, with valves configured such that it can drive flow in either direction. The reactors are charged and discharged by exchanging heat with the water glycol in the indoor and outdoor loops. Flow can be split off from either water glycol loop to exchange heat with either metal hydride reactor. The reactors are labelled low-temperature and high-temperature because the hydrides in them are chosen to have a relationship between

equilibrium pressure and temperature that will maximize how much flow will be temperature-driven. Thus, one reactor is at a lower temperature than the other. It should be noted that low-temperature and high-temperature are here used as relative terms: neither reactor will ever be colder than approximately -20°C or warmer than roughly 50°C.

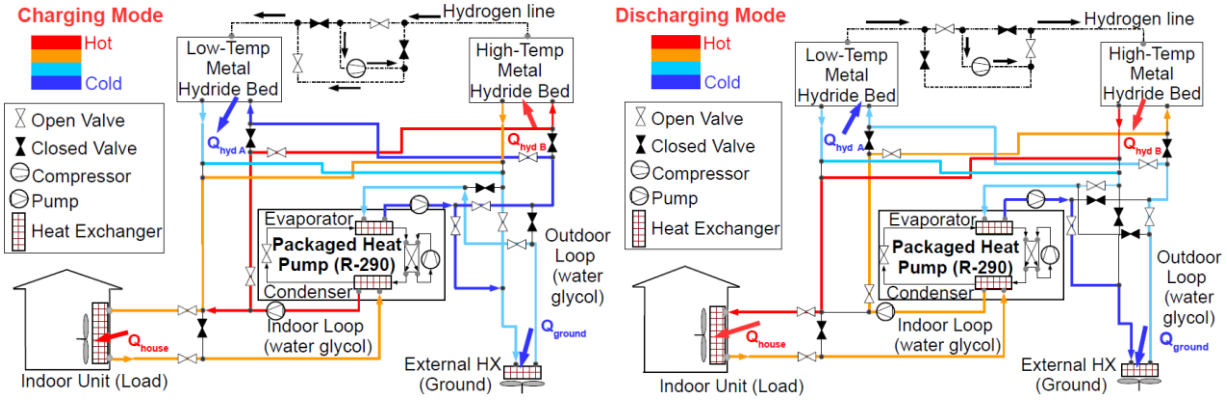

Figure 4-4. (a) Heating system in charging mode. Flow is diverted from the indoor loop to heat the high-temperature reactor; this, as well as the compressor if needed, drives the hydride to release hydrogen that flows to the low-temperature reactor, which absorbs the hydrogen and releases heat to the outdoor loop. (b) Heating system in discharge mode. Flow from the indoor loop to the high-temperature reactor is now at a lower temperature than in charging mode, and it is now heated by the high-temperature reactor, which thus delivers a portion of the heating load. This, and the compressor, if needed, drives hydrogen from the low-temperature reactor back to the high-temperature reactor. As the low-temperature reactor releases hydrogen, it absorbs heat from the outdoor loop.

Ultimately, the system operates in 6 modes: conventional heating and cooling mode with no interaction with the TES system, charging during heating or cooling, and discharging during heating or cooling.

The system operation in charging and discharging modes when cooling the house can be seen in Figure 4-3. In cooling mode, the evaporator in the heat pump provides the cooling load that will be delivered by the indoor loop, while the condenser heats the water glycol in the outdoor loop, which is restored to its original temperature by exchanging heat with the external heat exchanger. In charging mode, the outdoor loop heats the high-temperature reactor (metal hydride bed); this, as well as the compressor if necessary, drives a desorption reaction that releases hydrogen to flow to the low-temperature reactor, which absorbs the hydrogen and releases heat to the indoor loop. Then, in discharging mode, flow from the outdoor loop is diverted at a different

location (as seen in Figure 4-3, water glycol flows to the reactor from the heat pump when charging but from the external unit when discharging), where it is at a lower temperature, while the low-temperature reactor now desorbs hydrogen and absorbs heat from the indoor loop. The change in the temperature of the high-temperature reactor changes the equilibrium pressure, so that the hydrogen desorbed by the low-temperature reactor now flows back to the high-temperature reactor (with this flow driven by the compressor if the change in equilibrium pressure is insufficient), which absorbs it and releases heat to the outdoor loop. Since the low-temperature reactor transfers heat to the indoor loop when charging and absorbs heat from it when discharging, the metal hydride energy storage system can be used to shift a portion of the load from on-peak hours to off-peak.

As shown in Figure 4-4, the system is charged and discharged in heating mode in an analogous way as cooling mode, except for switching the connection of the water-glycol loop to the metal hydride reactors. In other words, the indoor loop heats the high-temperature reactor in charging mode and receives heat from it in discharging mode. As in cooling mode, the temperatures of the flow diverted from the outdoor and indoor loops and the compressor are used to drive the absorption and desorption reactions and the flow of hydrogen between the reactors. Compared to a conventional heat pump system, the heat pump has an increased heating load during charging and a decreased load during discharging enabling a load shift from on-peak to off-peak hours.

4.2 System Model

A diagram of the system model can be seen in Figure 4-5. This model consists of two main sub-models: one for the secondary (indoor and outdoor) loops and one of the metal hydride reactors (described in Chapter 3). External conditions are used to determine the load on the building (Section 4.2.1), which is then used as an input for the secondary loop model. The secondary loop model (Section 4.2.2) is solved iteratively to find a solution that satisfies the requirements for both the heat pump and the secondary loops, then uses a heat pump performance map (Section 4.2.3) to calculate the power required by the heat pump. Then, the calculated heat transfer rates, indoor and outdoor loop mass flow rates, and fluid inlet temperatures are used by the controller described in Section 3.3 to solve for the control inputs to the metal hydride reactors, and the state of the reactors calculated using the model described in Section 3.1. The target heat rates for the hydride reactors

are determined by the load-shifting control logic (Section 4.2.4), which determines when to charge and discharge the storage system. For a building with on-site solar PV, modified control logic is used for load-shifting (Section 4.2.5) and the solar power generation at each time step is calculated from weather conditions (Section 4.2.6).

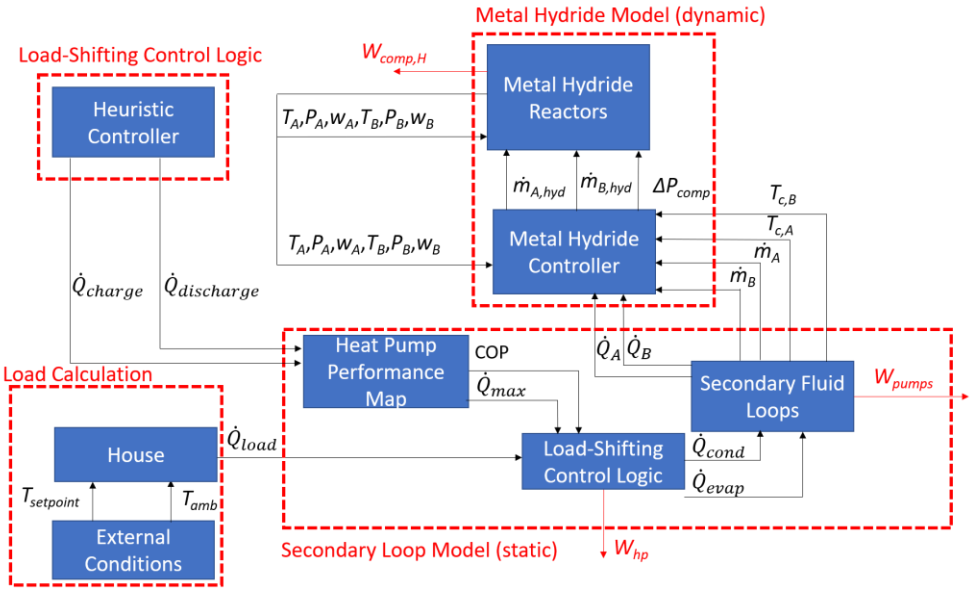

Figure 4-5. Diagram of the complete system model, showing the interaction between the static secondary loop model and the dynamic metal hydride model.

4.2.1 Load Calculation

For the residential model, the heating or cooling load at the house is calculated using a simple model that employs a quasi-steady-state assumption. This model calculates the load using an overall *UA*-value determined assuming that a cooling load of 3 tons (10.55 kW) is needed to maintain a setpoint temperature of 72°F (22.2°C) at an outdoor temperature of T_∞ = 95°F (35°C) from

$$\dot{Q}_{design\ load,house} = UA\left(T_{setpoint} - T_\infty + \theta_b\right) + \dot{g}. \quad (42)$$

In this equation, $\dot{g}$ is the internal gain, $T_{setpoint}$ is the desired temperature inside the home, and θ_b is a correction factor for heating by solar radiation. It is further assumed that this design load occurs when solar irradiation is at its maximum, and the internal gain is the average of its value across the entire time period used in the study (e.g., a year).

In estimating the overall *UA* using Eq. 42, the design solar temperature effect, θ_b, is

assumed to be 8.2°F (4.6°C) based on the ASHRAE recommendations for an unshaded wall [105]; a real house will have higher irradiation through the windows and lower irradiation on the unshaded walls, so this value is chosen as an intermediate value. The internal gain, $\dot{g}$, is assumed to be equal to the electric power consumed by the house excluding the HVAC system. Data for electric power consumption is taken from data for typical residential hourly electric loads from the Office of Energy Efficiency & Renewable Energy [106]; for estimating the value of *UA*, the average value for the time period studied is used. The heat gain rate due to solar radiation at the conditions used to calculate the design load is calculated with

$$\dot{Q}_{solar,max} = \dot{Q}_{design\ load,house} - \left[UA\left(T_{setpoint} - T_{\infty}\right) + \dot{g}\right] = UA \cdot \theta_b. \tag{43}$$

A simple model of solar heating effects is used in which the maximum solar heating effect is linearly scaled at each time step, according to the ratio of the horizontal irradiance for the time step to the maximum value for the year. This is given by

$$\dot{Q}_{solar} = \frac{GHI}{GHI_{max}} \dot{Q}_{solar,max}, \tag{44}$$

where *GHI* is the average global horizontal irradiance for the time step, and GHI_{max} is the maximum value of GHI in the weather data for that location.

The house heating or cooling load for any time step, $\dot{Q}_{load,house}$, is calculated using Eq. 45, with the values of $T_{setpoint}$, $\dot{g}$, and $\dot{Q}_{solar}$ determined using location-specific data:

$$\dot{Q}_{load,house} = UA\left(T_{setpoint} - T_{\infty}\right) + \dot{g} + \dot{Q}_{solar}. \tag{45}$$

For cooling, the setpoint is set to 72°F at all times except between 9 AM and 5 PM on weekdays, when it is 76°F. During heating, it is set to 68°F, and lowered to 64°F from 9 AM to 5 PM on weekdays. It is assumed that the system is only turned on for outdoor temperatures either 5°F greater or 15°F less than the setpoint.

For the commercial model, the heating and cooling loads, as well as the electricity demand from sources other than the HVAC system, are generated using an EnergyPlus model of a 3-story medium office building developed by the Department of Energy based on ASHRAE 90.1 standards [107]. This model is run with an input weather file for the location studied and the resulting cooling and heating loads on all the cooling and heating coils in the system are summed at each hour to determine the total load on the building at each hour for the year.

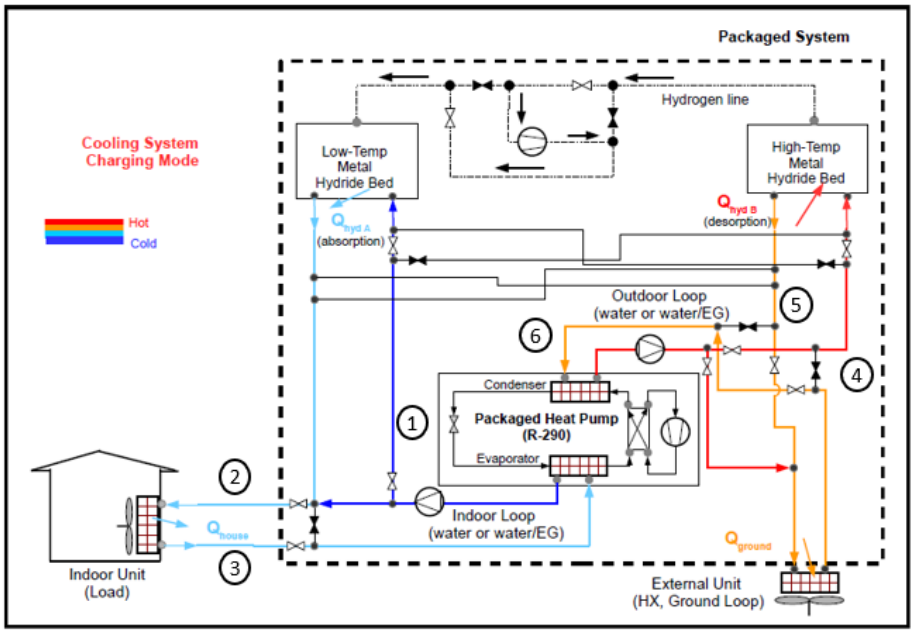

Figure 4-6. Diagram of the system in cooling charge mode, with the different points used in the secondary loops calculations labelled.

4.2.2 Secondary Loop Model

In each secondary loop, the temperature of the water-glycol mixture changes in the following locations: (1) where it exchanges heat with the heat pump, (2) where it exchanges heat with a hydride reactor, and (3) where it exchanges heat with either the indoor heat exchanger or the external heat exchanger. Since the fluid in each loop is heated or cooled at three different points, there are six different points where the temperature of the fluid must be solved for, labelled (1)-(6) in Figure 4-6. The change in the water-glycol temperature as it flows through each pump is neglected, but the change in pressure is estimated in order to calculate the pumping work required by the system.

Thus, calculating the thermodynamic state of the system requires solving for 6 temperatures, 6 heat transfer rates (one at each component), and 4 mass flow rates (the flow rate in the indoor and outdoor loops and the flow rate diverted to a reactor from each loop). The heat transfer rate from the indoor heat exchanger to the indoor loop, $\dot{Q}_{house}$, is known for given outdoor and setpoint temperatures. Load-shifting strategies (described in Sections 4.2.4 and 4.2.5) specify the ratio between the heat transfer rate from the hydride bed to the indoor loop, $\dot{Q}_{hyd,indoor}$, and the heat transfer rate from the heat pump to the inner loop, $\dot{Q}_{hp,indoor}$. Given the supply temperatures to

the heat pump, the COP and capacity of the heat pump can be calculated from the heat pump maps for an Emerson scroll compressor described in Section 4.2.3. Thus, the heat transfer rate from the heat pump to the outside loop, $\dot{Q}_{hp,outdoor}$, can be determined from the COP. Furthermore, to better control the hydride reactions, the ratio between the heat transfer rates in the two hydride reactors is set to a constant, k_r. As discussed in Section 3.4.1, the value for this ratio should be one that allows the reactors to operate predominantly in a near-equilibrium state, in order to avoid saturation of the control variables used to maintain these heat rates (discussed in Section 2.7). The values for k_r that best achieve this are k_r = 0.85 in charging mode and k_r = 0.75 in discharging mode.

The equations for heat transfer rates, when combined with energy balances performed on each of the 6 components, results in 10 equations. Nine of these equations are summarized in Eqs. 46-51 (the tenth is $\dot{Q}_{hp,in}$ being set by the load-shifting control logic shown in Figure 4-13):

$$\dot{Q}_{hp,indoor} = \dot{m}_{indoor} c_{wg} (T_1 - T_3) \tag{46}$$

$$\dot{Q}_{hyd,indoor} = \dot{m}_{indoor} c_{wg} (T_2 - T_1) \tag{47}$$

$$\dot{Q}_{house} = \dot{m}_{wg,indoor} c_{wg} (T_3 - T_2) = \begin{cases} -\dot{Q}_{load,house}, & cooling \\ -\left(\dot{Q}_{load,house} - \dot{Q}_{elec}\right), & heating \end{cases} \tag{48}$$

$$\dot{Q}_{hp,outdoor} = \dot{m}_{outdoor} c_{wg} (T_4 - T_6) = \begin{cases} 1 + \frac{1}{COP} \dot{Q}_{hp,indoor}, cooling \\ 1 - \frac{1}{COP} \dot{Q}_{hp,indoor}, heating \end{cases} \tag{49}$$

$$\dot{Q}_{hyd,outdoor} = \dot{m}_{outdoor} c_{wg} (T_5 - T_4) = -k_r \dot{Q}_{hyd,indoor} \tag{50}$$

$$\dot{Q}_{ground} = \dot{m}_{outdoor} c_{wg} (T_6 - T_5). \tag{51}$$

In these equations, $\dot{m}_{wg,indoor}$ is the indoor loop flow rate, $\dot{m}_{wg,outdoor}$ the outdoor loop flow rate, c_{wg} is the specific heat of the water glycol, T_n the temperature of the water glycol at location n shown in Figure 4-6 for n = 1 to 6, $\dot{Q}_{hp,indoor}$, $\dot{Q}_{hyd,indoor}$, and $\dot{Q}_{house}$, are the heat transfer rates to the water glycol in the indoor loop from the heat pump, hydride reactor, and indoor heat exchanger, respectively, and $\dot{Q}_{hp,outdoor}$, $\dot{Q}_{hyd,outdoor}$, and $\dot{Q}_{ground}$ are the heat transfer rates to the water glycol in the outdoor loop from the heat pump, hydride reactor, and external heat exchanger, respectively. $\dot{Q}_{elec}$ is the heat transfer rate to the house from auxiliary electric heating, which is used if the heating load at the house is greater than what can be met by the heat pump. The equations above are used for charging mode; for discharging mode, Eqs. 46-49 are still used, but since flow in the outdoor

loop now moves from the external unit to the hydride reactor rather than the other way around, the last two equations are

$$\dot{Q}_{ground} = \dot{m}_{wg,outdoor} c_{wg} (T_5 - T_4) \text{ and} \tag{52}$$

$$\dot{Q}_{hyd,outdoor} = \dot{m}_{wg,outdoor} c_{wg} (T_6 - T_5) = -k_r \dot{Q}_{hyd,indoor} \, . \tag{53}$$

Since the controller for the hydride reactor determines the mass flow rate of water glycol, $\dot{m}_{wg,r}$, sent to each reactor, there are 12 equations and 16 unknowns. Therefore, four variables must be specified to solve the system of equations. To avoid physically unrealistic operating temperatures, the outlet temperature at the house (T_3) is specified based on the indoor temperature, to ensure that flow leaves the house colder than room temperature in cooling mode and hotter than room temperature in heating mode. Similarly, the outlet temperature at the external heat exchanger (T_6 in charge mode, T_5 in discharge) is defined based on the ambient temperature, to ensure that flow leaves the external heat exchanger at a temperature above ambient temperature in cooling mode and below ambient temperature in heating mode.

In addition to these temperatures, the inlet temperatures of the hydride reactors are also defined in each case. Within the constraints imposed by the other defined temperature values, the values used for the hydride reactor inlet temperatures are selected based on the temperature-pressure relations, so that the resulting operating pressures will allow for temperature-driven flow in most cases while staying within the desired limits of hydrogen pressure. Since water glycol flows from the external heat exchanger to the hydride reactor in the outdoor loop during discharge mode, the inlet of the outdoor hydride reactor and the outlet of the external heat exchanger are both position 5. Thus, temperature must be defined in another position as well, so that the outlet temperature of the hydride reactor is also defined. This temperature is defined because it is also the inlet temperature to the heat pump, and thus used in calculating COP. Thus, T_1, T_3, and T_6 are always specified while T_4 is defined only if charging and T_5 only if discharging. The algorithm used to determine the values which are fixed for these temperatures is described below.

At each time step, the pump work is calculated from the water-glycol mass flow rate,

$$\dot{W}_{pumps} = \frac{\dot{m}_{wg,indoor}}{\rho_{wg}} \Delta P_{wg,indoor} + \frac{\dot{m}_{wg,outdoor}}{\rho_{wg}} \Delta P_{wg,outdoor} \tag{54}$$

$$\Delta P_{wg} = K_{loss,wg\ loop} \frac{\dot{m}_{wg}{}^2}{2 \rho_{wg} A_{c,wg\ loop}}. \tag{55}$$

The heat pump work is calculated using the COP and the heat transfer from the heat pump,

$$\dot{W}_{hp} = \frac{|\dot{Q}_{hp,indoor}|}{COP}. \quad (56)$$

The hydrogen compressor work is calculated inside the dynamic model using Eq. 19, as described in Section 3.1. Electric heating work is calculated from the electric heating load determined by the control logic explained in Section 4.2.4.

$$\dot{W}_{elec} = \dot{Q}_{elec}. \quad (57)$$

These work terms and an estimated value for typical non-HVAC work at a given time, are used to calculate the cost of electricity at each time step:

$$C_{tot} = C_{hour}\left(\left(\dot{W}_{hp} + \dot{W}_{pumps} + \dot{W}_{elec} + \dot{W}_{non-HVAC}\right)\Delta t + \int_0^{\Delta t} \dot{W}_{comp}\right). \quad (58)$$

In this equation, C_{tot} is the total operating cost for the time step and C_{hour} the electricity rate at that time of the day.

Secondary Loop Temperature Algorithm

The solution algorithm used to set the temperatures, mass flow rates, and heat transfer rates for cooling charge mode is shown in Figure 4-7. This includes control logic to find appropriate values for the water-glycol temperatures that do not violate any physical constraints. One particularly significant constraint is that the outlet temperature of the hydride reactor should not require the reactor to have a higher effectiveness than would be achieved if all of the water-glycol flow were diverted to the reactor. If initial heuristic values for temperature do not achieve this, alternate values are defined using target effectiveness values, $\varepsilon_{r,indoor,tar}$ and $\varepsilon_{r,outdoor,tar}$, that are lower than the maximum effectiveness, such that for charge mode (where T_4 is the reactor inlet in the outdoor loop):

$$T_2 = T_1 + \varepsilon_{r,indoor,tar}(T_{r,indoor} - T_1) \text{ and} \quad (59).$$

$$T_5 = T_4 + \varepsilon_{r,outdoor,tar}(T_{r,outdoor} - T_4)\,. \quad (60).$$

Since these target effectiveness values are defined to be less than those that the reactor will achieve if all flow is diverted to the reactor, it will be possible for the controller used in the dynamic model of the hydride reactors to achieve these outlet temperatures.

Similar control logic is used for each operating mode (cooling charge, cooling discharge, heating charge, and heating discharge). Different heuristic values are used for the secondary loop

operating temperatures for the different modes, due to the different constraints imposed by the house and hydride reactor temperatures. Furthermore, the hydride reactor is assumed to be at different operating temperatures in charge and discharge modes in defining these heuristic values. To keep the actual operating temperatures close to these assumed values, the reactors are heated or cooled by the secondary loops without allowing for hydrogen flow between them (which would sustain a reaction) if the reactor operating temperatures go outside of the acceptable range. Since the ratio of heat rates between the reactors is selected to minimize the change in temperature, such heating and cooling is generally done only between charging and discharging the system. The desired operating temperatures for the hydride reactors are heuristic values and not optimal ones and are selected primarily to reduce compressor work by allowing for more temperature-driven reactions. Optimization of the storage temperature, which is considered for a more abstract model in Chapter 6, is not considered for this model.

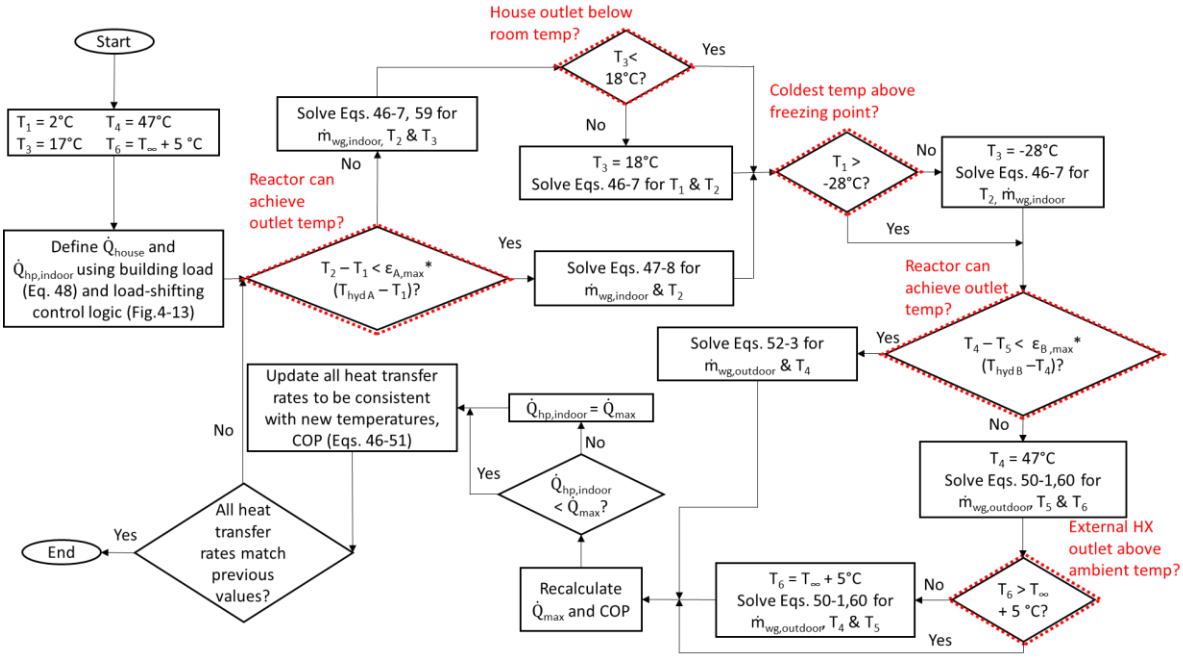

Figure 4-7. Calculation procedure used to find the temperatures, heat transfer rates, and mass flow rates for cooling charge mode. This control logic is used to find a set of operating conditions at each time step that satisfies Eqs. 46-53 while also ensuring that there are no physically unrealistic operating conditions (such as operating temperatures below the freezing point of water glycol or flow through a heat exchanger being heated above or cooled below the temperature of the other side of the heat exchanger).

In this way, the temperatures and heat transfer rates of the system are calculated at every time step. A time step of 15 minutes is used for these calculations, since this is the period also commonly used for calculating demand charges.

4.2.3 Heat Pump Model

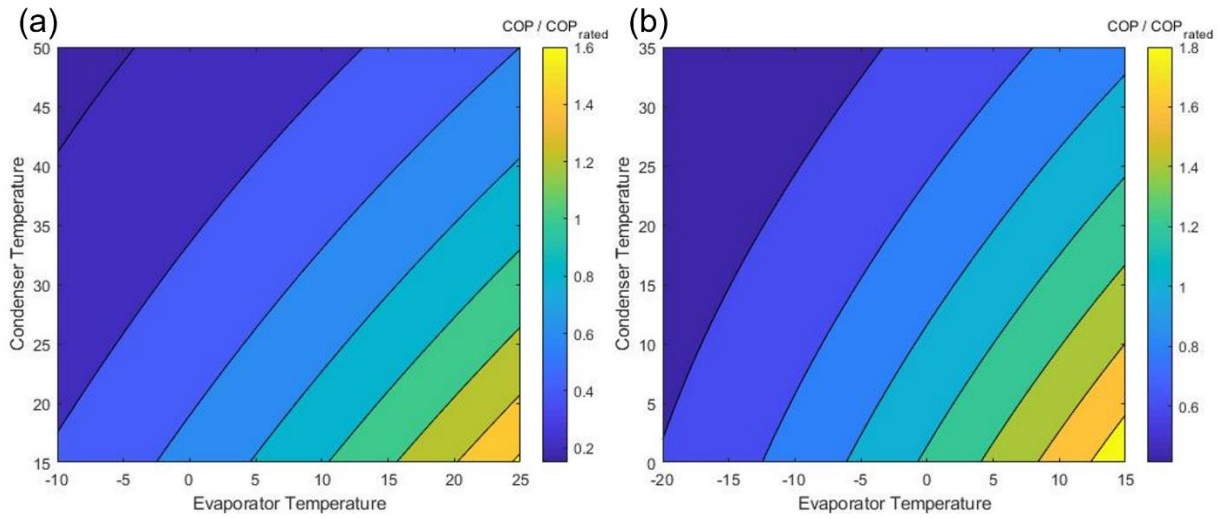

Figure 4-8. Normalized COP (COP/COP_{rated}) for the residential heat pump as a function of water glycol inlet temperature in the condenser and evaporator for (a) cooling and (b) heating

A model for the COP of the heat pump is needed to compute its power input requirement for a specified cooling or heating rate (i.e., heat pump load). In addition, a model for heat pump cooling or heating capacity ($\dot{Q}_{max}$) is needed in order to ensure that the load that is assigned to the heat pump does not exceed its capacity. Both the COP and the capacity are computed using quasi-steady-state performance maps defined in terms of the water-glycol supply temperatures to the evaporator and condenser.

The COP and cooling/heating capacity are normalized to rated values (COP_{rated} and $\dot{Q}_{max,rated}$) so that the rated value can be modified to represent a change in the size or performance of the heat pump. The normalized COP and capacity, defined as functions of the supply temperatures as equations for capacity and work for an Emerson ZH09KCU-TFM compressor as part of a model of a basic vapor-compression cycle (compressor, condenser, expansion valve, and evaporator). In addition to using the compressor maps to solve for the enthalpy change across the compressor, this model assumes superheat of 11°C and subcooling of 3°C.

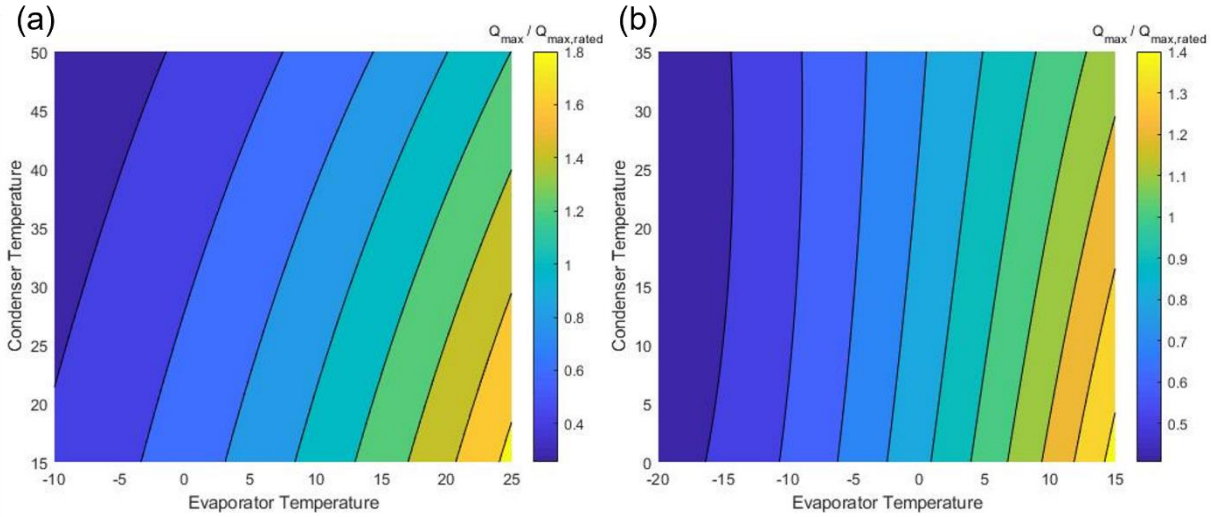

Figure 4-9. Normalized maximum heat pump capacity ($Q_{max}/Q_{max,\ rated}$) for the residential heat pump as a function of water glycol inlet temperature in the condenser and evaporator for (a) cooling and (b) heating

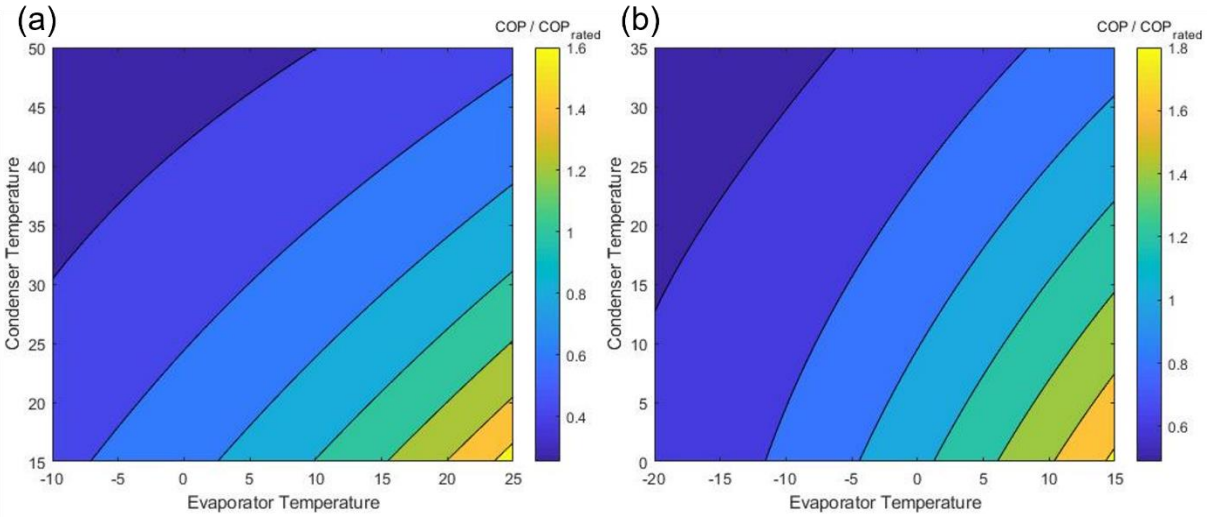

Figure 4-10. Normalized COP (COP/COP_{rated}) for the commercial heat pump as a function of water glycol inlet temperature in the condenser and evaporator for (a) cooling and (b) heating

The model also assumes values for the pressure drop and pinch point temperature for the evaporator and condenser, shown in Figure 4-8 and Figure 4-9, are calculated using the 10-factor equations for capacity and work for a Emerson ZH09KCU-TFM compressor as part of a model of a basic vapor-compression cycle (compressor, condenser, expansion valve, and evaporator). In addition to using the compressor maps to solve for the enthalpy change across the compressor, this model assumes superheat of 11°C and subcooling of 3°C. The model also assumes values for the

pressure drop and pinch point temperature for the evaporator and condenser.

Due to the much larger loads handled by the commercial system, a different compressor model is used for the commercial system. The compressor model used here is a Bitzer 6FEP-44P semi-hermetic reciprocating compressor, and the normalized capacity and COP are calculated using the same method as is used for the residential case. The capacity of this compressor is significantly less than the maximum load for the commercial building, but it is assumed that the commercial building uses multiple compressors in parallel to handle this. The normalized COP and capacity for the commercial case as functions of the supply temperatures, are shown in Figure 4-10 and Figure 4-11.

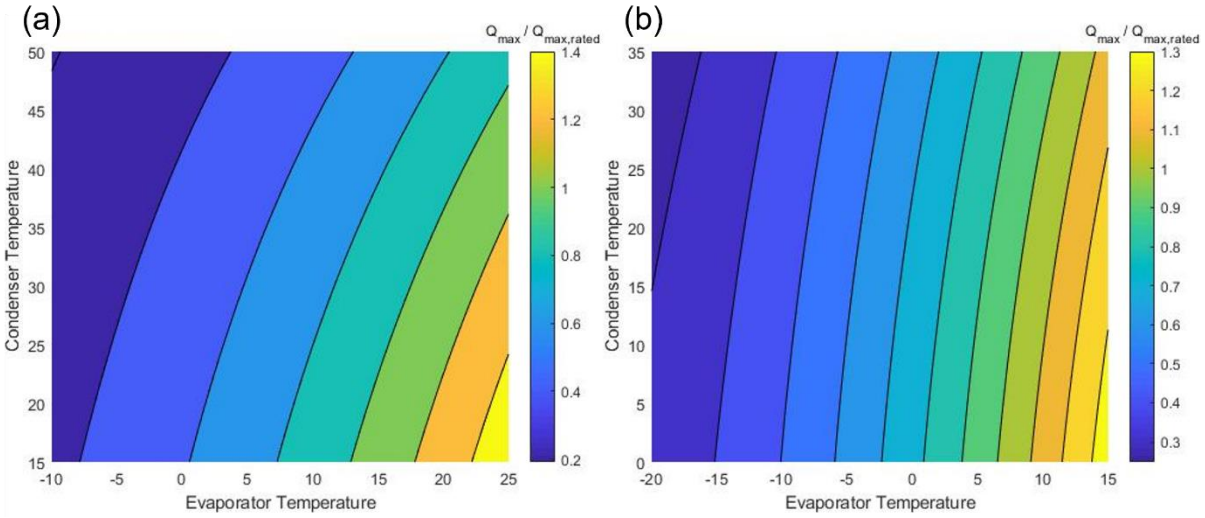

Figure 4-11. Normalized maximum heat pump capacity ($Q_{max}/Q_{max,\ rated}$) for the commercial heat pump as a function of water glycol inlet temperature in the condenser and evaporator for (a) cooling and (b) heating

4.2.4 Load-Shifting Control Logic

Here, we develop a heuristic load-limiting storage control strategy to determine the distribution of load between the heat pump and the reactors. Perfect knowledge of future building loads for each day is assumed for the purpose of assessing system performance. For the load-limiting control strategy, the system attempts to discharge the entire storage system during the on-peak period and fully charges it in the off-peak period. This strategy is similar to that described by Tam *et al*. [11], but differs from it in charge mode by not running the heat pump at full capacity

until the system is fully charged. Instead, the system uses a constant heat pump load for charging that is calculated as described in the next paragraph. The heat pump is not run at full capacity when charging in order to reduce the change in reactor temperature when charging begins. This is done in order to prevent the reactor temperature from becoming too close to the water-glycol temperature, thereby increasing the required pump work.

Figure 4-12 illustrates the calculation of the heat pump loads for one day. The charging load is calculated by increasing the average off-peak heat pump load by the load needed to fully charge the storage system over the full period. The discharging load is calculated by reducing the average on-peak heat pump load by the load provided by the storage system if fully discharged. Thus, at the beginning of each cycle (defined as a 24-hour period), the total building loads for the off-peak and on-peak periods, $\dot{Q}_{charge}$ and $\dot{Q}_{discharge}$ (respectively), are calculated using the following equations:

$$\dot{Q}_{charge} = \frac{\sum_{off} \dot{Q}_{load,house} + E_{stor,hyd}}{\Delta t_{off}} \tag{61}$$

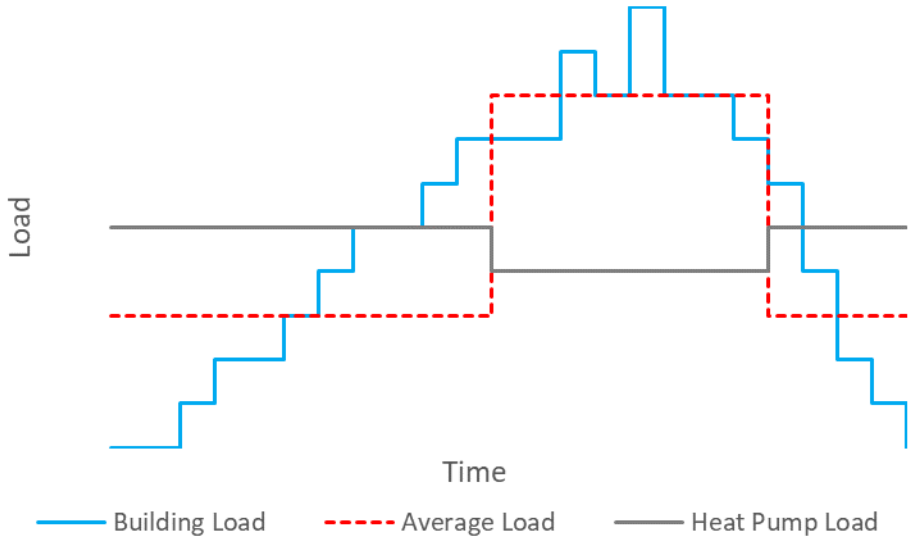

Figure 4-12. Heat pump loads for charging and discharging. The charging load is calculated by increasing the average off-peak heat pump load by the load needed to fully charge the storage system over the full period. The discharging load is calculated by reducing the average on-peak heat pump load by the load provided by the storage system if fully discharged.

$$\dot{Q}_{discharge} = \frac{\sum_{on} \dot{Q}_{load,house} - E_{stor,hyd}}{\Delta t_{on}}. \quad (62)$$

In these equations, $E_{stor,hyd}$ is difference in stored energy between a fully charged and a fully discharged storage system. For the purposes of this control logic, "fully charged" and "fully discharged" are defined as 90% and 10% of the maximum weight fraction that can be stored in the metal hydride, respectively. These values are used due to the higher compressor costs required as the weight fraction approaches its maximum or minimum value.

The method just described is used for the case where there is one on-peak period during each day (except for weekends). However, in some existing rate structures, there are two on-peak periods in a day during the winter (one in the morning and one in the evening). Since it is not feasible to fully charge the system in between these periods due to the high loads that occur during the day, the system still treats a full day as a cycle when operating under these rates. Thus, for cooling mode, the system is fully charged during the off-peak hours at night, and fully discharged over the course of the two on-peak periods during the day, while running conventionally in between these periods (for heating mode, it is charged in the afternoon and runs conventionally during the night, since heating loads are lower during the day).

Once the charging and discharging loads for the day have been determined, the model determines the operating mode of the system at each time step using the control logic shown in Figure 4-13. During on-peak hours, the heat pump provides the load calculated for discharging, with the storage system discharged to make up the difference between this and the building load. However, if the building load is less than the heat pump load for discharging, the system will not be discharged; instead, the heat pump will meet the building load without any heat transfer to and from the storage system (conventional operation). During off-peak hours, the storage system is discharged in cooling mode if the building load exceeds the capacity of the heat pump. In this case, the heat pump load is equal to its capacity and the storage system makes up the difference. If this condition occurs immediately before the on-peak period, the on-peak heat pump load is adjusted to make up for the difference between available and full storage capacity.

For heating mode (even in conventional systems), electric heating provides heating when the building heating load is greater than what can be provided by the heat pump. In this control

strategy, if the calculated heat pump load for charging or discharging (or the load at the building, if the system is running conventionally) exceeds the capacity of the heat pump, the heat pump load is set to the capacity of the heat pump and the difference between these values is provided by electric heating throughout the time period. Auxiliary heating is considered to be a part of the indoor heat exchanger and thus to have no effect on temperatures in the indoor loop.

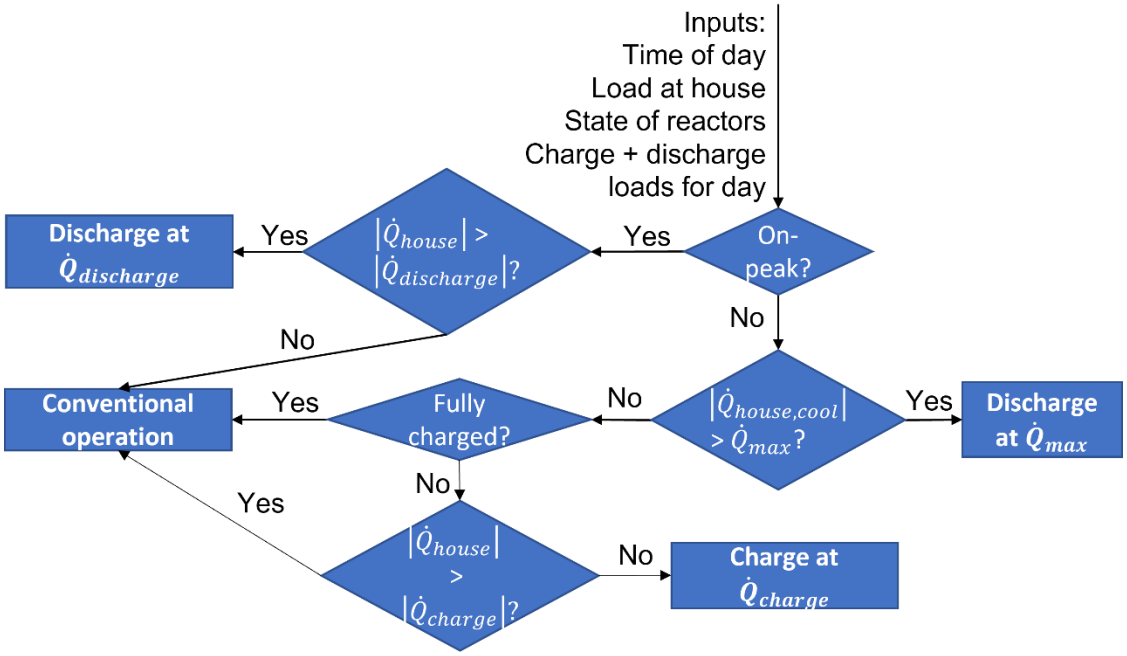

Figure 4-13. Flowchart showing the control logic for whether the energy storage system is charged, discharged, or not used at each time step.

During off-peak hours, the system is charged with the heat pump providing the calculated load for charging, with any load in excess of the building load being used to charge the storage system. However, if the storage system is already fully charged or if the building load is greater than the heat pump load for charging, the system runs in conventional operation instead. While the heat pump load for charging is calculated so the system will charge over the full off-peak period, in practice, the system will often be fully charged before the end of the off-peak period. This happens primarily for two reasons. First, the heat pump load is calculated assuming that the system runs at this load throughout the off-peak period. However, to do this, the system would have to discharge if there is a building load greater than the heat pump load for charging, but the system will instead run conventionally in that case. Since the system does not discharge at these times, it does not have to be charged to make up for any such discharging. Because of this, the system will

charge in less than the full off-peak period. The second reason is that if the system enters a charging period partially or fully charged, due to either a discharge period where the full storage capacity is not required or due to previous charging on the weekend (which has no on-peak periods), it will charge in less than the full off-peak period because the heat pump load for charging is calculated assuming the system needs to be fully charged.

4.2.5 Modified Load-Shifting Control Logic with On-Site Solar PV

The load-shifting control logic for the case of a building with on-site solar PV follows a similar logic to that described in Section 4.2.4. The heat pump loads for charging and discharging are calculated in the same way as described there. The calculated loads are used for charging in off-peak periods and discharging in on-peak periods, and the system runs in conventional operating mode (without using the storage system) if fully charged during off-peak hours. As before, the system may also be discharged during off-peak hours if the load required by the house is greater than what the heat pump can provide, but in heating mode, auxiliary electric heating is used instead to meet all heating loads greater than what can be met by the heat pump.

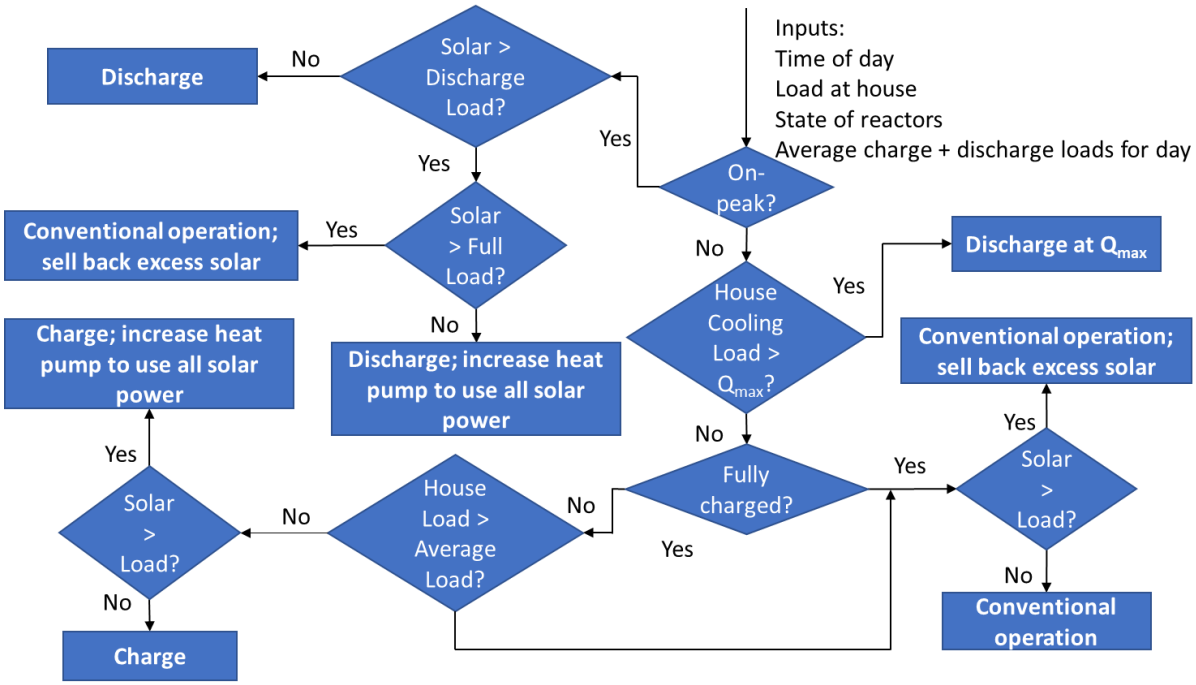

Figure 4-14. Diagram of the control logic used to modify the load at the heat pump when on-site solar PV is available.

However, since the system is trying to make maximum use of solar generation, the heat pump loads are sometimes modified based on the solar power available at the time. The control logic for this is shown in Figure 4-14. For discharging during on-peak periods, if the available solar power is greater than the power required to run the system at the average load calculated for the heat pump, then some of the load will be shifted back from the storage system to the heat pump so that all available solar power is used. If shifting all of the load from the storage system to the heat pump still results in excess solar power, then the system will run in conventional mode without using the storage system. Similarly, if there is excess solar power when the system is charging, then the load on the heat pump (and thus the load sent to charge the storage system) will be increased to use all available solar power (or until the heat pump is operating at full capacity). Thus, excess solar power is only sold back to the grid during on-peak hours if there is excess power even when operating conventionally. During off-peak hours, it is only sold back if there is excess power when the heat pump is operating at capacity or if the system is fully charged.

4.2.6 Solar Power Generation

When using this model to study a building with on-site solar PV, it is necessary to calculate the solar power generation from the solar radiation data for a particular time. The solar power generation, $\dot{W}_{solar}$, is calculated using the equation

$$\dot{W}_{solar} = \eta_{PV} A_{PV} I_T. \tag{63}$$

The efficiency of each solar panel, η_{PV}, is assumed to be 20% based on values for existing models, and the surface area, A_{PV}, of the solar array is determined as described in Section 5.1.1. The incident radiation on the solar panel, I_β, is calculated using the following equation [108].

$$I_\beta = \left(R_b + \frac{1-\cos\beta}{2}\rho_g\right) GHI + \left(\frac{1+\cos\beta}{2} - R_b\right) DHI. \tag{64}$$

Incident radiation is calculated in terms of the global horizontal incidence, GHI (the solar radiation incident on a horizontal surface), and the diffuse horizontal incidence, DHI. The term for GHI also includes a term for radiation reflected from the ground, calculated in terms of the reflectance of the ground, ρ_g. The slope of the solar panel, β, is 30°.

The ratio of beam radiation on the surface to horizontal radiation, R_b, is found using the following equations [109]:

$$R_b = \frac{\cos\theta}{\cos\theta_z} \tag{65}$$

$$\cos\theta = \sin\delta\sin\phi\cos\beta - \sin\delta\cos\phi\sin\beta\cos\gamma + \cos\delta\cos\phi\sin\beta\cos\omega + \cos\delta\sin\phi\sin\beta\cos\gamma\cos\omega + \cos\delta\sin\phi\sin\gamma\sin\omega \text{ , and} \tag{66}$$

$$GHI = DHI + DNI\cos\theta_z. \tag{67}$$

In these equations, DNI is the direct normal irradiation (the solar radiation on a surface oriented perpendicular to the beam), available from weather data, θ is the angle of incidence of the solar panel (angle between the normal of the panel surface and the beam radiation), θ_z is the zenith angle (angle of incidence of a horizontal surface), δ is the declination angle (angular position of the sun relative to the equator at noon), φ is the latitude of the location of the panel, γ is the surface azimuth angle of the panel (the direction the panel is facing), and ω is the hour angle (angular displacement of the sun due to the Earth's rotation) [109]. The solar panels for this model are south-facing and at a slope of 30°, and a value of 0.2 is assumed for the ground reflectance. Solar radiation data for each hour is used to calculate the resulting power generation for that hour.

This model for calculating solar power generation is used to incorporate solar PV into the static model of a building HVAC system. This model uses the building load calculations described in Section 4.2.1 and the heat pump performance maps given in Section 4.2.3 to solve for all heat transfer rates and water glycol temperatures in the system as described in Section 4.2.2. The basic model uses the load-shifting control logic in Section 4.2.4, while the model with solar PV uses the control logic in Section 4.2.5 and the model of solar power generation described in this section. This model, combined with the dynamic model and MPC of a two-reactor hydride system described in Chapter 3, is used to analyze the performance of this system compared to an HVAC system without energy storage in Chapter 5.

5. COST COMPARISON AND PAYBACK PERIOD FOR METAL HYDRIDE ENERGY STORAGE[4]

The model of a building HVAC system with metal hydride energy storage described in Chapters 3 and 4 is used first to analyze the performance of such a system over the course of a week and then to calculate the cost savings and payback periods for a full year of operation. This system is sized and its initial cost calculated in Section 5.1. The performance of the system in a residential building is analyzed in Section 5.2. The residential building is also analyzed with the addition of on-site solar generation in Section 5.3. The main results seen for residential TES using metal hydrides are discussed in Section 5.4. Finally, metal hydride TES is examined for a commercial building to see if the trends seen for residential storage are still applicable there in Section 5.5.

5.1 Initial Cost Calculations

To determine the operating costs and payback period of a metal hydride TES system, the system is first sized and the initial cost determined. This is done for a residential building in Section 5.1.1 and for a commercial building in Section 5.1.2.

5.1.1 Initial Costs for a Residential Building

Component Costs

The initial cost of the conventional system is the sum of the costs of the heat pump and the auxiliary electric heating system. For the energy storage system, the initial cost also includes the costs of the secondary loops with pumps and internal and external air-handling units, metal hydride reactors, and the compressor for pumping hydrogen. For the heat pump, the cost is estimated as a function of the rated capacity and SEER, based on a correlation developed by the Energy Efficiency and Renewable Energy Office [110]:

[4] Portions of this chapter are taken from the papers Krane et al. 2021 (2) [125] and Krane et al. 2022 [126].

$$C_{hp,initial} = 1.91 * 10^3 - 41.4SEER_{rated} + 7.48SEER_{rated}{}^2 + 589Q_{rated} - 16.4Q_{rated}{}^2. \quad (68)$$

An estimated cost of $10/kW capacity is determined for the auxiliary electric heating by examining the prices and maximum capacities of commercially-available units.

The most expensive component in the energy storage system is the metal hydride reactors. The reactor cost is determined by estimating the material costs for the hydrides, since this is much higher than the installation or material costs for the heat exchanger. Based on private correspondence with a supplier, a price of $20/kg is estimated for $LaNi_5$, but similar information was not available for $MmNi_{4.5}Cr_{0.5}$, which is not currently in use in large quantities. Comparing raw material prices for lanthanum and mischmetal [111] indicated that this material would likely be comparably priced to $LaNi_5$ if it were as commonly used. Therefore, a price of $24/kg is used for this material, as an approximation of the potential bulk price should the material become more commonly used. Both of these costs are reduced by 25% to account for the gains from recycling them at the end of their life cycle, so the actual values used are $15/kg for $LaNi_5$, and $18/kg for $MmNi_{4.5}Cr_{0.5}$.

The total cost of piping for an indoor secondary loop, including pump and air-handling unit, was estimated by Tam e*t al.* to be $1,301 [24]. Based on a cost breakdown for a secondary-loop system, the cost of the outdoor secondary loop, where the indoor air-handling system is replaced with an outdoor heat exchanger, is estimated to be $1,050. Since hydrogen compressors are usually used at much larger pressure ratios than the 10-bar limit imposed in this case, the cost of the compressor is estimated by comparing prices for air compressors with the appropriate operating pressures, resulting in an estimated cost of $200.

Sizing for Elizabeth City, NC

The primary location studied for the residential case is Elizabeth City, NC. We selected a city in the American South as the object of this study because this is the only region in the United States where electric heating, such as is used in our system, is more commonly used than gas heating [112]. For this study, the conventional system to which the system with energy storage is compared uses a SEER-17.5 heat pump with a rated maximum cooling capacity of 3 tons. This heat pump is sized to be able to meet the maximum cooling load for the year in this location. For

the energy storage system, the heat pump is downsized to a rated capacity of 2.5 tons, since this system can use energy storage to reduce the peak cooling load required for the heat pump. **The energy storage system is sized to be capable of storing enough energy to fill in the difference between load and heat pump capacity on the day with the highest cooling loads whenever the load is above the capacity of the heat pump**. The reactors are sized so that the low-temperature reactor can provide the load in cooling mode and the high-temperature reactor matches the storage capacity of the low-temperature reactor. Thus, this system requires one reactor with 470 kg $MmNi_{4.5}Cr_{0.5}$ and the other with 412 kg $LaNi_5$.

Table 5-1. Initial costs, by component, of the conventional system and the system with energy storage (both with and without downsizing the heat pump)

System	Initial Cost					
	Heat Pump	**Electric Heating**	**Hydrogen Compressor**	**Secondary Loops**	**Metal Hydrides**	**Total**
Conventional	$5096	$100	-	-	-	$5196
Storage w/ downsized heat pump	$4864	$110	$200	$2351	$14,640	$22,147
Storage w/out downsized heat pump	$5096	$100	$200	$2351	$14,640	$22,387

Using the prices and sizing just described, we can compare the initial cost of 3 systems: 1) conventional system without energy storage; 2) system with energy storage and a downsized heat pump; and 3) system with energy storage and without a downsized heat pump. The system with energy storage is studied both with and without a downsized heat pump to see whether the reduced initial cost from downsizing the heat pump is worth the increased operating cost from a greater reliance on auxiliary heating during the winter if the heat pump has a lower capacity. The initial costs of these systems can be seen in Table 5-1. These systems are compared to determine the annual change in operating costs for each of the systems that include energy storage. The payback period of the energy storage system is calculated from the initial and operating costs as

$$payback\ period = \frac{C_{initial,storage} - C_{initial,conv}}{C_{operating,conv} - C_{operating,storage}}. \quad (69)$$

For the case where a residential building with on-site solar PV is being considered, the heat pump is not downsized for the system with storage (based on the results comparing the downsized and full-size heat pumps for a building without PV). The hydride reactors are the same size as for

a building without solar PV. To ensure that the control logic for using excess solar power generation would be used, the solar panels are sized to a summer design day such that peak generation on that day exceeds power consumption at that time.

Table 5-2: Cost comparison between the conventional HVAC system and the system with metal hydride energy storage, for the case where both systems also include solar PV used for power generation.

System	Heat Pump	Electric Heating	Hydrogen Compressor	Secondary Loops	Metal Hydrides	Solar PV	Total
Conventional	$5096	$100	-	-	-	$12,600	$17,796
Energy Storage	$5096	$120	$200	$2351	$14,610	$12,600	$34,977

This results in a total surface area of 21 m^2 for the solar panels for the case study considered. A price of $600/$m^2$ is used in calculating the total price of the solar panels, based on costs for existing systems. It should be noted that since the heat pump and solar panels are the same size for the systems with and without storage, their costs have no effect on the difference in cost between the systems (and therefore no effect on the payback period). The costs of the system with on-site solar generation (with and without energy storage) are given in Table 5-2.

5.1.2 Initial Cost for Commercial Buildings

Component Costs

The HVAC and energy storage systems contain the same components for a commercial building as for a residential, but the cost of some of these components changes due to the larger scale. For the metal hydrides and auxiliary heating, it is assumed that the same cost per unit is still applicable. However, for the heat pump, the correlation used to estimate the cost for a residential building is not applicable; instead, an estimated cost of $1400/ton cooling capacity is used, based on examining the prices of existing units. For the secondary loops and hydrogen compressor, the costs are scaled up by a factor of 5 due to the increased size of the system.

Table 5-3. Initial costs for the HVAC system, with and without energy storage, for a commercial building in Charleston, SC.

System	Initial Cost				
	Heat Pump	Hydrogen Compressor	Secondary Loops	Metal Hydrides	Total
Conventional	$161,000	-	-	-	$161,000
Energy Storage	$105,000	$1000	$11,755	$863,100	$980,855

Sizing for Charleston, SC

For the medium office building used as our sample commercial building, a 115-ton heat pump is required to meet the maximum cooling load. With the use of energy storage, this can be downsized to a 75-ton heat pump. Due to the higher internal gain of the building, auxiliary electric heating is hardly ever used in either case, so the heat pump is downsized for use with energy storage. Due to the larger fluctuations in the cooling load during the day, and the much large cooling loads on the building, a much larger metal hydride energy storage system is needed if it is sized the same way as it is for the residential building, to be able to store enough energy to flatten the load on the hottest day of the year. For this location, 24.3 tons $LaNi_5$ and 27.7 tons $MmNi_{4.5}Cr_{0.5}$ are needed.

Table 5-4. Residential TOU rate structure for Elizabeth City, NC

Season	On-Peak Hours	On-Peak Rate	Off-Peak Rate
Winter	6-10 AM, Mon-Fri	27.6 ¢/kWh	5.52 ¢/kWh
Summer	2-7 PM, Mon-Fri	27.6 ¢/kWh	5.52 ¢/kWh

5.2 Residential Building Results

Short-term performance of a metal hydride TES system in a residential building is analyzed in Section 5.2.1 to show how the system is used for load shifting. Cost savings for existing utility rates are examined in Section 5.2.2. Cost savings and payback period are calculated for alternate utility rate structures in Section 5.2.3 and for alternate on-peak periods in Section 5.2.4.

5.2.1 Short-Term System Behavior

To demonstrate the behavior of the system, we evaluate the performance for a week in the summer and a week in the winter for a hypothetical house in Elizabeth City, NC. Data from Typical Meteorological Year 3 [113] for January 1-7 and June 1-7 is used for the temperature and solar irradiation, while data from the Office of Energy Efficiency & Renewable Energy on residential hourly electricity loads is used for the hourly non-HVAC electricity loads [106]. The TOU utility rate structure for this location is taken from the Utility Rate Database maintained by the National Renewable Energy Laboratory [114], and is summarized in Table 5-4.

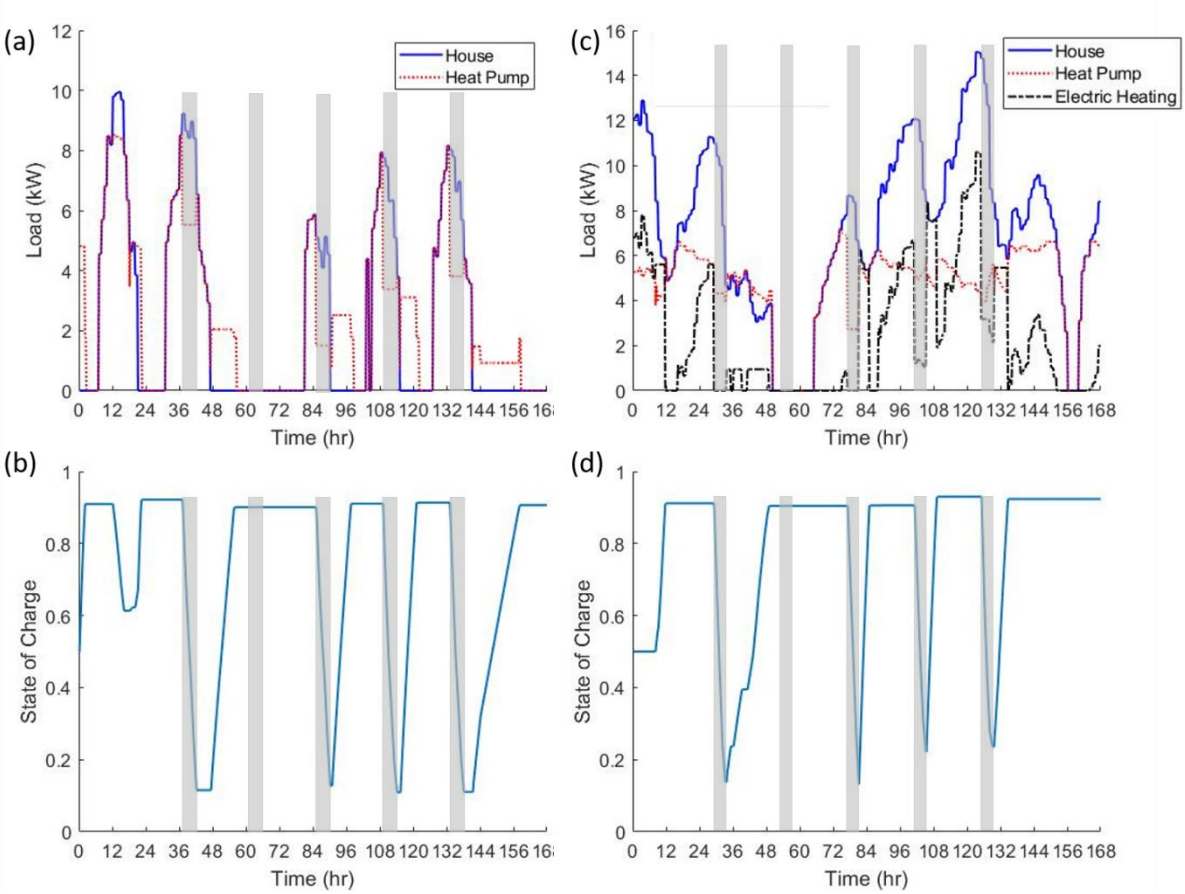

Figure 5-1. Results for sample weeks in winter and summer, starting at 1 am on Sunday. On-peak periods are shaded in gray. (a) Cooling load required by the house and produced by the heat pump for a week in summer. (b) State of charge of the hydride reactor system over time for the summer week. (c) Required heating load at the house, heat pump load, and electric heating over time for a week in winter. (d) State of charge of the hydride reactor system over time for the winter week.

Results for running the system for the representative summer and winter weeks are shown

in Figure 5-1. Both of these weeks begin at 1 am on Sunday. Considering the summer results in Figure 5-1a, the energy storage system is discharged during the weekday on-peak periods, except on Tuesday when there is no on-peak cooling load. It is also discharged once on a Sunday afternoon, when the load on the house exceeds the heat pump's capacity. The storage system is charged during off-peak hours, and primarily at night, when there is no home cooling load. Considering the results for winter in Figure 5-1c, the heat pump load varies primarily due to changes in heating capacity with changing ambient temperature. This is because most of the time, except for Tuesday, the house load exceeds the heat pump capacity and electric heating makes up the difference. The energy storage system does reduce the heat pump load by discharging on Monday and Wednesday. It is not needed due to lack of a load on Tuesday.

The main effect of the TES system when discharging in winter is to reduce the use of electric heating: on Monday and Wednesday, electric heating is eliminated and on Thursday and Friday, electric heating usage is reduced to less than a third of the rate immediately before the on-peak period starts. The energy storage system therefore primarily reduces the electric heating costs by moving a portion of this load from on-peak to off-peak hours. Since the heating loads in winter are larger than the cooling loads in summer (and the storage system is not sized for full storage even in the summer), some electric heating is still required (in addition to the heat pump) even during some of the on-peak periods. For both winter and summer, looking at the state-of charge for each week (see Figure 5-1b and Figure 5-1d), the system charges in significantly less time than the off-peak duration and in between charging and discharging, the conventional heat pump (and electric heating in winter) meets the load on the house.

The cost of running this system for each day in the summer week is shown in Figure 5-2, compared to the cost of running a conventional system, where the heat pump meets the entire cooling load. The electricity costs for the summer week are broken down by their source. The two main sources are (1) running the heat pump and (2) providing all non-HVAC electric loads. The energy storage system adds further operating costs compared to the conventional heat pump by (1) running the pumps for the secondary loops and (2) running the compressor to move hydrogen. The cost of running the pumps is negligible, but the cost of operating the compressor is not. The total operating costs for each component in the summer week period are presented in Table 5-5.

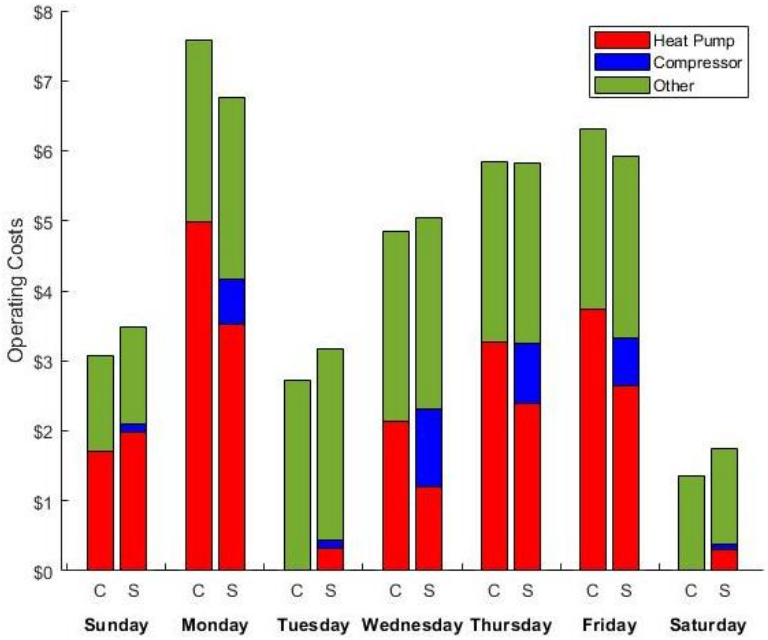

Figure 5-2. Comparison of operating costs for the summer week between the system with metal hydride energy storage (S) and a conventional system (C) where the load is entirely met by the heat pump, broken down by day and by component.

While the compressor operating costs are lower than the operating costs for the heat pump, the increased costs from running the hydrogen compressor are comparable to the reduction in heat pump costs from using the energy storage system. As a result, the operating costs for the system with energy storage are actually slightly larger than those of the conventional system. Looking at individual days in Figure 5-2, the conventional system is usually less expensive, but on the days with the highest loads (Monday and Friday) the energy storage system does reduce operating costs, and on Thursday, the operating cost is only 1¢ different between the two systems.

Table 5-5. Comparison of weekly electricity costs for the summer week using the metal hydride energy storage system as compared to a system without energy storage.

Component	**Conventional System Cost**	**Energy Storage System Cost**
Heat Pump	$15.80	$12.35
Hydrogen Compressor	$0.00	$3.65
Non-HVAC Loads	$15.95	$15.95
Total	**$31.75**	**$31.95**

For the winter week, the system with energy storage is compared to a conventional system and to a system with energy storage where the heat pump has not been downsized. This is because downsizing the heat pump, while reducing the initial cost, can lead to increased operating costs in

heating mode, due to the increased use of electric heating.

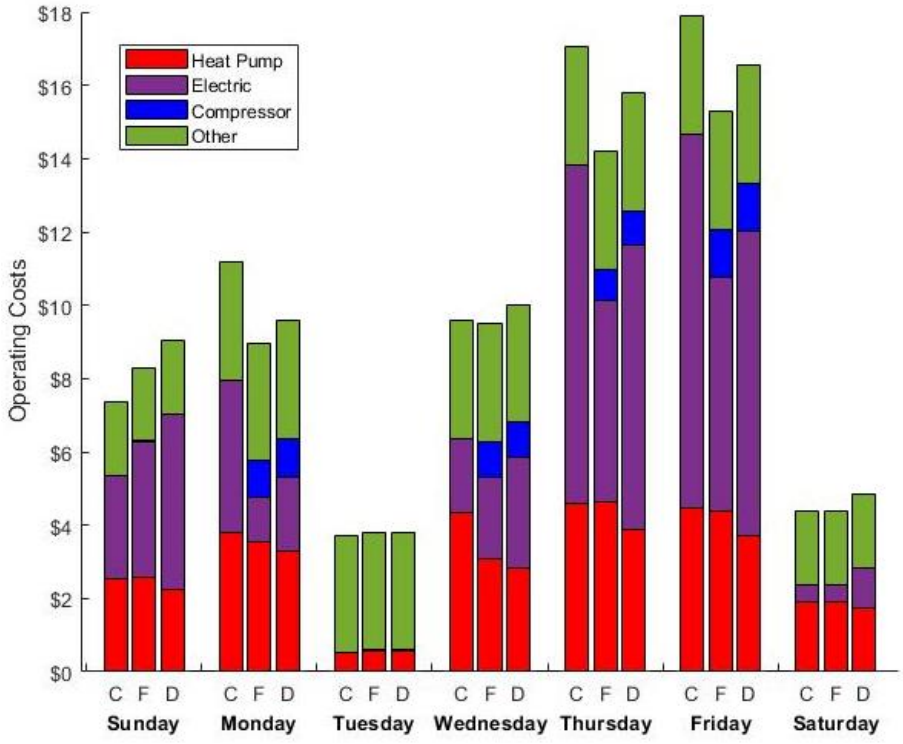

Figure 5-3. Comparison of operating costs for the winter week between the system with energy storage and the same heat pump capacity as the conventional system (F), the system with energy storage and a downsized heat pump (D), and the conventional system (C).

A comparison of the operating costs for these three systems for the winter week can be seen in Figure 5-3. The cost is decreased on days with high loads and on-peak periods, but some of these gains are lost on weekends and days without on-peak loads, where there are extra costs for charging the system but no cost reduction from discharging. Nonetheless, there are net cost savings for this case for both systems, unlike in cooling mode. Comparing the two different systems with energy storage, downsizing the heat pump leads to an increase in operating costs due to more of the heating load being met by electric heating rather than by the heat pump. The total costs for the week, seen in Table 5-6, show that both systems with energy storage reduce operating costs, but the system with a downsized heat pump does so only by 2.1%, whereas the system without a downsized heat pump achieves more significant cost savings, reducing the weekly operating cost by 9.2%. This indicates that, since the cost of compressing hydrogen is comparable to the reduced heat pump costs from load shifting, the primary way this system can reduce

operating costs is by reducing the on-peak electric heating during the winter.

Table 5-6. Comparison of weekly electricity costs for the week of January 1-7 using the metal hydride energy storage system, with and without downsizing the heat pump, compared to a system without energy storage.

Component	Conventional System Cost	Cost w/Storage and Downsized Heat Pump	Cost w/Storage and w/o Downsized Heat Pump
Heat Pump	$22.16	$18.25	$20.76
Hydrogen Compressor	$0.00	$4.28	$4.13
Electric Heating	$28.88	$27.01	$19.43
Non-HVAC Loads	$20.13	$20.13	$20.13
Total	**$71.17**	**$69.67**	**$64.65**

These results show that metal hydride energy storage reduces the operating costs of the heat pump and auxiliary heating, while adding increased operating costs for running the compressor. These costs for the compressor are significant enough to result in higher overall operating costs for the summer week. However, in the winter week, the increased cost savings from reducing the use of less-efficient auxiliary heating during the on-peak period outweigh the costs of running the compressor.

5.2.2 Cost Savings and Payback Period for Existing Rates

To determine the economic viability of the proposed systems, the model for each system is simulated for a calendar year for each of the three systems previously discussed using the weather data, utility rates, and hourly electricity loads for other systems applied to the house described in Section 3.1 for Elizabeth City, NC. The resulting annual operating costs, broken down by month and by component, for the three systems are shown in Figure 5-4. These costs show that downsizing the heat pump is not the right choice for this location, since it results in an increase in the total operating cost, with the hydrogen compressor and the increased electric heating outweighing the reduction in the heat pump costs. Even without downsizing, however, the system only achieves small cost savings, reducing the annual cost savings by only $13.12. While the system with storage consistently has lower heat pump costs and lower electric heating costs if not downsized, which system has lower operating costs overall varies from month to month, with the energy storage system primarily reducing costs in the winter months. These cost savings in the winter are due to the use of electric heating, which increases the on-peak operating costs and thus

provides a stronger incentive for the use of energy storage. Without this, as in the summer, the increased work from the compressor outweighs the reduced costs of operating the heat pump.

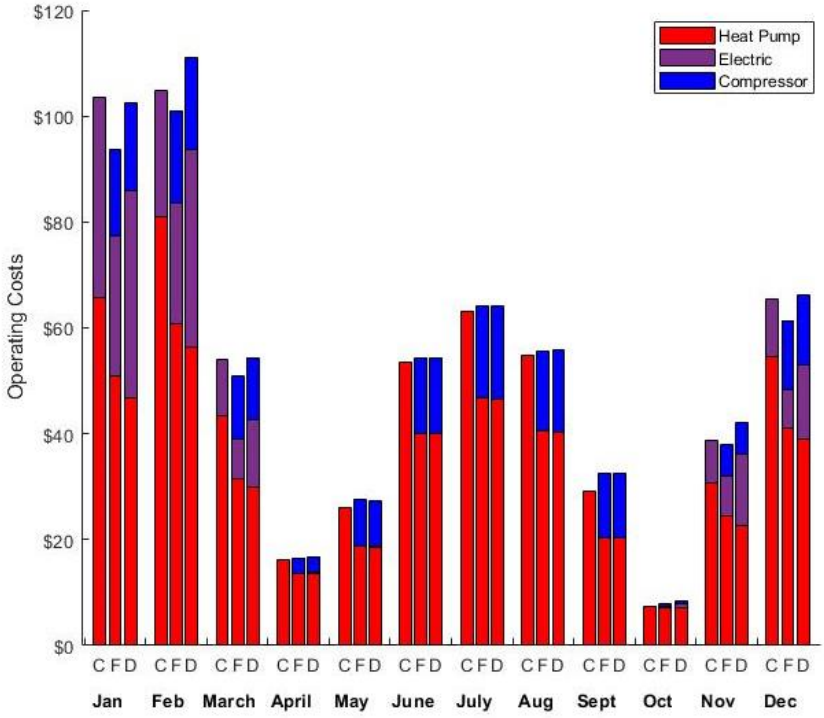

Figure 5-4. Comparison of HVAC system operating costs, by month, between the systems with energy storage to the conventional (C) system. The energy storage cases are shown with the full-size heat pump (F) and with a downsized heat pump (D).

5.2.3 Results for Different Utility Rates in Elizabeth City, NC

For this system to achieve large cost savings, the utility rates would have to be more favorable to energy storage, by having higher on-peak and lower off-peak rates. To evaluate the sensitivity of the payback period to the TOU rate structure, the operating costs for the year are calculated for a series of rate structures. These rate structures, given in Table 5-7, are designed to result in the same annual operating cost for the system without energy storage and differ in the ratio of the on-peak to off-peak rates. The rate structure in which this ratio equals 5 is the existing rate structure used for the previous results. All of these rates use the same on-peak period, as defined in Table 5-4. The higher the ratio of on-peak to off-peak rates, the more the rate structure incentivizes shifting the load away from the on-peak period. The resulting change in operating

cost, compared to the conventional system, and the payback period for the energy storage system with the different TOU rates is shown in Figure 5-5. The payback period is not shown for rates that did not result in cost savings or that resulted in cost savings low enough that the payback period exceeded 600 years.

Table 5-7. Rate structures used to examine how the cost savings from energy storage change with changes in how strongly the TOU rates incentivize load shifting. All of these rate structures result in the same annual operating cost for the conventional system.

Ratio of On-peak to Off-peak Rates	On-peak Rate	Off-peak Rate	Ratio of On-peak to Off-peak Rates	On-peak Rate	Off-peak Rate
1	$0.0894	$0.0894	8	$0.3431	$0.0429
2	$0.1548	$0.0774	10	$0.3734	$0.0373
3	$0.2048	$0.0683	12	$0.3968	$0.0331
4	$0.2442	$0.0610	15	$0.4232	$0.0282
5	$0.2760	$0.0552	18	$0.4429	$0.0246
6	$0.3023	$0.0504	20	$0.4535	$0.0227

As shown in Figure 5-5, any rates with a lower ratio than the existing rate structure do not result in any cost savings for this system. For cases with a higher ratio, the cost savings increase, reaching nearly $150 at a ratio of 20. The payback period becomes shorter as these cost savings increase but, as seen in Figure 5-5, is still too large, exceeding 100 years for all of the rate structures considered. Even if electricity were free during off-peak periods and the on-peak rate were $0.5772/kWh, the resulting payback period for this system would be 75 years.

In addition to these results, cost savings are also calculated for rate structures with a constant electricity rate and an on-peak demand charge. To determine whether the system can achieve better cost savings by reducing on-peak demand charges than by reducing on-peak electricity costs, the annual cost is calculated for a series of rate structures which use an on-peak demand charge instead of TOU energy rates. These rate structures, shown in Table 5-8, use the off-peak rates presented in Table 5-7 over the entire operating period with a demand charge. For each constant energy rate presented in Table 5-8, the on-peak demand charge is determined based on that which would result in the same conventional system operating cost. A case with free energy and only an on-peak demand charge is considered to evaluate the limit of how much cost savings can be improved by changing the rate structure. The demand charges considered here are mostly within the range of existing charges (rates examined in the NREL databased had on-peak demand

charges of up to $18.28/kW); however the rates used with these charges are mostly lower than is common ($0.0552/kWh is the lowest seen for existing rates) [114]. These rates are low because the TOU rates from Elizabeth City to which the total cost of all these rate structures is held constant for a conventional system are less expensive in terms of total cost than the majority of the other existing rate structures examined.

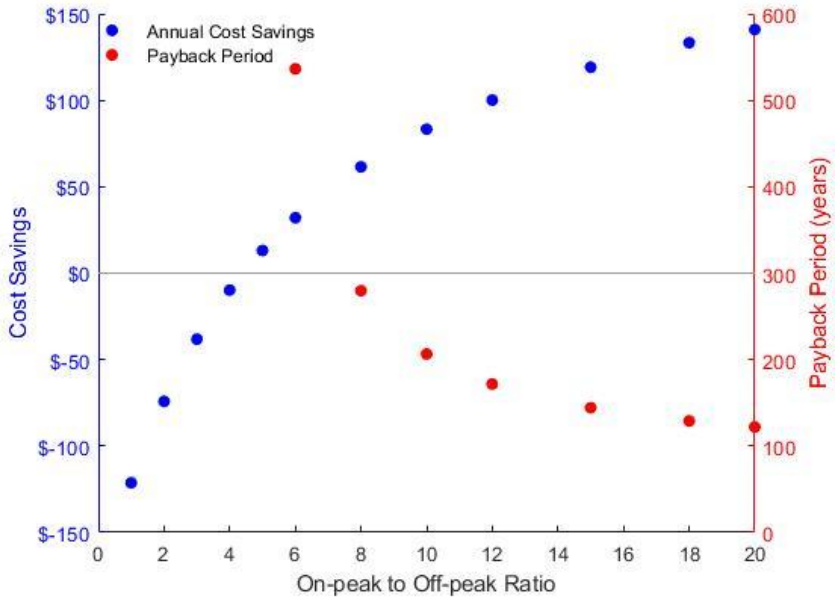

Figure 5-5. Annual cost savings and payback period from using energy storage, as compared to the conventional system, for the rate structures given in Table 5-7. Payback period is not shown for rates that did not result in cost savings, or that resulted in cost savings low enough that the payback period exceeded 600 years.

Table 5-8. Rate structures with a constant rate and an on-peak demand charge, used to analyze the performance of the energy storage system.

Constant Rate	On-Peak Demand Charge	Constant Rate	On-Peak Demand Charge
$0.0894	$0.00	$0.0373	$13.98
$0.0774	$3.22	$0.0331	$15.13
$0.0683	$5.68	$0.0282	$16.43
$0.0610	$7.62	$0.0246	$17.40
$0.0552	$9.19	$0.0227	$17.92
$0.0504	$10.48	$0.0000	$24.01
$0.0429	$12.49		

The resulting cost savings and payback periods for these rates are shown in Figure 5-6. The system achieves significantly larger cost savings for these rate structures: for the case where the constant rate is the same as the existing off-peak rate, it achieves annual cost savings of $101.65. This suggests that on-peak demand charges are more favorable to this energy storage system than higher on-peak rates. However, these payback periods are still too large; even if all operating costs come from on-peak demand charges, the payback period is approximately 37 years.

These results show that the cost savings the system achieves are strongly dependent on the utility rate structure in place. For rates that are more favorable to energy storage, it can achieve substantial cost savings; however, these cost savings do not result in a favorable payback period because of the high initial cost of the system.

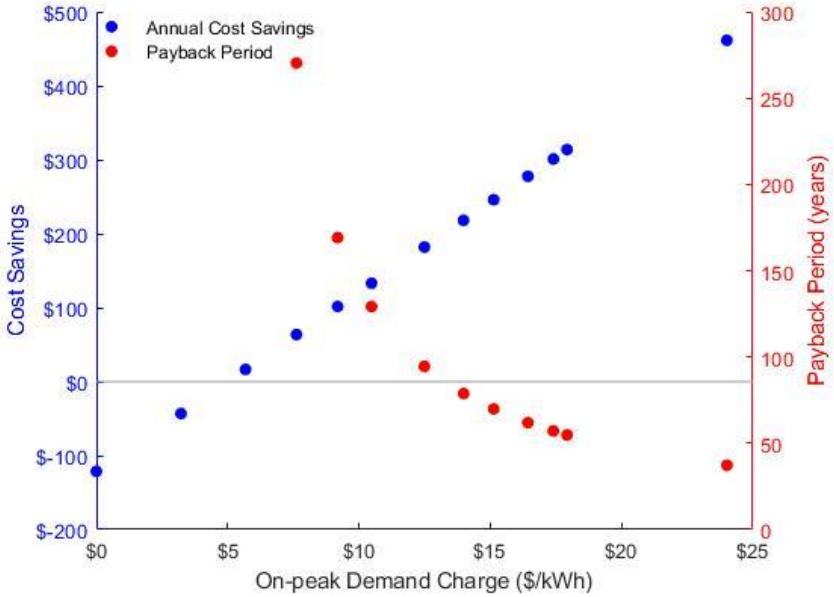

Figure 5-6. Annual cost savings and payback periods for the rate structures given in Table 5-8, plotted against the on-peak demand charge from those rate structures. Payback period is not shown for rates that did not result in cost savings, or that resulted in cost savings low enough that the payback period exceeded 300 years.

5.2.4 Results for Utility Rates with Different On-peak Periods

Electricity rate structures also vary in the time at which the on-peak period occurs. To evaluate the sensitivity of the payback period on this feature of the rate structure, the system is analyzed for a range of cases with different on-peak times, and different rates considered for each

of these cases. The on-peak periods considered are given in Table 5-9. Case 4 corresponds to the on-peak period for the existing utility rates used to generate results in Section 5.2.3. These cases are designed to consider the effect of having the winter on-peak period at different times of day (afternoon, morning, evening, morning and evening), and having the summer on-peak period be a longer or shorter period and of it being later in the afternoon.

For each of these cases, cost savings are calculated for different rate structures that are determined using the same method as in Section 5.2.3. For each case, the same number of rate structures, both with and without demand charges, are used as are described in Section 5.2.3. For each case, structures with TOU rates are determined by varying the ratio of the on-peak rates to the off-peak rates while holding the annual operating cost for a conventional system constant. The rate structures with an on-peak demand charge for each case have the same operating costs for the conventional system and constant electricity rates equal to the off-peak rates for the TOU rate structures studied. For each case, the rate structures are defined so that the rates for an on-peak to off-peak ratio of 5 are the same as existing rates. Note that this means the conventional system operating costs, while the same for all rates studied for a particular case, are not the same for different cases due to the different lengths of the on-peak periods.

Table 5-9. On-peak periods for which cost savings with different rate structures are analyzed.

Case	Summer On-peak Period	Winter On-peak Period
Case 1	12-8 PM	12-8 PM
Case 2	2-7 PM	2-7 PM
Case 3	12-8 PM	6-10 AM, 6-9 PM
Case 4	2-7 PM	6-10 AM
Case 5	3-9 PM	6-9 PM

The operating cost savings for different TOU rate structures for each case are shown in Figure 5-7. The cost savings from rate structures with on-peak demand charges are shown in Figure 5-8 where cost savings are plotted against the percentage of the conventional system operating costs that are due to the on-peak demand charge. In other words, the points corresponding to 0% represent constant rates with no demand charge and points corresponding to 100% represent rates in which all of the cost is due to an on-peak demand charge. This provides a metric that is meaningful across the different rate structures included in Figure 5-8.

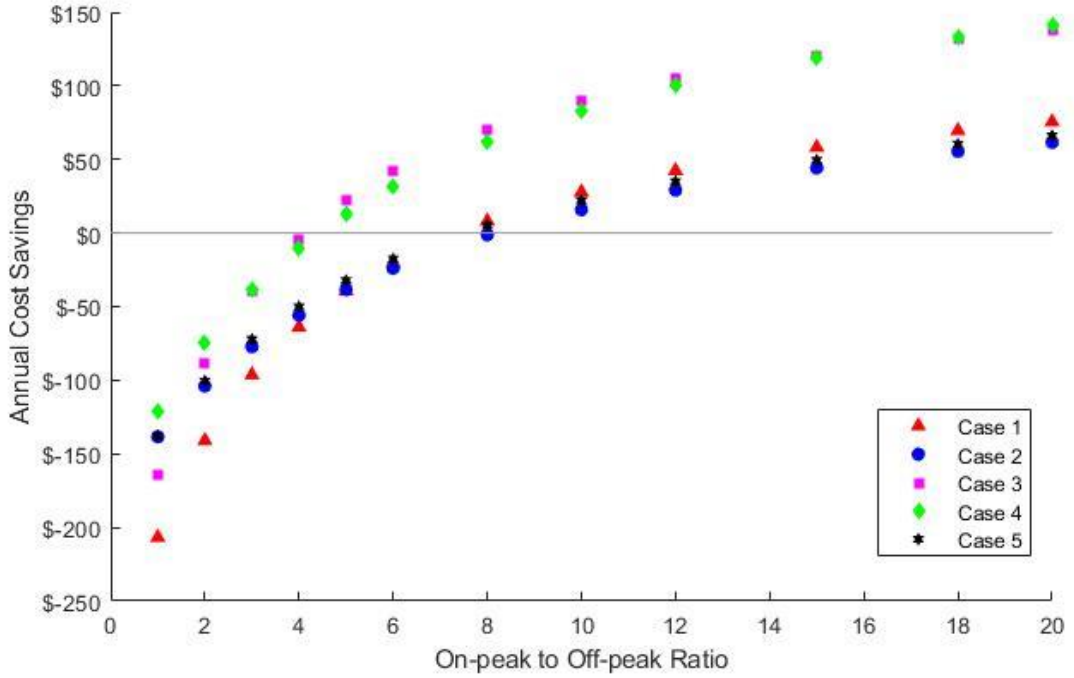

Figure 5-7. Annual operating cost savings from using energy storage for different TOU rate structures.

Across all the cases studied, we can see that the largest cost savings come from rate structures with on-peak demand charges. Cases 3 and 4 have the largest cost savings for both TOU rates and rates with an on-peak demand charge, with the largest cost savings coming from rates for Case 4 with an on-peak demand charge. These cases both have afternoon on-peak periods in the summer, and morning on-peak periods in the winter (with Case 3 also having a winter evening on-peak period). Cost savings are greatest for these cases because the winter on-peak periods in these cases required the greatest use of auxiliary electric heating for a conventional system. With energy storage, most of this on-peak auxiliary heating (>80% for Case 3, >90% for Case 4) did not have to be used since the load is met by the storage system instead. Since reducing the use of auxiliary electric heating provides a higher potential for cost savings than reducing the use of the heat pump, these cases have larger cost savings than those where there is less electric heating during the on-peak periods.

Since Case 4 has the same on-peak period as existing rates, these rates are the same ones discussed in more detail in Section 5.2.3, which did not achieve any payback periods less than 37 years. Since none of the other on-peak periods considered result in higher cost savings than these rates, none of them result in better payback periods. The large cost savings for some of these cases

(>$350 for the case where all the cost is due to an on-peak demand charge, >$250 for several rates with high on-peak demand charges and very low electricity rates) show the sensitivity of these results to the rate structures used. That even these large cost savings still result in a high payback period is due to the high initial cost of the system.

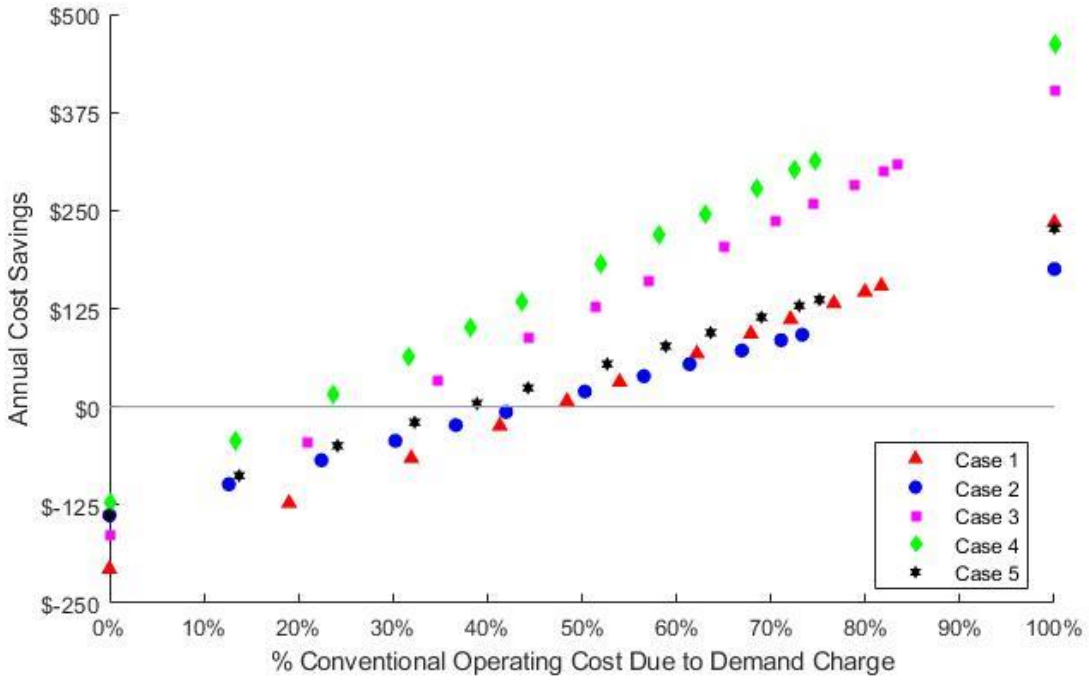

Figure 5-8. Annual operating cost savings from using energy storage for different rate structures with on-peak demand charges.

5.3 Residential Building with Solar PV Results

Metal hydride energy storage is next examined for a residential building with on-site solar power generation. The effect of solar PV on the short-term behavior of the metal hydride storage system is considered in Section 5.3.1, and the effect on annual cost savings and payback period in Section 5.3.2.

5.3.1 System Behavior on an Example Day for a Building with Solar PV

To show how the modified load-shifting control logic for a building with on-site solar PV (described in Section 4.2.5) works on a particular day, the model is run using temperature and solar

irradiation data for June 23 from the Typical Meteorological Year 3 (TMY3) data for Elizabeth City, NC [113]. The results for this example day can be seen in Figure 5-9. The storage system is partially discharged during each on-peak period, as seen in Figure 5-9b. While discharging, the heat pump is run at a low load, as seen in Figure 5-9a. However, for the last hour of the first on-peak period, the storage system is not used even though there is a cooling load larger than the load the heat pump had previously run at during this on-peak period. This is because there is enough solar power available at this time that all of the cooling load can be met with the heat pump without using any electricity from the grid. Since this is the case, the storage system is not used at this time to reduce the load on the heat pump.

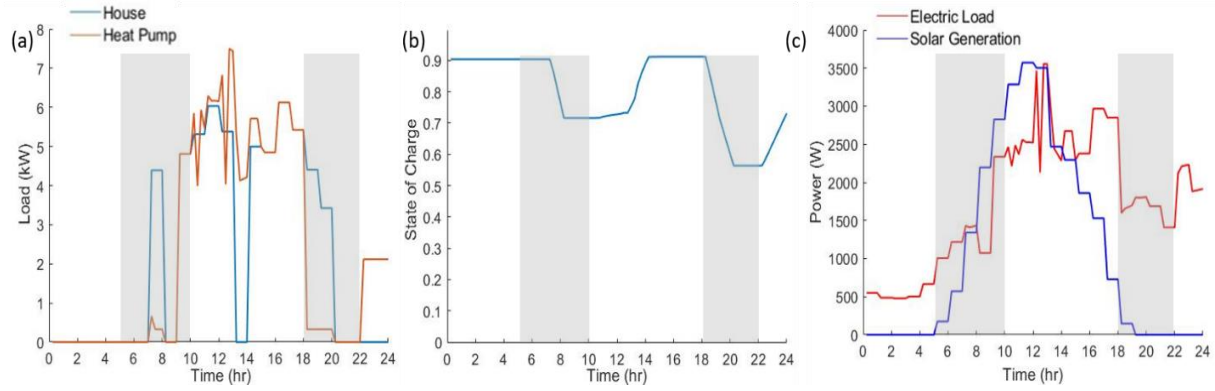

Figure 5-9: (a) Cooling loads at the house and heat pump, (b) reactor state of charge, and (c) total electric load for the house compared to solar power generation for an example summer day in Elizabeth City, NC. On-peak periods are highlighted in grey.

If no excess solar power were available, the system would not be charged in-between the morning and evening on-peak periods, since the heat pump loads for discharging are calculated so that the system will be fully discharged by the combination of the two periods, and then charged during off-peak hours at night, when the cooling load is lower. However, in this case, solar power generation during the afternoon on-peak period exceeds the power needed at the house, as seen in Figure 5-9c, so the excess solar power is sued to charge the storage system. While charging, the heat pump load exceeds the cooling load at the house, and the excess load charges the storage system. However, at two points during the afternoon the heat pump load goes below the cooling load at the house. This is because the system is adjusting the temperatures in the metal hydride reactors in order to keep them within the range of temperatures the system is designed to operate in. When this happens, some of the cooling load is being provided by the hydride reactors, because

the fluid in the indoor loop is being used to heat the hydride reactor connected to it. The system is also charged during the night after the end of the evening on-peak period. This charging is done at a constant heat pump load since it is using electricity from the grid and thus not trying to adjust the load in order to only use solar power.

5.3.2 Cost Savings and Payback Period for a Building with Solar PV

Rate Structures Analyzed

Table 5-10: On-peak periods examined as the basis for TOU utility rate structures. All on-peak periods are only on weekdays (Monday-Friday); rates are always off-peak on weekends.

	Morning	**Evening**	**Morning and Evening**
On-Peak Period	6-11 AM	7-11 PM	6-11 AM & 7-10 PM

Significant solar penetration is likely to lead to peak demand for electricity from the grid occurring in the morning and evening instead of the afternoon. The utility rate structures that are used to examine the performance of the metal hydride storage system have on-peak periods selected based on this. Therefore, three different on-peak schedules are examined, as shown in Table 5-10: one with on-peak rates in the morning, one with on-peak rates in the evening, and one with on-peak rates in both morning and evening.

For each of these three on-peak periods, a series of rate structures are analyzed. Different potential rate structures are evaluated by varying the ratio of the on-peak to off-peak rates to see how strongly the rates must incentivize load-shifting for the system to be economical, as in Section 5.2.3. Also as in Section 5.2.3, each rate structure is compared to an equivalent structure that uses an on-peak demand charge instead of a higher on-peak utility rate. In both cases, all rate structures are defined so that they result in the same annual operating cost for a system with no energy storage (but with solar power generation). Any difference in operating costs between two such rate structures is therefore due to the effect of the energy storage system.

All rate structures studied are defined to have the same total annual operating cost as a conventional system (with solar PV and no energy storage) with a flat utility rate of $0.12/kWh. Furthermore, all rate structures are defined as having an ACR which is equal to one-quarter of the

electricity rate. The rate structures defined in this way for the case with morning and evening peak periods are shown in Table 5-11. Note that for the cases with only morning or only evening peak periods, the rate structures will have different on-peak and off-peak rates for the same on-peak to off-peak ratio, since achieving the same annual operating cost for the conventional system requires different rates depending on the length of the on-peak period.

There are two sets of rate structures shown in Table 5-11; as in Section 5.2.3, one set uses TOU rates with a higher rate during the on-peak period, while the other uses a flat rate with an on-peak demand charge. These rates are defined as described in Section 5.2.3, with the only change being the rate structure used to determine the cost for the conventional system. By comparing results for these two rates, we can see whether the inclusion of solar PV changes whether on-peak demand charges or high on-peak rates result in higher cost savings.

Table 5-11: Rate structures used for the case with morning and evening on-peak periods. Rate structures with a high on-peak rate are defined by the on-peak to off-peak rate ratio. Each rate structure with a flat rate and an on-peak demand charge is defined to be equivalent to a structure with a high on-peak rate by having the same percentage of the operating costs for a conventional system occur in the on-peak period and having the flat rate equal the off-peak rate for the structure with a high on-peak rate.

		High On-Peak Rates				**On-Peak Demand Charge**			
% Conv. Cost On-Peak	**On-peak/ Off-peak Ratio**	**Summer**		**Winter**		**Summer**		**Winter**	
		On-peak Rate (/kWh)	**Off-peak Rate (/kWh)**	**On-peak Rate (/kWh)**	**Off-peak Rate (/kWh)**	**Flat Rate (/kWh)**	**On-peak Demand Charge (/kW)**	**Flat Rate (/kWh)**	**On-peak Demand Charge (/kW)**
35.5	1	$0.1200	$0.1200	$0.1200	$0.1200	$0.1200	$0.00	$0.1200	$0.00
52.3	2	$0.1729	$0.0864	$0.1791	$0.0895	$0.0864	$6.48	$0.0895	$5.90
68.7	4	$0.2217	$0.0554	$0.2376	$0.0594	$0.0554	$12.47	$0.0594	$11.74
73.3	5	$0.2350	$0.0470	$0.2542	$0.0508	$0.0470	$14.10	$0.0508	$13.40
76.7	6	$0.2447	$0.0408	$0.2666	$0.0444	$0.0408	$15.30	$0.0444	$14.64
81.4	8	$0.2582	$0.0323	$0.2840	$0.0355	$0.0323	$16.95	$0.0355	$16.37
84.6	10	$0.2669	$0.0267	$0.2955	$0.0296	$0.0267	$18.02	$0.0296	$17.52
89.1	15	$0.2796	$0.0186	$0.3125	$0.0208	$0.0186	$19.58	$0.0208	$19.21

Results

Using the system sized as described in Section 5.1.1, the model is run for a full year for a house in Elizabeth City, NC. TMY3 weather data [113] and EERE data on non-HVAC building loads [106] for the full year are used as described in the previous section. The annual operating cost calculated for the conventional system (with solar PV but no energy storage) is $1422.18. This cost is the same for all rate structures since these are defined to give the same annual operating cost if no storage is used. The majority of the operating cost is due to electrical loads other than the HVAC system, which has an operating cost of $622.33 for the flat rate of $0.12/kWh.

The operating cost savings for all the rate structures considered are shown in Figure 5-10. Cost savings are plotted against the percentage of the conventional system operating costs that occur during the on-peak period. The higher this value is, the larger the incentive to use energy storage. For each of the three on-peak periods considered (morning, evening, and morning and evening) rates with a high on- peak rate are compared to rates with a constant electricity rate and an on-peak demand charge.

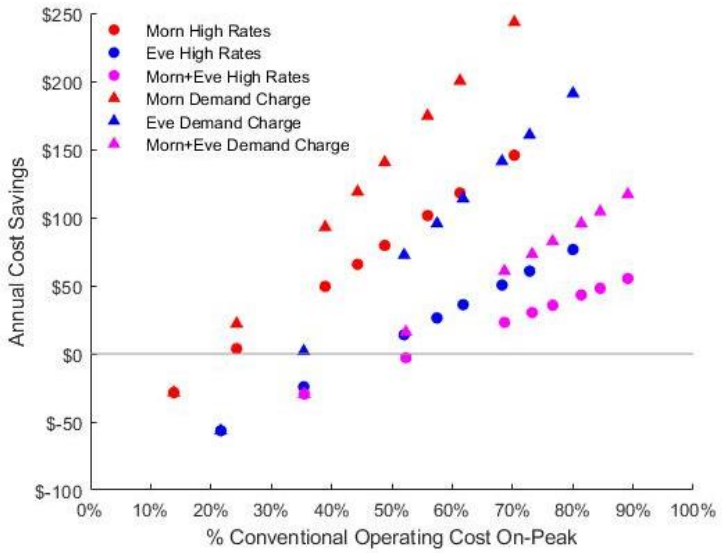

Figure 5-10: Annual cost savings for all TOU rates structures considered in this study, plotted as a function of the percentage of the conventional system operating cost that occurs during the on-peak period. Rates with high on-peak rates are compared to rates with an on-peak demand charge for rate structures with three different on-peak times (morning, evening, and morning and evening). The leftmost point in each series is a flat rate structure with no demand charge.

Estimated payback periods for the system with storage are presented in Figure 5-11 as function of the utility rates. While the system provides significant cost savings, the resulting payback periods are extremely long and not economically viable, even for the most favorable rate structures. As before, these high payback periods are primarily due to the extremely high cost of the metal hydrides and the loss in operating cost savings due to hydrogen compression.

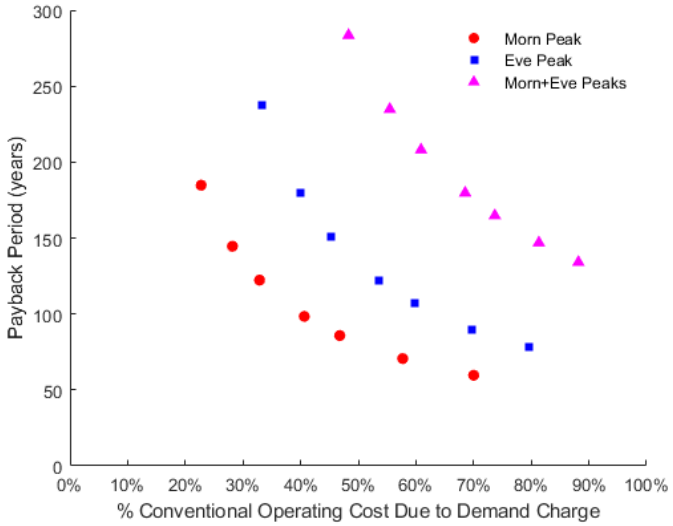

Figure 5-11: Payback periods calculated based on cost savings from different rate structure, plotted as a function of the percentage of the operating cost that is due to the on-peak demand charge for a conventional system. Payback period is calculated for the rate with an equivalent demand charge rather than rates with a higher on-peak rate, due to higher cost savings from rates with demand charges.

5.4 Discussion of Residential Results

The system proposed in this paper achieves the goal of providing year-round energy storage with a single system—both in heating and cooling modes—and enables cost savings on an annual basis. However, due to the high initial system cost and the reduced operating cost savings from compressing hydrogen, the system has a high payback period across a range of utility rate structures and so is not cost-effective for commercialization.

The high initial cost of the metal hydrides is a major factor in the high payback periods of the system, since 85.2% of the increase in initial cost for the system with energy storage is due to the cost of the hydrides. For the system to have a payback period of less than 10 years at existing rates, the initial cost of all components would have to decrease by 94%. This value is reduced for

rates more favorable to energy storage; however, even at the most favorable rates (where all operating costs are due to a high on-peak demand charge), a reduction in component cost by 73% would be required to achieve a 10-year payback period. Even if the system could eliminate all operating costs for heating and cooling, the payback period at existing rates in Elizabeth City, NC would still be 27.9 years. There are locations with more expensive utility rates and higher electricity demand for heating and cooling, but these would have to result in operating costs over 5 times as large before it would be even hypothetically possible for this system to achieve a 5-year payback period. Thus, while other things can be done to improve the cost-effectiveness of this system, a large reduction in the initial cost of the system, and particularly the cost of the metal hydrides, would be necessary for it to achieve a viable payback period. If the safety concerns from high-pressure storage could be managed, the initial cost of the system could be substantially reduced by replacing one of the hydride reactors with a hydrogen storage tank, although this would likely have the downside of increasing the cost of hydrogen compression as well.

The loss of operating cost savings from running the compressor is the other major contributor to the high payback period of the system. A storage system that is able to do the same load-shifting as the metal hydrides without the compressor operating costs would achieve much greater cost savings; for instance, at existing utility rates, the metal hydrides reduce heat pump and electric heating costs by $149.09, but $135.97 of this is lost running the compressor. Therefore, compressor costs would need to be substantially reduced for metal hydrides to compete with other forms of TES. Compressor costs would not be an issue if hydrogen flow were purely temperature-driven; however, this would require that the system operate at a wider range of temperatures and pressures, since the materials used in this paper are selected to minimize the required compressor work while operating within a narrow range of temperatures and pressures. Thus, reducing compressor work would require higher-pressure hydrogen storage in the hydride reactors, as well as a higher-temperature heat source to create a sufficient temperature difference to drive the reaction. If the system cannot be made purely temperature-driven, modifications to the target heat rates and controller to reduce compression costs might also be examined. Moreover, as mentioned in Section 4.2.2, optimization of the metal hydride operating temperatures is not considered in this part of the project. Similarly, heuristic control logic is used for charging and discharging the system rather than an optimal controller. Optimization of the operating temperatures and load-shifting control logic could improve the cost savings that this system can achieve.

These results also show that there is a high potential for cost savings from energy storage coupled with residential heating in buildings that use a heat pump supplemented by auxiliary electric heating. As seen in Figure 5-4, the metal hydride energy storage system achieves cost reductions of up to $10/month in months with heating loads large enough to require electric heating (even at rates where it fails to achieve any cost savings in months where electric heating is not used). This is due to the higher marginal cost savings from reducing the use of electric heating during on-peak periods than those from reducing the use of a heat pump. Because of this, 57.8% of the reduction in heat pump and electric heating costs (neglecting compressor costs) achieved by the system at existing rates occurs in the months of October-March. The results indicate that an energy storage system used with a residential heating system could achieve larger cost savings than an energy storage system with a cooling system for a location where heat pumps with auxiliary electric heating are used, but where there are significant heating loads in the winter that do require the use of auxiliary heating (such as the location studied here).

5.5 Commercial Building Results

The commercial model is run for a full year for a building in Charleston, SC, using a load profile calculated as discussed in Section 4.2.1. The operating costs for the conventional system and the system with energy storage are calculated using existing rates for this location, shown in Table 5-12. A monthly breakdown of the operating costs for the two systems is shown in Figure 5-12. The total operating costs for the year are shown in Table 5-13.

Table 5-12. Utility rate structures for commercial buildings in Charleston, SC

Time	On-peak Rate (/kWh)	On-peak Demand Charge (/kW)	Off-peak Rate (/kWh)	Off-peak Demand Charge (/kW)
June-September	$0.08414	$21.77	$0.04215	$4.68
October-May	$0.05475	$14.69	$0.04215	$4.68
Time	**On-peak Period**		**Off-peak Period**	
May-October	1-9 PM		12 AM- 1 PM, 9 PM- 12 AM	
November-April	6 AM- 12 PM, 5-9 PM		12-6 AM, 12-5 PM, 9 PM- 12 AM	

The energy storage system fails to deliver cost savings for this location at these rates; while it does significantly reduce the cost of the demand charges by lowering on-peak demand, the increased costs from running the compressor negate any benefits from this. Unlike with the

residential system, the monthly breakdown of the costs shown in Figure 5-12 does not show as large a variation in how the energy storage system compares to the conventional system. Furthermore, the energy storage system here does better in the summer, whereas for residential buildings it is best in winter. This is due to the absence of electric heating, which is the cause of the better performance in the winter for residential buildings. This system does best in summer because the loads are highest so it can bring about the most significant reduction in the demand charges.

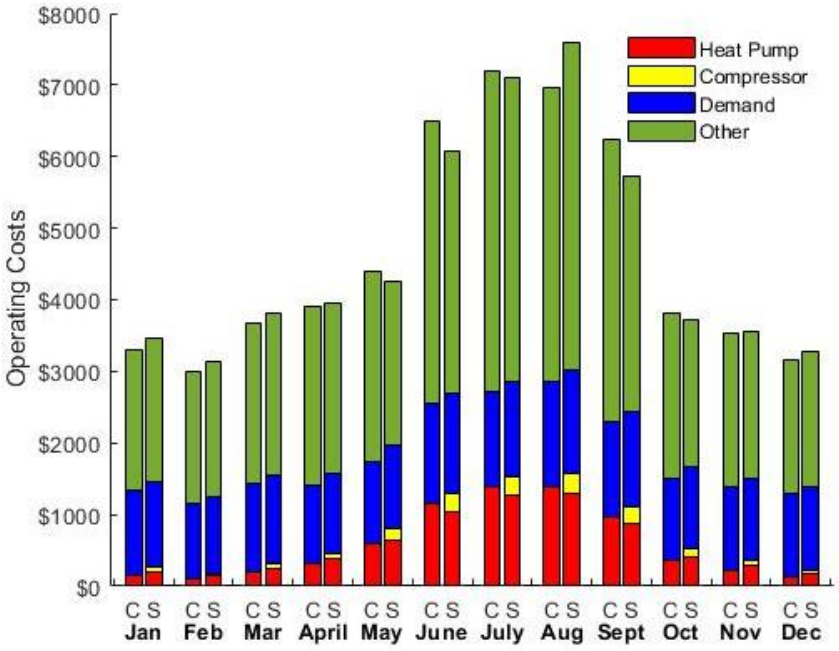

Figure 5-12. Operating costs by month for a commercial building, comparing a system with metal hydride energy storage to one without it.

The absence of electric heating here shows that while the South is an appropriate region to study this system for residential buildings, since there heating by heat pump with auxiliary electric heating is commonly used, it is not the right location to study this system in a commercial building. Instead, this system should be studied in a colder climate, where auxiliary heating is needed.

These results indicate that a larger scale does not solve the problems with the metal hydride energy storage system that are described in Section 5.2. The increased costs from compressing hydrogen mean that the system cannot achieve meaningful cost savings by shifting heat pump loads, and here there are no electric heating loads to shift. Furthermore, the difference in initial costs between systems does not improve with scale. Even with the heat pump downsized, the ratio

of the system costs for the commercial system in Table 5-3 is actually higher than that for the residential system given in Table 5-1. Thus, even if the system could achieve significant cost savings, these would still not lead to a reasonable payback period. These results, combined with those in Section 5.2, show that metal hydride energy storage is not suitable for either residential or commercial buildings. However, this is due to features specific to the metal hydride system- the high material cost and the cost of running the compressor- that might not be as significant for a different method of variable-temperature storage. To examine the potential of variable-temperature storage more generally, and to consider the problem of optimal operating temperatures for the storage system which is neglected in this chapter, a model, described in Chapter 6, is designed to study the optimization and performance of the abstract variable-temperature storage system.

Table 5-13. Annual operating costs for a commercial building in Charleston, SC with and without energy storage.

Component	**Conventional System Operating Cost**	**Operating Cost with Energy Storage**
Heat Pump	$6961.60	$6811.30
Hydrogen Compressor	$0	$2265.20
Non-HVAC Loads	$14,641.50	$14,641.50
Demand Charges	$33,663.90	$31,828.60
Total	**$55,267.00**	**$55,546.60**

6. VARIABLE-TEMPERATURE ENERGY STORAGE MODEL

In addition to the metal hydride system model, a model of a more generalized variable-temperature TES system integrated with a residential building HVAC system is also developed. This model is used to determine the optimal operating temperatures for a variable-temperature TES system and the potential improvement to system performance from dynamically tuning the operating temperature of such a system. A more generalized model is used in place of the model described in Chapters 3 and 4 to reduce computation time by eliminating the dynamic model (which is important given that the model must be run repeatedly as part of the optimization solver) and to obtain results that will be generally applicable for other variable-temperature TES systems. A description of this system model is given in Section 6.1. The heat pump model used here, described in Section 6.2, is more detailed than the one described in Section 4.2.3 and includes water glycol mass flow rate as an input in addition to condenser and evaporator inlet temperatures. The optimization function used to find the optimal storage temperatures is described in Section 6.3. In addition to the model described in Section 6.1, two other models are developed. The first, a modified version where the storage tank is charged with the outlet flow from the house, is described in Section 6.4. The second, a model of a system that uses two separate PCM storage tanks for cold storage and heat storage which is used as a benchmark for the variable-temperature model, is described in Section 6.5.

6.1 Variable-Temperature Storage Model

A diagram of the model used to analyze the performance of a variable-temperature storage system is shown in Figure 6-1. This model is used for a system architecture that is described in Section 6.1.1. Like the model described in Chapter 4, this model includes the calculation of building loads, load-shifting control logic, a model of the secondary loop, and a model of the storage tank. However, each of these components differs somewhat from the metal hydride system. The load calculations, described in Section 6.1.2, are now done entirely using EnergyPlus. The model of the storage tank, described in Section 6.1.3, is a part of the same static model as the secondary loop calculations, rather than a separate dynamic model with a controller. The algorithm for calculating the secondary loop temperatures is modified to work with the new storage system

and the absence of an outdoor loop, as described in Section 6.1.4. For load-shifting, different options are compared for the charging control logic, as described in Section 6.1.5. Furthermore, the model is now run inside of an optimization function (described in Section 6.3) that determines what operating temperature of the TES tank will maximize cost savings. To allow for more ways in which altering the PCT can affect system performance, a more detailed heat pump model is used so that the heat pump performance can be calculated in terms of the secondary loop mass flow rate, as described in Section 6.2.

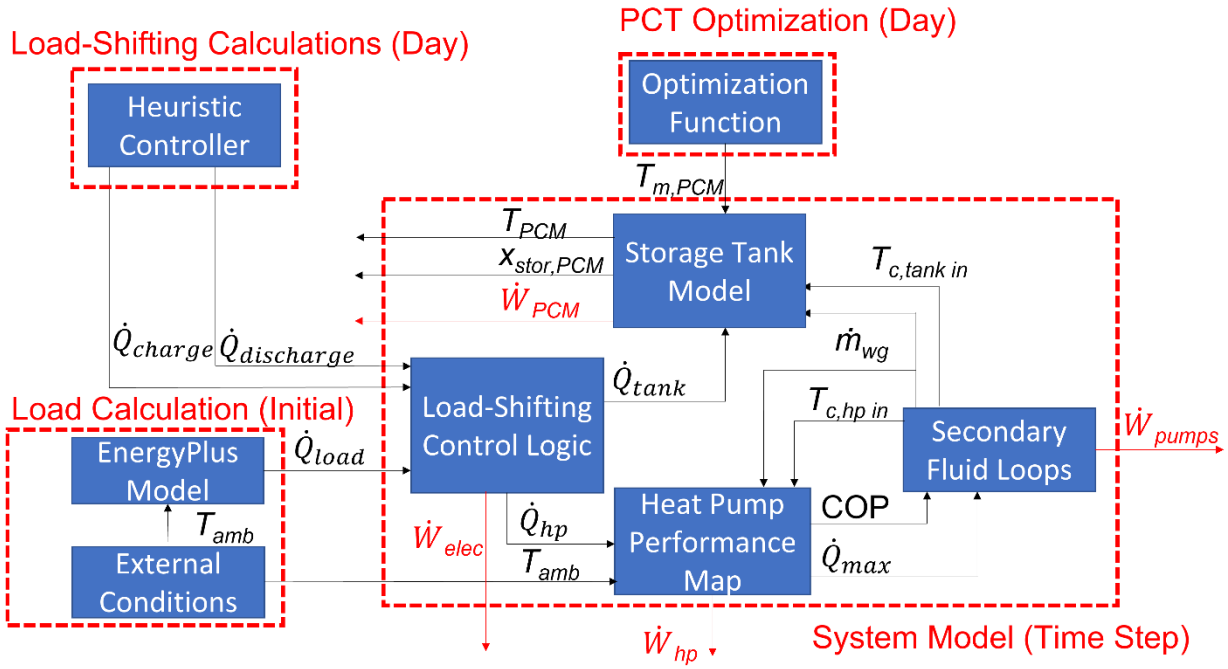

Figure 6-1. Diagram of the model used for the variable-temp storage system. At each time step, the model takes inputs from the load calculations performed before any other calculations in the model, as well as the load-shifting calculations and optimization of the storage tank operating temperature performed each day. Then, at each time step, the model determines the appropriate heat pump loads, calculates the heat pump work using the secondary loop model and heat pump performance map, and updates the state of the storage tank.

6.1.1 System Architecture

The system architecture for the variable-temperature storage system model is very similar to that of the residential HVAC system with ice storage, shown in Figure 2-1, that was modelled by Tam et al. [11,24]. The variable-temperature storage system is represented as a PCM storage tank where the phase-change temperature (PCT) of the PCM is treated as variable, rather than the

fixed value of 0°C used for ice storage. A diagram of this system is shown in Figure 6-2. A model of this architecture, instead of the model previously developed for a system with metal hydride energy storage, is used in order to reduce complexity and computation time. The reduced complexity primarily comes from the model only having one storage tank and one secondary loop, as compared to the two storage tanks and secondary loops used in the hydride model. The reduced computation time comes primarily from the simpler model of the storage system, described in 6.1.3. Like the system with metal hydride storage, this system has 6 operating modes, since it has conventional, charging, and discharging modes for both cooling and heating. In charging mode, flow from the indoor loop freezes (in cooling) or melts (in heating) the PCM; in discharge mode, the PCM is melted to cool (or frozen to heat) the fluid in the indoor loop and thus deliver a portion of the load to the house.

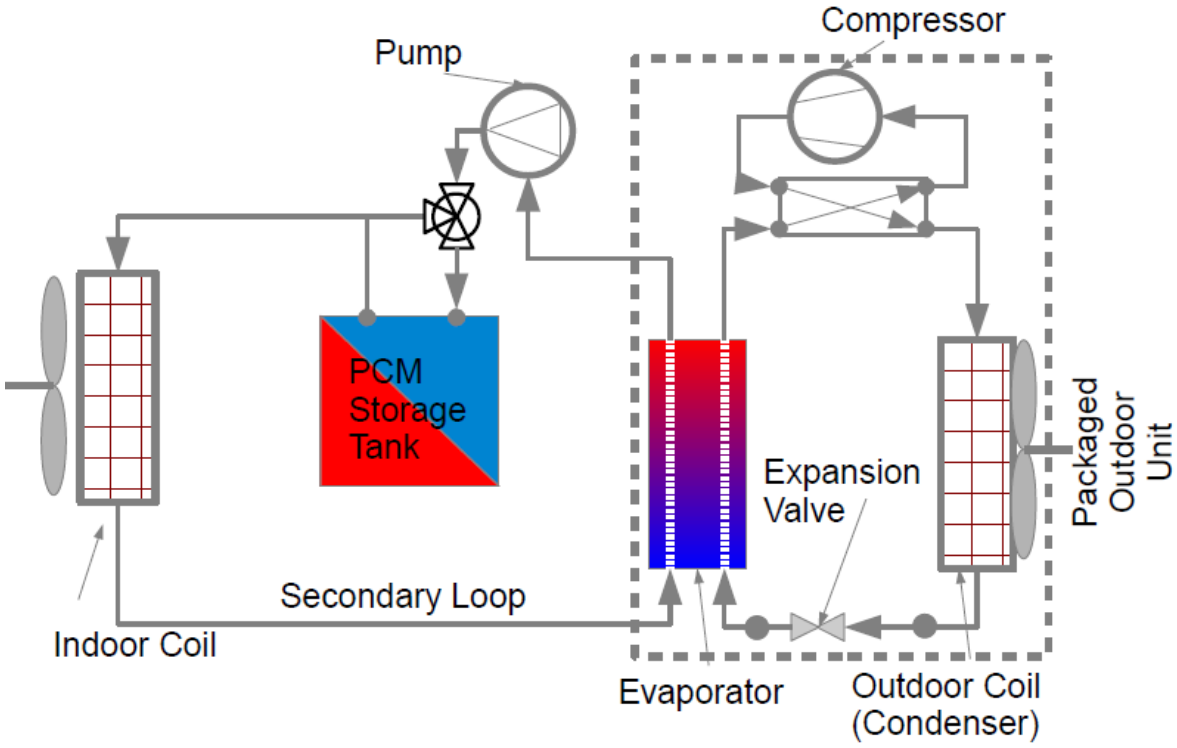

Figure 6-2. Schematic of the HVAC system with variable-temperature PCM storage.

6.1.2 Load Calculations

In order to obtain more accurate heating and cooling load profiles for the residential building in this model, an EnergyPlus model of a house is used to determine the required heating

and cooling loads instead of the model for calculating residential loads described in Section 4.2.1. Like the EnergyPlus model used to calculate commercial building loads for the metal hydride system model (also described in Section 4.2.1), the residential EnergyPlus models used were developed by the DOE with PNNL [115]. Multiple residential models are used because the DOE developed different versions of the residential model for different climate zones [115]. For each location studied, the model for the appropriate climate zone is used. For all locations, the model for a single-family house built on a slab using a heat pump for heating is used. As before, TMY3 weather data [113] is used as an input to the EnergyPlus model. The residential building represented in these models uses a single heat pump with auxiliary electric heating for heating and cooling. The cooling rate for this heat pump at each time step is used as the cooling load for the building at that time, while the sum of the heating rate for the heat pump and the auxiliary heating is used as the heating load at the building for each time step. In calculating the cooling and heating loads, the model used a cooling setpoint temperature of 23.9°C and a heating setpoint of 22.2°C.

6.1.3 Storage Tank Model

The TES system used for variable-temperature storage is modelled as PCM with a variable PCT. An energy balance on the storage tank gives us the equation:

$$\dot{Q}_{tank} = \dot{Q}_{lat} + \dot{Q}_{sens}. \tag{70}$$

In this equation, the storage tank is assumed to be insulated so that the only heat transfer in or out of the tank is the heat transfer to and from the circulating water glycol ($\dot{Q}_{tank}$). This heat transfer is equal to the sum of the latent heating ($\dot{Q}_{lat}$) and sensible heating ($\dot{Q}_{sens}$) in the storage tank. Sensible heating is included in this model because the storage tank does not stay at a fixed temperature, as an ice storage system does, due to the changes in the PCT. When the PCT changes, sensible heating or cooling is required to change the temperature of the PCM to match the new PCM. Therefore, sensible heating only occurs at times when the temperature of the storage tank (T_{PCM}) is different from the melt temperature of the PCM ($T_{m,PCM}$) since the system will not continue charging or discharging if $x_{stor} > 1$ or < 0. If the sensible heating or cooling load is delivered by the heat transfer from the water glycol ($\dot{Q}_{tank} = \dot{Q}_{sens}$), then the updated temperature is calculated from the sensible heating rate:

$$T_{PCM,new} = T_{PCM,old} - \frac{\dot{Q}_{sens}\Delta t}{m_{PCM}c_{PCM}}. \tag{71}$$

If the heat transfer to the tank is greater than the sensible heating load required to change the PCM temperature to the new PCT value, or if the sensible heating required has the opposite sign as the load being delivered to the tank, then the sensible heating rate and storage tank temperature at a given time step is calculated using the equations:

$$\dot{Q}_{sens} = \frac{m_{PCM} c_{PCM} (T_{PCM} - T_{m,PCM})}{\Delta t}, \text{ and} \tag{72}$$

$$T_{PCM,new} = T_{m,PCM}. \tag{73}$$

At every time step, the state of charge (x_{stor}) is updated based on the latent heating rate:

$$x_{stor,new} = x_{stor,old} + \frac{\dot{Q}_{lat} \Delta t}{m_{PCM} L_{PCM}}. \tag{74}$$

Since the heat exchanger effectiveness for the TES system is low in at least one mode (charging or discharging) for both very high and very low states of charge, the load-shifting control logic calculates the storage capacity so that the system will operate between the state of charge x_{stor} = 0.9 and x_{stor} = 0.1. Thus, the system will stop charging once x_{stor} = 0.9. However, while the load-shifting control logic calculates the heat pump load for discharge so that the system will end the on-peak period at x_{stor} = 0.1, if the state of charge does go below this value, the system will continue to discharge until entirely discharged (x_{stor} = 0):

$$\begin{aligned} if\ x_{stor,new} > 0.9 \quad &\rightarrow \quad \begin{cases} \dot{Q}_{lat} = \frac{\pm (0.9 - x_{stor,old}) E_{stor}}{\Delta t} \\ x_{stor,new} = 0.9 \end{cases} \\ if\ x_{stor,new} < 0 \quad &\rightarrow \quad \begin{cases} \dot{Q}_{lat} = \frac{\pm (-x_{stor,old}) E_{stor}}{\Delta t} \\ x_{stor,new} = 0 \end{cases} . \end{aligned} \tag{75}$$

The state of charge will only go above 0.9 as a result of sensible heating or cooling; if $\dot{Q}_{sens}$ is large enough to result in x_{stor} > 0.9 even for $\dot{Q}_{tank}$= 0, then x_{stor} will increase until either $\dot{Q}_{lat} = -\dot{Q}_{sens}$ or x_{stor} = 1:

$$if\ x_{stor,new} > 1 \quad \rightarrow \quad \begin{cases} \dot{Q}_{lat} = \frac{\pm (1 - x_{stor,old}) E_{stor}}{\Delta t} \\ \dot{Q}_{sens} = -\dot{Q}_{lat} \\ x_{stor,new} = 1 \\ T_{PCM,new} = T_{PCM} - \frac{\dot{Q}_{sens} \Delta t}{m_{PCM} c_{PCm}} \end{cases} . \tag{76}$$

In Eqs. 75 and 76, the ± is + in cooling mode and – in heating mode.

Since the system is variable-temperature, it can be used for storage in both cooling and heating mode. Which mode the system operates in is determined each day by whether there are

cooling or heating loads in the on-peak period. If there are no on-peak loads, the system stays in whatever mode it was in on the previous day. For cold storage, the state of charge represents the fraction of the PCM that is frozen whereas for heat storage, it represents the fraction that is melted. Because of this, when the storage system changes between cold storage and heat storage, the state of charge changes according to the equation:

$$x_{stor,new} = 1 - x_{stor,old.} \tag{77}$$

The storage tank model allows for an energy cost for changing the PCT to be included in the model. This energy cost is calculated using the equation

$$\dot{W}_{PCM} = \frac{w_{PCM} m_{PCM} \Delta T_{PCM}}{\Delta t}. \tag{78}$$

In this equation, w_{PCM} is the energy (in kJ) required to change the melt temperature of 1 kg of PCM by 1°C. This energy requirement is an input to the overall system model that can be set to any value, in order to compare how the system performance changes depending on the cost of changing the PCT.

To determine the required water glycol mass flow rate for the storage tank (and thus the minimum water glycol mass flow rate overall), the effectiveness of the storage tank heat exchanger is calculated as a function of the state of charge, using a correlation developed by West and Braun [116]:

$$\varepsilon_{charge} = 0.92 - 0.62x_{stor} + 4.93x_{stor}^2 - 17.05x_{stor}^3 + 24.02x_{stor}^4 - 12.12x_{stor}^5 \tag{79}$$

$$\varepsilon_{discharge} = 0.49 + 0.81x_{stor} - 0.98x_{stor}^2 + 0.67x_{stor}^2. \tag{80}$$

The mass flow rate of water glycol required by the storage tank is then calculated as

$$\dot{m}_{tank} = \frac{\dot{Q}_{tank}}{\varepsilon c_{wg}(T_{PCM} - T_{wg,in})}. \tag{81}$$

Table 6-1. Material properties used for the variable-temperature PCM.

Property	Value	Property	Value
Minimum PCT- Cooling	-10°C	Latent Heat	334 kJ/kg
Maximum PCT- Cooling	10°C	Specific Heat	4.18 kJ/kg-K
Minimum PCT- Heating	30°C	Density	1000 kg/m^3
Maximum PCT- Heating	50°C		

Except for the bounds on the PCT, the material properties of water are used for this PCM (since ice storage is the main benchmark for cold-storage TES). These material properties are given

in Table 6-1. A constant value is used for the specific heat of the PCM instead of accounting for the difference between the liquid-phase and solid-phase specific heat. Initial tests were done with a model where this was accounted for by making the specific heat a function of the state of charge. However, when this was done, it was possible to change the PCT at one state of charge and then change it back to its previous value at another state of charge, and thereby get a net increase in the state of charge from the sensible heating and cooling due to these changes in the PCT, even though there was no net change in the PCT. In a real system, such 'free' charging would not be possible due to energy costs for changing the PCT and because whatever method was used to change the PCT would affect the material properties of the PCM. For instance, in the metal hydride model, changing the operating temperature requires changing the pressure through the use of compressor work, so the cost of this would outweigh any benefits to the state of charge from changing the operating temperature. For an actual tunable PCM, such as the dual-ion battery design discussed in Section 2.5, changing the PCT requires altering the composition of the material, and thus its specific heat. However, since the effect of changing the PCT on specific heat is not considered in this model, and only some cases use a cost for changing the PCT, a constant specific heat is used to prevent any 'free' charging.

6.1.4 Secondary Loop Model

The model used for the secondary water glycol loop in this system is similar to that described in Section 4.2.2, except that it is simplified by the absence of an outdoor loop. Like the flow in the indoor loop in that model, the water glycol in the secondary loop changes temperature at three locations, shown in Figure 6-3. An energy balance on each component gives us the equations:

$$\dot{Q}_{hp} = \dot{m}_{wg} c_{wg} (T_1 - T_3) \tag{82}$$

$$\dot{Q}_{tank} = \dot{m}_{wg} c_{wg} (T_2 - T_1) \tag{83}$$

$$\dot{Q}_{house} = \dot{m}_{wg} c_{wg} (T_3 - T_2) = \begin{cases} -\dot{Q}_{load,house}, & cooling \\ -\left(\dot{Q}_{load,house} - \dot{Q}_{elec}\right), & heating. \end{cases} \tag{84}$$

With $\dot{Q}_{hp}$ being determined by the load-shifting control logic described in Section 6.1.5, this gives us 5 equations and 7 unknows (3 temperatures, 3 heat transfer rates, and the mass flow rate). Therefore, it is necessary to set the value of two temperatures in order to have a closed set

of equations. As in the model used with metal hydride storage, the inlet temperatures for the storage tank and heat pump (T_1 and T_3) are used for this. The tank inlet temperature T_1 needs to be defined in terms of T_{PCM} so that the storage tank is able to deliver the appropriate load. The heat pump inlet temperature T_3 is defined since it determines the performance of the heat pump, so the system should try to operate at the temperature that will optimize this performance. The following subsection describes the algorithm used to determine these temperatures and define the mass flow rate and heat transfer rates around them.

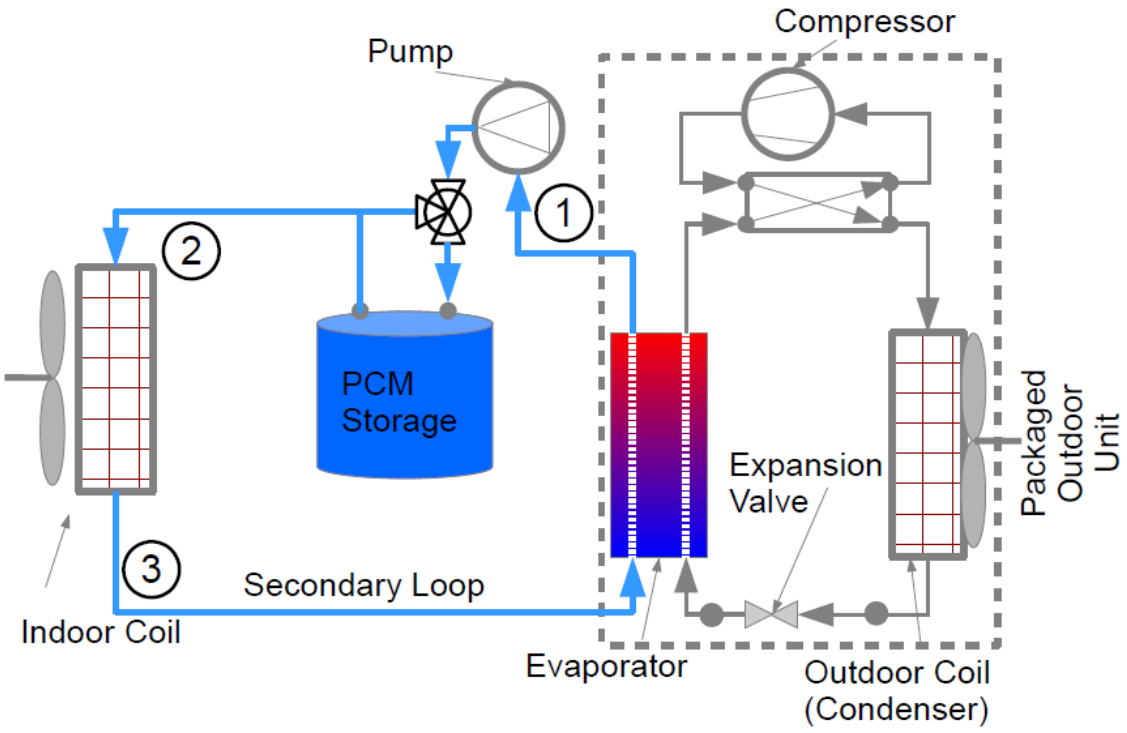

Figure 6-3. Diagram of the variable-temperature storage system (here shown operating in cooling mode) with the locations at which temperature is calculated in the model shown.

Heat pump and electric work are calculated using Eqs. 56 and 57, as in the model with metal hydride storage. Pump work is calculated using:

$$\dot{W}_{pump} = \frac{\dot{m}_{wg}}{\rho_{wg}} \Delta P_{wg.} \tag{85}$$

In this equation, ΔP_{wg} is calculated using Eq. 55. Using these work terms, in addition to the cost for changing the PCT defined by Eq. 78 and the assumed loads for non-HVAC work in the building (calculated using the EnergyPlus model), the operating cost at each time step is determined using:

$$C_{tot} = C_{hour}\left(\left(\dot{W}_{hp} + \dot{W}_{pump} + \dot{W}_{elec} + \dot{W}_{PCM} + \dot{W}_{non-HVAC}\right)\Delta t\right). \quad (86)$$

Secondary Loop Temperature Algorithm

Figure 6-4 shows the algorithm used to set the heuristic temperature values and then solve the secondary loop using those values. This algorithm includes control logic to ensure that the end result is physically possible and to avoid operating at conditions that are known to significantly reduce the performance of the system. The algorithm shown is used after the values of $\dot{Q}_{house}$ and $\dot{Q}_{hp}$ have been determined from the building load and the load-shifting control logic. The heat pump load is updated in this algorithm if changes to the operating temperatures and mass flow rate result in the capacity of the heat pump for those operating conditions being less than the heat pump load, in which case the heat pump load is reset to the calculated capacity. The heat transfer rate in the tank, $\dot{Q}_{tank}$, is calculated from $\dot{Q}_{house}$ and $\dot{Q}_{hp}$. This calculation is updated whenever $\dot{Q}_{hp}$ changes; this is not shown in Figure 6-4 to save space.

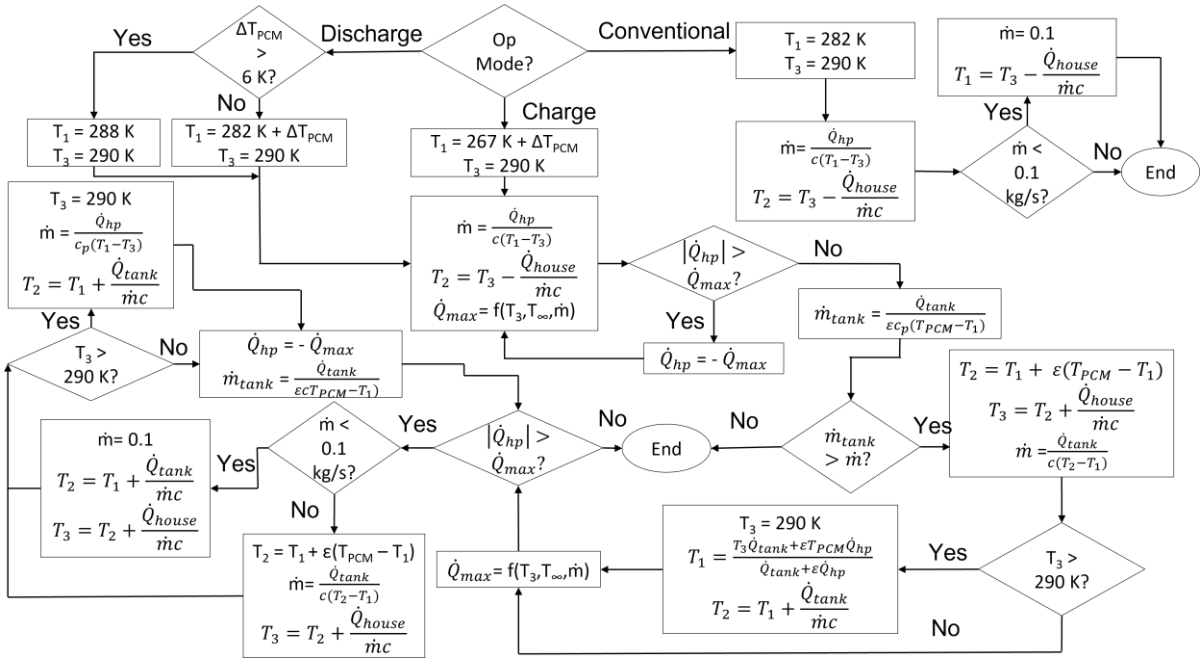

Figure 6-4. Diagram showing the control logic used to determine the operating temperatures and mass flow rate in the secondary loop for cooling mode.

For each operating mode, the algorithm initially sets heuristic setpoint values for T_1 and T_3. The value for T_1 is defined in terms of the melt temperature of the PCM (defined in Figure 6-4 by ΔT_{PCM}, the difference in PCT between the variable-temperature PCM and ice). The value for T_3 is initially set to be 290 K, or 16.9°C, which is assumed to be the maximum temperature at which water glycol can leave the house while delivering a cooling load there. Since COP increases the higher the value of T_3, the maximum value is used as the setpoint value since this will result in optimal performance. However, this maximum value is not always used in practice since it is not always possible for the system to operate at that temperature, particularly when charging the storage system. When this is the case, T_3 is defined in terms of T_1 and thus T_{PCM}. This means that changing the PCT can influence the performance of the heat pump through two different inputs to the heat pump model, since the variable PCT also affects the value of $\dot{m}_{wg}$ (since this is always calculated as a function of T_1).

The initial solution determined using the heuristic values of T_1 and T_3 must be changed if it is not possible for the system to operate at those temperatures. This can happen for two reasons: either (1) the heat pump load exceeds the heat pump capacity for these operating conditions, or (2) the mass flow rate required to deliver the load to the storage tank exceeds the water glycol mass flow rate in the secondary loop. In the first case, the magnitude of the heat pump load is set to equal the capacity and the temperatures and mass flow rates adjusted for the new value; this is repeated until the heat pump load does not exceed capacity.

For the second case, where the mass flow rate needs to be increased because the mass flow rate that needs to be sent to the storage tank exceeds the flow rate in the secondary loop, the tank outlet temperature is redefined so that the mass flow rate will equal the flow rate required by the storage tank and the house outlet temperature is adjusted accordingly. However, as seen in Figure 6-4, further checks must be made to ensure that there are no problems with this no solution. The solution is modified if the outlet temperature from the house is above its maximum possible value, or if the heat pump load is now above capacity. In solving for heat pump loads above capacity, if the mass flow rate in the secondary loop is consistently less than 0.1 kg/s, the temperatures are redefined around a flow rate of 0.1 kg/s. This is done because the COP and capacity decrease sharply for low values of $\dot{m}$ (see Section 6.2.2), so avoiding very low values will allow the system to operate at a higher capacity (and more efficiently) even if it does mean running at a less

favorable temperature. A similar increased mass flow rate is also always used in conventional mode, to improve performance in this operating mode.

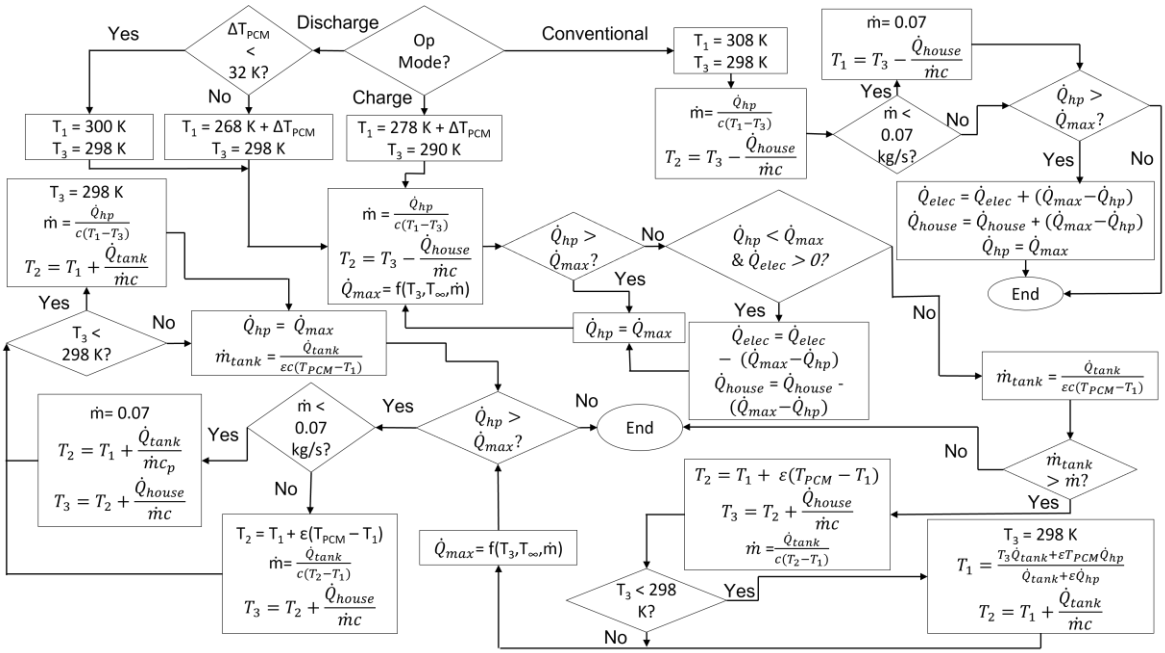

Figure 6-5. Diagram showing the control logic used to determine the operating temperatures and mass flow rate in the secondary loop for heating mode.

A very similar algorithm is used for heating mode, as shown in Figure 6-5. Here, different initial heuristic values, appropriate for heating, are used for the operating temperatures. Furthermore, when reducing the heat pump load due to its load exceeding capacity, the lost load is sometimes transferred to electric heating, and if the heat pump is operating below capacity with electric heating, some of the electric heating load is transferred to the heat pump. Finally, the cutoff for minimum mass flow rate in conventional operation or if the heat pump load exceeds capacity is lowered from 0.1 kg/s to 0.07 kg/s, because in heating mode, the optimal mass flow rate to operate as is lower and the capacity and COP do not decrease as much at low mass flow rates (as shown in Section 6.2.2).

6.1.5 Load-Shifting Control Logic

The load-shifting control logic used for the variable-temperature storage model is similar to the control logic used with metal hydride energy storage, as described in Section 4.2.4. For the

variable-temperature storage system, the same control logic is used to determine when and at what load to discharge the system, but three different alternatives are compared for charging the system.

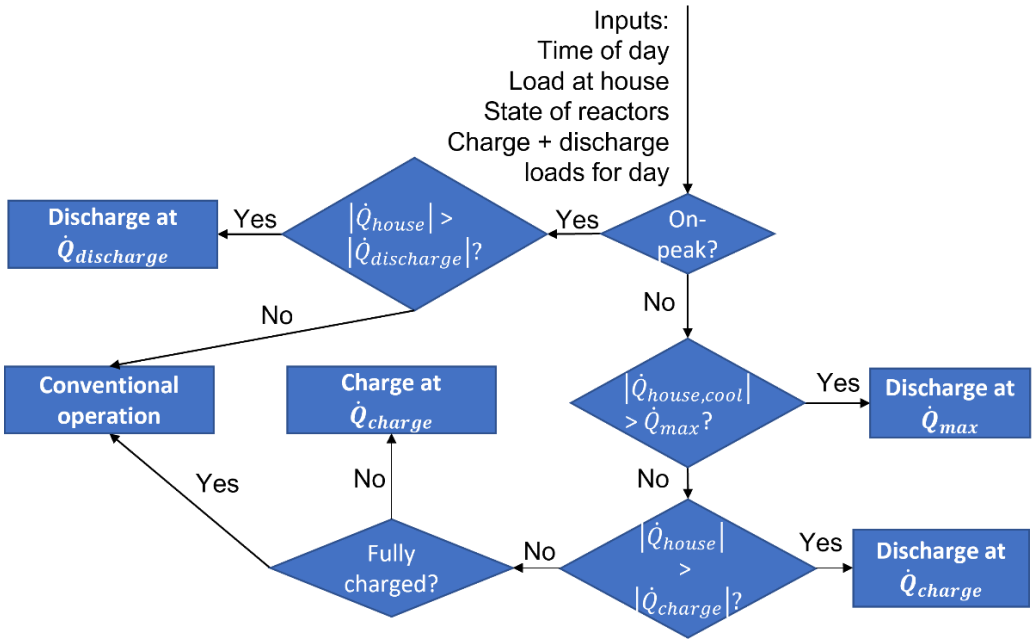

Figure 6-6. Flowchart showing the control logic for load-shifting with off-peak load limiting.

One of these three alternatives (charging at a flat load) is the control logic used for the metal hydrides. The second alternative (off-peak load-limiting) calculates $\dot{Q}_{charge}$ and $\dot{Q}_{discharge}$ using Eqs. 61 and 62, but discharges the storage system during off-peak hours if $|\dot{Q}_{house}| > |\dot{Q}_{charge}|$. The control logic used for load-shifting with off-peak load-limiting is shown in Figure 6-6. The third method (charging at capacity) is to charge the system as quickly as possible by running the heat pump at capacity, using any load in excess of the house load to charge the storage system, until the storage tank is fully charged. In this method, $\dot{Q}_{charge}$ is only used in heating mode to determine if auxiliary heating will be needed for the system to be fully charged.

The control logic used for load-shifting with charging at capacity is shown in Figure 6-7. These methods correspond to those used by Tam et al. [11] for rates with and without off-peak demand charges, respectively. All three methods handle rates with two on-peak periods described in Section 4.2.4.

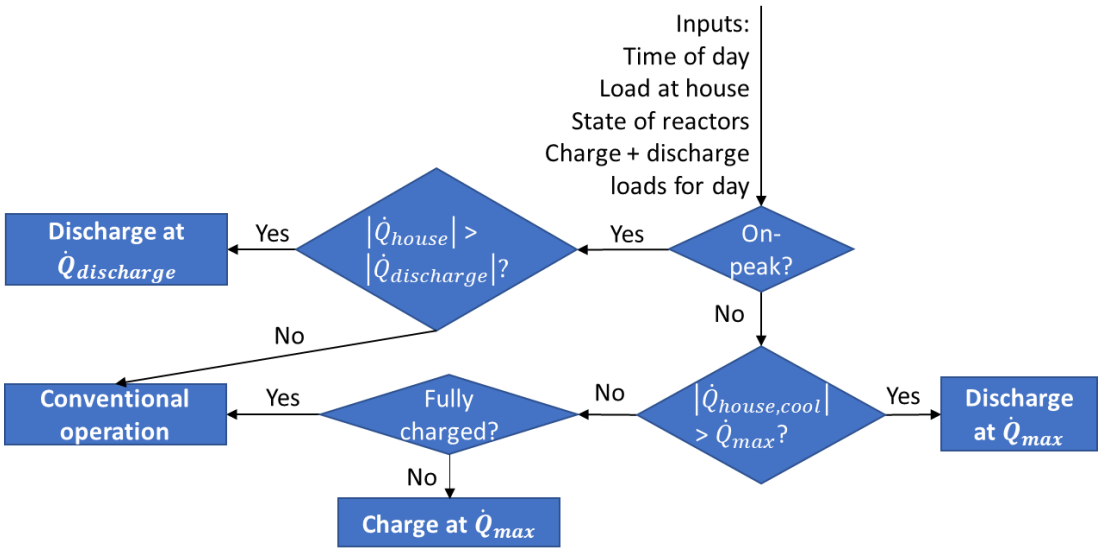

Figure 6-7. Flowchart showing the control logic for load-shifting with charging at capacity.

6.2 Heat Pump Model

6.2.1 Deriving the Heat Pump Correlations

In order to more fully assess the effect of using a variable PCT on heat pump performance, a more detailed heat pump model than the one described in Section 4.2.3 is needed. In that model, the heat pump performance is calculated from the inlet temperatures of the water glycol in the condenser and the evaporator. Since this model only uses one secondary loop, one of those temperatures would instead be simply the ambient temperature outside, and thus the inlet temperature in the secondary loop would be the only variable that affected heat pump performance that could be affected by changing the PCT. Changing the PCT would also affect pump work by changing the mass flow rate of water glycol, but pump work is not a significant driver of cost for the metal hydride system (see Section 5.2.1). However, in a real system, changing the mass flow rate of water glycol exchanging heat with the heat pump would also affect the performance of the heat pump. Therefore, this model calculates the COP and capacity of the heat pump in terms of the secondary loop mass flow rate, in addition to the water glycol temperature at the heat pump inlet and the ambient temperature.

In order to determine the effect of the mass flow rate on the heat pump performance, this model uses a more detailed model of the heat exchanger which exchanges heat with the secondary

loop (the evaporator in cooling mode, the condenser in heating mode) instead of assuming a pinch point temperature. A pinch point temperature is still assumed for the air heat exchanger (the condenser in cooling mode, the evaporator in heating mode). Since the mass flow rate of air in this heat exchanger is unconstrained, unlike the water glycol flow rate, and could therefore be set to any suitable value, it is less important to determine its effect on system performance. Similarly, the assumptions used for superheat, subcooling, heat exchanger pressure loss, and the expansion valve in Section 4.2.3 are still used. A 10-factor compressor model is still used, but in this case the map is for an Emerson YHV0211U-3X9-ABK scroll compressor [117], since this model performs better in heating mode.

Evaporator Model

Figure 6-8 shows a diagram of the model used for the evaporator. The heat exchanger being modelled is a plate heat exchanger, with a length (l_{HX}) of 0.6 m, a height (d_{HX}) of 0.25 m, a channel volume of 200 cm^3, and 300 plates. The model of the heat exchanger divides it into two zones. In the first (two-phase) zone, refrigerant enters the heat exchanger as a two-phase mixture and is heated until it becomes fully gaseous (q = 1). In the second (one-phase) zone, the gaseous refrigerant is superheated. Since water glycol flow moves counter-flow to the refrigerant, an energy balance on a pair of channels (where refrigerant is flowing through one and water glycol through the other) gives the equations:

$$\dot{Q}_{1P} = \dot{m}_{wg,ch} c_{wg} \left(T_{wg,in} - T_{wg,mid}\right) = \dot{m}_{ref,ch} \left(h_1 - h(q = 1, P_1)\right) \quad (87)$$

$$\dot{Q}_{2P} = \dot{m}_{wg,ch} c_{wg} \left(T_{wg,mid} - T_{wg,out}\right) = \dot{m}_{ref,ch} (h(q = 1, P_1) - h_4). \quad (88)$$

The effectiveness of the two-phase zone is calculated using the relation for a heat exchanger where one side is constant-temperature [103], since the refrigerant does not change temperature until it becomes one-phase. For the one-phase zone, it is assumed that a counter-flow effectiveness relation for a pair of channels can be used for the plate heat exchanger as a whole [118]. Thus, the effectiveness for each zone is calculated and used as follows:

$$\varepsilon_{1P} = \frac{1 - e^{-(1-C^*)NTU_{1P}}}{1 - C^* e^{-(1-C^*)NTU_{1P}}} \quad (89)$$

$$\varepsilon_{2P} = 1 - e^{-(1-C^*)NTU_{2P}}. \quad (90)$$

$$\dot{Q}_{1P} = \varepsilon_{1P} \dot{m}_{ref,ch} \left(h\left(T = T_{wg,in}, P_4\right) - h(q = 1, P_1)\right) \quad (91)$$

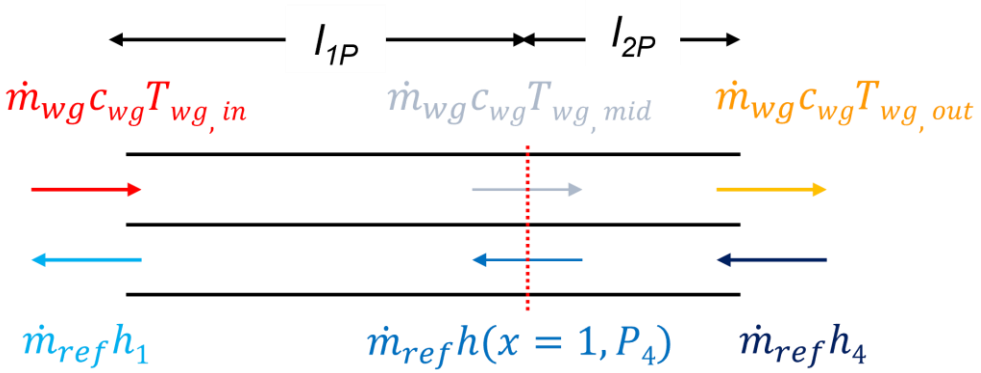

Figure 6-8. Diagram of the flow in the plate heat exchanger used as an evaporator in cooling mode. In the two-phase (2P) zone, refrigerant is heated until it is fully gas. In the one-phase (1P) zone, gaseous refrigerant is superheated.

$$\dot{Q}_{2P} = \varepsilon_{2P}\dot{m}_{wg,ch}c_{wg}\left(T_{wg,mid} - T_4\right) \tag{92}$$

The number of transfer units in each section is calculated using the equations:

$$NTU_{1P} = \frac{h_{conv,ref,1P}h_{conv,wg}}{h_{conv,ref,1P}+h_{conv,wg}}\frac{l_{1P}d_{HX}}{\dot{m}_{wg,ch}c_{wg}} \tag{93}$$

$$NTU_{2P} = \frac{h_{conv,ref,2p}h_{conv,wg}}{h_{conv,ref,2p}+h_{conv,wg}}\frac{l_{1P}d_{HX}}{\dot{m}_{wg,ch}c_{wg}} \tag{94}$$

The water glycol and one-phase refrigerant heat transfer coefficients are calculated using Eq. 2 (with the material properties updated). A correlation developed by Ayub for evaporation in a plate heat exchanger [119] is used to calculate the two-phase refrigerant heat transfer coefficient:

$$h_{conv,ref,2p} = \left(0.1121\frac{ft*lb_m}{BTU}\right)^{0.4124}\frac{k_{ref,L}}{D_{Hy,ch}}\left(\frac{Re_L^2 L_{ref}}{L_{2P}}\right)^{0.4124}\left(\frac{P_{ref}}{P_{c,ref}}\right)^{0.12}\left(\frac{65°}{\theta}\right)^{0.35}. \tag{95}$$

In this equation, θ is the chevron angle, assumed to be 40°. These equations are solved using the assumptions for superheat and pressure drop discussed above, as well as knowledge of the total length of, and heat transfer in, the evaporator:

$$\dot{Q}_{evap} = \frac{n_{plates}}{2}\left(\dot{Q}_{1P} + \dot{Q}_{2P}\right) \tag{96}$$

$$l_{HX} = l_{2P} + l_{1P} \tag{97}$$

Since the evaporation temperature, T_{evap}, is determined based on T_1 and the assumed superheat, and the ten-factor compressor model uses T_{evap} as an input, the evaporator model will affect the heat pump COP and capacity, which are calculated using the compressor model.

Condenser Model

A diagram of the model used for the condenser is shown in Figure 6-9. Since the condenser in heating mode is the same heat exchanger that is used as an evaporator in cooling mode, the same dimensions are used. The calculations for the condenser differ primarily in that here flow is entering as a gas and leaving as a liquid (while in the evaporator, flow is already two-phase when entering), meaning that three zones are needed to model the condenser instead of two. The energy balances for these zones are:

$$\dot{Q}_G = \dot{m}_{wg,c} c_{wg} \left(T_{wg,mid,G} - T_{wg,out}\right) = \dot{m}_{r,ch} \left(h(q=1,P_2) - h_2\right) \quad (98)$$

$$\dot{Q}_{2P} = \dot{m}_{wg,ch} c_{wg} \left(T_{wg,mid,L} - T_{wg,mid,G}\right) = \dot{m}_{ref,ch} \left(h(q=1,P_2) - h(x=0,P_2)\right) \quad (99)$$

$$\dot{Q}_L = \dot{m}_{wg,ch} c_{wg} \left(T_{wg,in} - T_{wg,mid,L}\right) = \dot{m}_{ref,ch} \left(h_3 - h(q=0,P_2)\right). \quad (100)$$

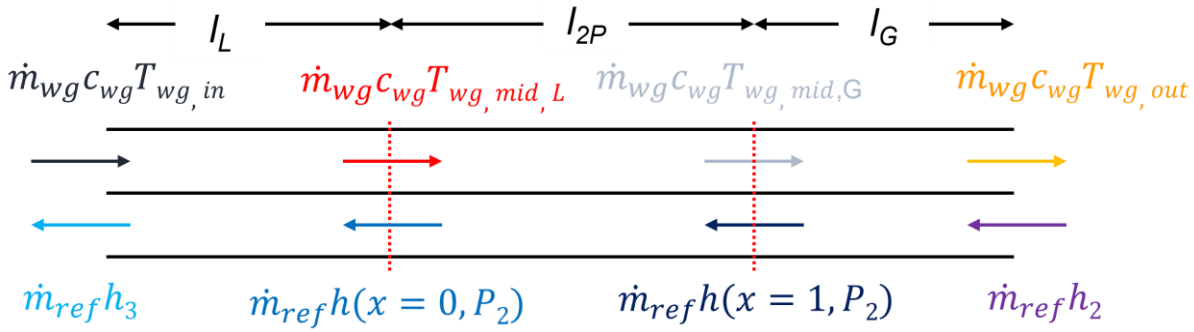

Figure 6-9. Diagram of the flow in the plate heat exchanger used as a condenser in heating mode. In the gas (G) zone, gaseous refrigerant is cooled until it reaches saturation temperature. In the two-phase (2P) zone, refrigerant is cooled until it is fully liquid. In the liquid (L) zone, liquid refrigerant is subcooled.

As with the evaporator, a constant-temperature effectiveness relation is used for the two-phase zone, and a counterflow effectiveness relation is used for both of the one-phase zones. Thus, for the two-phase zone, Eqs. 90 and 94 are used to find the effectiveness, with the only difference being that h_{2p} is now calculated using a correlation for condensation in a plate heat exchanger developed by Yan et al. [120]:

$$Nu = \frac{h_{conv,ref,2p} D_{Hy,ch}}{k_{ref,L}} = 4.118 Re^{0.4} \mathrm{Pr}^{\frac{1}{3}}. \quad (101)$$

For both the liquid and the gas phases, Eqs. 89 and 93 are used to find the effectiveness (in terms of the length of the particular zone, l_G or l_L). The effectiveness values for these three zones are then used in the equations:

$$\dot{Q}_G = \varepsilon_G \dot{m}_{r,ch} c_{p,ref} \left(T_{wg,mid,G} - T_2\right) \tag{102}$$

$$\dot{Q}_{2P} = \varepsilon_{2P} \dot{m}_{wg,ch} c_{wg} \left(T_{wg,mid,L} - T_4\right) \tag{103}$$

$$\dot{Q}_L = \varepsilon_L \dot{m}_{r,ch} c_{p,ref} \left(T_{wg,in} - T_{cond}\right). \tag{104}$$

As in the evaporator model, the known total heat transfer and length are also used in solving the condenser:

$$\dot{Q}_{cond} = \frac{n_{plates}}{2} \left(\dot{Q}_G + \dot{Q}_{2P} + \dot{Q}_L\right) \tag{105}$$

$$l_{HX} = l_G + l_{2P} + l_L. \tag{106}$$

These equations are then used to solve the condenser. The solution for the condenser, combined with the assumed superheat, subcooling, and pressure drop, is used to solve the heat pump. The condenser calculations affect the ultimate heat pump performance calculations since the condensation temperature, T_{cond}, is both an input to the compressor model and an output of the condenser model (since it is a function of T_3 and the assumed subcooling). However, since T_2 is both an output of the compressor model and an input of the condenser model, the two models are solved iteratively together, unlike in cooling mode where the compressor and evaporator models can be solved independently since the compressor solution does not affect any of the inputs to the evaporator model.

Table 6-2. Ambient and water glycol temperatures for which results are shown in Figure 6-10 and Figure 6-12.

Ambient Temperature	Value	Water Glycol Temperature	Value
$T_{air,1}$	20°C	$T_{wg,1}$	0°C
$T_{air,2}$	30°C	$T_{wg,2}$	10°C
$T_{air,3}$	40°C	$T_{wg,3}$	18.5°C
$T_{air,4}$	-10°C	$T_{wg,4}$	20°C
$T_{air,5}$	0°C	$T_{wg,5}$	30°C
$T_{air,6}$	10°C	$T_{wg,6}$	40°C
$T_{air,7}$	15°C		

6.2.2 Correlations for Cooling and Heating Mode

The heat pump model described in Section 6.2.1 is used to develop 20-factor correlations for COP and capacity in terms of ambient temperature, water glycol inlet temperature, and water glycol mass flow rate for both heating and cooling mode. These correlations are of the form:

$$COP\ (or\ Q_{max}) = a_1 T_\infty + a_2 {T_\infty}^2 + a_3 {T_\infty}^3 + a_4 T_{wg,in} + a_5 {T_{wg,in}}^2 + a_6 {T_{wg,in}}^3 + a_7 \dot{m}_{wg} + a_8 {\dot{m}_{wg}}^2 + a_9 {\dot{m}_{wg}}^3 + a_{10} T_\infty T_{wg,in} + a_{11} T_\infty \dot{m}_{wg} + a_{12} \dot{m}_{wg} T_{wg,in} + a_{13} {T_\infty}^2 T_{wg,in} + a_{14} {T_\infty}^2 \dot{m}_{wg} + a_{15} \dot{m}_{wg} {T_{wg,in}}^2 + a_{16} T_\infty {T_{wg,in}}^2 + a_{17} T_\infty {\dot{m}_{wg}}^2 + a_{18} {\dot{m}_{wg}}^2 T_{wg,in} + a_{19} T_\infty T_{wg,in} \dot{m}_{wg} + a_{20}. \quad (107)$$

To obtain these correlations for cooling mode, the model is run for mass flow rates from 0.11 kg/s to 0.50 kg/s, ambient temperatures from 20°C to 45°C, and water glycol inlet temperatures from 0°C to 20°C. For heating mode, the model is run for mass flow rates from 0.05 kg/s to 0.45 kg/s, ambient temperatures from -100°C to 15°C, and water glycol inlet temperatures from 20°C to 42°C. For COP and capacity in both operating modes, a correlation is found that minimizes error compared to the output of this model, and these correlations are used to calculate COP and capacity in the system model described in Section 6.1.

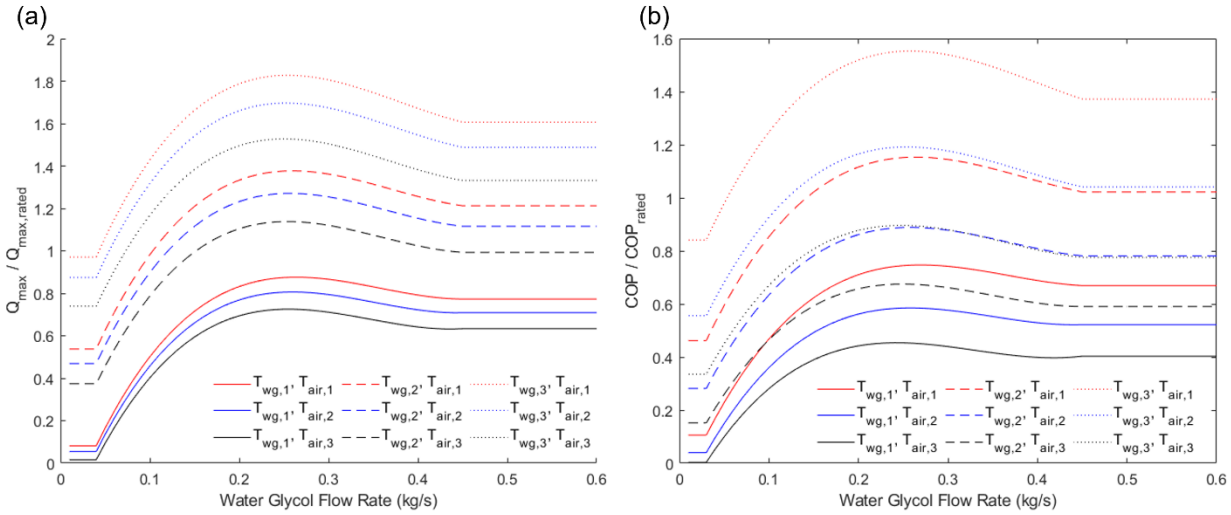

Figure 6-10. (a) Capacity and (b) COP in cooling mode as a function of mass flow rate for a range of water glycol and air temperatures. The COP correlation is used for 0.03 kg/s < $\dot{m}_{wg}$ < 0.45 kg/s and the capacity correlation for 0.04 kg/s < $\dot{m}_{wg}$ < 0.45 kg/s; outside this range, neither changes with $\dot{m}_{wg}$.

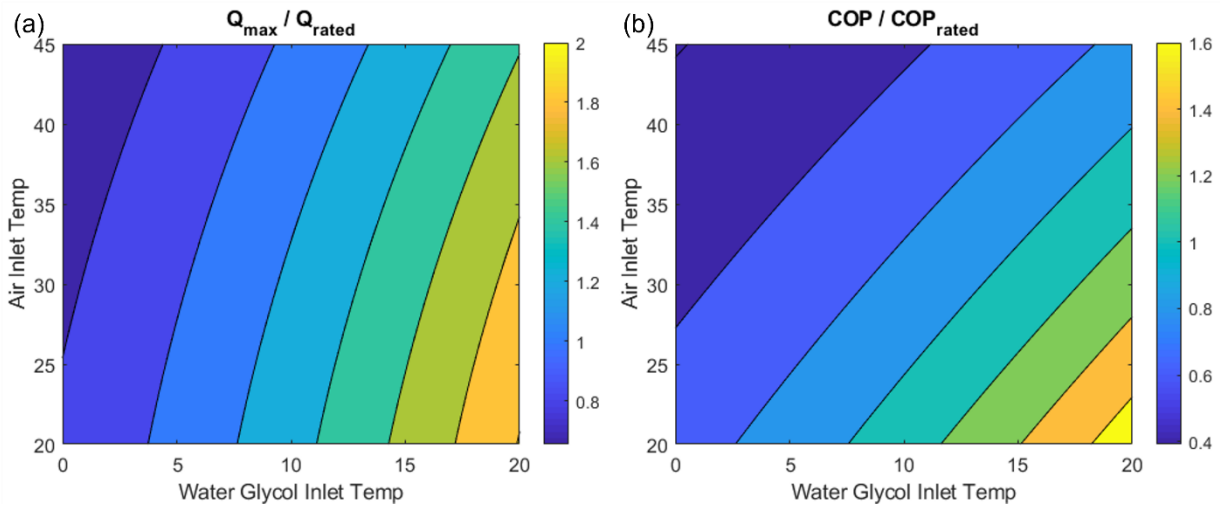

Figure 6-11. (a) Capacity and (b) COP in cooling mode as a function of air and water glycol temperature for a mass flow rate of 0.2 kg/s.

These correlations are only accurate within a certain range; for high mass flow rates, each of them starts to see an increase in the COP and capacity as mass flow rate increases, which is not present in the output of the heat pump model. Therefore, each correlation is only used up to a certain maximum mass flow rate; above this value, the COP and capacity are treated as a constant.

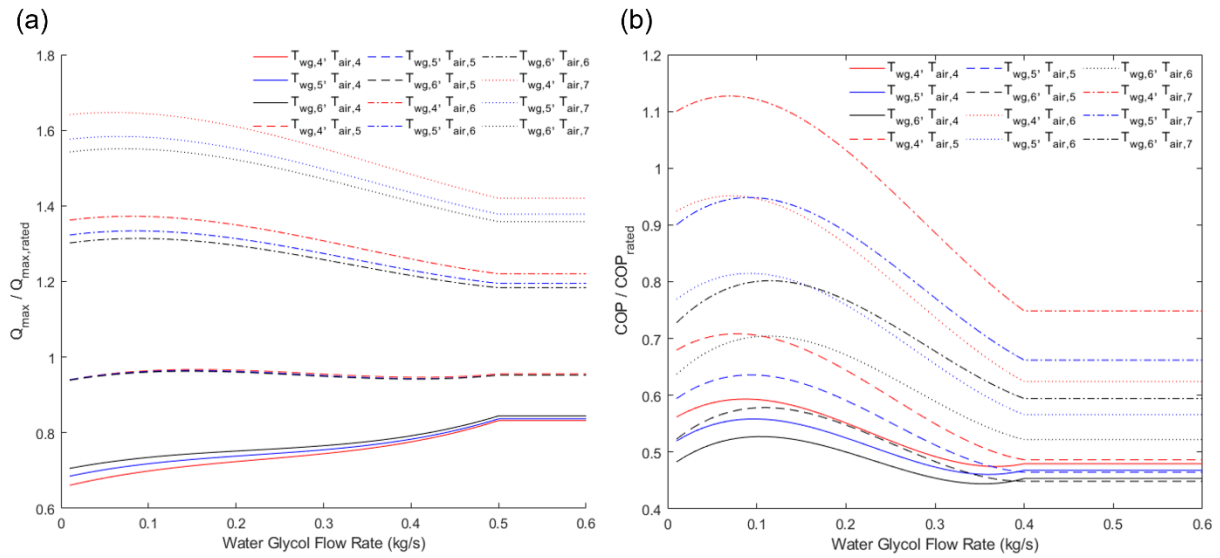

Figure 6-12. (a) Capacity and (b) COP in heating mode as a function of mass flow rate for a range of water glycol and air temperatures. The COP correlation is used for $\dot{m}_{wg}$ < 0.4 kg/s and the capacity correlation for $\dot{m}_{wg}$ < 0.5 kg/s; outside this range, neither changes with $\dot{m}_{wg}$.

Similarly, the COP and capacity are also treated as constant for very small mass flow rates in cooling mode, to reduce the likelihood a non-physical below-zero result (this is also avoided by the control logic that avoids low mass flow rates described in Section 6.1.4). However, the range in which the correlations are valid is the range in which the system usually operates, except for occasional very high or low loads.

For cooling mode, the dependence of COP and Q_{max} on mass flow rate for different ambient and water glycol temperatures can be seen in Figure 6-10. The ambient and water glycol temperatures for which results are plotted in this figure and the heating results in Figure 6-12 are given in Table 6-2. The temperature-dependence of COP and Q_{max} for a fixed mass flow rate can be seen in Figure 6-11. As seen in Figure 6-10, the optimal mass flow rate is in the range $0.2 < \dot{m}_{wg} < 0.25$ across a range of operating temperatures, with the exact value depending on these temperatures. The results in Figure 6-11 show that the COP and capacity have a similar dependence on the ambient and water glycol inlet temperatures as in the heat pump model described in Section 4.2.3.

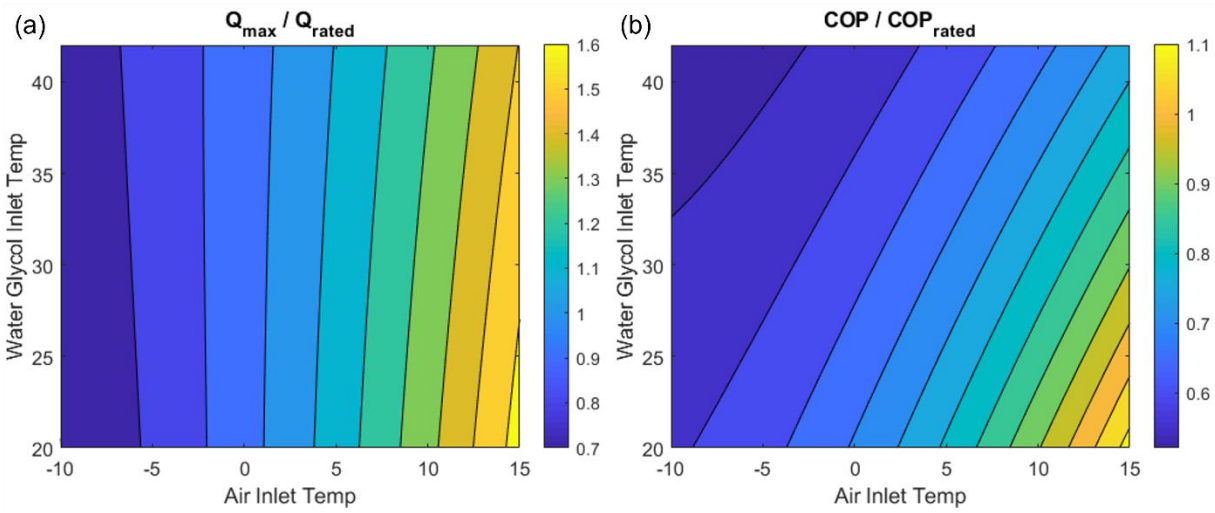

Figure 6-13. (a) Capacity and (b) COP in heating mode as a function of air and water glycol temperature for a mass flow rate of 0.1 kg/s.

For heating mode, the dependence of COP and Q_{max} on mass flow rate for different ambient and water glycol temperatures can be seen in Figure 6-12. The temperature-dependence of COP and Q_{max} for a fixed mass flow rate can be seen in Figure 6-13. Here, the optimal mass flow rate is significantly lower than in cooling mode, being somewhere closer to $\dot{m}_{wg} = 0.1$ kg/s, with the

exact value depending on the operating temperature. As with cooling mode, the temperature-dependence of the COP and capacity is very similar to that seen in Section 4.2.3. Worth noting in these results is that capacity is primarily dependent on the ambient temperature, unlike capacity in cooling mode and COP in both modes, which are more affected by changes in the water glycol temperature and mass flow rate.

6.3 The Optimization Problem for Determining the Phase-Change Temperature

The model described in Section 6.1 is used to determine the electricity consumption and resulting operating costs for a variable-temperature TES system given input values for the PCT of the storage material at each time step. To determine the potential cost savings from variable-temperature TES, an optimization problem is solved to determine which values for the PCT result in the lowest operating costs for the building. This optimization problem is solved for each day in the simulation, with each day starting at the end condition from the case which achieved optimal results the previous day. The optimization problem being solved has the form

$$\begin{aligned} &\min costfnc\left(T_{m,PCM}(t), T_{\infty}(t), \dot{Q}_{load,house}(t)\right) \\ &s.t\ T_{m,PCM,min} < T_{m,PCM} < T_{m,PCM,max}. \end{aligned} \tag{108}$$

In this equation, the minimum and maximum PCT values, $T_{m,PCM,min}$ and $T_{m,PCM,max}$, are given in Table 6-1 and the cost function is calculated (for rates without demand charges) using:

$$costfnc\left(T_{m,PCM}(t), T_{\infty}(t), \dot{Q}_{load,house}(t)\right) = \sum_{day} C_{tot} + C_{pen,rem\ charge}. \tag{109}$$

The cost penalty $C_{pen,rem\ charge}$, which is included in the cost function for optimization but not in the actual operating cost calculations, is intended to represent the approximate cost of charging the system from its state at the end of the day if the system is not fully charged at that time:

$$C_{pen,rem\ charge} = C_{off-peak}\frac{(0.9-x_{stor})E_{stor,PCM}}{COP_{est}}. \tag{110}$$

This penalty is used because the optimization period (a calendar day) does not align with one cycle of charging and discharging the storage system (which would start either at the beginning or the end of the on-peak period). Therefore, without this cost penalty, there is the possibility of the solver finding a solution that minimizes cost for the day by doing less charging after the on-peak period, thereby reducing the operating costs for the day by transferring some of these costs to the next day (resulting in higher overall costs, since the solver can only reduce the rate of

charging by changing the PCT to one where the heat pump is less efficient). With the penalty $C_{pen,rem\,charge}$ included, this is no longer optimal even when only considering one day. Solving the optimization problem for a time period of a week is examined as an alternate way to avoid this problem (since the period would end during the weekend, when the system would not be in the middle of a charge-discharge cycle due to the lack of an on-peak period). However, for most cases, it results in an increased computation time without improving the performance compared to optimizing for a day while using the cost penalty given in Eq. 110.

For rates with demand charges, the cost function is modified to penalize increasing the peak work for the month so far, since this results in increased costs at the end of the month when demand charges are calculated. Thus, the modified cost function used for rates with demand charges is

$$costfnc\left(T_{m,PCM}(t), T_{\infty}(t), \dot{Q}_{load,house}(t)\right) = \sum_{day} C_{tot} + C_{pen,partial\,charge} + C_{pen,demand}. \tag{111}$$

The penalty for increasing the peak work that determines the cost from demand charges, $C_{pen,demand}$, is calculated by:

$$C_{pen,demand} = C_{demand,on-peak} \max\left(\dot{W}_{max,on-peak,day} - \dot{W}_{max,on-peak,prev}, 0\right) + C_{demand,off-peak} + \max\left(\dot{W}_{max,off-peak,day} - \dot{W}_{max,off-peak,prev}, 0\right). \tag{112}$$

In this equation, $\dot{W}_{max,on-peak,day}$ and $\dot{W}_{max,off-peak,day}$ are the maximum on-peak and off-peak work for the day, while $\dot{W}_{max,on-peak,prev}$ and $\dot{W}_{max,off-peak,prev}$ are the maximum on-peak and off-peak work for previous days that month.

The optimization problem is solved by surrogate optimization, using the surrogateopt function from Matlab. In testing, this function was found to consistently outperform any of the algorithms used by the fmincon function (Interior Point, Active Set, and Sequential Quadratic Programming). This superiority is likely because surrogateopt is searching for a global, rather than a local, minimum, and because its memory retains the best solution it has found so far and outputs that rather than the solution from its final iteration.

The optimization problem is solved for different frequencies for changing the PCT. As a benchmark, all cases are compared to the case where a constant PCT of 10°C is used for cooling mode and a constant PCT of 30°C is used for heating mode. These values are used as the benchmark because they result in the most favorable water glycol inlet temperatures, and thus are

generally most likely to result in optimal cost savings. Optimal PCT values and resulting cost savings are calculated for the case where a single PCT is used each day, as well as for shorter time steps that the length of a day is evenly divisible by (1, 2, 3, 4, 6, 8, and 12 hours). In addition to comparing results for fixed time steps, optimal PCT values are also calculated for an algorithm that uses two PCT values for a day based on the operating mode of the system, as described in Section 6.3.1.

6.3.1 Optimal Temperatures for Charge and Discharge Mode

Using a constant time step may not be the way to get the largest cost savings from the fewest changes in the PCT because one major reason to change the PCT is to account for a change in the operation mode- from charging to discharging- since the operating temperatures are defined differently in terms of PCT for different operating modes. Since a constant time step might not line up with the on-peak and off-peak periods (unless a 1-hour step is used), better results could be obtained if the PCT is defined based on whether the system is charging or discharging. However, simply using one value of the PCT when charging and one when discharging was found in initial tests to not work as well as using a constant time step of any length shorter than a full day. This is because when the PCT is decreased in cooling mode, or increased in heating mode, the state of charge decreases. In cooling mode, this happens because the PCM is now at a temperature above its melt temperature, so some of the PCM melts until this provides enough cooling to bring the temperature down to the new PCT. Similarly, in heating mode, some of the PCM freezes until the temperature increases to the new PCT. Thus, if this happens when the system begins to discharge, the lost charge cannot be made up by charging (since it is already an on-peak period) and so less of the load will be met by the storage system. Therefore, to examine a strategy that uses different PCTs for charging and discharging, it is necessary to switch to the discharge PCT during the off-peak period so that any charging needed to make up for lost charge can be done before the on-peak period.

The next simplest alternate would be to use one PCT from the end of the off-peak period until the system is fully charged, then switch to the other PCT and stay at it until the end of the on-peak period. However, if the system becomes fully charged before the end of the day (which is common when using the load-shifting control logic shown in Figure 6-7), then changing the PCT

in a way that lowers the state of charge will increase costs for that calendar day but lower costs on the next calendar day. Since the system uses calendar days as its optimization period, this would discourage changes to the PCT that would save costs overall because the cost savings would only occur in the next optimization period.

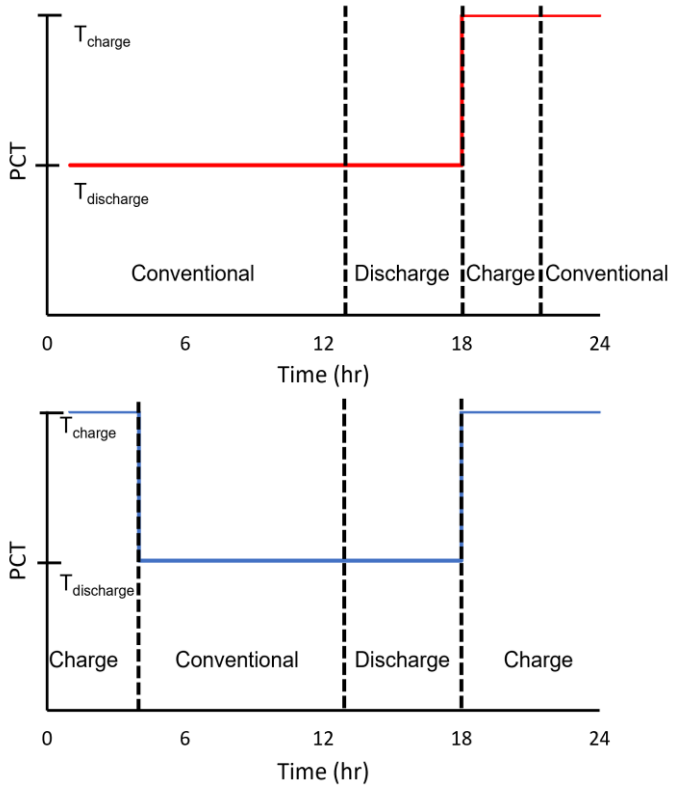

Figure 6-14. Diagram showing the operating mode and PCT for a system using the logic described in this section to determine the PCT for two cases, one (top) where the system finishes charging before the end of the day and the other (bottom) where it finishes charging in the morning. The discharge period shown in both figures corresponds to the on-peak period.

To avoid this issue, the control logic for determining the PCT instead stays at the charge value until the end of the calendar day even if the system becomes fully charged. This results in the cycle of charging and discharging lining up more closely with a calendar day, since if the system does finish charging before the end of the calendar day, each calendar day will include the system running conventionally until the on-peak period, fully discharging during the on-peak period, and fully charging afterwards. If the system does not finish charging by the end of the day, the mismatch between a calendar day and a cycle is still not a concern since any change in the PCT will still occur on the same day as whatever benefits it brings. A diagram showing when the PCT changes according to this control logic can be seen in Figure 6-14.

6.4 Alternate Design for Charging Mode

For the residential ice storage system considered by Tam *et al.* [11,24] and the metal hydride system described in Chapter 4, when a load is being delivered to both the house and the storage tank, the water glycol in the secondary loop flows from the heat pump to the storage tank to the indoor unit, and then back to the heat pump, as shown in Figure 2-1 and Figure 4-3. This is done in charging mode for ice storage since the storage tank needs to be charged at a temperature lower than the phase-change temperature, which for a fixed-temperature system must be lower than the temperature at which the load is delivered to the house. In discharging mode, it is done to improve the performance of the heat pump, since it provides its cooling load first before the storage tank, and thus operates at a higher evaporation temperature than if it was cooling a flow that had already been cooled by discharging the storage tank.

While this reason still applies for the variable-temperature storage case, it is no longer the case that the PCM must be charged at a lower temperature than the house is cooled at, since it is possible to increase the PCT while charging and then decrease it before discharging. Therefore, it may be more efficient in charging mode for the water glycol to flow from the heat pump to the indoor unit, and then to the storage tank, if the PCM does not need to be charged at a lower temperature than the house. This would allow the storage tank to be charged at higher temperatures than would be possible if the outlet flow from the storage tank were then used to provide the cooling load at the house. Charging the storage tank at this higher temperature would in turn allow the heat pump to operate at a higher temperature than the maximum outlet temperature of the house.

A diagram of a system that uses this proposed design is shown in Figure 6-15. While the logic behind this system design has been described for, and the system in Figure 6-15 is shown in, cooling mode, the same logic also applies to heating mode. Charging the storage tank with the house outlet flow in heating mode allows for the heat pump to operate at a lower condensation temperature, and thus a higher COP.

Since this system design requires the use of higher PCT values in charging mode than are possible in discharge mode, the PCT must always change from the higher value to the lower before the beginning of the on-peak period. Therefore, this model is always used with the control logic for different PCT values for charge and discharge modes described in Section 6.3.1, rather than using a time step for tuning the PCT. However, one modification is made to this control logic. Since the optimal temperature for charging is often outside the range of possible temperatures for

discharge, the problem of the system not switching to an appropriate discharge temperature if the cost benefits occur on the next calendar day is lessened (since the system must switch to a different temperature for discharge mode due to the different bounds). Furthermore, in heating mode, if there is an on-peak period in the morning, the system only has a few hours to make up any charge lost due to the change in PCT if this occurs at the beginning of the calendar day (this is only the case if there is not also an evening on-peak period, since in that case, the system is charged in the afternoon rather than at night). Since the loss of charge is greater for this system due to the larger change in PCT, and since heating loads are often high in the early hours of the day, the system would not always be able to make up the lost charge before the beginning of the on-peak period. Therefore, for the case of heating mode with a morning (and no evening) on-peak period, the PCT changes from the charge to discharge value as soon as the system is fully charged, even if this is before the end of the calendar day.

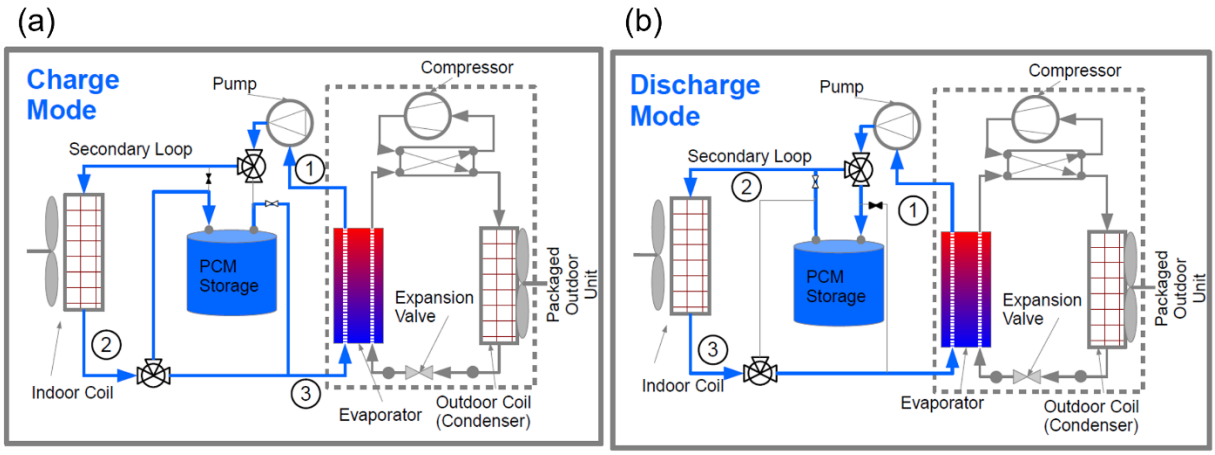

Figure 6-15. Diagram of the proposed alternate system design, where the storage tank is charged with the outlet flow from the house rather than the house cooled with the outlet flow from the storage tank. The system is shown in (a) cooling charge mode and (b) cooling discharge mode, but the secondary loop flow is the same for heating mode.

The model of this system is very similar to the system model described in Section 6.1, using the same load calculations, storage tank model, and load-shifting control logic. Other than the changes to the minimum and maximum PCT values in charging mode seen in Table 6-3, the only difference is in the secondary loops model. Here, Eq. 82 is still used, and Eqs. 83-84 are still used if the system is operating in discharge mode (or in charge mode after switching to the discharge temperature for the PCM). However, when charging the system with the PCM at a higher

PCT (or a lower PCT, in heating mode), the modified flow in the secondary loop means that the energy balances on the storage tank and the house are now

$$\dot{Q}_{house} = \dot{m}_{wg} c_{wg} (T_2 - T_1) = \begin{cases} -\dot{Q}_{load,house}, & cooling \\ -\left(\dot{Q}_{load,house} - \dot{Q}_{elec}\right), & heating. \end{cases} \quad (113)$$

$$\dot{Q}_{tank} = \dot{m}_{wg} c_{wg} (T_3 - T_2). \quad (114)$$

In addition, the algorithm used to determine the operating temperatures in the secondary loop is modified for charging mode to reflect the change in system design. The algorithms described by Figure 6-4 and Figure 6-5 are still used for conventional operation, discharge mode, and charge mode when operating at the discharge PCT (to make up the charge lost after the PCT has been lowered from its charge value). However, a different algorithm is used when charging at the charge PCT. This algorithm for cooling mode is shown in Figure 6-16. Since the house outlet is now T_2 instead of T_3, it is this value that is initially defined as 290 K. To ensure the best performance of the heat pump, the tank outlet temperature T_3 is defined based on the assumption that all of the water glycol is sent to the storage tank ($\dot{m}_{wg} = \dot{m}_{tank}$), since this will maximize the inlet temperature to the heat pump.

Table 6-3. Minimum and maximum values of the PCT used by the model where the storage system is charged with the outlet flow from the house.

Operating Mode	**Minimum PCT**	**Maximum PCT**
Cooling Charge	5°C	25°C
Cooling Discharge	-10°C	10°C
Heating Charge	30°C	50°C
Heating Discharge	15°C	35°C

Most of the rest of the algorithm involves checking for the same things as in Figure 6-4: that the heat pump load does not exceed capacity, that the mass flow rate in the storage tank is not greater than the secondary loop mass flow rate, and that the mass flow rate is not a low value that will hurt the system performance. In addition, the control logic also includes a check to prevent low values for the house inlet temperature, T_1, since this temperature is freely-defined in this algorithm instead of being a setpoint value and might be set to unrealistically low values without this restriction.

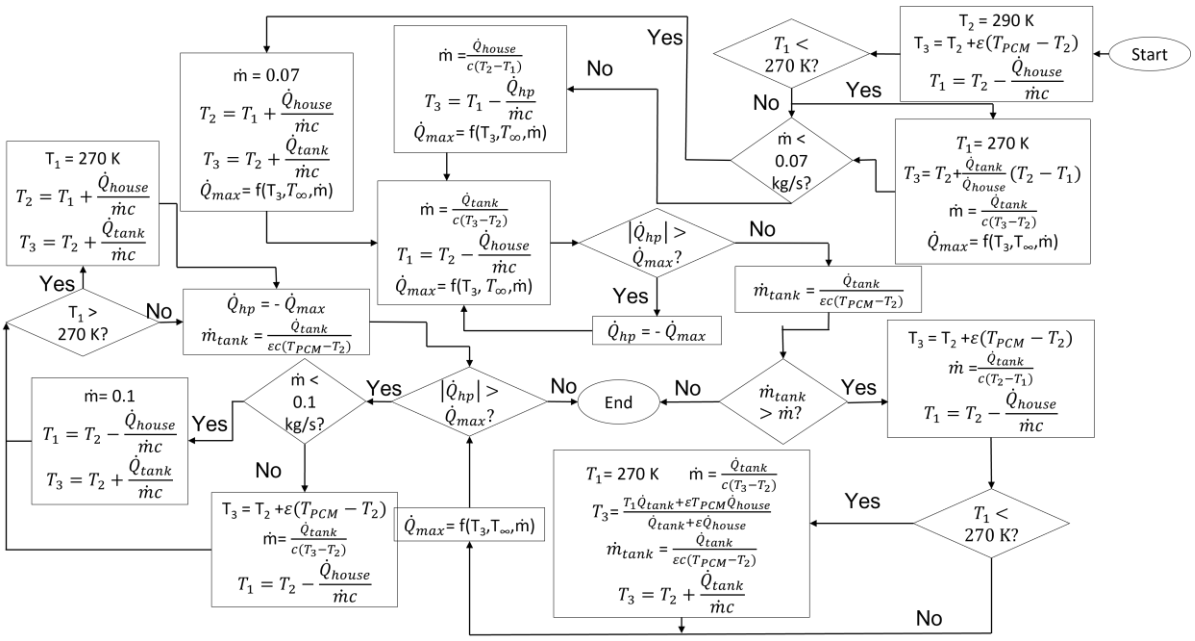

Figure 6-16. Diagram showing the control logic used to determine the operating temperatures and mass flow rate in the secondary loop when the storage tank is being charged with the house outlet flow in cooling mode.

6.5 2-PCM Model

In addition to the variable-temperature storage models described in Sections 6.1 and 6.4, a model of a system that uses two separate PCMs for cold storage and heat storage is also created for use as a benchmark against which variable-temperature storage could be compared. The system architecture for this model is shown in Figure 6-17; it differs from the variable-temperature storage model only by having two storage tanks, only one of which is being charged or discharged at any given time. The model uses the same load calculations and load-shifting control logic as the variable-temperature storage model, and the secondary loop model differs only in that all values in the secondary loop temperature algorithm that are defined in terms of the variable PCT in Section 6.1.4 are instead fixed values, since the PCT does not change for the PCMs used in this model.

The most significant differences between this model and the variable-temperature storage model are in the storage tank model. Since there is no change in the PCT, both PCMs always remain at the same temperature throughout operation, so $\dot{Q}_{sens}$ = 0 (and thus $\dot{Q}_{tank} = \dot{Q}_{lat}$) at all times. Eqs. 74-75 and 79-81 are still used to update the state of charge and determine the required

mass flow rate as they are for the variable-temperature storage model. However, Eq. 76 is not used since it is only applicable in cases with sensible heating. While the logic used to determine whether the cold storage or heat storage system will be charged and discharged on a particular day is the same as that described in Section 6.1.3, Eq. 77 is not used since the same system is not used for storage in both cases. Instead, the model keeps track of two separate state- of-charge values for heating and cooling, $x_{stor,cool}$ and $x_{stor,heat}$.

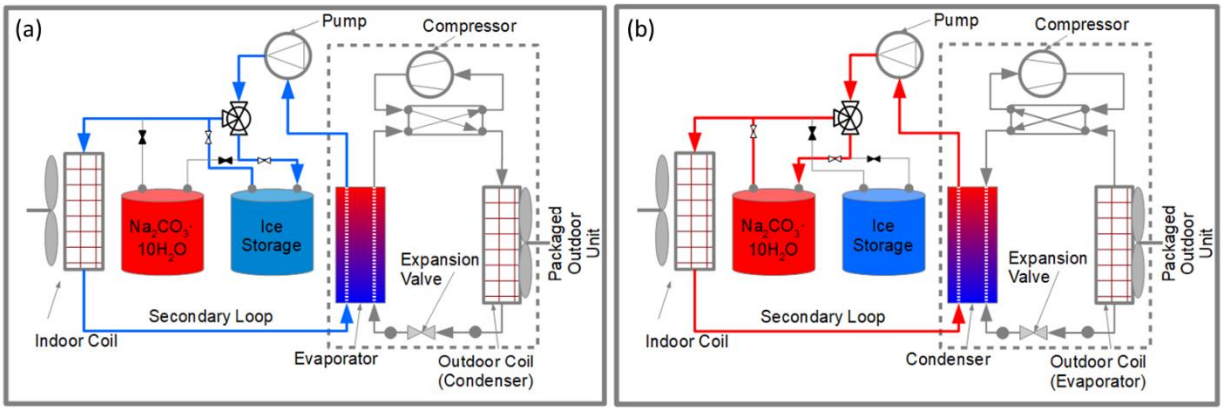

Figure 6-17. Diagram of the system with 2 PCMs used for TES, shown operating in (a) cooling mode with a PCM for cold storage and (b) heating mode with a PCM for heat storage.

In addition to using different equations for the storage tank, the material properties of the PCMs are also different since in this model, different PCMs (with different properties, shown in Table 6-4) are used for heating and cooling. Ice storage is used for cold storage since this is the most commonly-used form of cold storage in practice. Sodium carbonate decahydrate is selected as the material for heat storage. It is selected based on a review of the properties and costs of PCMs for heat storage as a low-cost option with a melt temperature high enough to allow it to be used for heat storage, but low enough not to be detrimental to heat pump performance [121]. The melting temperature of this material is taken from Rao et al. [122], and the latent heat from Guion et al. [123].

Table 6-4. Material properties of the PCMs used for cold storage and heat storage in the 2-PCM model.

Property	**Cold Storage PCM**	**Heat Storage PCM**
Latent Heat	334 kJ/kg	179.8 kJ/kg
Density	1000 kg/m^3	1434 kg/m^3
Melt Temperature	0°C	33.9°C

7. EXAMINATION OF DYNAMIC TUNING OF VARIABLE-TEMPERATURE STORAGE

The variable-temperature storage model described in Chapter 6 has the potential to bring cost savings by reducing the initial cost of year-round storage by using one storage tank instead of two and by reducing operating costs through dynamic tuning of the PCT. This chapter focuses on the potential for cost savings through dynamic tuning. System performance is analyzed on the scale of a week or a month to see how dynamic tuning can bring about cost savings and how significant these cost savings are. Results for single-week periods in the summer and winter are first analyzed in Section 7.1 for a house in Elizabeth City, NC with existing utility rates to see how varying the PCT can lead to cost savings. Based on these results, a rules-based controller is developed for setting PCT values for charge and discharge modes in Section 7.2. Next, how performance changes with rates and load profiles is examined by solving the system model for different rate structures - examining different ratios between on-peak and off-peak rates, rates with on-peak demand charges, and alternate on-peak periods - and different locations for a time period of a month in Section 7.3. These results, and the extent to which they are dependent on particular features of the system model, are discussed in Section 7.4.

7.1 Short-Term Results for Dynamic Tuning of the PCT

The performance of the variable-temperature TES system is analyzed first for a house in Elizabeth City, NC. Heating and cooling loads, and non-HVAC electric loads, are calculated using the EnergyPlus model described in Section 6.1.2. The utility rate structure given in Table 5-4 is used in this analysis. In Section 7.1.1, the different load-shifting control strategies discussed in Section 6.1.5 are compared for the 2-PCM model described in Section 6.5 as well as a version of the variable-temperature model where the PCT only changes when shifting between cooling and heating modes. These results are used to determine which load-shifting strategy should be used for the variable-temperature model with dynamic tuning. The effect of dynamic tuning in cooling mode is analyzed for a week in June in Section 7.1.2. Dynamic tuning in heating mode is examined for a week in January in Section 7.1.3. These results are summarized and compared to results for weeks in February and July in Section 7.1.4. The effect of the varying the specific heat of the PCM

on the cost savings from dynamic tuning is considered in Section 7.1.5. All of these results are calculated without including a cost function for changing the PCT. Section 7.1.6 examines how adding this cost function affects the performance of the system. All results in this section, as well as Sections 7.2 and 7.3, are for a system with a 2-ton heat pump and a 50-gallon PCM storage tank (or 2 such tanks for the system with different PCMs for heat storage and cold storage). For all simulations in this and subsequent sections, it is assumed that the first day of the simulation is a Sunday.

7.1.1 Comparison of Load-Shifting Control Strategies

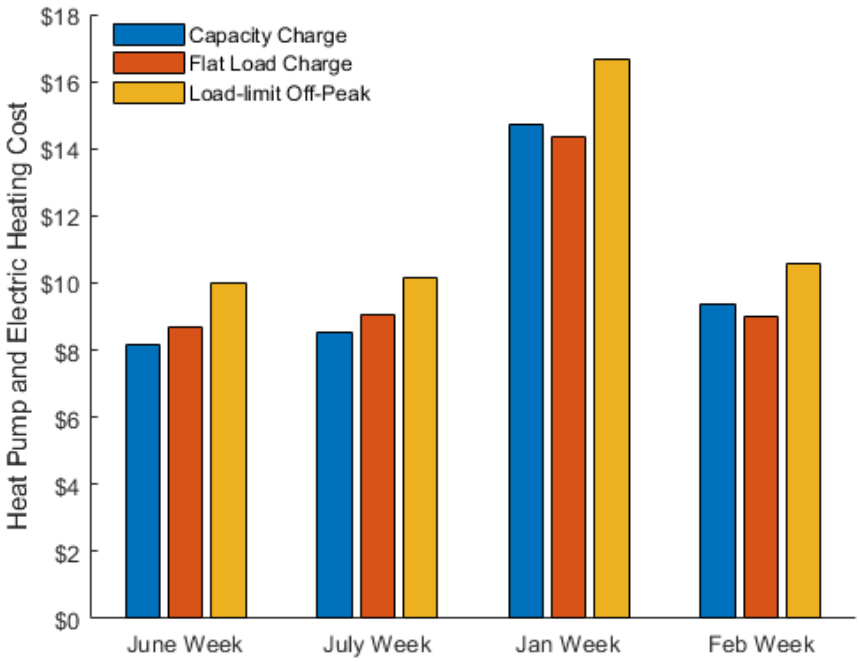

Figure 7-1. Cost comparison between the load-shifting strategies discussed in Section 6.1.5 for cold storage for a week in June and a week in July, and for heat storage for a week in January and a week in February. Results are for the model with separate PCMs for heat and cold storage.

The three load-shifting control strategies described in Section 6.1.5 - charging at capacity (see Figure 6-7), charging at a flat load (see Figure 4-13), and load-limiting during the off-peak period (see Figure 6-6) - are compared using the 2-PCM model (described in Section 6.5). This comparison is first done for the weeks of June 1-7 and July 1-7 (to examine performance in cooling

mode), as well as January 1-7 and February 1-7 (to examine performance in heating mode). The resulting operating costs can be seen in Figure 7-1. Heat pump and electric heating costs are shown, since non-HVAC costs do not change with different control strategies and pump work is found to be negligible, as in the metal hydride model.

From the results in Figure 7-1, we can see that load-limiting off-peak is consistently the most expensive strategy. This is because this strategy involves discharging the system during off-peak hours, which requires increased charging of the system to allow for it to be discharged more. In general, the effect of the lower COP when charging the system at a lower heat pump inlet temperature outweighs the benefit of reducing the heat pump loads at times with more extreme ambient temperatures by discharging. Only when the rates are also higher when the system discharges does the system achieve cost savings from using storage. This strategy may be more effective for rates with off-peak demand charges, since it can reduce peak work during the off-peak hours and thus the demand charges, but for rates without them it is less cost-effective than other strategies.

While load-limiting off-peak is consistently the least cost-effective strategy, the most cost-effective strategy is different for cooling and heating modes. In cooling mode, the lowest costs come when charging at capacity, while in heating mode, the lowest costs come from charging at a flat load. This difference is likely due to the optimal mass flow rates in heating mode being lower than those for cooling mode (as shown in Section 6.2.2). Since charging at a flat rate means charging at lower heat pump loads, it usually involves charging at lower mass flow rates. Since heating mode has lower optimal mass flow rates, it is more likely that reducing the mass flow rate will improve performance than it is for cooling mode.

Since these results indicate that different strategies work best for heating and cooling mode, a full year is studied to see whether it would be better to use different strategies for heat storage and cold storage than a single strategy for both. A comparison is done for a full year of operation between all three control strategies, used consistently throughout the year, and a fourth option of charging cold storage at capacity and charging heat storage at a flat load. This full-year analysis is done using both the 2-PCM model and the variable-temperature model. For simplicity, the variable-temperature model is run without dynamic tuning, using a PCT of 10°C for cold storage and 30°C for heat storage. The results of this comparison, for both models, can be seen in Figure 7-2. These results show that using different load-shifting strategies for cooling and heating modes

leads to superior results than using any control strategy consistently throughout the year. Therefore, for all subsequent results in this chapter, the load-shifting control logic shown in Figure 4-13 (charging at a flat load) is always used for heat storage and the load-shifting control logic shown in Figure 6-7 (charging at capacity) is always used for cold storage.

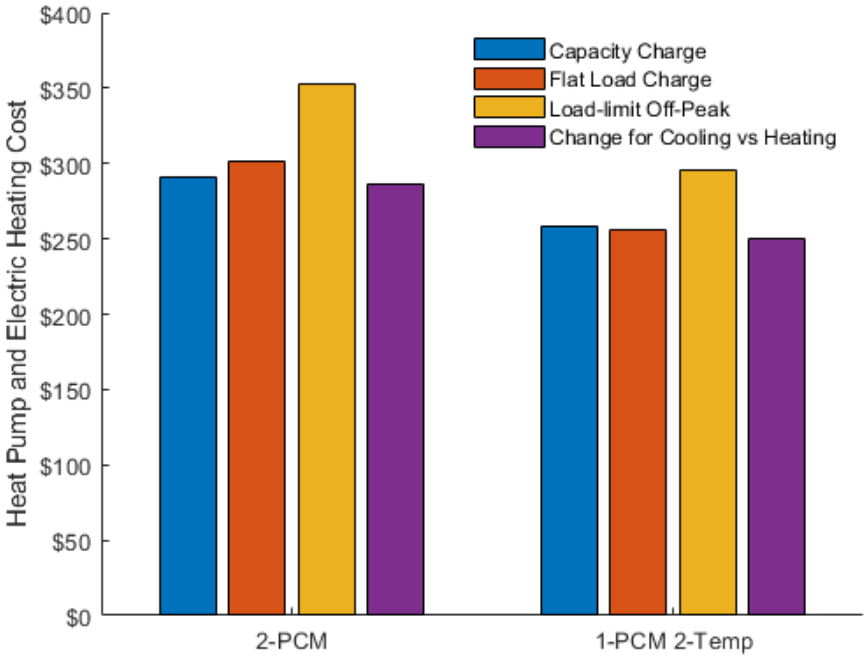

Figure 7-2. Cost comparison between load-shifting strategies for a full year, including the option of using different control strategies for cold storage and heat storage (charge at capacity for cold storage, charge at a flat load for heat storage). Results are shown for both the 2-PCM model and the variable-temperature model with constant temperatures for cold storage and heat storage.

7.1.2 Results for a Summer Week in Elizabeth City, NC

To examine the potential benefits of dynamically tuning the PCT and how to obtain them, the performance of the variable-temperature system is analyzed for the week of June 1-7. This is done using multiple strategies for dynamic tuning. As a benchmark, one case uses a constant PCT of 10°C throughout, while other cases use a fixed time step for changing the PCT, ranging from every 24 hours to every hour. Another strategy is to use two PCTs a day according to the control logic in Section 6.3.1. Finally, the previous strategy is also used with the model where the storage

system is charged using the house outlet flow as described in Section 6.4. The resulting operating costs for the week for each of these cases can be seen in Figure 7-3.

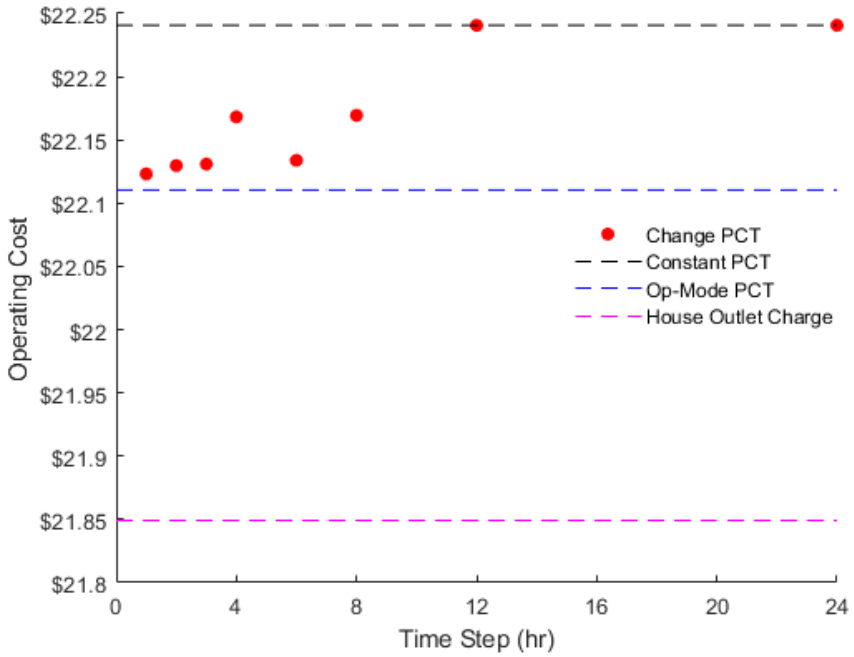

Figure 7-3. Total operating costs (including non-HVAC loads) for the week of June 1-7 as a function of the time step used for changing the PCT, compared to the cases with a constant PCT of 10°C, two temperatures a day for charging and discharging (Op-Mode PCT), and the storage tank being charged with the house outlet flow (House Outlet Charge).

Looking at the results for fixed time steps in Figure 7-3, we can see that using a 24-hour or a 12-hour time step results in the same operating costs as the case with a constant PCT, since for these time steps changing the PCT does not result in cost savings. However, as the time step decreases, changing the PCT does result in cost savings, particularly for time steps of 6 hours or of 3 hours or less. However, these cost savings are small compared to the overall cost- in the best case, they are still less than $0.15/week. The case with different PCT values for charge and discharge outperforms any fixed time step, but only by ~$0.01. Larger cost savings, around $0.40/week, can be obtained by using the method where the house outlet flow charges the storage tank. These results indicate that it is possible to improve the performance of the system by dynamically tuning the PCT, but the cost savings for doing so in cooling mode are limited. To see how the PCT is tuned to obtain these cost savings, more detailed results are shown below for the

cases that resulted in the highest cost savings: using two temperatures for charge and discharge, using a 1-hour time step, and charging with the house outlet flow.

Charge and Discharge Temperatures

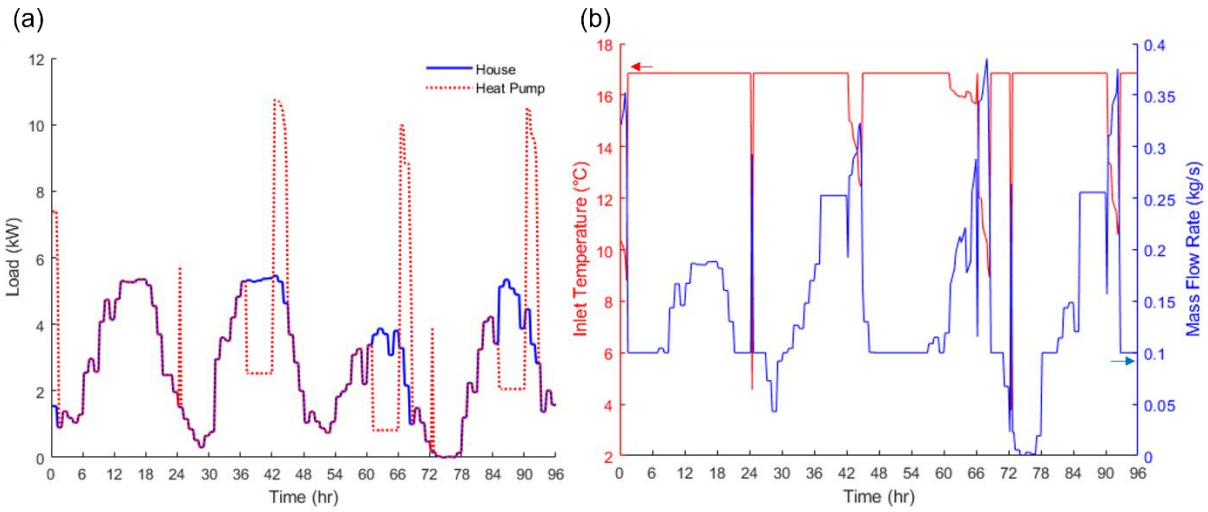

Figure 7-4. (a) House and heat pump loads and (b) water glycol mass flow rate and heat pump inlet temperature for June 1-4 for the case where different PCT values are used for charging and discharging the system.

To see how using different PCT values for charge and discharge as described in Section 6.3.1 results in cost savings, key system parameters are shown in Figure 7-4 and Figure 7-5 for the period of June 1-4. A 4-day period is used instead of the full week so that the results can be seen more clearly. The cooling loads at the house and the heat pump, and the mass flow rate and inlet temperature of the heat pump, can be seen in Figure 7-4. The PCT and state of charge of the storage system can be seen in Figure 7-5. The heat pump loads shown in Figure 7-4a differ from the house loads when the system is charging or discharging. Because of the load-shifting control logic used, the system charges quickly at a high, but non-constant load (because it charges at the capacity of the chiller, which changes with ambient temperature) while it discharges at a constant heat pump load. However, we can also see two sudden spikes where the heat pump load exceeds the house load at t = 24 hours and t = 72 hours. As seen in Figure 7-5a, the PCT decreases at these times, since the control logic switches to the discharge value for a day at the beginning of the day if the

system is finished charging. The state of charge decreases at these times as the PCM melts until its temperature reaches the PCT. The spikes in the heat pump load are the system charging to make up for this lost charge.

The PCT is always 10°C when charging but is lowered for two of the three discharge periods. This indicates that the optimal way to change the PCT between operation modes is to charge the system at the highest PCT but sometimes lower the PCT when discharging the system. The maximum PCT is used in charging mode because here flow must leave the heat pump and enter the storage tank at a lower temperature than the PCT in order to charge the tank. For charging mode, this constraint is usually more restrictive than the maximum outlet temperature possible in the house, and so the heat pump inlet temperature is less than this maximum temperature, as seen in Figure 7-4b. Therefore, increasing the PCT increases the heat pump inlet temperature, thereby increasing its COP.

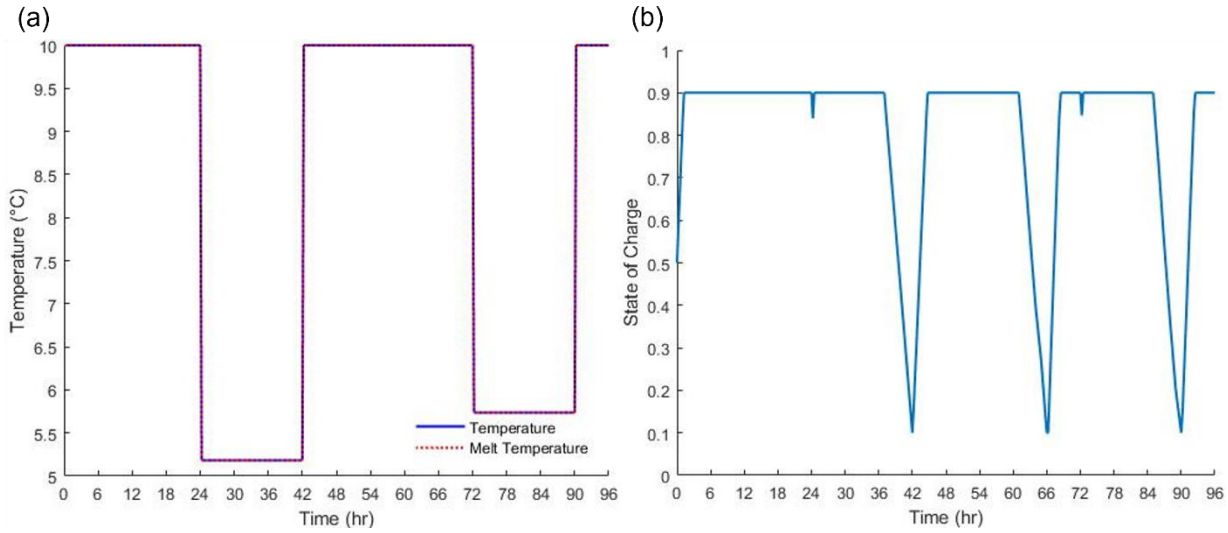

Figure 7-5. (a) PCT and operating temperature and (b) state of charge of the storage tank for June 1-4 for the case where different PCT values are used for charging and discharging the system.

It can also be seen in Figure 7-4b that the heat pump inlet temperature when the system is discharging is usually constant, since here flow is not constrained by storage tank outlet temperature because the constraint on house outlet temperature is more restrictive. This is because the flow here leaves the storage tank at a temperature above the PCT, so flow enters the house at a higher temperature than it does in cooling mode. This means that in discharge mode, it is possible to reduce the PCT without reducing the heat pump inlet temperature. Thus, lowering the PCT will

improve performance if it leads to a more optimal mass flow rate. Because of this, the PCT is lowered on the 2nd and 4th days, in order to increase the change in water glycol temperature when delivering the cooling load and thus reduce the mass flow rate. As can be seen in Figure 7-4b, the mass flow rate is a constant value close to 0.25 kg/s during both of these periods, which is around the optimal value. However, on the 3rd day the heat pump and house loads are lower, so the mass flow rate is already lower than the optimal value for most of the period. Therefore, the PCT is not lowered on this day, since it would lead to a lower COP.

As seen in Figure 7-3, this method for changing the PCT outperforms any fixed time step, indicating that lowering the PCT when discharging in order to optimize the mass flow rate is the best way to get cost savings from dynamically tuning the PCT in cooling mode. This explains why fixed times steps of 3 and 6 hours result in lower costs than steps of 4 or 8 hours; the former time steps allow the PCT to be changed at the end of the on-peak period, which makes it possible to lower the PCT for the entire on-peak period without also charging the system at this lower value.

1-Hour Time Step

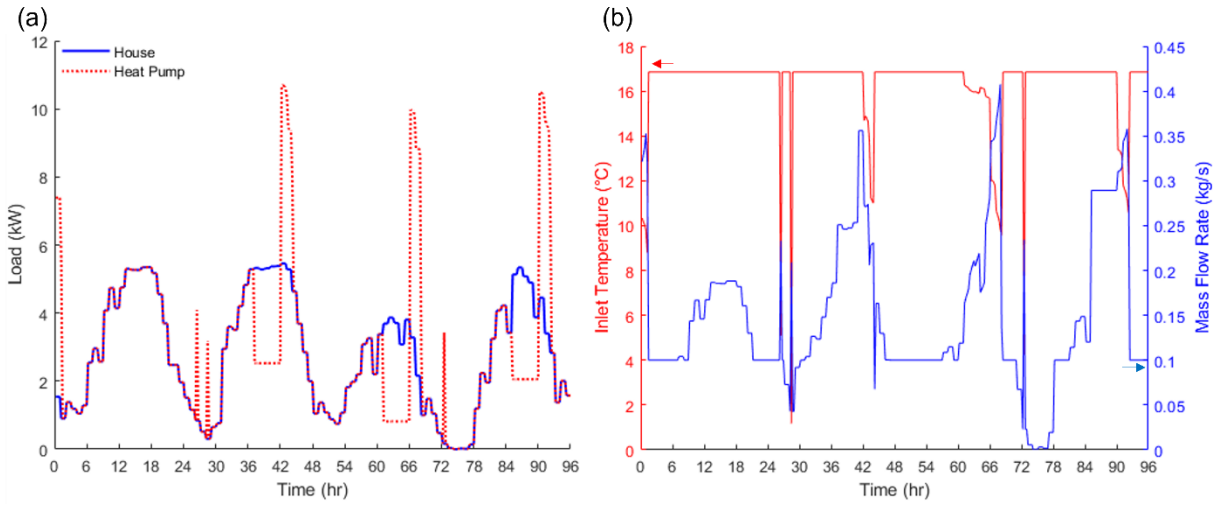

Figure 7-6. (a) House and heat pump loads and (b) water glycol mass flow rate and heat pump inlet temperature for June 1-4 for the case with a 1-hour time step for updating the PCT.

For the case with a 1-hour time step, the cooling loads at the house and the heat pump for June 1-4, and the mass flow rate and inlet temperature of the heat pump, can be seen in Figure 7-6.

The PCT and state of charge can be seen in Figure 7-7. While the results for the 1st and 3rd days are very similar to the previous case, the PCT values seen in Figure 7-7a are slightly different on the 4th day and very different on the 2nd, with the PCT increasing and decreasing across the entire range of possible values repeatedly over the course of the day. This leads to similar fluctuations in the state of charge, as the PCM melts and freezes with the changes in its temperature. These changes in the state of charge require additional charging at two time steps, resulting in the spikes in the heat pump load seen in Figure 7-6a.

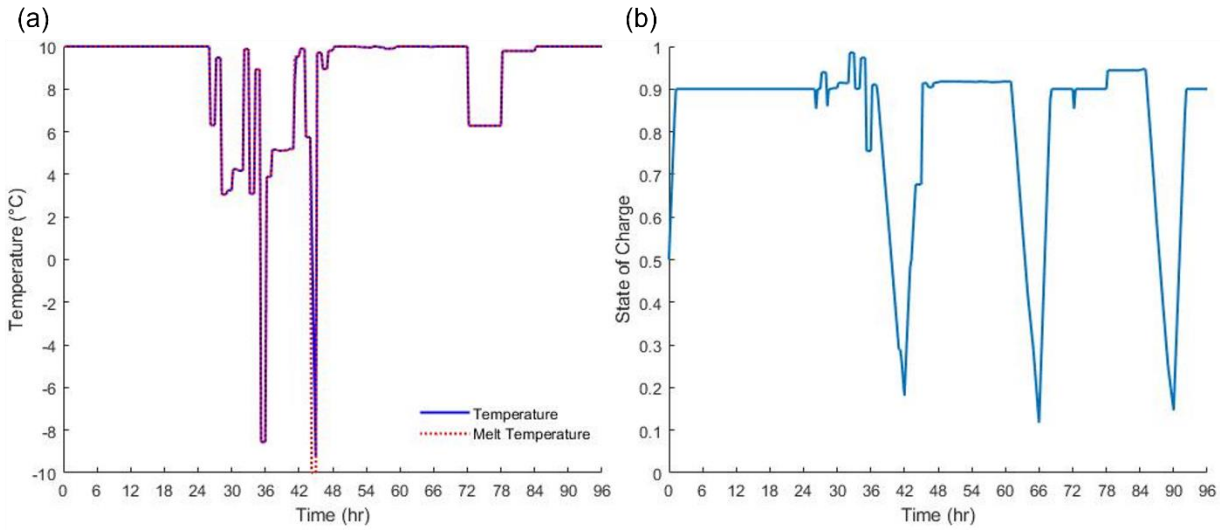

Figure 7-7. (a) PCT and operating temperature and (b) state of charge of the storage tank for June 1-4 for the case with a 1-hour time step for updating the PCT.

There are two overall effects from all these changes in the PCT. The first is that during the actual on-peak period, the PCT is at a lower temperature similar to those used in the previous case which optimizes the mass flow rate as discussed. The other effect is that the changes to the PCT result in additional charging of the system at two points as mentioned above. This results in the system ending the discharge period at a higher state of charge, since the increase in the PCT at the beginning of the on-peak period led to an increase in the state of charge. Thus, in essence, changing the PCT in the morning shifted some of the charging load from after the on-peak period to before it. This leads to cost savings if the charging is being moved to a time when it is done at a higher COP. This can happen if increased loads at the house at one time at the house allow the system to charge at a higher temperature, but that is not the case here. Instead, improved performance comes from the charging at these two points in the morning happening at near-optimal mass flow rates (as seen in Figure 7-6b, at both times the mass flow rate is in the range of 0.2-0.25 kg/s). Something

similar happens on the 4th day; however, here the PCT returns to a higher value before the on-peak period.

While these results involve more frequent changes to the PCT, they ultimately result in slightly lower cost savings than the simpler method where only two temperatures (charge and discharge) are used each day. Furthermore, a significant portion of these savings come from using lower PCTs during the on-peak period as in the previous case. Two methods of getting cost savings from dynamic tuning have been identified: changing the PCT in order to shift charging loads to times when the system operates more effectively and lowering the PCT in discharge mode to improve the mass flow rate. However, while both can lead to cost savings, the latter results in greater savings for fewer changes in the PCT. The smaller and less frequent changes to the PCT are advantageous because they mean any cost for changing the PCT (not considered here) will be lower.

Charging with House Outlet Flow

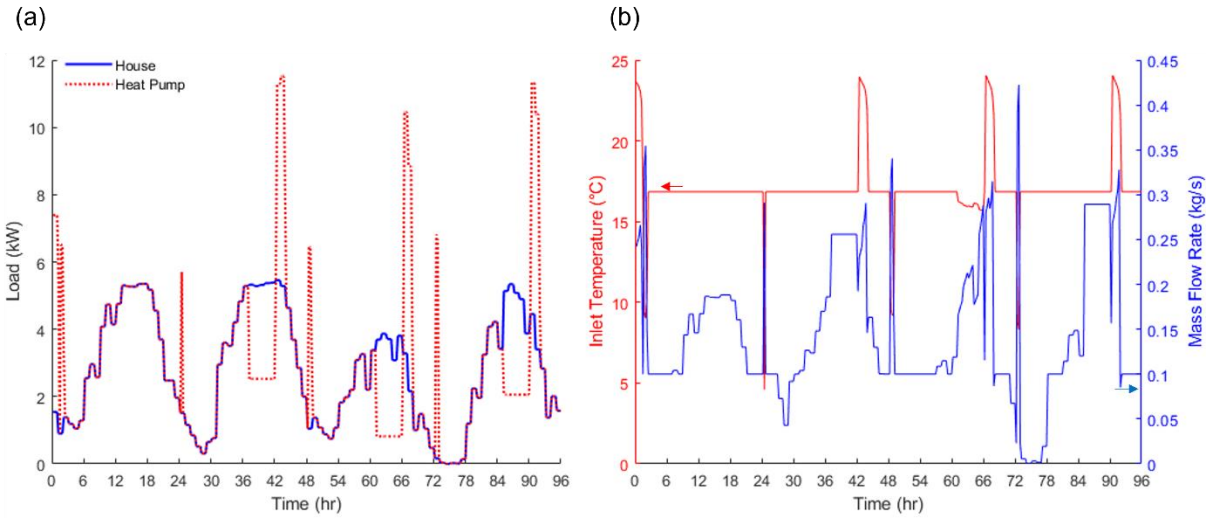

Figure 7-8. (a) House and heat pump loads and (b) water glycol mass flow rate and heat pump inlet temperature for June 1-4 for the case where the storage tank is charged with the house outlet flow.

For the case where the storage tank is charged with the house outlet flow for June 1-4, the cooling loads at the house and the heat pump, and the mass flow rate and inlet temperature of the heat pump, can be seen in Figure 7-8. The PCT and state of charge can be seen in Figure 7-9. These

results follow a similar pattern to the case with two temperatures for charging and discharging, where higher temperatures are used for charging and lower values for discharging. The difference is that here the temperatures for charging the system are higher, since redirecting the flow so that the storage tank is charged with the house outlet flow allows for higher PCT values to be used in charging.

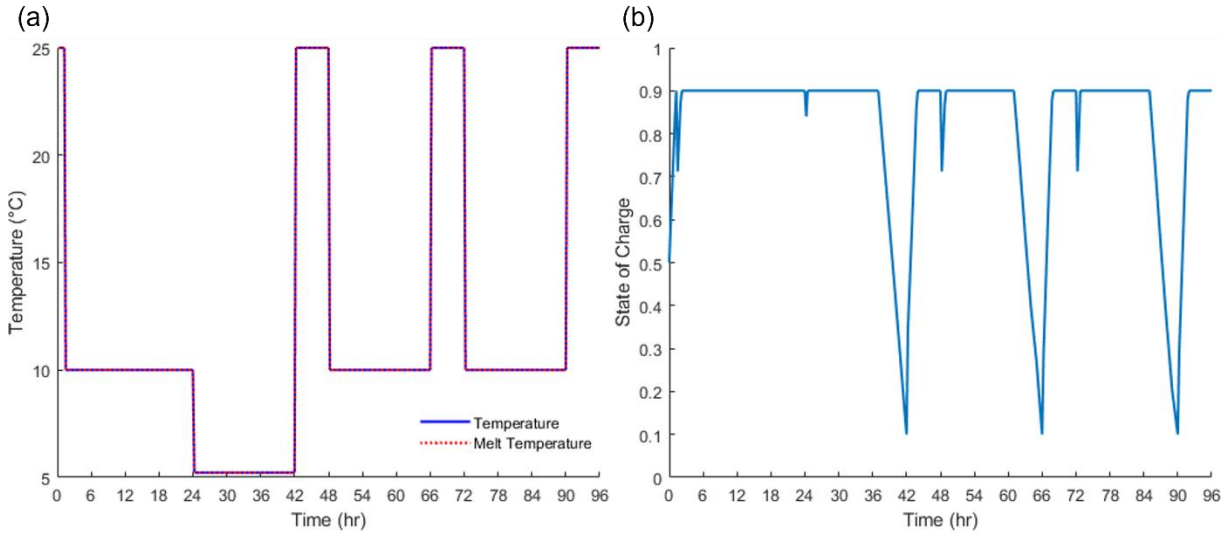

Figure 7-9. (a) PCT and operating temperature and (b) state of charge of the storage tank for June 1-4 for the case where the storage tank is charged with the house outlet flow.

As seen in Figure 7-9a, the maximum PCT possible (25°C) is used whenever the system is being charged, so as to maximize the heat pump inlet temperature. This results in the system being charged at heat pump inlet temperatures around 6°C higher than the maximum outlet temperature at the house, as seen in Figure 7-8b. This increased heat pump temperature results in a significantly higher COP, and thus the reduced operating costs seen in Figure 7-3.

One other difference that can be seen between this case and the case with two temperatures for charging and discharging is that the difference between the PCT values for charging and discharging is much larger (~15-20°C instead of ~5°C). Therefore, the loss of charge when lowering the PCT, and thus the charging that must be done at the lower operating temperature, is greater. This is one considerable limitation on the cost savings obtained using this system design: around 25% of the charging must still be done at a lower temperature because of the lost charge when lowering the PCT. Despite this, however, the cost savings from using this method are still

significantly greater than those from any other method for dynamically tuning the PCT in cooling mode.

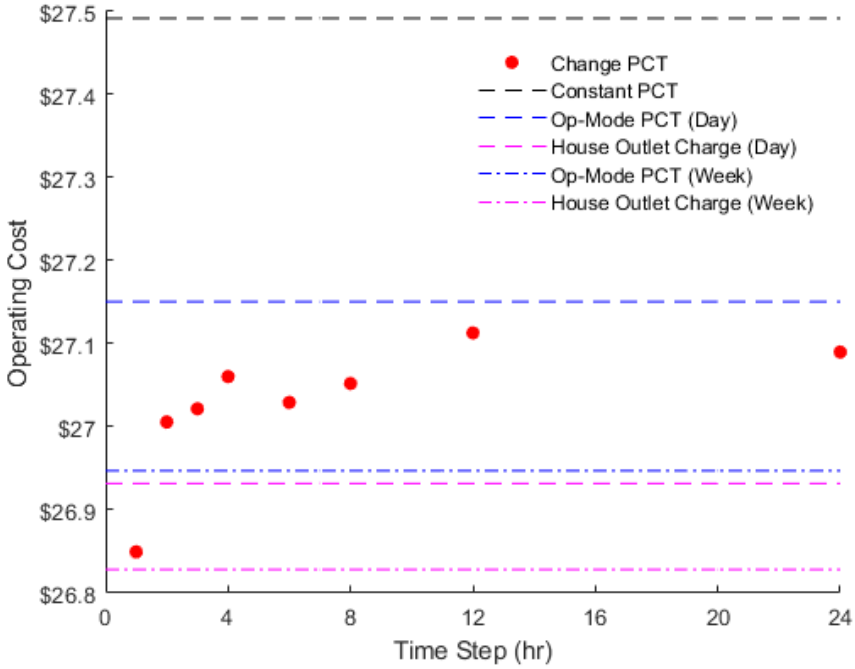

Figure 7-10. Total operating costs (including non-HVAC loads) for the week of January 1-7 as a function of the time step used for changing the PCT, compared to the cases with a constant PCT of 30°C, two temperatures a day for charging and discharging (Op-Mode PCT), and the storage tank being charged with the house outlet flow (House Outlet Charge). Results for the last two cases are shown using both a day and a week as the time period considered by the optimization function.

7.1.3 Results for a Winter Week in Elizabeth City, NC

To see the effect of dynamically tuning the PCT in heating mode, the model is run for the week of January 1-7 in Elizabeth City, NC for all of the same cases that are used in cooling mode. The resulting operating costs can be seen in Figure 7-10. Three major differences can be seen between these results and the results for cooling mode. The first is that changing from a constant PCT to a 24-hour time step results in significant cost savings of around $0.40/week. The second is that the maximum cost savings from a fixed time step are much greater, around $0.65/week instead of $0.15/week. The third is that using two temperatures for charging and discharging results in lower cost savings compared to using a fixed time step when using a day as the time

period for the optimization function (which is done for all the results in Section 7.1.2). However, using a week as the optimization period resulted in larger cost savings for this case, as well as the case where the tank is charged with the house outlet flow. This is not the case in cooling mode, where using a week as the optimization period was examined but did not improve system performance (and so results from it are not shown in Section 7.1.2).

To understand why the results are different from those for cooling mode, we will look in more detail at the cases with the most different results: using a 24-hour time step, a 1-hour time step, and charging and discharging temperatures.

24-Hour Time Step

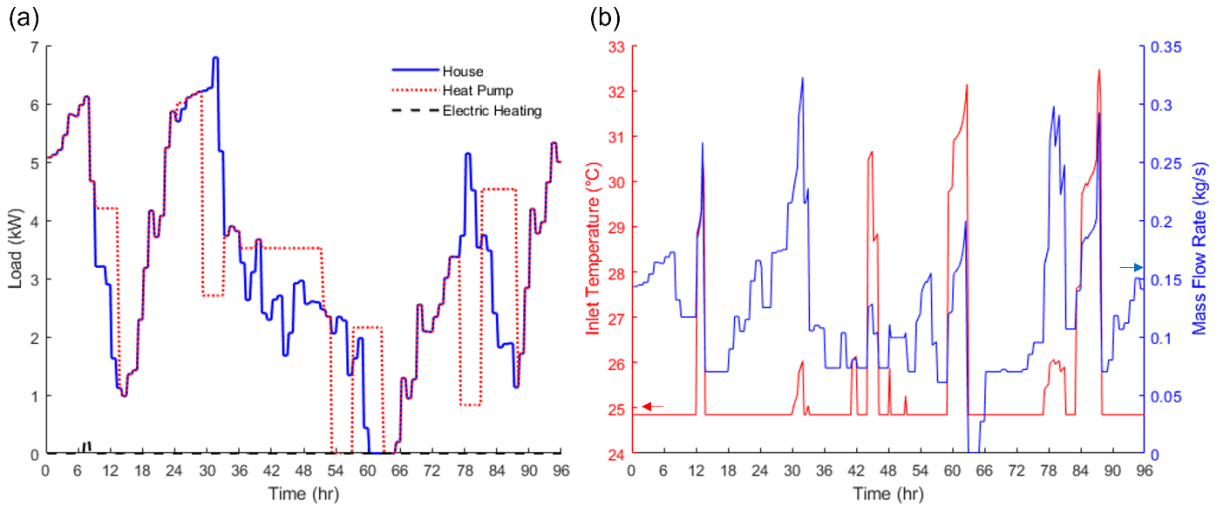

Figure 7-11. (a) House, heat pump, and electric heating loads and (b) water glycol mass flow rate and heat pump inlet temperature for January 1-4 for the case with a 24-hour time step for updating the PCT.

The heating loads at the house and the heat pump for the case with a 24-hour time step, and the mass flow rate and inlet temperature of the heat pump, can be seen in Figure 7-11. The PCT and state of charge can be seen in Figure 7-12. Looking at the loads in Figure 7-11a, we can see that that the heating loads are generally not large enough to require the use of auxiliary heating, except briefly on the 1st day. The different control logic used for charging heat storage can also be seen here: the heat pump loads when charging are constant on each day, and significantly lower than the maximum loads met by the heat pump. Because of this, the system generally takes more

time to charge than it does in cooling mode, on one day only finishing charging shortly before the end of the off-peak period.

As seen in Figure 7-12a, the PCT values for the 1st and 3rd days are very close to the minimum value, which is used when a constant value is used for heat storage (30°C). However, on the 2nd and 4th days, higher PCT values are used. One reason these values are used is the high mass flow rate when discharging on these days (as seen in Figure 7-11b), which would be even higher if a lower PCT were used. Lowering the mass flow rate reduces the heat pump work when discharging on these days. However, it cannot reduce heat pump work when discharging on the 3rd day since there the entire on-peak load is met using the storage tank instead of the heat pump. Increasing the PCT also leads to a higher heat pump inlet temperature, particularly when charging, which does lower the performance of the heat pump.

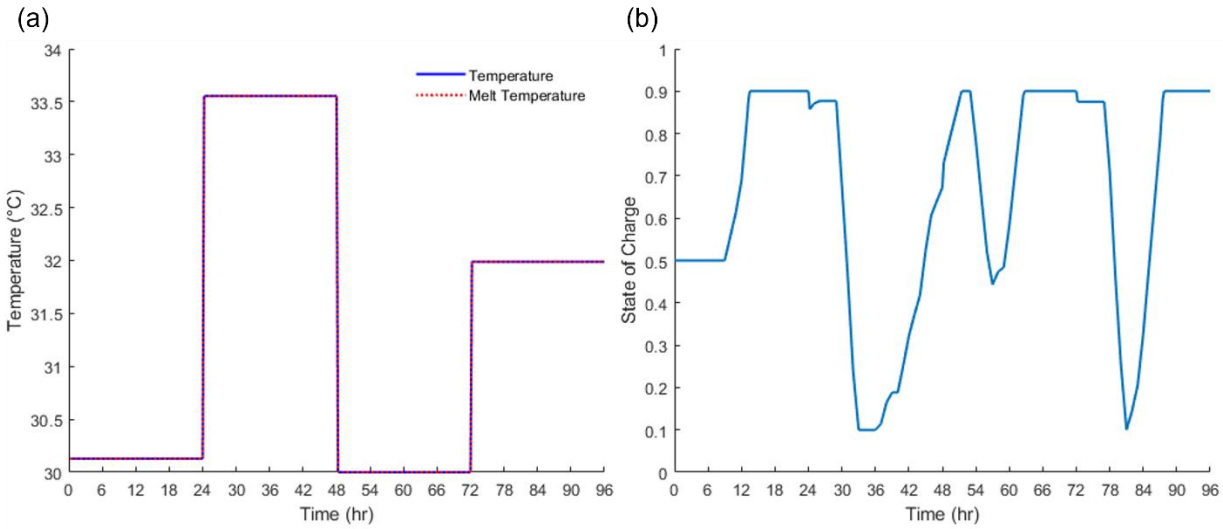

Figure 7-12. (a) PCT and operating temperature and (b) state of charge of the storage tank of the storage tank for January 1-4 for the case with a 24-hour time step for updating the PCT.

However, the overall gains from lowering the mass flow rate are greater than the losses from increasing the heat pump inlet temperature. This happens because the COP is less strongly dependent on the water glycol temperature than it is in cooling mode, as can be seen by comparing Figure 6-11 with Figure 6-13. Therefore, it is more likely that the effect of the mass flow rate will outweigh the effect of the inlet temperature than it is in cooling mode. Given the weaker dependence of COP on inlet temperature, it is possible that increasing the PCT to reduce the mass flow rate might sometimes lead to cost savings during charging.

1-Hour Time Step

The heating loads at the house and the heat pump for the case with a 24-hour time step, and the mass flow rate and inlet temperature of the heat pump, can be seen in Figure 7-13. The PCT and state of charge can be seen in Figure 7-14. The most obvious difference between this case and the case with a 24-hour time step is that the PCT is changing rapidly throughout the entire time in this case, with the exception of morning on the 3rd day. Despite these frequent changes, a significant reason for the improved performance relative to the 24-hour time step is that the model can lower the PCT when charging on the 2nd and 4th days, thereby lowering the heat pump inlet temperature. The fluctuations during the on-peak period on the 2nd day (seen between t = 30 hours and t= 36 hours in Figure 7-14a) also allow the system to operate at a lower inlet temperature (except one brief point where it is significantly higher) while remaining near the optimal mass flow rate, as seen in Figure 7-13b. Similarly, the fluctuations in the PCT when charging on the 4th day (seen between t = 78 hours and t= 84 hours in Figure 7-14a) allow for the system to charge alternatively at a high and a low (near-optimal) mass flow rate, as seen in Figure 7-13b, rather than consistently charging at a high mass flow rate, as in Figure 7-11b. Overall, these results show that there is significantly more potential for cost savings from frequent changes to the PCT in heating mode than there are in cooling mode.

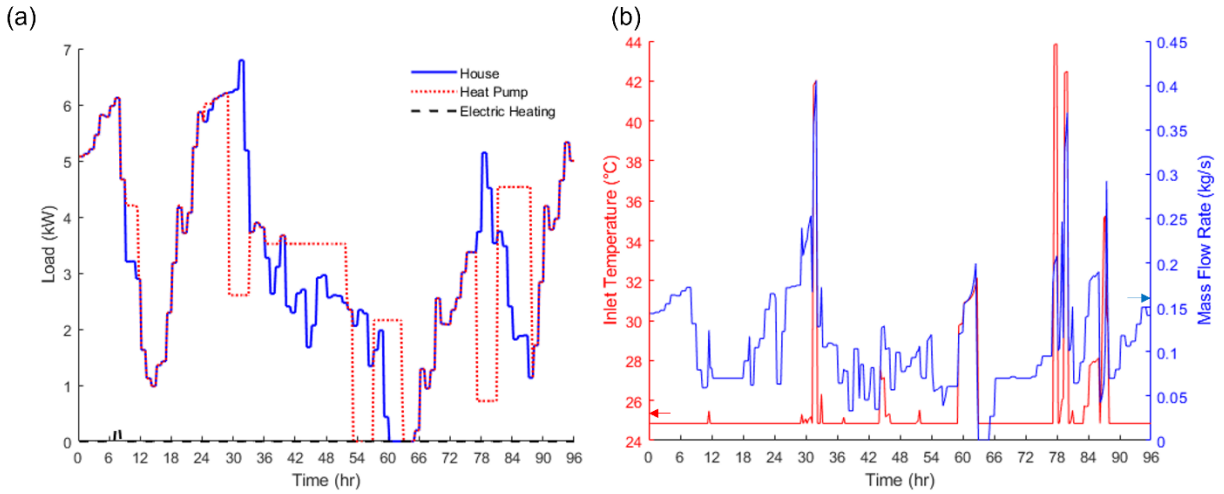

Figure 7-13. (a) House, heat pump, and electric heating loads and (b) water glycol mass flow rate and heat pump inlet temperature for January 1-4 for the case with a 1-hour time step for updating the PCT.

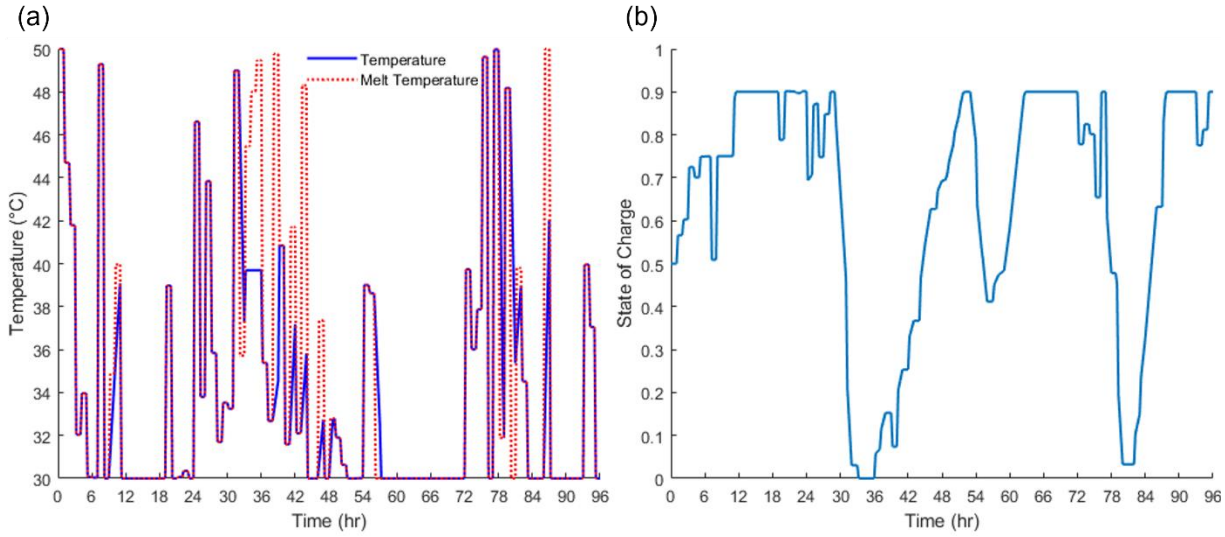

Figure 7-14. (a) PCT and operating temperature and (b) state of charge of the storage tank of the storage tank for January 1-4 for the case with a 1-hour time step for updating the PCT.

These increased cost savings from frequent changes to the PCT to reduce the mass flow rate are obtainable in part because, unlike in cooling mode, the system is not consistently constrained by house temperature in discharge mode and storage tank temperature in charge mode, as can be seen by looking at the inlet temperatures in Figure 7-13b. This means that adjusting the PCT to optimize the mass flow rate is more important in charge mode and that the system cannot necessarily operate consistently at the optimal mass flow rate in discharge mode. Both of these factors increase the incentive to make more frequent changes to the PCT.

One other thing that should be noted is that the system starts at a high PCT and then reduces this value in order to charge the system using sensible heating. That this results in lower operating costs is an artifact of the initial conditions for this simulation, not something that could be used to reduce costs in a real system (since the heating needed to start the PCM out at a higher temperature is not accounted for). This is not done in cooling mode because there the system begins charging immediately, so there would be significant losses in performance if the PCM did not start out with a high PCT. Since the system runs conventionally for the first few hours in heating mode, until the house load decreases below the heat pump load for charging, it is feasible in this case. To avoid this issue, all results in Section 7.2 and after use an initial storage tank temperature of 10°C in cooling mode and 30°C in heating mode, regardless of the initial PCT value.

Charge and Discharge Temperatures

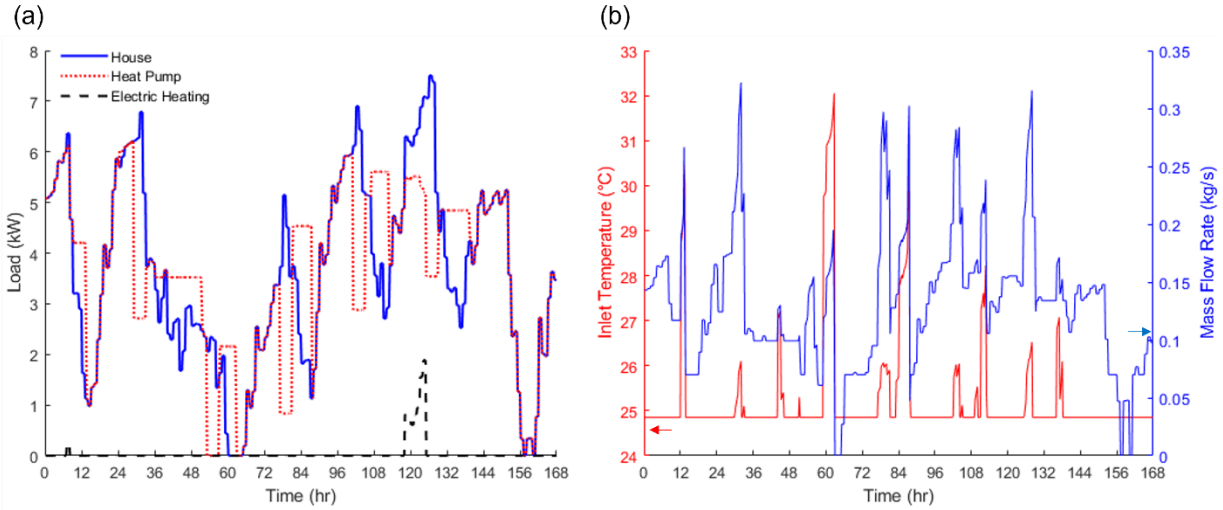

Figure 7-15. (a) House, heat pump, and electric heating loads and (b) water glycol mass flow rate and heat pump inlet temperature for January 1-7 for the case where different PCT values are used for charging and discharging the system and a day is used as the optimization period.

To understand why using two temperatures for charge and discharge results in worse results than using a single temperature for each day if a day is used as the optimization period, the results for the former case are shown in Figure 7-15 and Figure 7-16 (loads and water glycol flow rate and heat pump inlet temperature in Figure 7-15, PCT and state of charge in Figure 7-16). These results are shown for the full week because, unlike the previous cases shown, the last three days are particularly significant for understanding the results. This is because it is only on the 5th and 6th days that the system performs worse than it does when a 24-hour time step is used. For the first four days, using two temperatures a day does result in reduced operating costs.

In Figure 7-16a, we can see that the PCT is changed in a way similar to cooling mode, except that the system now uses higher temperatures when discharging since in heating mode, these lead to lower flow rates while lower temperatures are desirable in charging because heat pump performance is better for lower water glycol temperatures. The system performs worse than the system with a 24-hour time step because on the later days, consistently operating at a higher temperature outperforms switching between lower values for charging and higher values for discharging. This is because the system loses charge at the beginning of the day when it changes to a higher PCT. Because the system only charges if the house load is below the set heat pump

load for charging and there only a few hours with high heating loads before the on-peak period starts, the system starts the on-peak period not fully charged, thereby reducing the cost savings from energy storage since the system is not fully discharged during the on-peak period. However, the optimization function does not see this when using a day as the optimization period because the benefits from lowering the PCT to charge (better mass flow rates and inlet temperatures, as seen in Figure 7-15b) occur on the same day, while the downsides (the system losing charge when the PCT increases in the morning) do not occur until the next day, outside the optimization period.

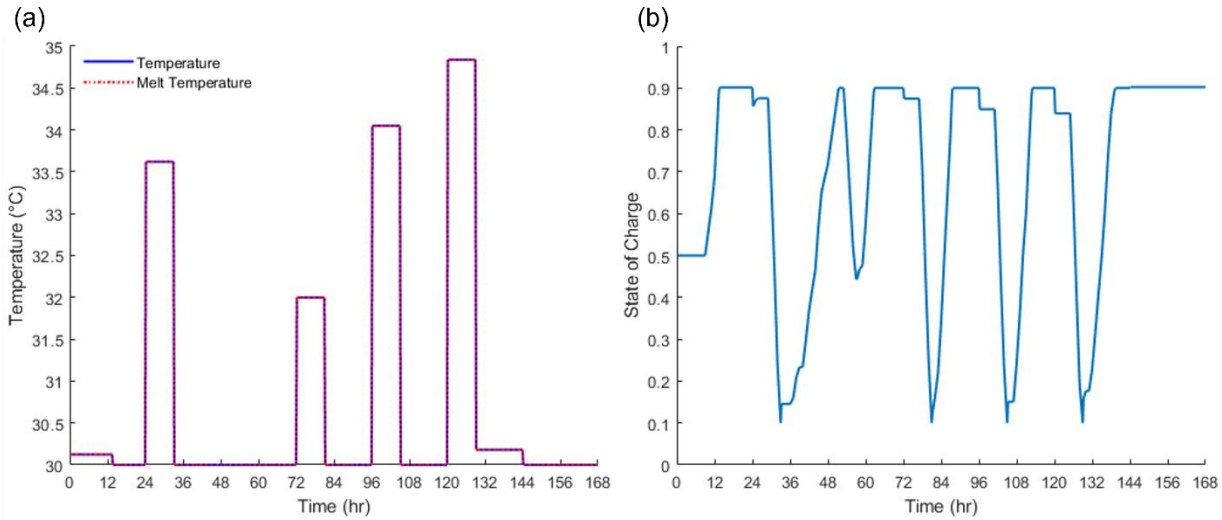

Figure 7-16. (a) PCT and operating temperature and (b) state of charge of the storage tank of the storage tank for January 1-7 for the case where different PCT values are used for charging and discharging the system and a day is used as the optimization period.

Using a week as the time period for optimization avoids this problem, since then both the costs and benefits of lowering the PCT are considered. Because of this, the system gets larger cost savings (as seen in Figure 7-10) in this case by using a higher PCT value for charging on days 3-5. Using a week as the time period for optimization usually does not improve performance but does increase computation time. However, in this case, the combination of load-shifting control logic that does not charge the system at times with high loads and a short time period with high loads before the on-peak period creates a situation where there are significant losses that are difficult to account for in the cost function used when optimizing for a day. Because of this, using a week as the time period for optimization does result in a more optimal solution for the case where two temperatures are used for charging and discharging in heating mode.

7.1.4 Overall Comparison of Short-Term Results with No Cost Function

The operating costs in cooling mode for different systems and methods for optimizing the PCT are summarized for the week in June discussed in Section 7.1.2 and for the week of July 1-7 in Figure 7-17. Similarly, the operating costs in heating mode for the week in January discussed in Section 7.1.3 and for the week of February 1-7 are compared in Figure 7-18. For both heating and cooling modes, we can see that the relative performance of the different cases studied is very similar for both weeks studied. This indicates that the trends in the results discussed in Sections 7.1.2 and 7.1.3 are not heavily dependent on the particular load profiles for those weeks. These figures also show how the cost savings from changing how the PCT is dynamically tuned compare to the cost savings from using TES, or from using TES at a single favorable temperature. As can be seen in Figure 7-17, the operating cost savings from using ice storage compared to a conventional system, or from using a PCT of 10°C instead of ice storage, are significant (> $1/week for each).

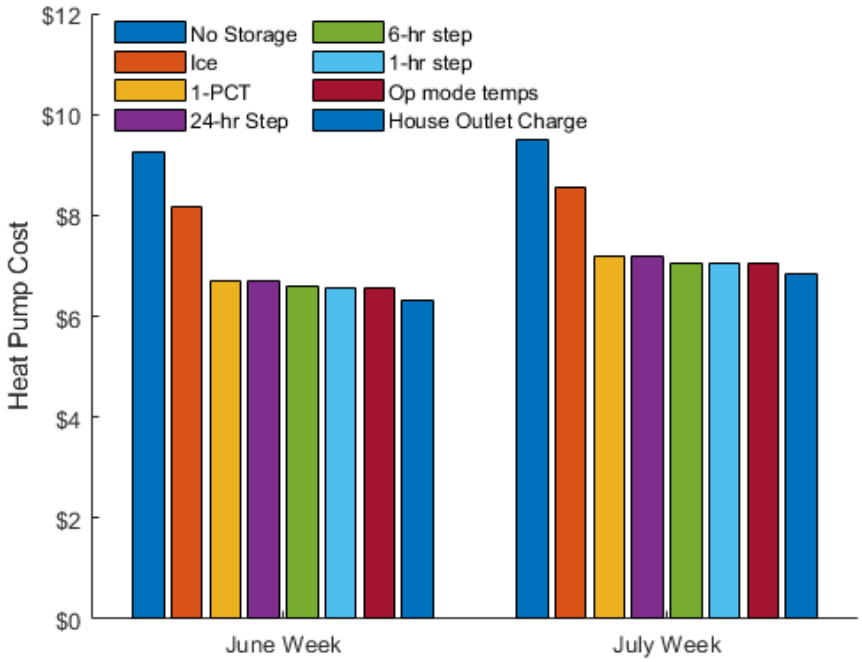

Figure 7-17. Comparison of operating costs in cooling mode for a conventional system (No Storage), a system with ice storage (Ice), a system with a constant PCT of 10°C (1-PCT), and a system with a dynamically-tuned PCT with different time steps (24-hr step, 6-hr step, and 1-hr step), as well as two temperatures for charge and discharge (Op mode temps) and two temperatures with the house outlet flow used to charge the TES system (House Outlet Charge)

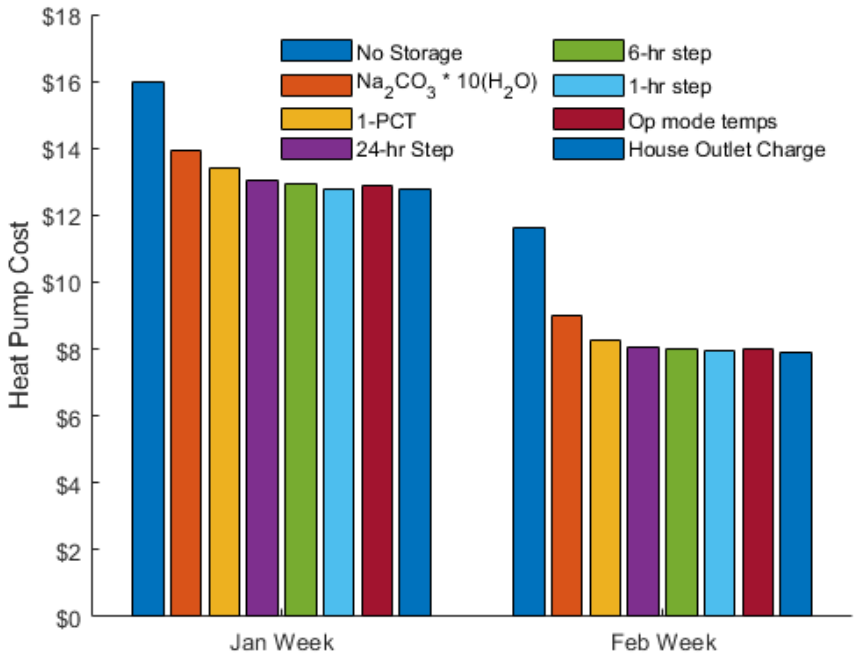

Figure 7-18. Comparison of operating costs in heating mode for a conventional system (No storage), a system a real PCM for heat storage (Na_2CO_3*10(H_2O)), a system with a constant PCT of 10°C (1-PCT), and a system with a dynamically-tuned PCT with different time steps (24-hr step, 6-hr step, and 1-hr step), as well as two temperatures for charge and discharge (Op mode temps) and two temperatures with the house outlet flow used to charge the TES system (House Outlet Charge)

Compared to these savings, the cost savings from dynamic tuning are small: <$0.20 a week without using the house outlet flow for charging, and only ~$0.40/week when doing so. In comparison, we can see that in heating mode, the cost savings from using sodium carbonate decahydrate for TES are larger than those from using ice, while the cost savings from switching to a storage temperature of 30°C are smaller. This is because switching to using the variable-temperature system with fixed temperatures for heat storage and cold storage involves a smaller change in the PCT compared to the real PCM for heat storage than it does for cold storage (3.9°C instead of 10°C). Furthermore, there are more significant cost savings from dynamically tuning the PCT, the majority of which can be obtained simply by using a different constant value for the PCT every day.

Overall, these results show that dynamic tuning of the PCM can be used to obtain cost savings. However, in cooling mode, the savings from dynamically tuning the PCT are small, and most of the improvement over ice storage can be obtained by using a PCM with a fixed PCT close

to 10°C. Larger potential cost savings can be obtained in heating mode. Maximizing these requires frequent alteration of the PCT, but the majority of these savings can be obtained simply by changing the PCT once a day. Since pump work is negligible compared to heat pump work in this system, all of these cost savings are the result of improving the performance of the heat pump. This performance depends on both the water glycol temperature at the heat pump inlet and its mass flow rate. Running at the highest possible PCT in cooling mode and the lowest possible PCT in heating mode always results in the most favorable inlet temperature, but changes to the PCT can improve the heat pump performance by moving towards a more optimal mass flow rate.

7.1.5 Effect of Specific Heat on Dynamic Tuning

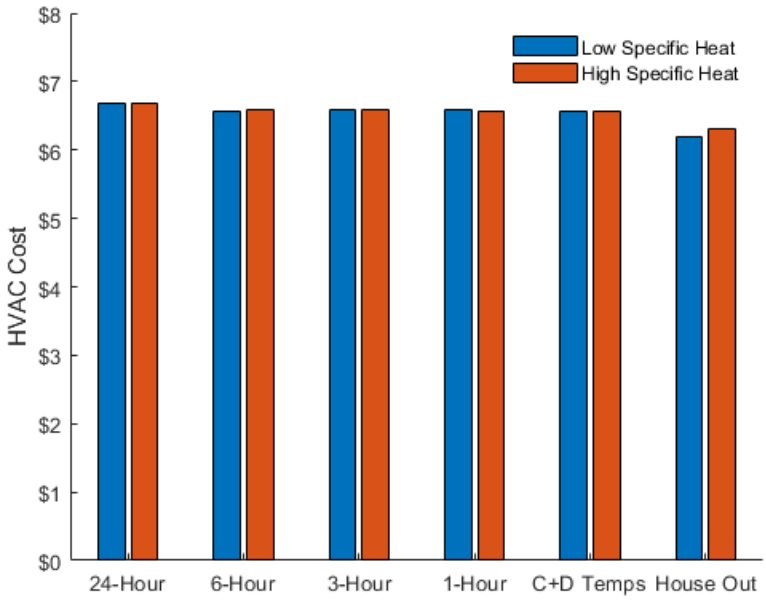

Figure 7-19. Comparison of operating costs for the week of June 1-7 for different specific heats of the PCM. Results are shown for different fixed-hour time steps (24-Hour, etc.), as well as two temperatures for charge and discharge (C+D Temps) and charging with the house outlet flow (House Out).

The material properties of water are used for the variable-temperature PCM as discussed in Section 6.1.3. Since a simplified model is used for the storage tank, the only material properties used are the latent heat and specific heat (density is used in calculating the size of the system but does not affect its performance). These properties determine the magnitude of the heat transfer required to change the state of charge and temperature, respectively, of the PCM (as seen in Eqs. 74 and 72). Therefore, the ratio of these properties will determine what change in state of charge

will occur when the PCM changes temperature. Since this change in the state of charge plays a significant role in the results shown in Sections 7.1.2 and 7.1.3, several of the cases studies in these sections are re-run for a modified specific heat $c_{PCM,new} = \frac{c_{PCM,old}}{2}$ to see how cost savings would change if changing the temperature of the PCM had less of an effect on the state of charge.

The operating costs for several cases using the lower specific heat are compared to the results from Section 7.1.2 for the week of June 1-7 in Figure 7-19. The effect of varying the specific heat is noticeable primarily for the case where the system is charged with the house outlet flow, where it results in a lower operating cost. This is because a lower specific heat reduces the state of charge that is lost when the PCT is lowered from the high value used for charging, thereby reducing the fraction of the charging that is done at a lower PCT and thus lower heat pump inlet temperature. This same effect also occurs in the case where different temperatures are used for charge and discharge without house outlet charging; however, in this case the change in temperature is much smaller and so the effect on the operating costs is not significant.

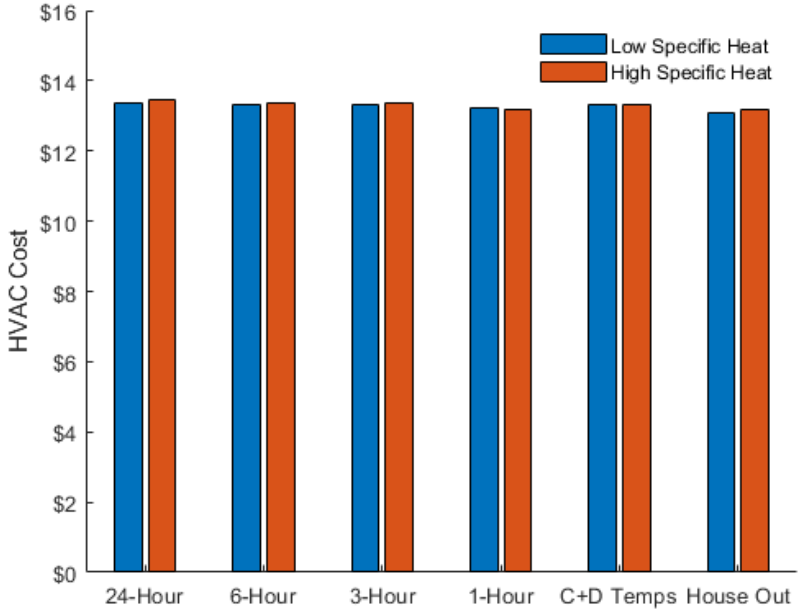

Figure 7-20. Comparison of operating costs for the week of January 1-7 for different specific heats of the PCM. Results are shown for different fixed-hour time steps (24-Hour, etc.), as well as two temperatures for charge and discharge (C+D Temps) and charging with the house outlet flow (House Out).

The operating costs for the same cases are compared for the week of January 1-7 in Figure 7-20 to see the effect of changing the specific heat in heating mode. Once again, this results in

lower costs for charge and discharge temps and charging with the house outlet flow, but only in the latter case is the cost reduction significant. For smaller fixed time steps, costs are actually higher when the specific heat is lower - a pattern that can also be seen in Figure 7-19. This is because the method of reducing costs by shifting charging loads by changing the PCT is less effective for this case, since when doing this a larger change in the state of charge per change in the PCT is desirable.

Overall, these results show that a higher ratio of latent heat to specific heat results in increased cost savings from dynamic tuning when it is used to operate at optimal mass flow rates in discharge mode but can reduce cost savings if dynamic tuning is used to shift charging loads from after the on-peak period to before, and that both of these effects are generally small even for a large change in the specific heat. Therefore, it is desirable for the PCM to have a high latent heat-to-specific heat ratio if dynamic tuning is used to set temperatures based on operating mode, but this is not likely to be significant except in the case where the system is charged with the house outlet flow.

7.1.6 Effects of a Cost Function for Tuning the PCT

All results shown so far have assumed that there is no cost associated with changing the PCT of the storage tank. However, this is not a realistic assumption, since in any real system, energy would be required to change the PCT. This is true for both a thermochemical storage system (for example, compressing hydrogen in a metal hydride system in order to change the pressure and thus the reaction temperature) or a latent heat storage system (work is required for both optical activation as in Han et al. [30] or storing ions in a battery as in Lau et al. [29]). Therefore, in this section, we will examine how the results for the weeks in June and January examined in Sections 7.1.2 and 7.1.3 change if the model includes a term for the energy required to change the PCT of the storage system, as given in Eq. 78.

Cooling Mode

To examine the effect of adding a cost function for the PCT, the model is run for the week of June 1-7 while increasing the specific energy required to change the PCT, w_{PCM}. The resulting operating costs for different fixed time steps, and for the case with temperatures for charging and

discharging, are shown in Figure 7-21. As can be seen there, once the cost for changing the PCT reaches 2 kJ/(kg K), dynamically tuning the PCT is no longer cost-effective for any case, and the operating costs for all cases are the same as the case with a fixed PCT of 10°C. The results for the case where the system is charged with the house outlet flow are not shown here. For that system, the cost continues increasing past the constant-temperature case, since the secondary loop temperature algorithm assumes a higher PCT in charging mode and leads to worse results if this is not used. Like the other cases, charging with the house outlet flow no longer results in cost savings for a cost of 2 kJ/(kg K) to change the PCT. That this system is no longer cost-effective for the same energy requirement even though it gets higher cost savings for no cost is due to it requiring larger changes in the PCT to obtain those savings.

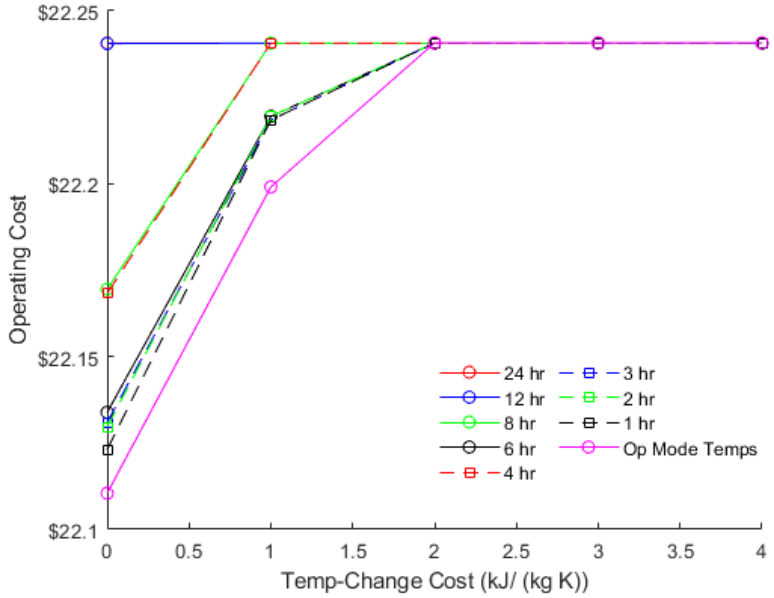

Figure 7-21. Operating costs for the variable-temperature system as a function of the energy requirement for changing the PCT for the week of June 1-7 in Elizabeth City, NC.

These results suggest that dynamic tuning of the storage temperature is likely not to be cost-effective in cooling mode, unless the energy requirements for doing it are low. For perspective, a cost of 2 kJ/(kg K) would mean that the energy required to change from a PCT of 10°C to one of 5°C (approximately the range of a typical change between charging and discharging modes) would be only 3% of the storage capacity of the TES system. But this energy requirement would

already be enough to negate any cost savings from changing the PCT in that fashion. The maximum cost function at which the system achieves cost savings is approximately an order of magnitude less than what is currently achievable on a prototype scale for varying the PCT of a PCM, since the system examined by Lau et al. [29] has a cost of 13.5 kJ/(kg K), or 6.8 kJ/(kg K) if the released electrical energy is used, for a temperature change of 6.5°C.

Heating Mode

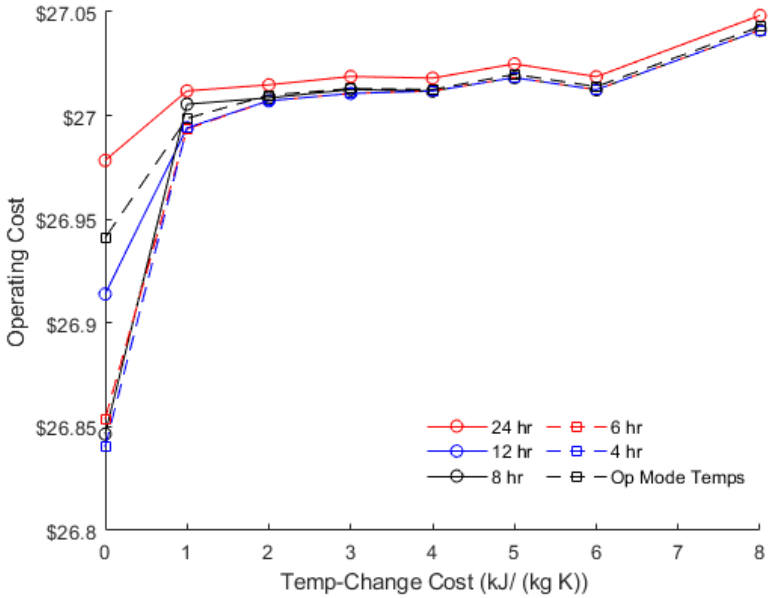

Figure 7-22. Operating costs for the variable-temperature system as a function of the energy requirement for changing the PCT for the week of January 1-7 in Elizabeth City, NC.

The results for cases with a PCT cost for the week of January examined in Section 7.1.3 are shown in Figure 7-22. These results are calculated using a week as the optimization period. This was done to avoid an issue that occurred when a day was used for optimization where the system would achieve cost savings in one day by ending at a PCT that would result in higher costs the next day when the PCT would need to change to a different value, thereby increasing the overall operating costs. Due to the increased computation time required with a week time step, fixed time steps lower than 4 hours are not included. From these results, we can see that there is a significant decrease in the cost savings once any cost is added, followed by a small increase in the operating costs with the cost for changing the PCT as it continues to increase. However, for energy

requirements up to 8 kJ/(kg K), the results do not plateau completely at one point the way they do for cooling mode.

To understand what the optimizer is doing to get these results for the different costs, the PCT values used for a 4-hour time step at different costs are plotted in Figure 7-23. The large variations in the PCT, going all the way from 30°C to 50°C multiple times in the week, that occur without any cost function are greatly reduced once a cost function is added. However, for a low value (1 kJ/(kg K)), there is still significant variation in the PCT, although within a 2-3°C range. For higher values, this flattens out almost completely, with the PCT changing by only ~0.4°C. Finally, once even this change is no longer cost-effective, the optimizer changes to a different solution, with a higher PCT that never changes significantly at all. These results indicate that the system is still able to make some variation to the PCT at higher costs than in cooling mode, but only small changes of less than 1°C. In both cases, cost savings can be obtained for a cost around 1 kJ/(kg K), but not significantly after that. As in cooling mode, the case where the system charges with the house outlet flow increases in cost rapidly once a cost is added for changing the PCT; for a cost of only 1 kJ/(kg K), it is already more expensive than any other method is for a cost of 8 kJ/(kg K).

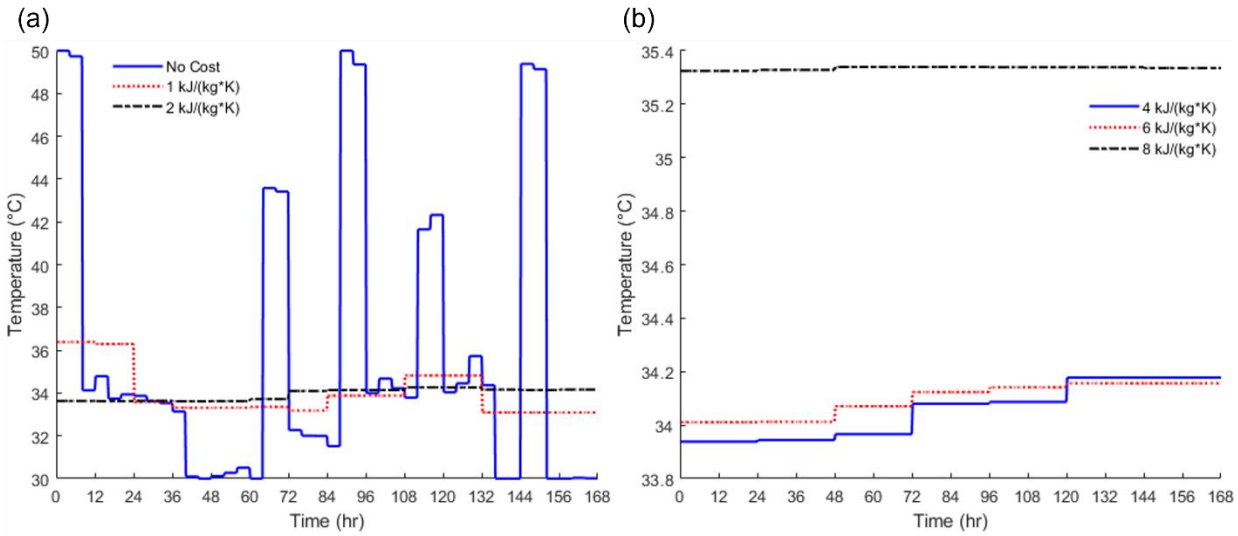

Figure 7-23. Comparison of the PCT for the week of January 1-7 at different PCT costs: (a) Cases with low PCT costs (<= 2 kJ/(kg K)), (b) cases with higher costs

One important thing to note here is that while in cooling mode, the system runs at the highest possible PCT if a constant value is used, here the constant PCT used when the cost for

dynamic tuning is prohibitive is not the lowest possible value. This indicates that in addition to the constant PCT value of 30°C used as a benchmark previously, it would also make sense for future cases to compare results to using a single optimal PCT for the entire time period studied.

7.2 Rules-Based Controller for Setting Charge and Discharge PCT Values

From the results shown in Section 7.1, it can be seen that in both cooling and heating modes, using two temperatures for charging and discharging results in cost savings that are close to the maximum possible for dynamic tuning. To see how those cost savings might be obtained in a real system, a rules-based controller is designed that sets the PCT values for charge and discharge modes according to control logic designed to achieve cost savings as close to optimal as possible.

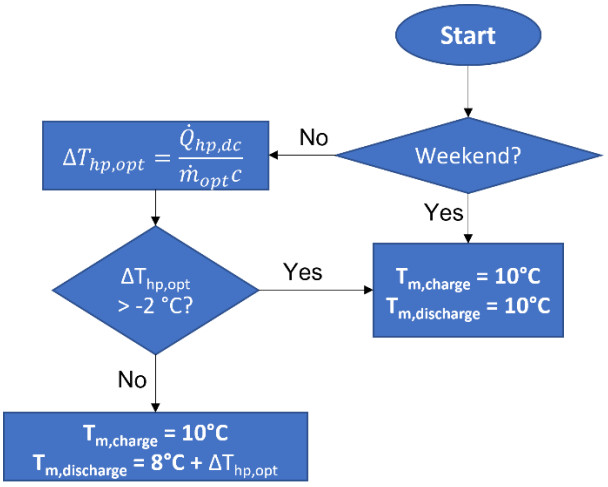

Figure 7-24. Algorithm for setting the PCT values for charging and discharging in cooling mode.

7.2.1 Rules-Based Controller for Cooling Mode

The control logic used for setting the PCT in cooling mode is simple. As seen in Figure 6-4, the algorithm used to set the temperatures in the secondary loop, while it also includes modifications to the temperatures and flow rate if the heat pump load exceeds capacity, essentially uses one of two operating conditions for a given heat pump load. The first of these is where the heat pump inlet temperature is defined as the maximum outlet temperature from the house (290

K). This is used unless the mass flow rate required for this condition is lower than the mass flow rate required to deliver the load to or from the storage tank. In that case, the mass flow rate is defined as the mass flow rate required by the storage tank. The water glycol temperatures are defined in terms of this mass flow rate and the tank inlet (heat pump outlet) temperature, which is a function of the PCT. Thus, in the first case, the heat pump inlet temperature is fixed and the PCT only affects performance by affecting the mass flow rate. In the second case, however, the heat pump inlet temperature is a function of the PCT, and thus the PCT should be maximized in order to maximize the inlet temperature.

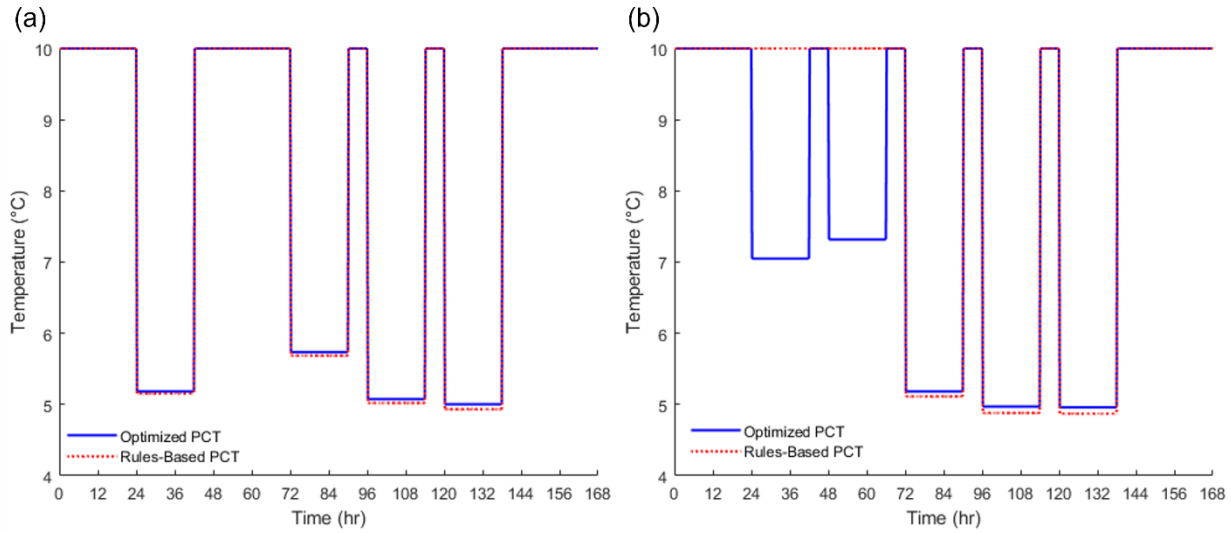

Figure 7-25. Comparison of the PCT for the weeks of (a) June 1-7 and (b) July 1-7 between the rules-based controller and the values found by the optimization function.

The algorithm used to set the PCT in cooling mode, shown in Figure 7-24, is based on examining the results for cooling mode and finding that operating temperatures are generally constrained by the storage tank when charging, but by the house outlet temperature when discharging. Therefore, the best option in charging mode is to charge at the highest PCT possible (10°C), in order to maximize the heat pump inlet temperature. But in discharge mode, where the PCT can generally be lowered without lowering the heat pump inlet temperature, the PCT is instead set so that the temperature difference across the heat pump results in an optimal mass flow rate. A single value can be used for the whole on-peak period to accomplish this, since the load-shifting control logic uses a flat heat pump load when discharging. Since the tank inlet temperature only changes with the PCT if the PCT is less than 6°C (as shown in Figure 6-4) in order to maintain

a minimum temperature difference across the heat pump, a value of 10°C is used for any case where the PCT would otherwise be between 6°C and 10°. A value of 0.25 kg/s is used for the optimal mass flow rate, based on the COP function shown in Figure 6-12.

To test the effectiveness of this algorithm, the system is analyzed using it to set the PCT for the same weeks in June and February shown in Section 7.1.4. The PCT values from the rules-based method and the optimizer are compared in Figure 7-25, and the resulting operating costs in Figure 7-26. The PCT values are very similar at all times except the first two on-peak periods in July, when the optimizer lowers the PCT by ~3°C while the rules-based controller does not change the PCT. However, since T_m > 6°C for both cases, this does not significantly affect the performance. As shown in Figure 7-25, operating costs are virtually identical for both weeks, with the rules-based controller obtaining >98% of the cost savings that the optimal controller achieves (relative to a constant PCT of 10°C) in both cases.

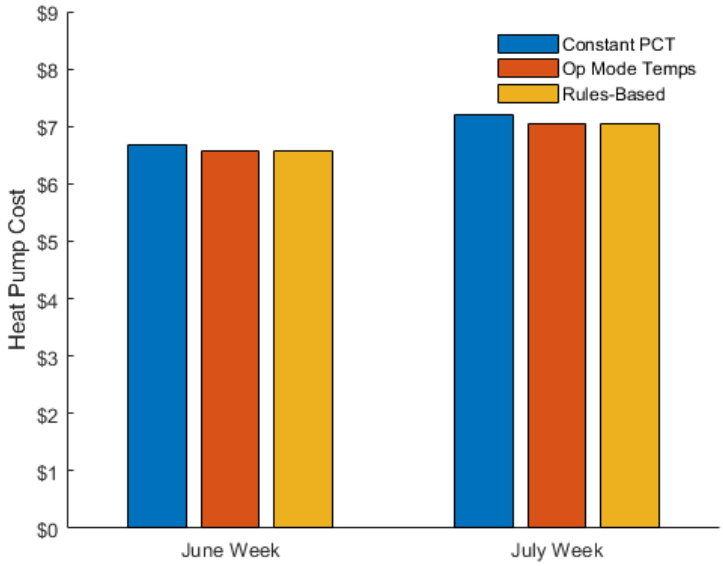

Figure 7-26. Operating costs for the rules-based controller for the weeks of June 1-7 and July 1-7, compared to optimal results for charge and discharge temperatures and a constant PCT of 10°C.

7.2.2 Rules-Based Controller for Heating Mode

While a very simple algorithm is sufficient to achieve cost savings very close to optimal for cooling mode, there are several factors that cause heating mode to require more complicated

control logic. First, as noted in Section 7.1.3, increasing the PCT at the beginning of the day sometimes leads to the system not being able to discharge fully, because the state of charge is lowered by the change in the PCT but the system cannot be charged to make up for this because the loads in the morning are too high. Second, the system is more likely to be constrained by the house rather than the storage tank when charging, since the temperature difference between the house outlet and the closest PCT is smaller and the control logic for charging makes it more likely the system will be charged at times with significant heating loads. Third, and most significantly, the optimal mass flow rate is less than half that for cooling mode, with a value of 0.1 kg/s being used based on the performance map shown in Figure 6-12. This lower optimal mass flow rate means that operating at the optimal flow rate is often not possible in discharge mode because the mass flow rate required by the storage tank is larger than the optimal value.

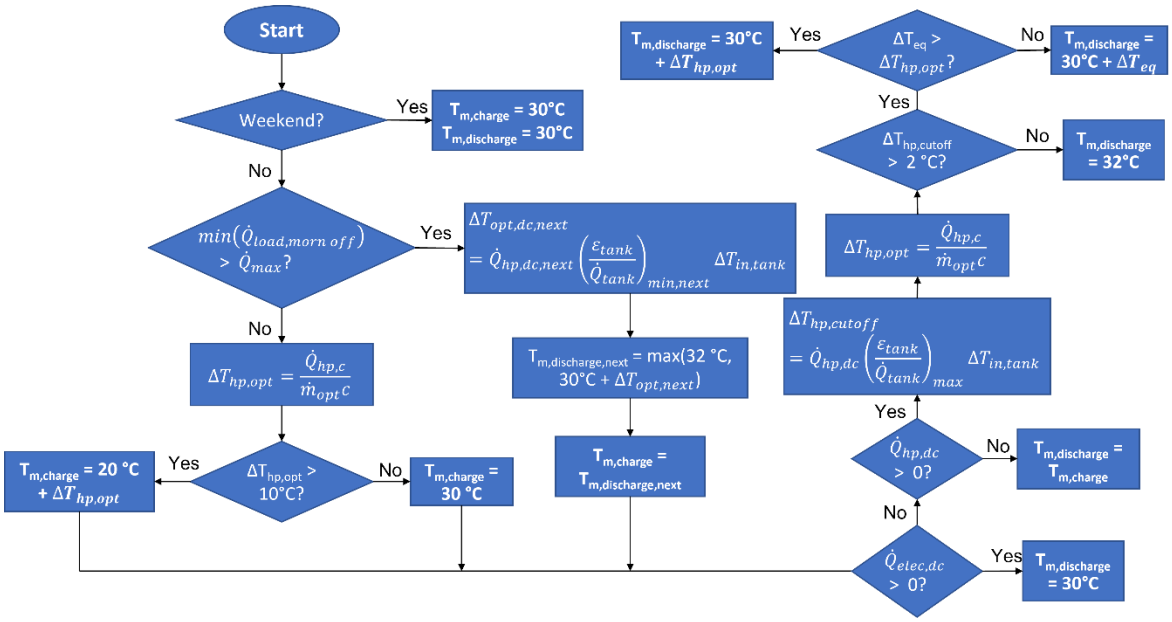

Figure 7-27. Algorithm for setting the PCT values for charging and discharging in heating mode.

The algorithm that determines the PCT in heating mode is shown in Figure 7-27. Unlike in cooling mode, the system does not always charge at the same PCT. Instead, to avoid a case where the system loses charge from changing to the discharge PCT and not being able to charge in the morning, the system will charge at the discharge value of the PCT for the next day if the load before the on-peak period on the next day is always greater than the heat pump capacity. Even if this is not the case, the PCT is also sometimes increased to allow for charging at the PCT that will

achieve the optimal mass flow rate if the operating temperatures are constrained by the house rather than the storage tank.

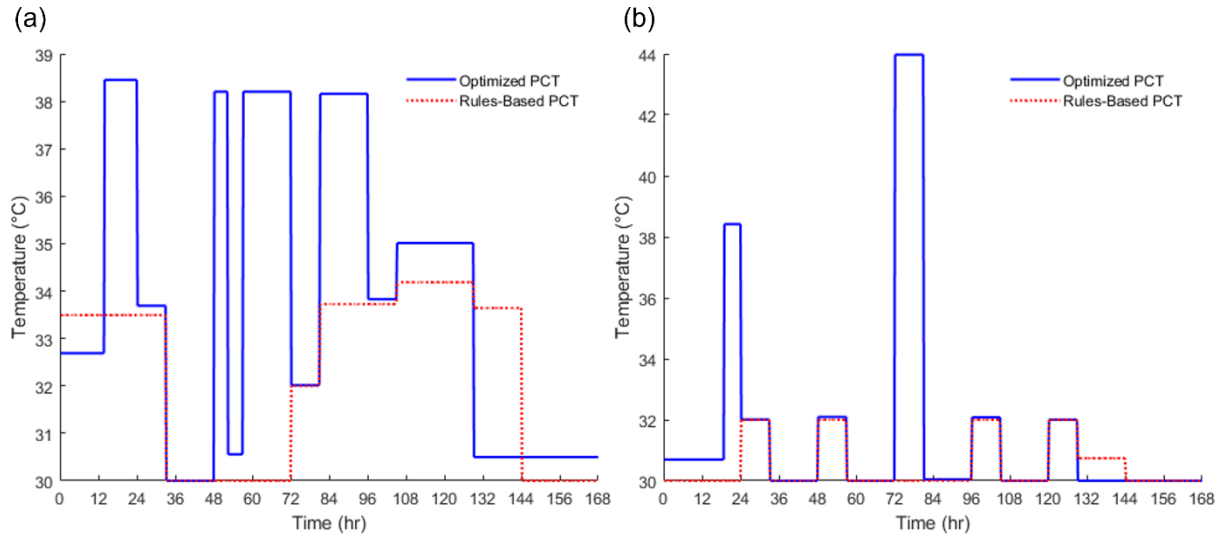

Figure 7-28. Comparison of the PCT for the weeks of (a) January 1-7 and (b) February 1-7 between the rules-based controller and the values found by the optimization function.

The PCT value used for discharge mode is primarily determined by whether the system can operate at the optimal mass flow rate or if this is prevented by the constraint imposed by the storage tank. If the system can operate at the optimal flow rate, it does so in the same way it does for cooling mode (with the values used to set the PCT updated to reflect the heating temperature algorithm shown in Figure 6-5). However, if the system cannot operate at the optimal mass flow rate, it tries to operate as close as it can to the cutoff point between the system being constrained by the house outlet and the system being constrained by the tank outlet. This is done because for PCT values below the cutoff, increasing the PCT improves performance by lowering the mass flow rate. However, for PCT values above the cutoff, increasing the PCT instead increases the heat pump inlet temperature, thereby making the system performance worse. Therefore, the algorithm sets the PCT to the value that results in the system operating at the cutoff point for the time in the on-peak period the mass flow rate required by the storage tank is lowest (so the PCT will be above the cutoff for the rest of the period). In addition to this, the system will also operate at the minimum PCT for cases where auxiliary electric heating is needed even while discharging the storage system, since increasing the mass flow rate increases the capacity of the heat pump at low ambient

temperatures, thereby reducing the use of auxiliary heating. No such cases occur in Elizabeth City, but one is discussed in Section 7.3.3.

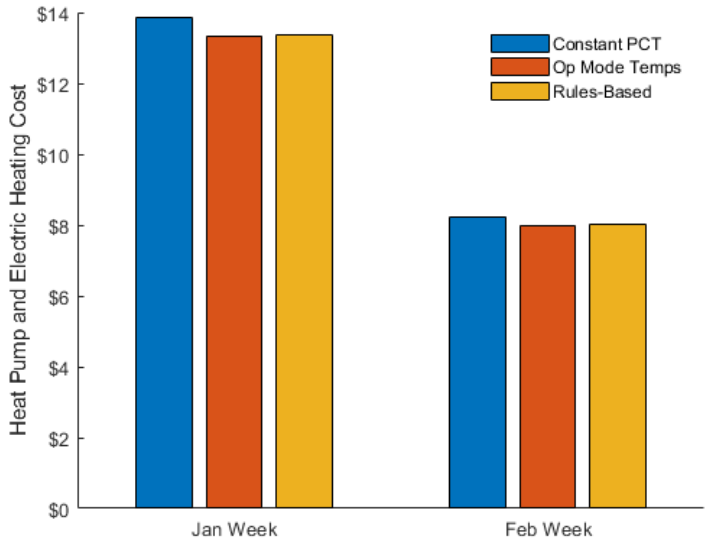

Figure 7-29. Operating costs for the rules-based controller for the weeks of January 1-7 and February 1-7, compared to optimal results for charge and discharge temperatures and a constant PCT of 30°C.

To test the effectiveness of this algorithm, the system is analyzed using it to set the PCT for the same weeks in January and February shown in Section 7.1.4. The PCT values from the rules-based method and the optimizer are compared in Figure 8-4, and the resulting operating costs in Figure 8-5. Unlike cooling mode, here the rules-based controller does use significantly different temperatures than the optimizer, particularly for the week in January. In particular, the optimizer repeatedly uses higher PCT values than those used by the rules-based controller. However, this does not result in significantly lower cost savings. The rules-based controller achieves 97.9% of the cost savings (relative to the constant-PCT case) from the optimal charge and discharge temperatures the week in January, and 94.1% of the cost savings for the week in February. Therefore, while unlike in cooling mode, this algorithm sets the PCT to significantly different values than those used by the optimizer, like in cooling mode it is able to achieve near-optimal cost savings.

7.3 Effect of Location and Rate Structure on Results with Dynamic Tuning

Having examined how dynamically tuning the PCT can achieve cost savings in Section 7.1 and used this to develop a rules-based controller for tuning the PCT in Section 7.2, the next step is to examine how these results change if different rate structures or different locations are studied. In Section 7.3.1, the effect of varying the ratio of on-peak to off-peak rates and of adding an on-peak demand charge are considered. Next, rates with different on-peak periods are considered in Section 7.3.2. Finally, in Section 7.3.3, the system is studied in a location with higher heating loads than Elizabeth City (Kansas City, MO) and a location with lower heating loads and higher cooling loads (Phoenix, AZ).

7.3.1 Comparing Different Rate Structures for the Existing On-Peak Period

To examine how the TOU rate structures influence the ways in which dynamic tuning is used, and whether the rules-based controller still achieves near-optimal cost savings for different rates, the system is analyzed for Elizabeth City, NC with four different rate structures. These rate structures, given in Table 7-1, have the same on-peak period as the existing rates used in Section 7.1 and are defined in a manner similar to the rates used in Section 5.2.3. That is, all these rates result in the same annual operating cost if no TES is used. In this case, they are defined so that the annual costs for that case are the same as those for a flat rate of $0.12/kWh. This flat rate is used instead of using the existing rates as in Section 5.2.3 because the existing rates for this location are lower than average for utility rates in the United States, so a higher value that is closer to more common rates is used instead.

Table 7-1. Rate structures (with the same on-peak period as existing rates) used to examine how different rates effect the performance of a variable-temperature TES system.

Rate Structure	Off-Peak Rate	On-Peak Rate	On-Peak Demand Charge
Low Incentive	$0.1041	$0.2081	$0
High Incentive	$0.0744	$0.3721	$0
Low Incentive w/Demand	$0.1041	$0.1561	$3.22
High Incentive w/Demand	$0.0744	$0.1488	$13.81

As in Section 5.2.3, these rates are defined by varying the ratio of on-peak to off-peak rates and whether an on-peak demand charge is used. However, unlike in that case, on-peak rates that

are higher than the off-peak rates are used for the case with an on-peak demand charge. This is done since most existing rates with demand charges still use different off-peak and on-peak rates as well. Looking at rates with only an on-peak demand charge is useful for looking at maximum potential cost savings, as in Section 5.2.3, but less useful for understanding how the system will behave for existing rate structures.

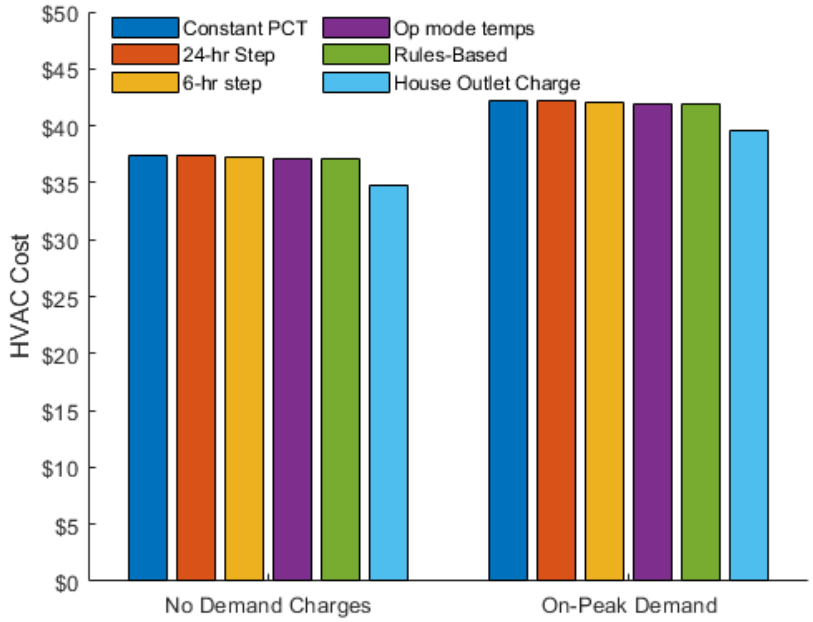

Figure 7-30. Comparison of operating costs for different dynamic-tuning cases for the month of June in Elizabeth City, NC using the low-incentive rates from Table 7-1. The cost shown is the sum of heat pump operating costs and the monthly demand charge.

Two rates without demand charges are used: one with an on-peak to off-peak ratio of 2 (called the 'Low Incentive' case since a lower ratio provides less incentive to use energy storage) and one with a ratio of 5 (the 'High Incentive' case). The ratio of 5, used in existing rates for Elizabeth City, is used as the high-incentive value since these rates had one of the highest ratios of any existing rates examined in the NREL database [114]. For the rates with on-peak demand charges, the ratio of on-peak to off-peak rates is lowered to 1.5 for the Low-Incentive case and 2 for the High-Incentive case, and in each case the on-peak demand charge is calculated to result in an increase in cost for a conventional system equal to the reduction in cost from the lower on-peak rates.

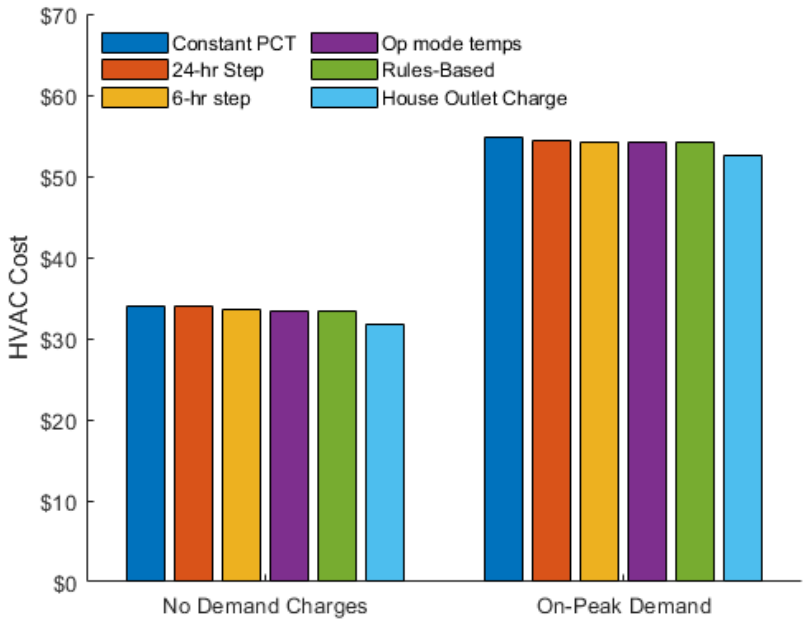

Figure 7-31. Comparison of operating costs for different dynamic-tuning cases for the month of June in Elizabeth City, NC using the high-incentive rates from Table 7-1. The cost shown is the sum of heat pump operating costs and the monthly demand charge.

Since demand charges are applied on a monthly basis, the system is studied for a full month in the summer (June) and a full month in the winter (January). For the summer month, optimal solutions for two fixed time steps (24 hours and 6 hours), as well as the case with charge and discharge temperatures and the case where the tank is charged with the house outlet flow, are compared to a fixed PCT of 10°C and the rules-based controller. Results for the low-incentive rates are shown in Figure 7-30, and for the high incentive rates in Figure 7-31. In both images, the costs from non-HVAC loads are not included, but the full cost from the demand charge (including the effect of non-HVAC loads) is. This means that a higher cost is shown for rates with an on-peak demand charge, although the total operating cost (including non-HVAC loads) for these cases will be comparable to the total cost without demand charges.

Comparing these results, we can see that using an on-peak demand charge does not have much of an effect on the use of dynamic tuning: for both sets of rates, the same trends hold between cases for rates with and without an on-peak demand charge. The one exception to this is that for the high-incentive rates, there is a small reduction in cost (relative to the constant PCT of 10°C) when using a 24-hour time step, which is not the case for any of the other rates. This is because usually, when a 24-hour time step is used, a constant PCT of 10°C is still used since the benefits

of charging at this temperature outweigh those of discharging at a lower temperature. However, with a large on-peak demand charge, some small cost savings can be obtained by using a lower PCT on the days with the highest on-peak loads, since this reduces the on-peak demand charge.

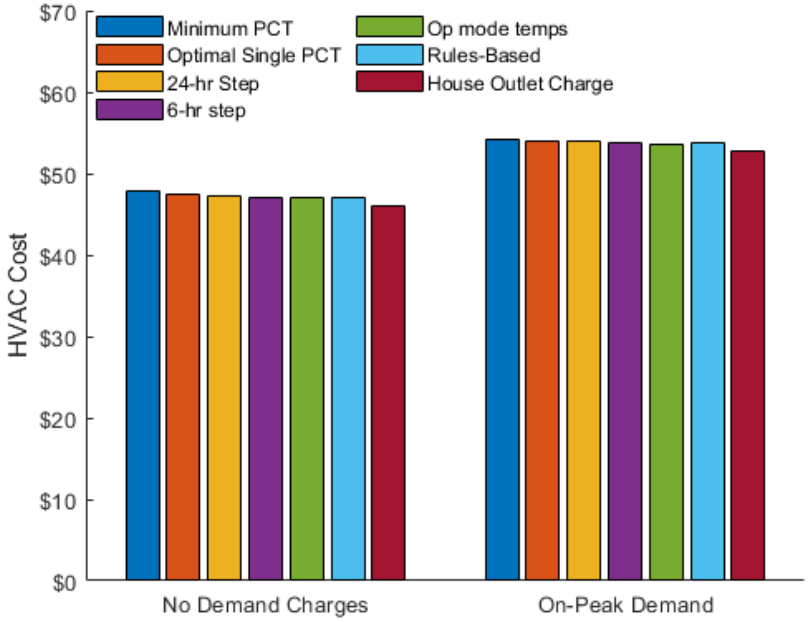

Figure 7-32. Comparison of operating costs for different dynamic-tuning cases for the month of January in Elizabeth City, NC using the low-incentive rates from Table 7-1. The cost shown is the sum of heat pump and electric heating operating costs and the monthly demand charge.

One other trend of note is that while the overall costs are higher in Figure 7-30 than in Figure 7-31, and the savings from most methods of dynamic tuning lower, the cost savings from charging with the house outlet flow are actually larger in this case. The lower costs savings overall are due to these rates having less incentive for energy storage, which also means less incentive for optimizing the PCT for discharging. The higher cost savings from charging with the house outlet flow come from the fact that this system reduces costs when charging during the off-peak periods; since the off-peak rates are higher for the low-incentive rates, reducing costs when charging results in higher cost savings than it does for the high-incentive rates. Thus, while using charge and discharge temperatures saves $0.45 for the high-incentive case with no demand charge but only $0.22 for the low-incentive, charging with the outlet flow saves $2.57 for the low-incentive case as compared to $2.08 for the high-incentive case.

As these numbers indicate, the cost savings from dynamic tuning are still limited for all cases except the house outlet charge case, as in Section 7.1.2. As in Section 7.2.1, the rules-based

controller is able to perform essentially as well as using optimal temperatures for charging and discharging.

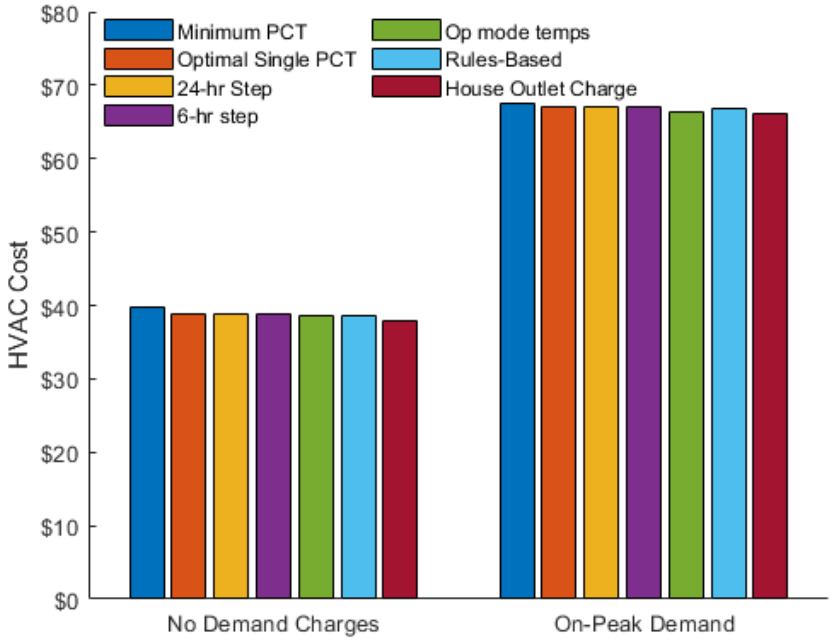

Figure 7-33. Comparison of operating costs for different dynamic-tuning cases for the month of January in Elizabeth City, NC using the high-incentive rates from Table 7-1. The cost shown is the sum of heat pump and electric heating operating costs and the monthly demand charge.

For the month of January, results are shown for the low-incentive case in Figure 7-32, and for the high-incentive case in Figure 7-33. The six cases compared in cooling mode are also shown for these cases. However, another case is also considered: in addition to using a constant PCT of 30°C (Minimum PCT), there is also a case where a single PCT is used throughout the month, but this value is optimized to minimize cost savings (Optimal Single Temperature). As can be seen in Figure 7-32 and Figure 7-33, this method is able to achieve the majority (>67% in all cases) of the cost savings from using a 24-hour time step compared to the minimum PCT. This confirms what is indicated by the results in Section 7.1.6: the optimal PCT for heating mode is not necessarily the minimum value. This is because the minimum value is sometimes not even the optimal value for charging, as discussed in Section 7.1.3, and only rarely the optimal value for discharge mode, whereas it always is at least for charging in cooling mode. The optimal PCT values used for this case are similar for all four rate structures, all within the range of 32.9°C - 33.6°C.

Looking at the performance of the rules-based controller, we can see that it is effective for rates without demand and with a low on-peak demand charge, achieving >90% of the cost savings compared to the minimum-PCT case, and >80% of the cost savings compared to the optimal single-PCT case, that using optimal temperatures for charge and discharge does. However, it is less effective for the high-incentive case with an on-peak demand charge, where it only achieves 55% of the cost savings relative to the minimum-PCT case and only 19% compared to the optimal single PCT case. This is likely because the controller algorithm is based on how the optimizer minimizes costs for rates without demand charges, so if different strategies, that prioritize reducing peak loads, are best for rates with high on-peak demand charges, the controller will not do as well as these. However, while the rules-based controller performs less optimally for this case, it still achieves significantly higher cost savings than either single-PCT case, showing it is an effective algorithm for reducing cost even when it is not the optimal one.

As in cooling mode, the cost savings from dynamic tuning in heating mode are larger for high-incentive cases. However, this difference is due to the savings from using a single optimal temperature ($1.00 high-incentive vs. $0.38 low-incentive) and not the further savings from using charge and discharge temperatures ($0.27 high-incentive, $0.33 low-incentive). Furthermore, the cost savings from using the house outlet flow are not larger for the low-incentive case as they are in cooling, but only a few cents different between the two cases. This is likely due to the COP depending less strongly on heat pump inlet temperature for heating, which means that cost savings from optimizing flow rate are larger while the savings from charging at lower temperatures by using the house outlet flow are lower than in cooling mode. This would also explain why charging with the house outlet flow achieves lower additional cost savings compared to other dynamic tuning strategies than it does for cooling mode.

7.3.2 Comparing Different On-Peak Periods

Having examined the effect of different utility rates with the same on-peak period, the next step is to see if the effect of dynamic tuning is substantially different for rates with different on-peak periods. To study this, two alternate on-peak periods are considered. For the first, the morning on-peak period in the winter is replaced by an afternoon on-peak period. This on-peak period is common in locations where more homes use gas heating or where heating loads are very low, since

in either case peak loads in winter are primarily determined by non-HVAC loads. In this structure, the same on-peak period is used in the summer and the winter, which is the same as the summer on-peak period used in the existing rates for Elizabeth City. The second alternate on-peak period examines the effect of extending the on-peak period by using a summer on-peak period that starts earlier in the afternoon and goes later into the evening and two on-peak periods in the winter: one in the morning and one in the evening.

Table 7-2. Different on-peak periods used to study how varying the on-peak period affects dynamic tuning of the PCT. The SAWM period is the one used by existing rates.

On-Peak Periods	Summer On-Peak Period	Winter On-Peak Period
Summer Afternoon, Winter Morning (SAWM)	2-7 pm	6-10 am
Summer Afternoon, Winter Afternoon (SAWA)	2-7 pm	2-7 pm
Summer Afternoon and Evening, Winter Morning and Evening (SAEWME)	12-8 pm	6-10 am, 6-9 pm

Table 7-3. Rate structures (with the same on-peak period as existing rates) used for the SAWA on-peak period.

Rate Structure	Off-Peak Rate	On-Peak Rate	On-Peak Demand Charge
Low Incentive	$0.1037	$0.2074	$0
High Incentive	$0.0737	$0.3686	$0
Low Incentive w/Demand	$0.1037	$0.1556	$3.61
High Incentive w/Demand	$0.0737	$0.1474	$15.39

Table 7-4. Rate structures (with the same on-peak period as existing rates) used for the SAEWME on-peak period.

Rate Structure	Off-Peak Rate	On-Peak Rate	On-Peak Demand Charge
Low Incentive	$0.0949	$0.1899	$0
High Incentive	$0.0584	$0.2919	$0
Low Incentive w/Demand	$0.0949	$0.1424	$4.82
High Incentive w/Demand	$0.0584	$0.1167	$17.77

The on-peak periods for these rates, along with the existing on-peak periods used in previous sections, are given in Table 7-2. The rates used in the case with summer and winter afternoon (SAWA) on-peak periods are shown in Table 7-3. Rates for the case with summer

afternoon and evening and winter morning and evening (SAEWME) on-peak periods are shown in Table 7-4. These rate structures are defined in the same way as the ones used in Section 7.3.1. This method results in different rates for different on-peak periods since the different on-peak periods result in different operating costs for a conventional system. Results for the low-incentive rates are not shown here, but these rates are used in the optimal sizing of the system in Section 8.1. Similarly, for the SAWA case, only the winter results are shown here since results for a summer afternoon on-peak period have already been considered.

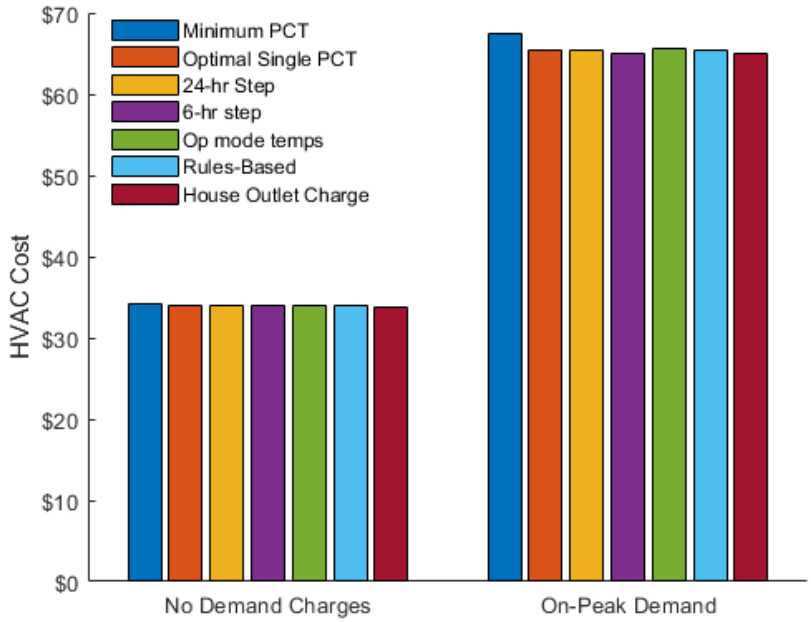

Figure 7-34. Comparison of operating costs for different dynamic-tuning cases for the month of January in Elizabeth City, NC using the high-incentive rates from Table 7-3 with the SAWA on-peak period from Table 7-2. The cost shown is the sum of heat pump and electric heating operating costs and the monthly demand charge.

Results for the high-incentive rates with a summer afternoon on-peak period are shown in Figure 7-34. As can be seen by comparing these results to Figure 7-33, the potential for cost savings from dynamic tuning here is lower for rates without demand charges ($0.31 from charge and discharge temperatures, $0.57 from charging with the house outlet flow) but higher for rates with demand charges ($1.97 from charge and discharge temperatures, $2.43 from charging with the house outlet flow). This difference is primarily due to the difference in cost savings from using an optimal single PCT: $1.77 with a demand charge, but only $0.26 without one. This difference is not due to the selection of very different PCT values (32.8°C is used without demand, 32.0°C

with demand). Instead, it implies that shifting to an optimal temperature results in a larger percentage reduction in peak load than it does in the total load. This is not universally true; the opposite is the case for the SAWM results.

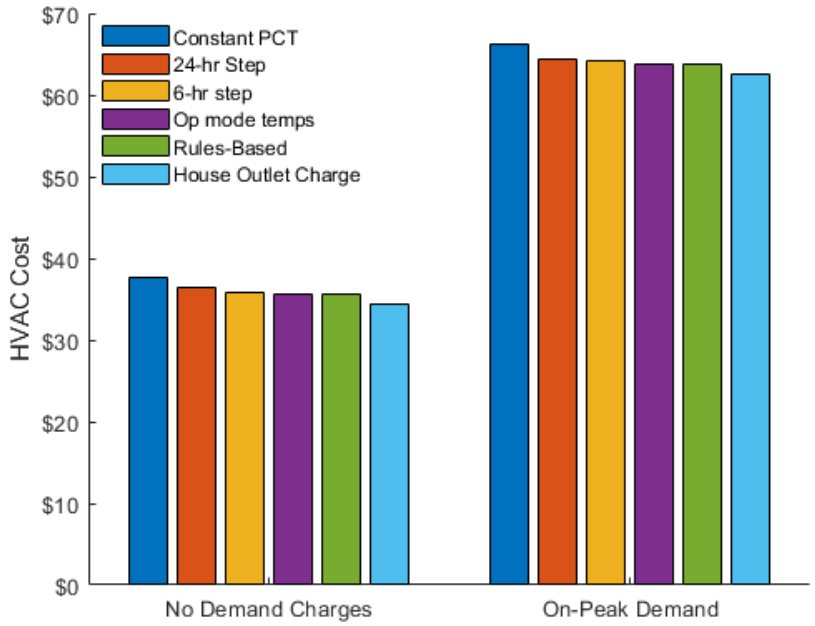

Figure 7-35. Comparison of operating costs for different dynamic-tuning cases for the month of June in Elizabeth City, NC using the high-incentive rates from Table 7-4 with the SAEWME on-peak period from Table 7-2. The cost shown is the sum of heat pump and electric heating operating costs and the monthly demand charge.

The performance of the rules-based controller is also the opposite of the SAWM results, since it does better for the case with a demand charge (actually beating the optimized case, likely due to the optimizer losing some cost savings by trying to prevent an increase in demand charges at a time that did not turn out to be the peak load) than it does for the case without one. For both cases, the rules-based controller is able to outperform a single optimal PCT and thereby obtain the majority of the benefits from dynamic tuning, as in the SAWM case.

Results for a month in June using the high-incentive rates for the SAEWME on-peak period are shown in Figure 7-35. These results show substantially larger cost savings from dynamic tuning than is obtained for the SAWM case. In particular, there are significant cost savings from using a 24-hour time step as compared to a constant PCT ($1.33 without demand, $1.74 with demand) when there are none at all for the SAWM case. Further cost savings can be obtained by using two temperatures a day: charge and discharge temperatures result in savings of $1.99 without demand

and $2.32 with demand. Costs can be lowered further the system is charged with the house outlet flow, but the cost savings for this case compared to using charge and discharge temperatures are comparable to the SAWM case.

These larger cost savings are not due to a different strategy for setting the PCT, since the rules-based controller achieves >98% of the cost savings from optimal temperatures for charging and discharging. Instead, they are a result of the longer on-peak period, which means that more of the on-peak load is being met by the heat pump and less by the TES system. This means that there are larger potential cost savings from operating at optimal temperatures during the on-peak period than there are for a shorter on-peak period. Because of this, operating at the optimal PCT for discharge rather than the optimal PCT for charge for a full day sometimes results in cost savings; this explains the cost savings from a 24-hour time step. These cost savings are even greater if optimal temperatures are used for both charging and discharging the system.

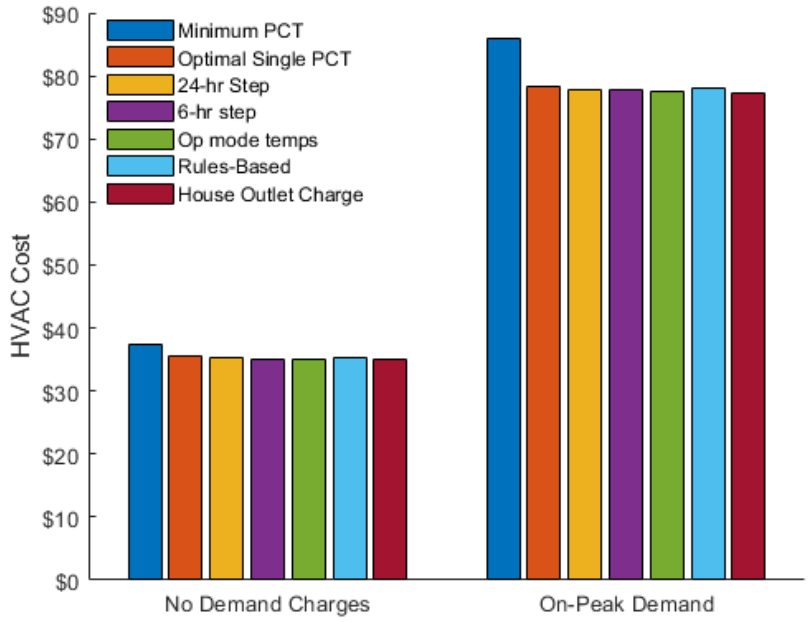

Figure 7-36. Comparison of operating costs for different dynamic-tuning cases for the month of January in Elizabeth City, NC using the high-incentive rates from Table 7-4 with the SAEWME on-peak period from Table 7-2. The cost shown is the sum of heat pump and electric heating operating costs and the monthly demand charge.

The effect of a longer on-peak period in the winter can be seen by looking at the results for January with the high-incentive rates for the SAEWME case in Figure 7-36. The most striking feature here is how much the costs can be reduced using a single optimal PCT instead of using a

PCT of 30°C for rates with an on-peak demand charge. The operating costs are reduced by $7.53, a change 3 times greater than any other seen in previous results. This reduction is due to a much higher PCT (38.9°C) being used for the single-value case than any previous case, indicating that the value is being set primarily to optimize for the on-peak period rather than the off-peak period. Using this value instead of 30°C reduces the mass flow rate at the point where the peak load occurs by ~60%, thereby greatly increasing the COP at that time. Cost can be reduced by almost $1 more by using different temperatures for charge and discharge; however, the rules-based controller only is able to achieve ~25% of this improvement.

The higher PCT used for a single value and the large cost savings associated with it are due to the same effect seen in the cooling results previously: a longer on-peak period means more heat pump work during the on-peak period and thus more potential cost savings from optimizing the system during discharge. These savings are much smaller for rates without a demand charge - $2.38 for optimal charge and discharge temperatures - but are still significantly larger than those for either a morning or an afternoon on-peak period. This is again due to the increased potential for cost savings by optimizing in discharge mode due to the longer on-peak period. This results in the single optimal PCT value for this case being 35.1°C, lower that the case with on-peak demand charges but higher than the SAWM or SAWA cases.

These results indicate that longer on-peak periods result in a larger potential for cost savings from dynamic tuning. However, it should be noted that this is due to the increased heat pump work during these periods. This increased heat pump work is in turn due to the TES system not being re-sized for the longer period, since optimal sizing is likely to be larger for a longer on-peak period. It appears that dynamic tuning is most effective when the TES system is more frequently providing partial rather than full storage. This suggests a tradeoff where larger storage systems mean more overall cost savings from storage, while there are larger savings from dynamic tuning for smaller systems. The determining factor, then, in how much dynamic tuning can reduce costs is how close the sizing at which dynamic tuning results in maximal cost savings is to the optimal sizing for the system when considering overall cost savings and payback period.

The rules-based controller is shown to consistently achieve significant cost savings compared to a fixed PCT of 10°C in cooling or 30°C in heating. However, while its performance is consistently near-identical to optimal values for cooling, it often achieves significantly less than optimal savings in heating mode. Its performance in heating mode is worst for rates with on-peak

demand charges and with longer on-peak periods, suggesting that there may be potential improvements that could be made to it for such rate structures. In such cases, it still consistently outperforms a single optimal PCT for the month but achieves significantly lower cost savings than optimal temperatures for charging and discharging, or sometimes even less than a single optimal temperature for each day.

Table 7-5. Rate structures (with the same on-peak period as existing rates) used to examine how different rates effect the performance of a variable-temperature TES system.

Location	Demand Charge?	Off-Peak Rate	On-Peak Rate	On-Peak Demand Charge
Kansas City, MO	No	$0.0730	$0.3650	$0
Kansas City, MO	Yes	$0.0730	$0.1460	$11.54
Phoenix, AZ	No	$0.0719	$0.3597	$0
Phoenix, AZ	Yes	$0.0719	$0.1439	$15.35

7.3.3 Comparing Different Locations

To see how the effects of dynamic tuning change for significantly different load profiles, month-long analysis like that conducted in the previous two sections is performed for houses in Phoenix, AZ and Kansas City, MO. In both cases, the effect of dynamic tuning is examined for the months of June and January using the SAWM on-peak period from Table 7-2. High-incentive rate structures, with and without demand charges, are used for both locations in this analysis. These rate structures are determined by the same method used in Section 7.3.1 and are given in Table 7-5.

Kansas City, MO

Results for the month of June in Kansas City can be seen in Figure 7-37. The main difference between these results and those for Elizabeth City for this on-peak period is that here there are larger cost savings for using a 24-hour time step ($0.41 instead of none for rates without demand charges, $0.88 instead of $0.33 for rates with demand charges). Cost savings for using charge and discharge temperatures or for charging with the house outlet flow, relative to the 24-hour time step case, are comparable to those for Elizabeth City; however, these cost savings are larger compared to the constant-PCT case due to the cost savings from using a 24-hour time step.

As in Elizabeth City, the rules-based controller is effective at achieving cost savings very close (>95%) to the optimizer for charge and discharge temperatures.

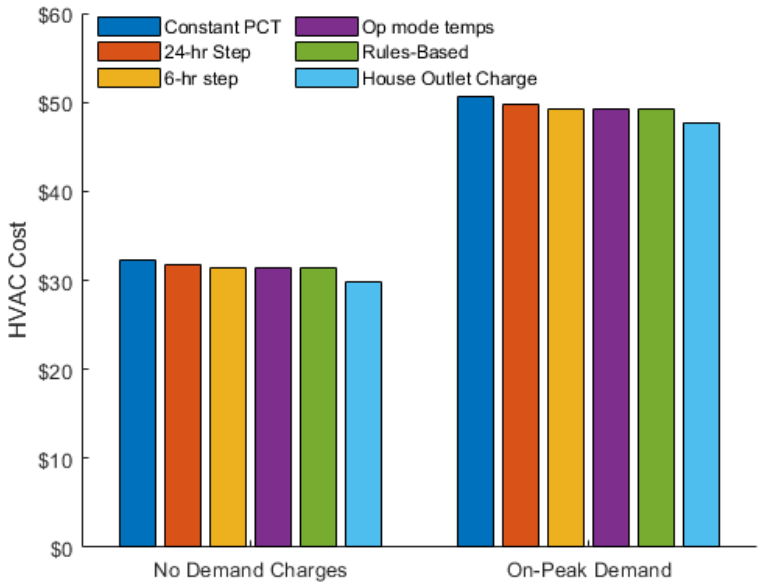

Figure 7-37. Comparison of operating costs for different dynamic-tuning cases for the month of June in Kansas City, MO using the rates from Table 7-5 with the SAWM on-peak period from Table 7-2. The cost shown is the sum of heat pump operating costs and the monthly demand charge.

Results for the month of January can be seen in Figure 7-38. Here, operating costs are much higher than they are for Elizabeth City, since this location has significantly higher heating loads, and a large portion of these loads must be met with auxiliary heating rather than the heat pump. However, this large increase in the heating loads does not result in a similar increase in the cost savings from dynamic tuning, with cost savings from all strategies other than charging with house outlet flow being <$1.50, and savings with house outlet charging still <$3.00. The rules-based controller is capable of achieving significant cost savings for this case, but significantly less than the optimal solution: 60% relative to a PCT of 30°C for rates without demand charges, and 49% for rates with demand charges.

One major reason these cost savings are not larger is that the increased loads mean that electric heating is sometimes needed in the on-peak period even after loads have been reduced by the use of storage. This use of auxiliary heating means that the optimal solution when discharging is to increase the mass flow rate, since this increases the heat pump capacity at low ambient

temperatures (as shown in Figure 6-12). This reduces the use of auxiliary heating, which can improve performance even if the COP is reduced. This means that using the minimum PCT is the best strategy for more on-peak periods, which reduces the potential cost savings from dynamic tunning since there are less times when it is desirable to change the PCT. Because of this, the cost savings from using an optimal single PCT are lower than for Elizabeth City, and a value of 32°C is used as the optimal PCT for both cases. In addition, in this case the mass flow rates for these on-peak periods are often above the value at which the correlation saturates as described in Section 6.2.2. Therefore, the model does not accurately capture the loss of COP for some of these cases, so the benefits of increasing the mass flow rate to increase the capacity are overestimated.

Overall, the summer results for this location do not show any important new trends, since cooling loads are similar to those for Elizabeth City, while the winter results do show differences due to the use of on-peak electric heating. These winter results, combined with those for the SAEWME case in Elizabeth City, suggest that dynamic tuning will lead to the largest cost savings in the winter if the TES system is sized to prevent the need for auxiliary heating during the on-peak period for as much of the winter as possible.

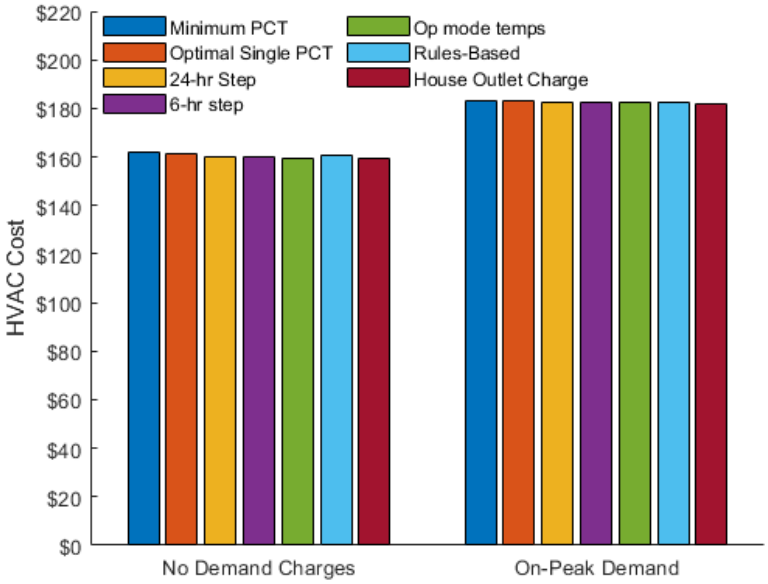

Figure 7-38. Comparison of operating costs for different dynamic-tuning cases for the month of January in Kansas City, MO using the rates from Table 7-5 with the SAWM on-peak period from Table 7-2. The cost shown is the sum of heat pump and electric heating operating costs and the monthly demand charge.

Phoenix, AZ

Results for the month of June in Phoenix can be seen in Figure 7-39. Due to the larger cooling loads for this location, the operating costs for all cases are substantially higher than they are for either Kansas City or Elizabeth City. Unlike the higher heating loads in Kansas City, however, these higher cooling loads do translate into larger cost savings from dynamic tuning. Using two temperatures for charging and discharging results in cost savings of $5.55 for rates without demand charges and $4.80 for rates with demand charges, while charging with the house outlet flow results in cost savings of $6.75 for the first case and $5.91 for the second. Since there is no effect like that of on-peak auxiliary heating that changes the strategy for dynamic tuning, higher cooling loads translate to higher cost savings from dynamic tuning. As with the SAEWME case for Elizabeth City, it should be noted that the storage tank is not re-sized for these large loads and so the cost savings might be different for an optimally-sized system.

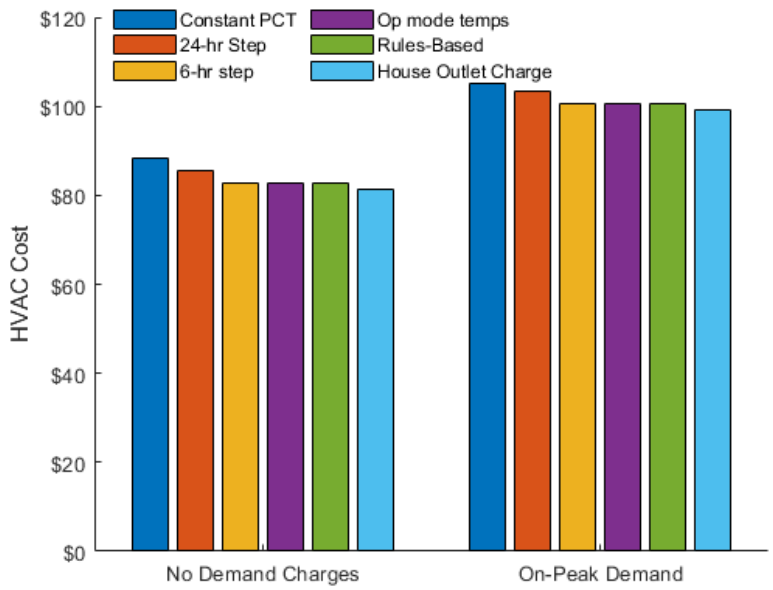

Figure 7-39. Comparison of operating costs for different dynamic-tuning cases for the month of June in Phoenix, AZ using the rates from Table 7-5 with the SAWM on-peak period from Table 7-2. The cost shown is the sum of heat pump operating costs and the monthly demand charge.

Results for the month of January in Phoenix can be seen in Figure 7-40. Here, operating costs are lower than in other locations due to the low heating loads in Phoenix. As a result of these

low loads, the cost savings for dynamic tuning are also lower- even for charging with the house outlet flow, cost savings are less than $1 for both cases. Here, the rules-based controller achieves virtually the same cost savings as optimal temperatures for charging and discharging. This, combined with previous results, strongly suggests that this controller does best in heating mode for cases with lower heating loads, but that there is more room for improvement in how it handles cases where there are higher heating loads. Other than the performance of the rules-based controller, the trend in how different cases compare here is similar to other cases with higher loads.

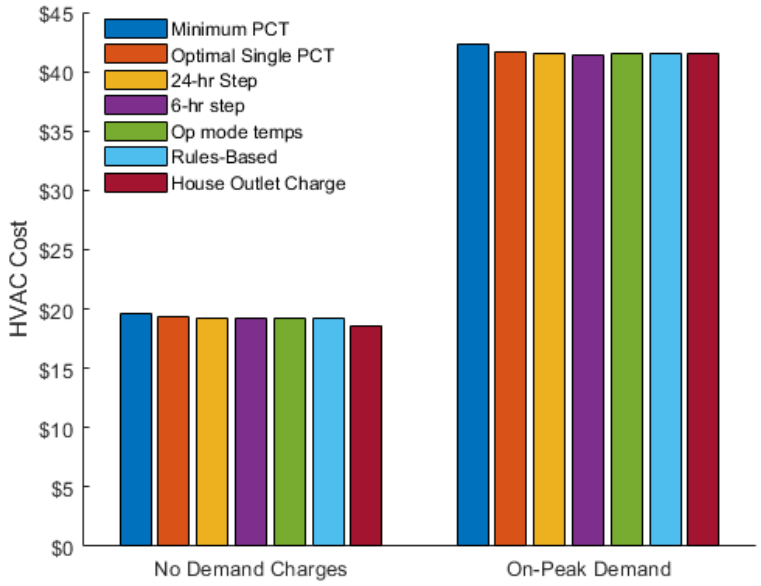

Figure 7-40. Comparison of operating costs for different dynamic-tuning cases for the month of January in Phoenix, AZ using the rates from Table 7-5 with the SAWM on-peak period from Table 7-2. The cost shown is the sum of heat pump and electric heating operating costs and the monthly demand charge.

7.4 Discussion

Dynamic tuning of the PCT can achieve cost savings through shifting the water glycol mass flow rate and heat pump inlet temperature towards values at which the heat pump performs more efficiently. In cooling mode, this is done by charging the storage system using the highest PCT possible in order to maximize the inlet temperature, while discharging at whatever PCT value results in the system operating at an optimal mass flow rate. This is done because in charging mode the main constraint on the heat pump inlet temperature is the constraint on the storage tank outlet

temperature, which must be lower than the PCT. However, in discharge mode, the heat pump inlet temperature is generally more constrained by the house outlet temperature. Thus, the PCT can be lowered in order to change the mass flow rate (by changing the temperature difference across the heat pump) without lowering the inlet temperature. Cost savings from dynamic tuning can also come from lowering the PCT after charging to a lower value than the PCT used for discharge mode. This results in a loss of charge, since the PCM partially melts as the temperature is lowered to the PCT, after which the system is charged to make up for this loss. Since the state of charge increases when the PCT is raised after the discharge period, the net effect of this change in the PCT is to shift some of the charging load from after the on-peak period to an earlier time when the heat pump can operate more efficiently. However, this method generally results in less cost savings than using different temperatures for charging and discharging.

In heating mode, similar logic is used to set a low PCT for charging and a higher value for discharging. However, the lower optimal mass flow rates for heating mean that it is often not possible to discharge at the optimal value, because the storage tank is a more significant constraint than the house at lower flow rates. In addition, a lower PCT is used for discharge with electric heating since a higher mass flow rate increases the capacity of the heat pump. Another difference is that the COP for heating mode is more strongly dependent on mass flow rate relative to heat pump inlet temperature. Thus, frequent changes to the PCT to improve the flow rate are more likely to result in cost savings, so there are higher cost savings from a short time step for this case. The combination of all these factors makes it more complex to develop rules for setting the operating PCT for heating mode than it is for cooling mode, and more likely for the rules-based results to fall short of optimal results.

The strategies for setting the PCT described above are designed for a particular system. Changes to the physical components of this system (the compressor and refrigerant-to-water glycol heat exchanger in the heat pump) or to the control strategies used by it (for load shifting and for setting the operating temperatures in the secondary loop) could affect these results. The primary effect of the design of the refrigerant-to-water glycol heat exchanger is that this largely determines the optimal water glycol mass flow rate, with a larger heat exchanger meaning a larger optimal flow rate. For a smaller, less effective, heat exchanger, the optimal mass flow rate being less than the flow rate required by the storage tank might be a significant concern in cooling mode as well as heating mode. Similarly, the relative importance of optimizing inlet temperature and mass flow

rate in heating mode depends in part on the heat pump model used. For a different model, where the inlet temperature has a stronger effect on heat pump performance in heating mode, varying the PCT in charging mode to improve the mass flow rate might be less desirable. Furthermore, it is desirable to use a lower PCT for on-peak periods with auxiliary heating because of how the capacity of the heat pump changes with mass flow rate. For this compressor, it increases slightly with mass flow rate for ambient temperatures below approximately -3°C. Since auxiliary heating is generally not used during an on-peak period if temperatures are higher than this, it is desirable to increase the mass flow rate to increase the capacity. For a different compressor model, this logic might not be applicable.

In addition to the components of the heat pump, the control logic used for the system also has an effect on how dynamic tuning is used to obtain cost savings. The use of a flat heat pump load for charging the system in heating mode allows for the rules-based controller to set a PCT for charging that optimizes the mass flow rate; if the system charged at capacity, this would require more frequent changes to the PCT. The algorithm used for the secondary loop temperature setpoints also has a large effect on the optimal PCT values, since all effects the PCT has on system performance depend on how the setpoint for storage tank inlet temperature is defined in terms of the PCT. If the difference between the setpoint temperature and the PCT were changed, this would affect what PCT would result in an optimal mass flow rate. However, it would have less effect on how to achieve the optimal inlet temperature since the storage tank inlet temperature would still increase if the PCT increased, or vice versa. Imposing a different temperature difference at the tank inlet would affect the limits at which this temperature no longer changes with the PCT, such as not increasing for $T_m > 6$°C when discharging in cooling mode.

Nonetheless, while some changes to the temperature setpoints might affect how dynamic tuning is used, there would still be a basic division between setpoints for the case where the system is constrained by the tank outlet temperature and setpoints for the case where it is constrained by the house outlet temperature. It would likewise always be the case that the storage tank would be more likely to be the relevant constraint in charging mode, since there the flow must enter the tank at a temperature below (in cooling mode, above in heating mode) the PCT, while it operates at a higher (lower in heating mode) temperature when discharging. Therefore, for most control strategies and heat pumps it would still be true that it is more important to optimize the inlet temperature when charging and the mass flow rate when discharging. Thus, it would usually be

the case that higher PCTs are used for charging than for discharging in cooling mode, and lower PCTs in heating mode, and that switching between these values would be one of the most promising ways to get cost savings from dynamic tuning.

Cost savings from dynamic tuning are limited (<$3/month) for many cases, and therefore these savings are outweighed by the cost for changing the PCT if this cost is 2 kJ/(kg K) or greater. However, larger savings (up to $8.73/month) can be obtained for cases with longer on-peak periods or higher on-peak loads. This is because the cost savings from operating at the optimal PCT when discharging increase as the loads met by the heat pump during the on-peak period increase (since the larger the load met by the heat pump, the larger the savings from operating at a higher COP). However, these larger savings are for cases where the same storage tank size is used for different on-peak periods and locations, even though longer on-peak periods or higher loads would also create an incentive to use a larger storage tank. To see whether these on-peak periods and loads still increase the incentive for dynamic tuning if the system is sized to account for them, the storage system would have to be sized for each location and rate structure so as to minimize the payback period. Then, the cost savings from dynamic tuning with these optimally-size systems could be compared. This optimal sizing and comparison of cost savings is done in Chapter 8.

8. YEAR-ROUND VARIABLE TEMPERATURE STORAGE RESULTS

In this chapter, the potential of year-round variable-temperature storage is examined by looking at the performance of the system modelled in Chapter 6 over a full year. The optimal sizing of such a system (and the resulting payback period) for different locations and rate structures is determined and compared to that of a system with separate heat storage and cold storage tanks in Section 8.1. Optimal sizing is determined using constant PCT values for heating and cooling mode without dynamic tuning. The effect of dynamic tuning on the year-round performance of an optimally-sized system is considered in Section 8.2, which examines the cost savings for a full year from using dynamic tuning of the PCT for a system sized as determined in Section 8.1.

8.1 Optimal Sizing for Year-Round Storage

The results shown in Sections 7.1-7.3 all used a 50-gallon TES storage tank and did not examine the effect of modifying the size of the storage system. In this section, we examine the optimal sizing for TES tanks for the locations and rate structures discussed in Section 7.3, for both the 2-PCM and the variable-temperature system. Optimal sizing for each of these is calculated as the sizing that results in the shortest payback period for the complete system compared to a conventional system with no storage tank or secondary loop. Section 8.1.1 describes how the initial costs are calculated. In Section 8.1.2, the optimal sizing for a 2-PCM system is determined. In Section 8.1.3, the optimal sizing for a variable-temperature storage system is determined and compared to the results for the 2-PCM system to see how the use of a single storage tank for heating and cooling affects the sizing of the system.

8.1.1 Initial Cost Calculations

The initial cost of a system with variable-temperature TES, or with two PCMs used for cold storage and heat storage, is the combined cost of the heat pump, auxiliary electric heating, TES system, and secondary loop. Except for the storage tank, the initial cost for each of these components is calculated the same way as in Section 5.1.1: Eq. 68 is used to calculate the cost of the heat pump, a cost of $10/kW is used for electric heating, and a cost of $1301 is used for the

secondary loop. For auxiliary heating, it is assumed that the capacity must be an integer value, in kW, with a minimum value of 2 kW if any auxiliary heating is used, so the maximum electric heating needed by the system used in rounded up to this value.

For the 2-PCM model, a cost of $9/gallon is used for the ice storage tank, based on Tam et al. [24]. The cost for the heat storage tank is calculated by assuming that the costs for the tank, piping and installation will be comparable to an ice storage tank, and any difference in cost is due to the material cost. Therefore, the cost of the storage tank is $9/gallon plus the material cost of sodium carbonate decahydrate. Hirschey et al. [121] give a price range of $0.18-0.26/kg for this material. Based on this price range, and the density given in Table 6-4, a material cost of $1.10/gal is used, resulting in an overall cost of $10.10/gal for the heat storage tank.

For the variable-temperature storage system, determining an initial cost is more difficult because the system being considered is a generalized one and so is not based on any specific material. A value in the range of $9-$19.10/gal would be most appropriate, since it is not likely that any variable-temperature storage system would be less expensive to install than ice storage, but any variable-temperature TES system that cost more than the combined cost of existing cold storage and heat storage systems would likely not be economically viable, since it would lose the advantage of lowering the initial cost of year-round storage. Therefore, a value of $15.15/gal (a 50% increase on the cost of heat storage) is used, in order to see what the optimal sizing and payback period would be if variable-temperature storage could be done at a cost significantly less than that of two separate storage tanks, but still significantly more than that of a single tank for cold or heat storage.

Table 8-1. Initial cost for a conventional system in Elizabeth City, NC, compared to the cost of the systems with TES described in Section 7.1, with 50-gallon storage tanks (either one variable-temperature tank, or two tanks for cold storage and heat storage).

		System	
Cost	**Conventional**	**2-PCM**	**Variable-Temperature**
Heat Pump	$4588.65	$4588.65	$4588.65
Storage	$0	$955	$757.50
Secondary Loop	$0	$1301	$1301
Auxiliary Heating	$30	$20	$20
Total	**$4618.65**	**$6864.65**	**$6667.15**

As an example of how systems costs compare for the different systems considered, the cost of the conventional system, system with 2-PCM storage, and system with variable-temperature storage used to obtain the results given in Section 7.1 are shown in Table 8-1. These costs are shown to give an idea of the relative costs of the different components; they do not match the costs of the system when optimally sized for any particular rate structure or location.

Table 8-2. Minimum and maximum heat pump capacities considered when determining optimal sizing of the system with TES, compared to the heat pump capacity used for the conventional system results used a benchmark for calculating the payback period.

Location	Minimum Capacity	Maximum Capacity	Conventional Capacity
Elizabeth City, NC	1.5 tons	3 tons	2 tons
Kansas City, MO	1.5 tons	4 tons	2 tons
Phoenix, AZ	2 tons	2.5 tons	2.5 tons

8.1.2 Optimal Sizing for a 2-PCM System

The optimal sizing of a storage system and its resulting payback period is first examined for a system with two separate PCMs for heat storage and cold storage to see whether heat storage or cold storage is more economically viable for different locations and rates. This analysis is done for the three locations discussed in Section 7.3. For each location, the optimal sizing and resulting payback period is calculated for 12 different rate structures (3 different on-peak periods with 4 different rates each). The rate structures used for Elizabeth City are given in Table 7-1, Table 7-3, and Table 7-4; the rates used for Kansas City and Phoenix are calculated by the same method using the conventional-system results for that location. For all cases, the payback period is calculated using Eq. 69 by comparing operating and initial costs to a conventional system with no secondary loop or storage tanks.

At each location, the optimal sizing of the storage tanks and the heat pump is considered. This is done by solving for the optimal sizing of the storage tanks for heat pump capacities at increments of 0.5 tons across a range of feasible sizes. This range goes from capacities lower than that required to meet the full cooling load, but which are capable of meeting peak cooling loads with the aid of TES, to capacities higher than that of the conventional system which could reduce costs by reducing the use of auxiliary heating. The minimum and maximum capacities considered for the heat pump, as well as the capacity used for the conventional system, are shown in Table

8-2. The minimum capacity the capacity used for the conventional system are determined as discussed in Section 5.1.1. The maximum capacity considered for Elizabeth City and Phoenix is the capacity at which no auxiliary heating is needed; for Kansas City, a maximum capacity of twice the capacity required for cooling is used, to reduce computation time since the capacity required for no auxiliary heating is even larger. For the storage tanks, a maximum size of 150 gal is used in finding the optimal size. The minimum size is 0 gal unless the heat pump is downsized, in which case the minimum size for cold storage is the size required to allow for downsizing, calculated as described in Section 5.1.1 (the minimum is always 0 gal for heat storage).

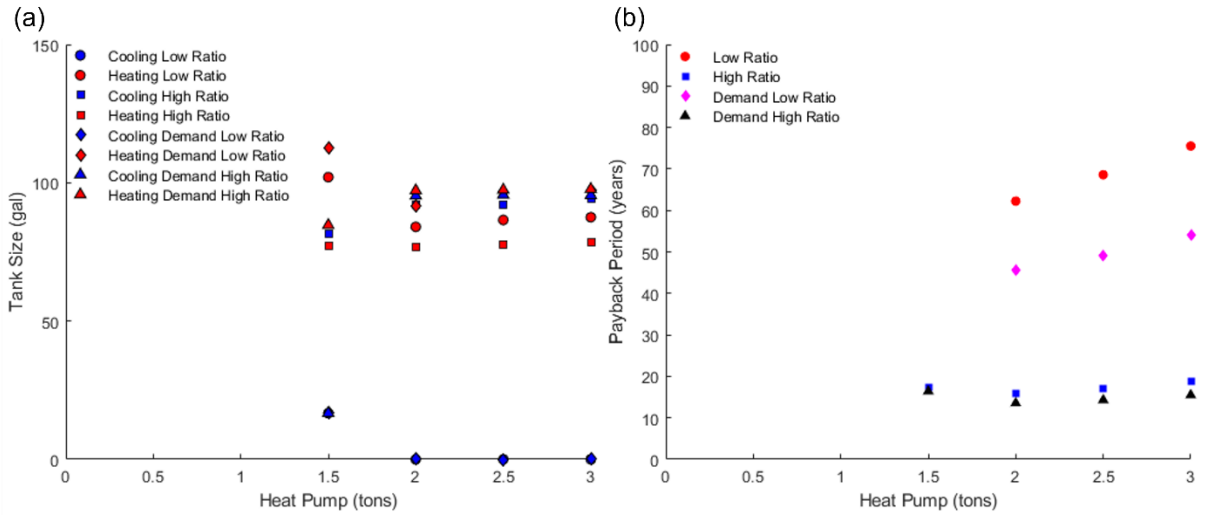

Figure 8-1. (a) Optimal sizing and (b) resulting payback period for a 2-PCM system for SAWM on-peak periods in Elizabeth City, NC. Results are shown for four cases: a low ratio of on-peak to off-peak rates (Low Ratio), the same structure with some of the on-peak rate increased replaced by an on-peak demand charge (Demand Low Ratio), a high on-peak to off-peak ratio (High Ratio) and the high-ratio case with some of the on-peak rate increased replaced by an on-peak demand charge (Demand High Ratio).

Elizabeth City, NC

Optimal sizing and the resulting payback period for rates with a summer afternoon and a winter morning (SAWM) on-peak period are shown in Figure 8-1. For rates that less strongly incentivize energy storage, the optimal result is to only use heat storage, with all cases having either no cold storage or the minimum amount allowed. However, for rates that more strongly

incentivize energy storage, both heat storage and cold storage are used, with the cold storage tank being larger for rates without demand charges and only slightly smaller for rates with demand charges. This pattern holds true even for heat pumps large enough not to use auxiliary heating, so it is not entirely due to the increased cost savings from reducing the use of auxiliary heating. Instead, one reason why the heat storage system is better at achieving cost savings for rates with a lower incentive for storage is that it has a PCT closer to the ideal value than the cold storage system, so the energy efficiency losses from charging are lower, allowing it to achieve cost savings at a lower on-peak to off-peak ratio than the cooling system.

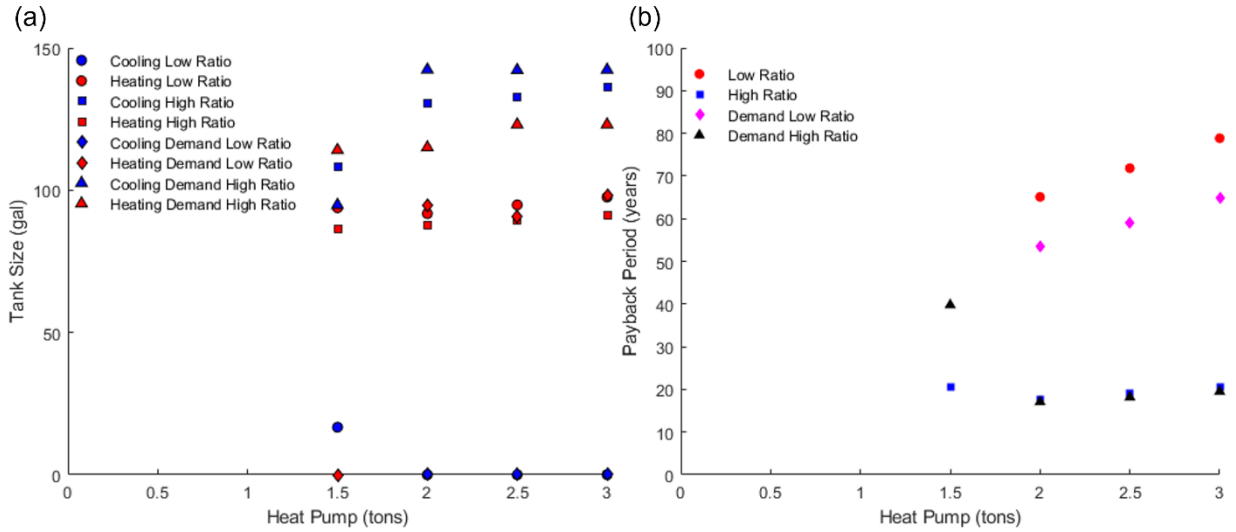

Figure 8-2. (a) Optimal sizing and (b) resulting payback period for a 2-PCM system for SAEWME on-peak periods in Elizabeth City, NC. Results are shown for four different rate structures, as described in the caption for Figure 8-1.

The increased initial cost of the heat storage system is not sufficient to discourage the use of it compared to cold storage, since comparable storage tank sizes are used for both cold and heat storage, and heat storage is even more viable at low-incentive rates. This is because the difference in the initial costs does not have a large effect on the payback period- for both high-incentive cases, the payback period decreases by only 0.4 years at optimal sizing if the cost of heat storage is the same as that of cold storage. Similarly, the payback period is not highly sensitive to an increase in the cost of heat storage, increasing 0.4 years for a 10% increase in the initial cost. Both these changes to the payback period are not accounting for any change to the optimal sizing because of

the change in the initial cost; the payback period might be slightly lower for the new optimal sizing in both cases.

From the payback period results, we can see that neither decreasing nor increasing the heat pump capacity results in a reduced payback period, with downsizing resulting in particularly poor results (payback periods of >100 years) for rates which less strongly incentivize energy storage. Like the metal hydride system, the payback period is shorter for rates with on-peak demand charges, although this difference is smaller for rates more favorable to energy storage.

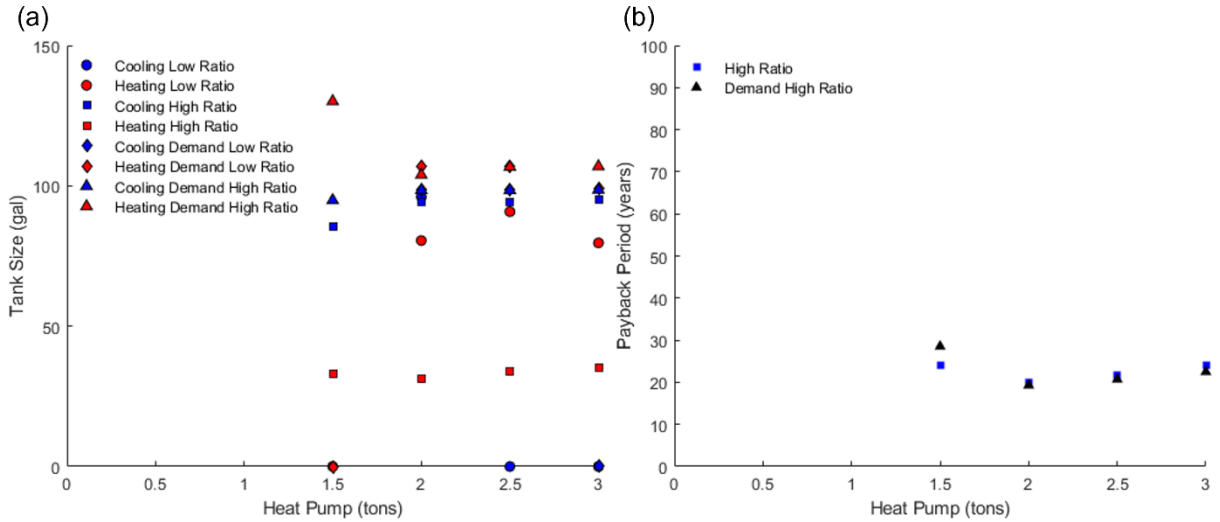

Figure 8-3. (a) Optimal sizing and (b) resulting payback period for a 2-PCM system for SAWA on-peak periods in Elizabeth City, NC. Results are shown for four different rate structures, as described in the caption for Figure 8-1.

Optimal sizing and the resulting payback period for rates with a summer afternoon and evening on-peak period and two winter on-peak periods in the morning and the evening are shown in Figure 8-2. As before, cold storage is only used for rates with that more strongly incentivize energy storage, and neither downsizing nor upsizing the heat pump results in cost savings. The primary difference between this case and the previous one is that the optimal sizing tends to be significantly larger, particularly for cold storage. This larger sizing is due to longer on-peak periods, which increase the total on-peak load and thus incentivize more use of storage. Another difference is that heat storage is not able to achieve cost savings for rates with a low incentive for storage and a demand charge. The minimum payback period across all rates is somewhat larger than for the SAWM on-peak period (17.1 years instead of 13.6).

Results for the case with an afternoon on-peak period in both the summer and the winter can be seen in Figure 8-3. Optimal sizing for cold storage is similar to the SAWM case, since the same on-peak period is used for the cooling season. The one exception is that cold storage is used for rates with less incentive for storage if the heat pump is not upsized. The optimal sizing for heat storage tends to be lower than the SAWM case for rates structures without demand charges, but higher for rates with an on-peak demand charge. The smaller sizing is likely due to the lower on-peak loads in the winter for this rate structure, which reduces the incentive for a larger storage tank in heating, but the reason for larger sizing with on-peak demand charges is less apparent. This reduced incentive would also explain why cold storage might be more favorable relative to heat storage for some rates where it is less favorable with different on-peak periods. The lower on-peak heating loads contribute to the higher payback periods seen in Figure 8-3. The reduced cost savings from heat storage result in no rates with a low incentive for energy storage resulting in an on-peak period of less than 100 years. For rates with a high incentive for energy storage, the payback period is still larger than previous cases, with the lowest value being 19.3 years.

In general, these results show that many of the trends seen for metal hydride storage for this location (described in Section 5.2) are applicable for other forms of TES. These trends include lower cost savings from winter afternoon on-peak periods, downsizing the heat pump resulting in a longer payback period, and on-peak demand charges resulting in larger cost savings than high on-peak rates. However, the payback periods here are much lower than they are for metal hydrides due to the much lower costs of the storage materials.

Kansas City, MO

Optimal sizing and the resulting payback period for a house in Kansas City with rates with a SAWM on-peak period are shown in Figure 8-4. From these results, we can see that heat storage is more strongly incentivized relative to cold storage here, to the point that cold storage is not used for most of the cases studied. Another difference is that here increasing the capacity of the heat pump past what is required for cooling mode does result in a reduced payback period, with the optimal heat pump capacity being 3 tons instead of the 2 tons required for cooling. Both of these differences are due to the significantly higher heating loads in this location. A further difference is that rates with an on-peak demand charge result in a higher payback period than rates without one

for heat pump capacities of 3 tons or less. This is due to the increased use of auxiliary heating; if TES is not sufficient to eliminate the use of this during the on-peak period, it can result in a large increase in the peak work. Once the heat pump is large enough that this does not happen, rates with on-peak demand charges start to do slightly better than those without. A final significant difference is the much lower payback periods for rates with lower incentives for energy storage if the heat pump capacity is above the requirement for cooling. These lower payback periods are due to a significant fraction of the cost savings in these cases coming from the reduced use of auxiliary heating due to the larger heat pump, rather than any savings due to the TES system. However, the lower payback period for rates that more strongly incentivize energy storage show that some of the cost savings are coming from the use of storage.

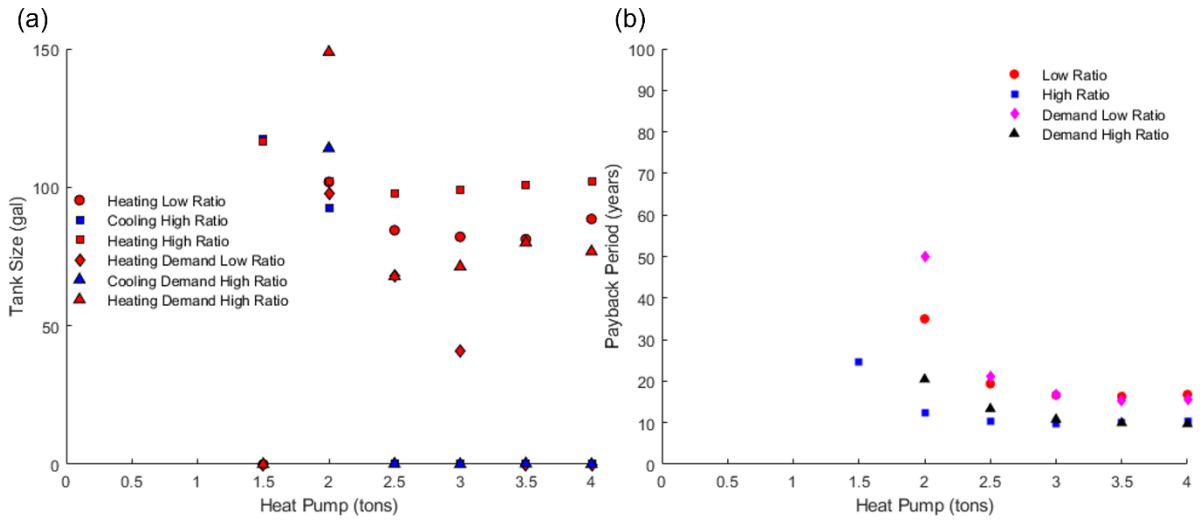

Figure 8-4. (a) Optimal sizing and (b) resulting payback period for a 2-PCM system for SAWM on-peak periods in Kansas City, MO. Results are shown for four different rate structures, as described in the caption for Figure 8-1.

The optimal sizing and resulting payback period for the other two on-peak periods considered in this location are summarized in Table 8-3. For the SAEWME case, the lowest payback period is actually for the case with a high ratio and on-peak demand, but in this case the cost savings are obtained entirely from using a 4-ton heat pump without any storage. The results shown are for the case with the lowest payback period that actually used storage. That the lowest payback period comes purely from increasing the heat pump capacity and that the optimal sizing of the heat pump with storage is larger is due to the longer on-peak period, which increases the on-

peak use of electric heating. The most significant feature of the SAWA results is that here it is optimal to make more use of cold storage than heat storage (instead of not using cold storage, as in the other cases) since the cost savings from heat storage are lower due to the reduced heating loads during the winter on-peak period. These lower on-peak loads also mean that in cases with a larger heat pump, using TES only reduces the payback period for rates with a high incentive for energy storage.

Table 8-3. Optimal sizing for 2-PCM storage and optimal rate structure, with resulting payback period, for the SAEWME and SAWA on-peak periods in Kansas City, MO.

On-Peak Period	Optimal Sizing			Payback Period	Rate Structure
	Heat Pump	Cold Storage	Heat Storage		
SAEWME	3.5 tons	0 gal	127 gal	11.3 years	High Ratio
SAWA	3.5 tons	113 gal	37 gal	13.9 years	High Ratio w/Demand Charge

Phoenix, AZ

The optimal sizing results for the SAWM case in Phoenix, AZ are shown in Figure 8-5. As can be seen, the optimal sizing for cold storage is much larger than it is for other locations, and much larger than it is for heat storage. This is due to the larger cooling loads and lower heating loads in this location. For rates that strongly incentivize energy storage, there is very little difference between those with an on-peak demand charge and those without. Both result in payback periods in the range of 11-13 years for both heat pump capacities, with the lowest value being 11.4 years for rates without a demand charge and a downsized heat pump.

The optimal sizing and resulting payback period for the other two on-peak periods considered in this location are summarized in Table 8-4. Notably, heat storage is not used at all in either of these cases. The optimal cold storage for the SAEWME case is the upper bound imposed on storage tank size; this is the only case for which this limit actually affects the results. In both cases, as with the SAWM case, the lowest payback period comes from a downsized heat pump and rates without an on-peak demand charge.

The different results for heat pump sizing in these three cases indicate that the optimal heat pump size can vary considerably with climate: downsizing is cost-effective if heating loads are lower than cooling (meaning auxiliary heating is not used), while increasing the capacity can lead

to lower payback periods in locations with higher heating loads. For locations (like Elizabeth City) where heating and cooling loads are similar, neither downsizing nor upsizing is cost-effective since auxiliary heating costs are too low to justify the increased initial cost of a larger heat pump but will increase significantly if the heat pump is downsized. Likewise, the sizing of the storage tanks is also dependent on climate, with the optimal choice being to only use cold storage for some rates in warm locations, while the optimal choice for colder locations can sometimes be to only use heat storage. However, for a number of cases considered, using both heat storage and cold storage is the optimal solution.

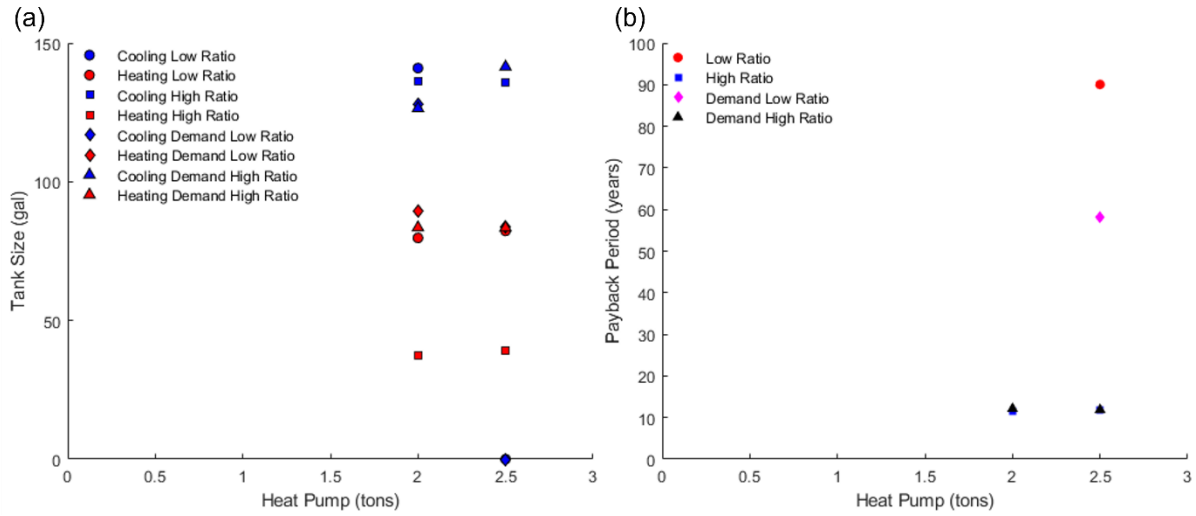

Figure 8-5. (a) Optimal sizing and (b) resulting payback period for a 2-PCM system for SAWM on-peak periods in Phoenix, AZ. Results are shown for four different rate structures, as described in the caption for Figure 8-1.

Table 8-4. Optimal sizing for 2-PCM storage and optimal rate structure, with resulting payback period, for the SAEWME and SAWA on-peak periods in Phoenix, AZ.

On-Peak Period	Optimal Sizing			Payback Period	Rate Structure
	Heat Pump	Cold Storage	Heat Storage		
SAEWME	2 tons	150 gal	0 gal	14.9 years	High Ratio
SAWA	2 tons	131 gal	0 gal	10.4 years	High Ratio

8.1.3 Optimal Sizing for a Variable-Temperature System

The variable-temperature storage system is sized for the same locations and rate structures as the 2-PCM system, using the same conventional-system results as a benchmark in calculating the payback period. The minimum and maximum heat pump sizes given in Table 8-2 are also used for the variable-temperature system. Since the same tank is used for both cold storage and heat storage, the minimum size of the cold storage tank used in Section 8.1.2 for cases with a downsized heat pump is used for the single tank for all similar cases; otherwise, a range of 0-150 gal is used, as before. All results are calculated without using dynamic tuning; instead, a PCT of 10°C is used for cold storage and a PCT of 30°C for heat storage.

Elizabeth City, NC

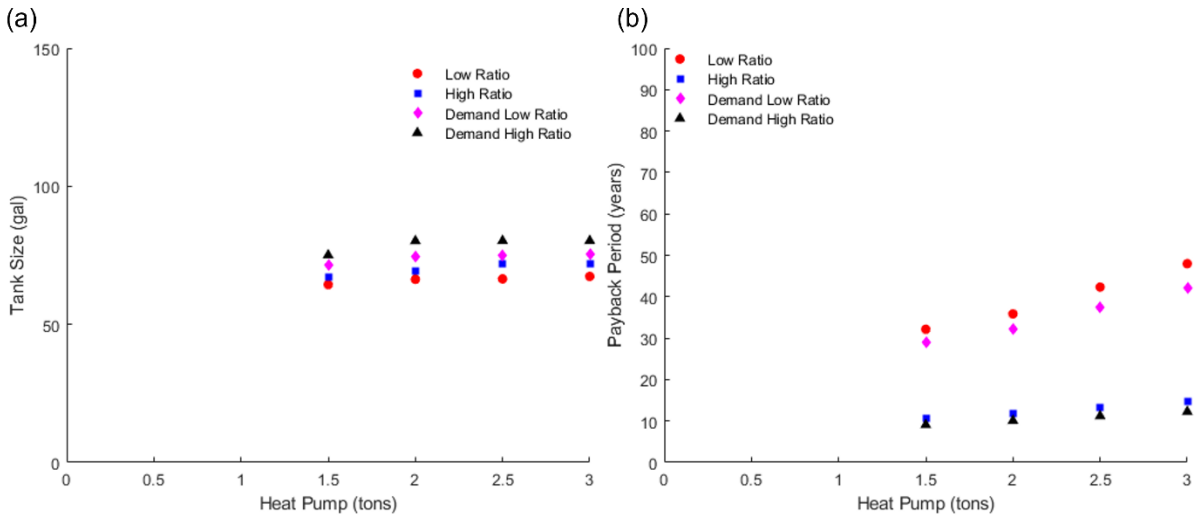

Figure 8-6. (a) Optimal sizing and (b) resulting payback period for a variable-temperature PCM storage system for SAWM on-peak periods in Elizabeth City, NC. Results are shown for four different rate structures, as described in the caption for Figure 8-1.

Optimal sizing and the resulting payback period for the SAWM on-peak period are shown in Figure 8-6. Comparing these results to those for the 2-PCM system shown in Figure 8-1, we can see that the optimal sizing for the storage tank tends to be smaller, and the payback period shorter, for variable-temperature storage. Another significant difference is that downsizing the heat pump does result in a shorter payback period, unlike in the 2-PCM case. Overall, the shortest payback period is 9.1 years, for high-incentive rates with an on-peak demand charge and a downsized heat

pump. This shows that a single TES system for both heating and cooling can reduce the payback period for storage if the system costs less than the cost of two separate heat storage and cold storage tanks. Results for other cases in this location are summarized in Table 8-5. Optimal sizing is larger and the payback period longer than for the SAWM case for both of these cases, as it is for the 2-PCM system. In both cases, variable-temperature storage results in a shorter payback period using a smaller storage tank than using separate PCMs for heat and cold storage. One notable feature of all three cases is that rates with demand charges not only result in a shorter payback period, as they did for the 2-PCM case, but also in a larger optimal size for the storage tank.

Table 8-5. Optimal sizing for variable-temperature storage and optimal rate structure, with resulting payback period, for the SAEWME and SAWA on-peak periods in Elizabeth City, NC.

On-Peak Period	Optimal Sizing		Payback Period	Rate Structure
	Heat Pump	Storage Tank		
SAEWME	1.5 tons	95 gal	12.3 years	High Ratio w/Demand Charge
SAWA	1.5 tons	86 gal	14.8 years	High Ratio w/Demand Charge

Kansas City, MO

Optimal sizing and the resulting payback period for the SAWM on-peak period are shown in Figure 8-7. Here, the payback period for the optimally-sized system is even shorter than it is for Elizabeth City, and significantly shorter than it is for this location with a 2-PCM system. The shortest payback period is 6.6 years for a 2.5-ton heat pump and a high-incentive rate structure with an on-peak demand charge. The optimal sizing is smallest for the heat pump size at which the payback period is lowest, as seen in Figure 8-7a. These results show two significant trends for the variable-temperature storage system: the optimal sizing of the heat pump tends to be smaller than it is for 2-PCM storage (downsized in Elizabeth City, 2.5 tons instead of 3 tons in this case) and the optimal sizing of the storage system tends to be smallest at this heat pump size. Both of these trends hold for other on-peak periods in this location. The results for these on-peak periods are summarized in Table 8-6. As in Elizabeth City, the optimal sizing for the storage tank is smaller than the larger storage tank used in the 2-PCM system (here, the heat storage tank).

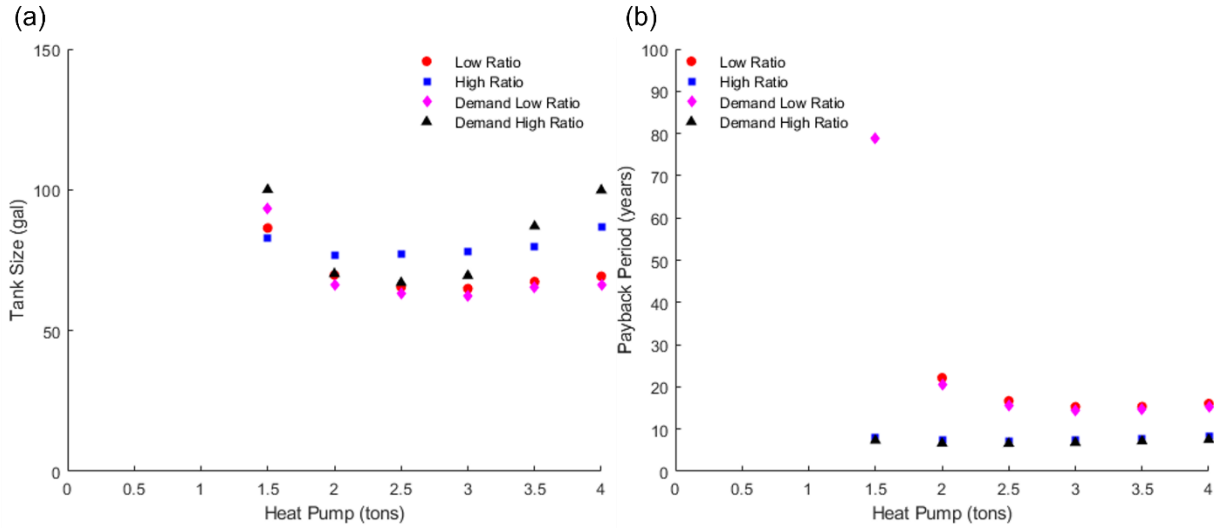

Figure 8-7. (a) Optimal sizing and (b) resulting payback period for a variable-temperature PCM storage system for SAWM on-peak periods in Kansas City, MO. Results are shown for four different rate structures, as described in the caption for Figure 8-1.

Table 8-6. Optimal sizing for variable-temperature storage and optimal rate structure, with resulting payback period, for the SAEWME and SAWA on-peak periods in Kansas City, MO.

On-Peak Period	Optimal Sizing		Payback Period	Rate Structure
	Heat Pump	Storage Tank		
SAEWME	2.5 tons	82 gal	7.7 years	High Ratio w/Demand Charge
SAWA	3 tons	74 gal	10.6 years	High Ratio w/Demand Charge

These results also show that the payback periods are once again lower for this case than they are for 2-PCM storage. Unlike the results with the 2-PCM system, it is not the case for any of the on-peak periods that the lowest payback period across all rates comes from increasing the heat pump capacity without using any storage, although this is still the optimal solution for low-incentive rate structures with a SAWA on-peak period. This demonstrates that, for high-incentive rates, the use of a single storage tank year-round allows TES to be more cost-effective than increasing the heat pump size, which is not always the case for 2-PCM storage. One other notable feature of the results in Table 8-6 is that the SAWA on-peak period has a larger optimal size for the heat pump. The lower on-peak loads for this case mean that less auxiliary heating is needed during the on-peak hours, but more is used during off-peak hours. On-peak auxiliary heating is more expensive, but also can be reduced or removed by the use of TES, while off-peak auxiliary heating is not. The larger optimal capacity for the SAWA case suggests that enough of the on-peak

load that would be met by auxiliary heating is taken by TES instead that shifting more auxiliary heating to the off-peak period increases the incentive for a larger heat pump.

Phoenix, AZ

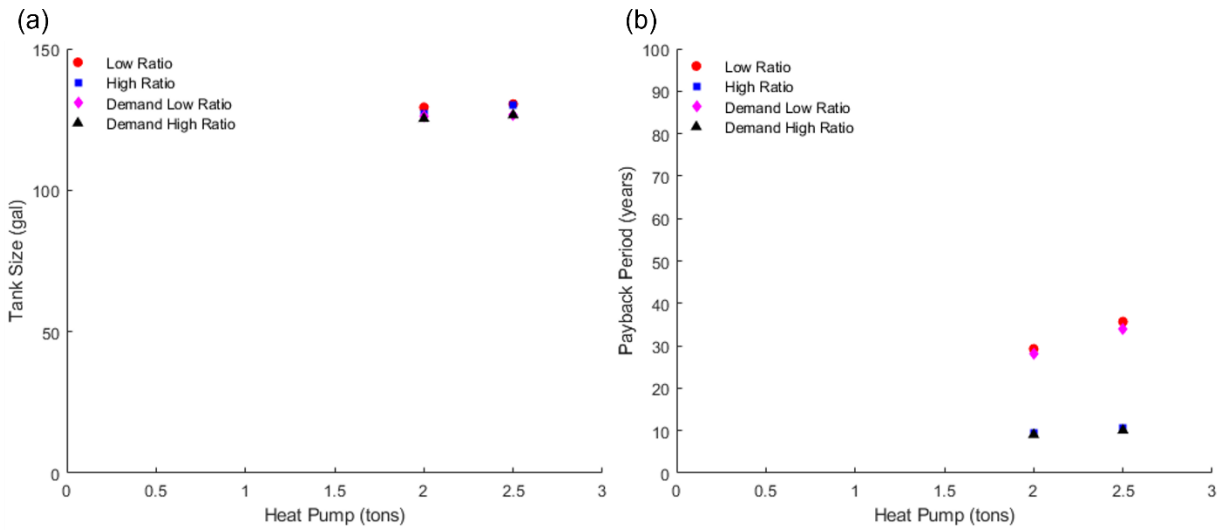

Figure 8-8. (a) Optimal sizing and (b) resulting payback period for a variable-temperature PCM storage system for SAWM on-peak periods in Phoenix, AZ. Results are shown for four different rate structures, as described in the caption for Figure 8-1.

Optimal sizing and the resulting payback period for the SAWM on-peak period are shown in Figure 8-8. Here, the optimal sizing of the storage system is much larger than it is for the previous locations, but still smaller than the sizing for cold storage for this location seen in Section 8.1.2. Even though there is a much greater use for cold storage than heat storage in this location, the payback period for a single storage tank is still lower than the payback period for using separate heat and cold storage systems. The best case value is 9.1 years for high-incentive rates with an on-peak demand charge. As shown in Table 8-7, this is also the case for the other on-peak periods studied. The SAEWME case uses the maximum-size storage tank, which is also the case for cold storage in the 2-PCM model. In all cases, it is the downsized heat pump that results in a shorter payback period. However, the SAWA and SAEWME cases have a lower payback period for rates without a demand charge than for rates with one, unlike the SAWM case (and all cases for Elizabeth City and Kansas City).

Table 8-7. Optimal sizing for variable-temperature storage and optimal rate structure, with resulting payback period, for the SAEWME and SAWA on-peak periods in Phoenix, AZ.

On-Peak Period	Optimal Sizing		Payback Period	Rate Structure
	Heat Pump	Storage Tank		
SAEWME	2 tons	150 gal	12.2 years	High Ratio
SAWA	2 tons	127 gal	10.0 years	High Ratio

Overall, the results for sizing a variable-temperature storage system show that such a system for heating and cooling could result in a significantly lower payback period for most cases if the variable-temperature storage system has an initial cost in-between that of one fixed-temperature storage system and that of two such systems. This is true even for locations where heating loads are substantially higher than cooling loads, and locations where cooling loads are substantially higher. These results also show that the optimal sizing of the heat pump used with variable-temperature storage tends to be lower than the optimal sizing of the heat pump for use with separate heat storage and cold storage.

8.2 Year-Round Results with Dynamic Tuning of the PCT

The effect of dynamic tuning for an optimally-sized variable-temperature storage system is considered here by studying the effect of dynamic tuning in systems sized based on the results in Section 8.1.3. For each system studied, a comparison is made between four cases: using constant PCT values of 10°C in cooling mode and 30°C in heating (the case used to size the system), using the rules-based controller to set the PCT, using optimal PCT values for charging and discharging each day, and using these optimal temperatures where the storage tank is charged using the house outlet flow. Each of these cases is considered for the high-incentive rates used in Section 8.1, both with and without demand charges, for the SAWM and SAEWME on-peak periods. These periods are considered since the first tended to result in the shortest payback periods in Section 8.1 and the second in the highest savings from dynamic tuning in Section 7.3.

In solving these cases, several changes are made to the rules-based controller that improve its performance for the larger storage systems used here. These changes are summarized in Section 8.2.1. Results are then shown for each of the three locations previously studied: for Elizabeth City, NC in Section 8.2.2, for Kansas City, MO in Section 8.2.3, and for Phoenix, AZ in Section 8.2.4.

8.2.1 Modifications to the Rules-Based Controller

The rules-based controller uses the same control logic for cooling mode as before, but two significant modifications have been made to how it operates in heating mode. The first change is that the system now operates at the minimum PCT in charging mode if there is auxiliary heating used (previously, it had only done so in discharge mode). The discharge PCT is also not increased for this case in order to avoid additional charging with auxiliary heating from the loss of state of charge when changing the PCT. The second change to the control logic has to do with setting the PCT for charging to the value that optimizes the mass flow rate. As described in Section 7.1.3, this is only beneficial in cases where the storage tank is not a constraint when charging. While such cases are more common in heating mode than in cooling mode, it is still often the case that the storage tank is the primary constraint, particularly for times with low heating loads. Therefore, the rules-based controller now only increases the PCT to the value that optimizes the mass flow rate if the average load at the house is sufficiently large that the house will be a more significant constraint than the storage tank at that average house load. The updated algorithm that includes these changes is shown in Figure 8-9.

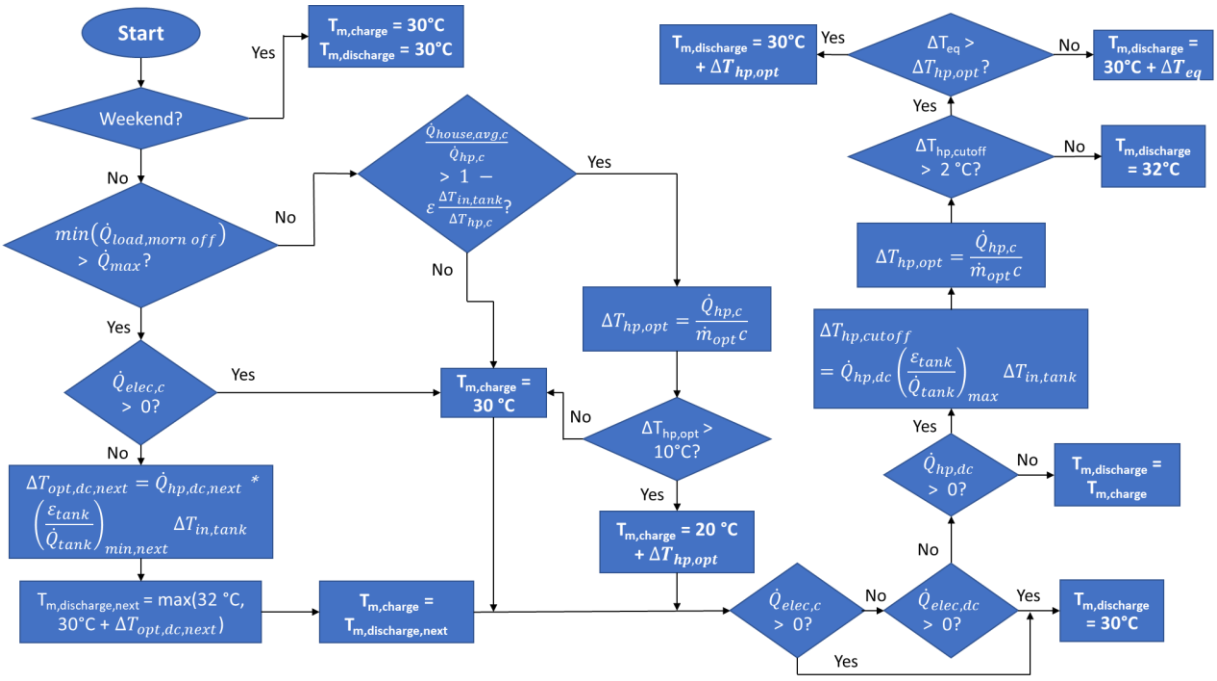

Figure 8-9. Updated algorithm for setting the PCT values for charging and discharging in heating mode.

8.2.2 Results for Elizabeth City, NC

Operating costs for the four cases considered [(1) constant PCTs for cooling and heating modes, (2) optimal temperatures for charge and discharge, (3) the rules-based controller, and (4) optimal charge and discharge temperatures for a system where the tank is charged with the house outlet flow] are shown for the case with SAWM on-peak periods in Elizabeth City, NC in Figure 8-10. These results are for the case with high-incentive rates with no on-peak demand charge. The costs of operating the HVAC system (heat pump and electric heating) are shown in Figure 8-10; costs from non-HVAC building electricity usage, which are the same for all cases, are not. From these results, we can see that the operating costs are comparable for all four cases, but that there are some cost savings that can be gained from dynamic tuning.

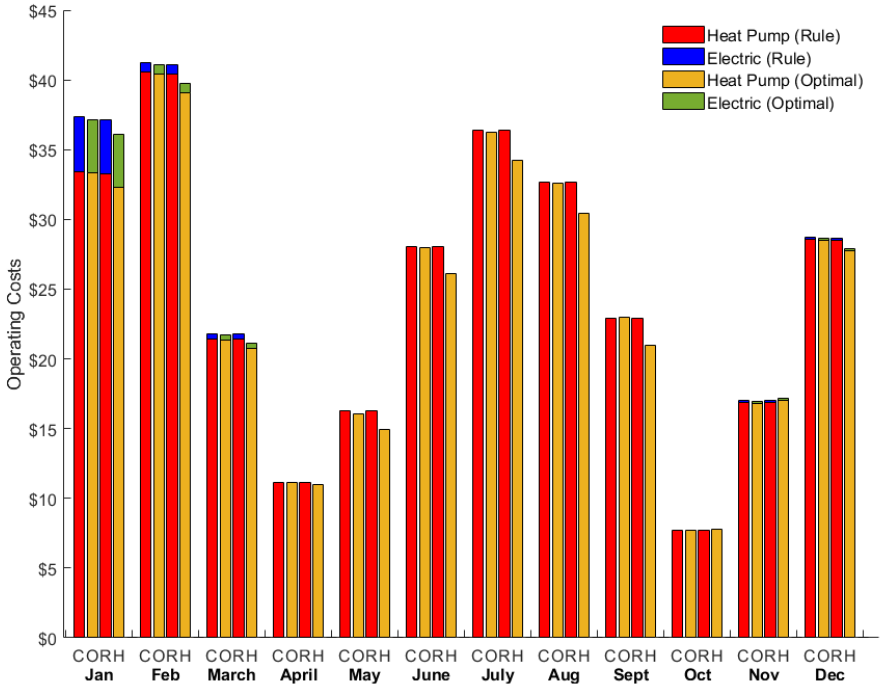

Figure 8-10. Monthly operating costs in Elizabeth City, NC for different dynamic-tuning cases for high-incentive utility rates with no demand charge and a SAWM on-peak period. Four cases are compared: (1) constant (C) PCTs for heating and cooling, (2) optimal PCTs for each operating mode (O) - charge and discharge, (3) PCTs for charge and discharge set by the rules-based controller (R), and (4) optimal PCTs for charge and discharge where the tank is charged with the house outlet flow (H). For ease of viewing, different colors are used for the two cases where the PCT is set by rule (C and R) and the two cases where optimal values are used (O and H).

Table 8-8. Comparison of annual operating costs for the SAWM case in Elizabeth City, NC for rates with and without an on-peak demand charge

		Annual Operating Costs				
Case	**Demand?**	**Heat Pump**	**Auxiliary**	**Non-HVAC**	**Demand**	**Total**
Constant PCT	No	$295.94	$5.34	$1023.7	$0.00	$1325.02
Rules-Based	No	$295.63	$5.25	$1023.7	$0.00	$1324.61
Op-Mode Temps	No	$295.07	$5.11	$1023.7	$0.00	$1323.92
House Outlet Charge	No	$282.34	$5.23	$1023.7	$0.00	$1311.31
Constant PCT	Yes	$274.81	$5.60	$758.73	$238.35	$1277.51
Rules-Based	Yes	$274.77	$5.49	$758.73	$238.27	$1277.26
Op-Mode Temps	Yes	$275.32	$5.14	$758.73	$236.16	$1275.36
House Outlet Charge	Yes	$261.04	$5.37	$758.73	$245.76	$1270.91

Cost savings from dynamic tuning are very low in the summer for the two cases where house outlet charging is not used. This is due to the storage tank being larger here than in Chapter 7. With this larger storage tank, it is only rarely the case that the heat pump load during the on-peak period is large enough to allow for cost savings from lowering the PCT in discharge mode. Because of this, the rules-based controller is not able to achieve noticeable cost savings in cooling mode, since it relies on this method for setting the discharge PCT. However, the case with optimal PCT values for charge and discharge modes achieves some limited cost savings in the summer ($0.52 over a four-month period) by lowering the discharge PCT on certain days in order to shift loads from after the on-peak period to before it, as discussed in Section 7.1.2. The rules-based controller achieves more cost savings in the winter months since the minimum discharge heat pump load required for cost savings to be achieved by changing the discharge PCT is lower in heating mode and the PCT is sometimes changed in charging mode as well. However, cost savings in the winter are still lower than those achieved by the optimizer for charge and discharge temperatures.

Cost savings are much higher for the case where the storage tank is charged with the house outlet flow, which achieves approximately 8 times the cost reduction from using optimal charge and discharge temperatures without changing the flow direction. This is because charging with the house outlet flow allows for substantial cost savings in charging mode, so increasing the size of the storage tank does not decrease the potential cost savings for this case.

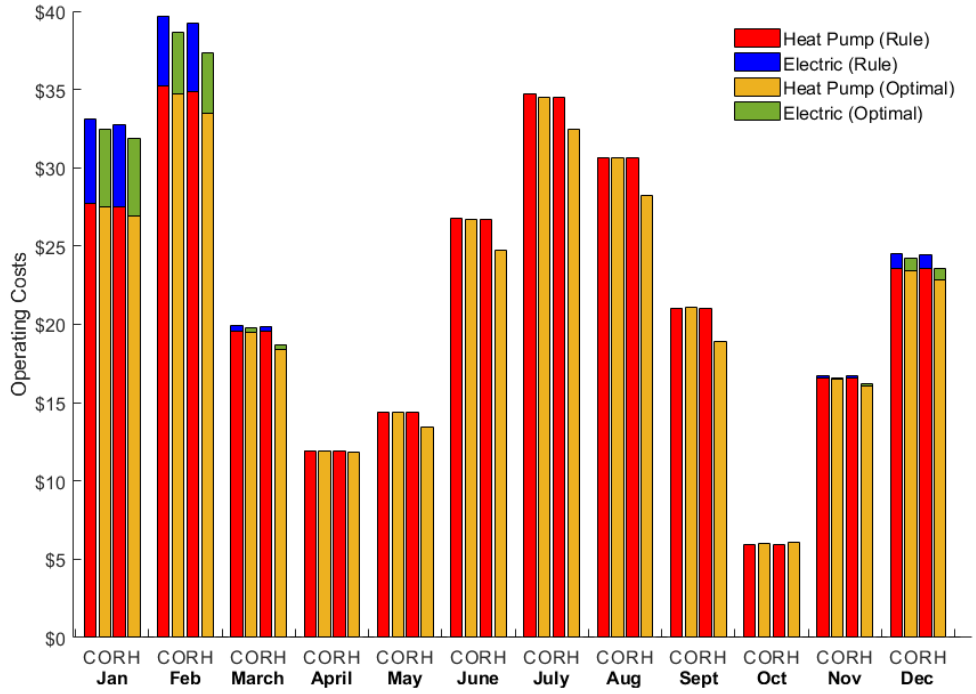

Figure 8-11. Monthly operating costs in Elizabeth City, NC for different dynamic-tuning cases for high-incentive utility rates with no demand charge and a SAEWME on-peak period. Four cases are compared: (1) constant (C) PCTs for heating and cooling, (2) optimal PCTs for each operating mode (O) - charge and discharge, (3) PCTs for charge and discharge set by the rules-based controller (R), and (4) optimal PCTs for charge and discharge where the tank is charged with the house outlet flow (H).

Total operating costs for the year (including non-HVAC costs) are shown and compared to those for rates with an on-peak demand charge in Table 8-8. These results show using an on-peak demand charge does not have a major effect on the potential cost savings from dynamic tuning but does somewhat lower the cost savings for the case where the system is charged with the house outlet flow. The rules-based controller is also less effective for rates with on-peak demand, achieving only 11.1% of the cost savings achieved by optimal PCT values, as compared to 37.3% for the case without a demand charge. Note that the operating costs are lower overall for the case with a demand charge because a larger storage tank is used for that case, since the optimal sizing is larger as discussed in Section 8.1.3; this is also the case for most other on-peak periods and locations in this section.

Table 8-9. Comparison of annual operating costs for the SAEWME case in Elizabeth City, NC for rates with and without an on-peak demand charge

		Annual Operating Costs				
Case	**Demand?**	**Heat Pump**	**Auxiliary**	**Non-HVAC**	**Demand**	**Total**
Constant PCT	No	$268.21	$11.21	$1052.03	$0.00	$1331.46
Rules-Based	No	$267.29	$11.00	$1052.03	$0.00	$1330.32
Op-Mode Temps	No	$266.86	$10.07	$1052.03	$0.00	$1328.96
House Outlet Charge	No	$253.46	$10.02	$1052.03	$0.00	$1315.51
Constant PCT	Yes	$228.33	$12.82	$657.42	$417.74	$1316.30
Rules-Based	Yes	$228.42	$12.59	$657.42	$413.33	$1311.75
Op-Mode Temps	Yes	$229.05	$11.45	$657.42	$413.84	$1311.77
House Outlet Charge	Yes	$213.79	$11.64	$657.42	$417.16	$1300.02

Monthly operating costs for the case with a SAEWME on-peak period are shown in Figure 8-11. The cost savings from dynamic tuning are only slightly larger than in the previous case, indicating that the increased cost savings from dynamic tuning seen for similar cases in Section 7.3 are primarily due to the storage tank not being re-sized. If the storage tank is sized to minimize the payback period for each rate structure, then a larger storage tank is used for cases with higher on-peak periods, reducing the potential cost savings from dynamic tuning. Because of this, the cost savings from using optimal temperatures for charge and discharge modes, while almost 40% greater than in the SAWM case, are still less than $2.00 for the entire year. In other words, the cost savings from dynamic tuning for the whole year are less than what is obtained for a single month for a smaller storage tank. For this location, the optimal sizing for minimizing the payback period is substantially larger than the sizing that would result in the largest cost savings from dynamic tuning for all rate structures. As with the SAWM case, charging with the house outlet flow achieves several times the cost savings that other methods of dynamic tuning achieve.

Total operating costs for the year (including non-HVAC costs) for the SAEWME on-peak periods, both with and without an on-peak demand charge, are shown in Table 8-9. These results show that cost savings are larger for the case with an on-peak demand charge, but still less than $5.00/year unless house outlet charging is used. The rules-based controller performs better for this on-peak period than it did for the SAWM period, partly because it is able to achieve some cost

savings in the summer due to higher on-peak heat pump loads, as seen in in Figure 8-11. The rules-based controller obtains 45.4% of the cost savings from optimal PCT values for rates without demand charges and cost savings virtually identical to the optimal case for rates with a demand charge.

8.2.3 Results for Kansas City, MO

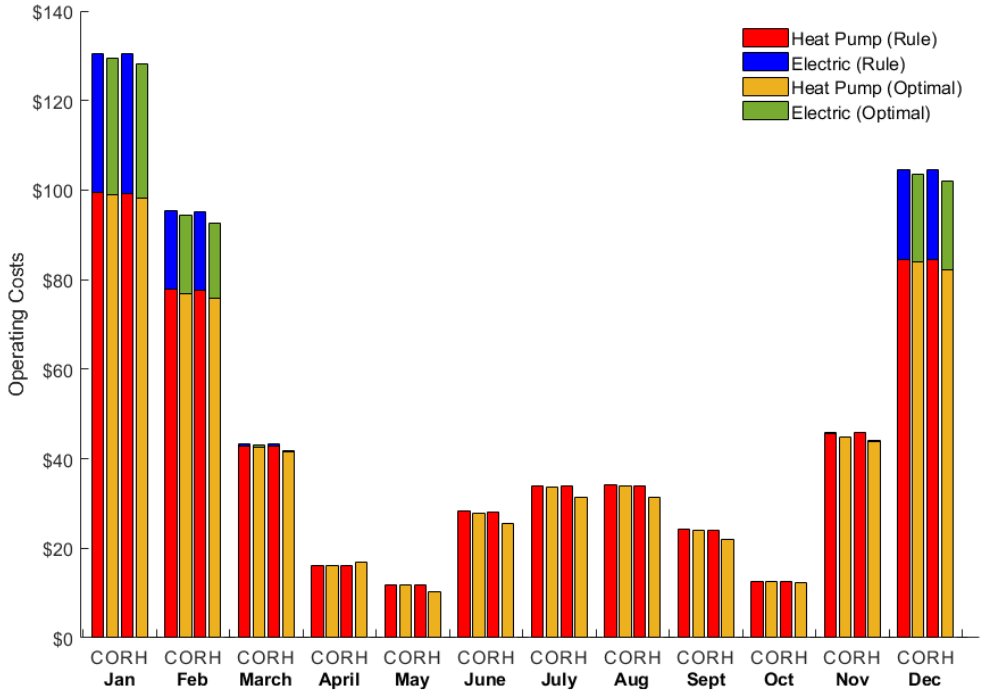

Figure 8-12. Monthly operating costs in Kansas City, MO for different dynamic-tuning cases for high-incentive utility rates with no demand charge and a SAWM on-peak period. Four cases are compared: (1) constant (C) PCTs for heating and cooling, (2) optimal PCTs for each operating mode (O) - charge and discharge, (3) PCTs for charge and discharge set by the rules-based controller (R), and (4) optimal PCTs for charge and discharge where the tank is charged with the house outlet flow (H).

Operating costs for the four methods for setting the PCT that are considered for Elizabeth City in Section 8.2.2 are shown for the SAWM case in Kansas City, MO in Figure 8-12. Here, heating loads are significantly higher in the winter, leading to operating costs that are three times as high as those in the summer. These heating loads mean that electric heating costs are much more

significant than they are in Elizabeth City, even though a 2.5-ton heat pump is used here instead of a 1.5-ton one.

These higher heating loads do lead to an increase in the cost savings from dynamic tuning, but these are still limited to around $5 for optimal charge and discharge temperatures and around $22 for charging with the house outlet flow. The larger heating loads are the main factor in these higher cost savings, since the largest cost savings occur in the coldest months (January, February, and December). However, cost savings are also slightly higher for cooling than for this on-peak period in Elizabeth City, with the rules-based controller being able to achieve some cost savings in August.

The rules-based controller performs worse than it did for this on-peak period in Elizabeth City, achieving only 17.7% cost savings compared to the optimal case. These lower savings are primarily due to it not achieving the same cost reductions in the peak heating months that the optimal case does. Given how much auxiliary heating is used during these months, this suggests that there are likely strategies for reducing operating costs by dynamic tuning when auxiliary heating is being used which are not currently incorporated into the rules-based controller.

Table 8-10. Comparison of annual operating costs for the SAWM case in Kansas City, MO for rates with and without an on-peak demand charge.

		Annual Operating Costs				
Case	**Demand?**	**Heat Pump**	**Auxiliary**	**Non-HVAC**	**Demand**	**Total**
Constant PCT	No	$511.23	$69.23	$1004.26	$0.00	$1584.71
Rules-Based	No	$510.31	$69.21	$1004.26	$0.00	$1583.77
Op-Mode Temps	No	$507.18	$68.01	$1004.26	$0.00	$1579.45
House Outlet Charge	No	$491.57	$67.04	$1004.26	$0.00	$1562.87
Constant PCT	Yes	$468.16	$66.45	$744.29	$291.37	$1570.27
Rules-Based	Yes	$467.12	$66.38	$744.29	$289.81	$1567.61
Op-Mode Temps	Yes	$465.80	$65.26	$744.29	$288.11	$1563.46
House Outlet Charge	Yes	$450.69	$64.83	$744.29	$299.26	$1559.08

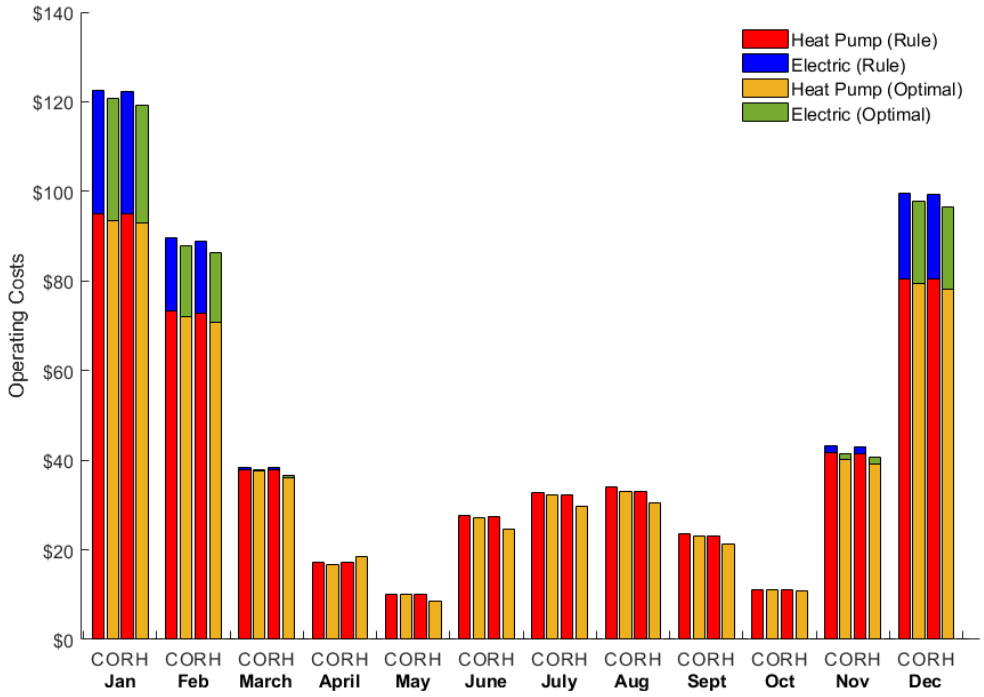

Figure 8-13. Monthly operating costs in Kansas City, MO for different dynamic-tuning cases for high-incentive utility rates with no demand charge and a SAEWME on-peak period. Four cases are compared: (1) constant (C) PCTs for heating and cooling, (2) optimal PCTs for each operating mode (O) - charge and discharge, (3) PCTs for charge and discharge set by the rules-based controller (R), and (4) optimal PCTs for charge and discharge where the tank is charged with the house outlet flow (H).

The total operating costs for this case are compared to those with the same on-peak period but with an on-peak demand charge in Table 8-10. Cost savings for the rates with an on-peak demand charge are higher for optimal charge and discharge temperatures, but still less than $7/year. The rules-based controller is more effective at achieving these cost savings, obtaining 39.2% of the savings achieved by the optimal controller. Savings are comparatively lower for the case where the tank is charged with the house outlet flow due to higher costs from the demand charge, which is also the case for this rate structure in Elizabeth City.

Monthly operating costs for the SAEWME on-peak period can be seen in Figure 8-13. As in Elizabeth City, cost savings for this case are higher than for the SAWM on-peak period- approximately $10/year for using optimal temperatures for charge and discharge, and over $25 for charging the storage tank with the house outlet flow. However, also like Elizabeth City, these cost savings are limited since the storage tank size has been increased to account for the higher on-peak

loads for these rates. The rules-based controller is more effective than it is for the SAWM on-peak period, achieving 32.1% of the cost savings that the optimal PCTs for charge and discharge achieve. This is due in part to higher on-peak heat pump loads in the summer, which allow for more cost savings from the strategy used by the rules-based controller in cooling, as compared to the strategy of shifting loads to before the on-peak period that is used by the optimal controller when on-peak heat pump loads are low.

Table 8-11. Comparison of annual operating costs for the SAEWME case in Kansas City, MO for rates with and without an on-peak demand charge.

		Annual Operating Costs				
Case	**Demand?**	**Heat Pump**	**Auxiliary**	**Non-HVAC**	**Demand**	**Total**
Constant PCT	No	$484.85	$64.82	$1054.05	$0.00	$1603.72
Rules-Based	No	$482.03	$64.36	$1054.05	$0.00	$1600.44
Op-Mode Temps	No	$476.15	$63.29	$1054.05	$0.00	$1593.50
House Outlet Charge	No	$461.18	$62.06	$1054.05	$0.00	$1577.28
Constant PCT	Yes	$405.98	$57.75	$658.68	$474.34	$1596.74
Rules-Based	Yes	$402.04	$57.57	$658.68	$460.52	$1578.81
Op-Mode Temps	Yes	$401.65	$56.74	$658.68	$454.24	$1571.31
House Outlet Charge	Yes	$386.17	$54.84	$658.68	$454.72	$1554.42

The total operating costs for this case are compared to those with the same on-peak period but with an on-peak demand charge in Table 8-11. Cost savings for the case with an on-peak demand charge are the highest seen so far, with savings of $25.40/year for optimal charge and discharge temperatures and $42.29/year for charging with the house outlet flow. As in Elizabeth City, the rules-based controller is most effective for the SAEWME case with a demand charge, achieving 70.5% of the cost savings from optimal charge and discharge temperatures. In general, the modifications made to the rules-based controller in Section 8.2.1 appear to have made it more effective for cases with an on-peak demand charge.

8.2.4 Results for Phoenix, AZ

A comparison of monthly operating costs for the SAWM on-peak period in Phoenix, AZ can be seen in Figure 8-14. Here, heating loads in the winter months are much lower than cooling

loads in the summer, such that operating costs for the HVAC system are 3-4 times as high in the summer. Despite this, the use of a much larger storage tank for this case means that the rules-based controller does not achieve any cost savings because on-peak heat pump loads are never large enough for it to change the PCT away from the values used in the constant-value case. Some limited cost savings - around $1.50/year - can be obtained by using optimal charge and discharge temperatures, primarily by shifting loads from after the on-peak period to before as previously discussed. While the cost savings from optimal charge and discharge temperatures are small in this case, the cost savings for charging with the house outlet flow are some of the highest seen for any location or rate structure. This is again because this method obtains cost savings by optimizing the PCT for charging and so still improves performance significantly when a large storage tank is used.

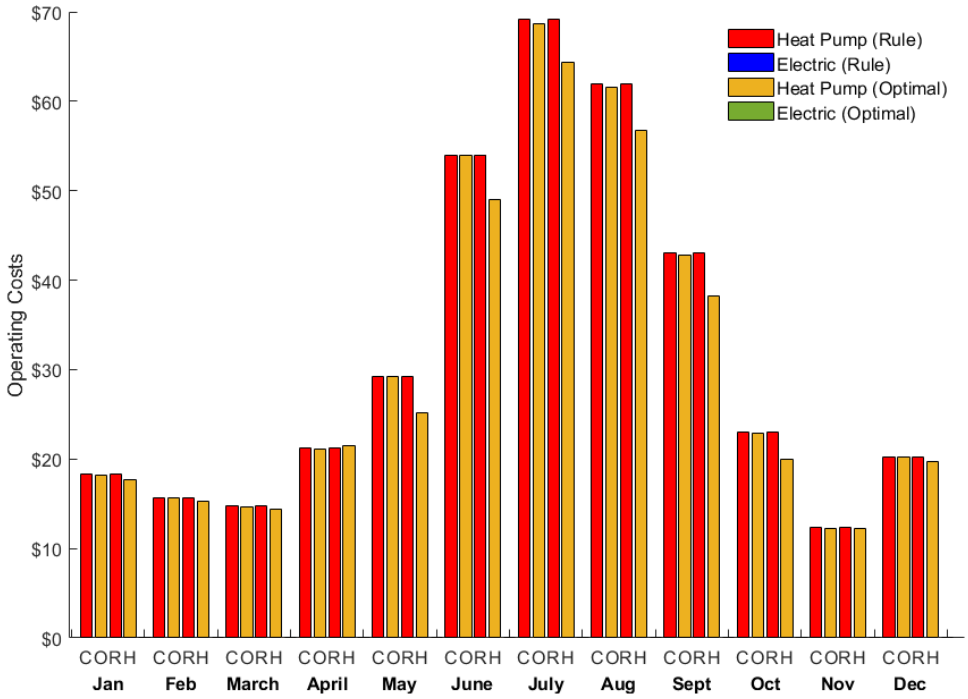

Figure 8-14. Monthly operating costs in Phoenix, AZ for different dynamic-tuning cases for high-incentive utility rates with no demand charge and a SAWM on-peak period. Four cases are compared: (1) constant (C) PCTs for heating and cooling, (2) optimal PCTs for each operating mode (O) - charge and discharge, (3) PCTs for charge and discharge set by the rules-based controller (R), and (4) optimal PCTs for charge and discharge where the tank is charged with the house outlet flow (H).

Table 8-12. Comparison of annual operating costs for the SAWM case in Phoenix, AZ for rates with and without an on-peak demand charge.

		Annual Operating Costs				
Case	**Demand?**	**Heat Pump**	**Auxiliary**	**Non-HVAC**	**Demand**	**Total**
Constant PCT	No	$382.69	$0.00	$989.76	$0.00	$1372.45
Rules-Based	No	$385.69	$0.00	$989.76	$0.00	$1372.45
Op-Mode Temps	No	$381.23	$0.00	$989.76	$0.00	$1370.99
House Outlet Charge	No	$354.28	$0.00	$989.76	$0.00	$1344.04
Constant PCT	Yes	$372.83	$0.00	$733.54	$250.91	$1357.29
Rules-Based	Yes	$372.83	$0.00	$733.54	$250.91	$1357.29
Op-Mode Temps	Yes	$372.34	$0.00	$733.54	$249.70	$1355.59
House Outlet Charge	Yes	$345.31	$0.00	$733.54	$249.74	$1328.60

The total operating costs for the case with SAWM on-peak periods, with and without an on-peak demand charge, are given in Table 8-12. Cost savings for the rates with an on-peak demand charge are comparable for all cases to those from the rates without them. The rules-based controller does not achieve any cost savings for rates with on-peak demand, since it still consistently sets the PCTs to the values used in the constant-PCT case (10°C in cooling mode, 30°C in heating mode). The failure of the rules-based controller to reduce operating costs for a location in which the bulk of the operating costs come from cooling loads suggest that the strategy used for setting the PCT in cooling is not suited for optimally-sized systems. Heat pump loads for such systems in cooling mode are usually not large enough during the on-peak periods for lowering the PCT to optimize the mass flow rate to achieve cost savings. Instead, the best strategy would be to find a way to determine on which days lowering the PCT in the morning to shift a portion of the charging load from the evening to the morning would result in cost savings. However, it should be noted that the minimum on-peak heating loads required for lowering the PCT to achieve cost savings depends on the PCT value at which the tank inlet temperature stops increasing with the PCT (in order to maintain a minimum temperature difference across the heat pump), which is 6°C in this case. A different temperature algorithm, where the difference between the PCT and the tank inlet temperature in discharge mode is smaller and thus the PCT for which the tank inlet

temperature stops increasing is higher, might provide a greater opportunity for cost savings from discharging at an optimal flow rate even for lower heat pump loads.

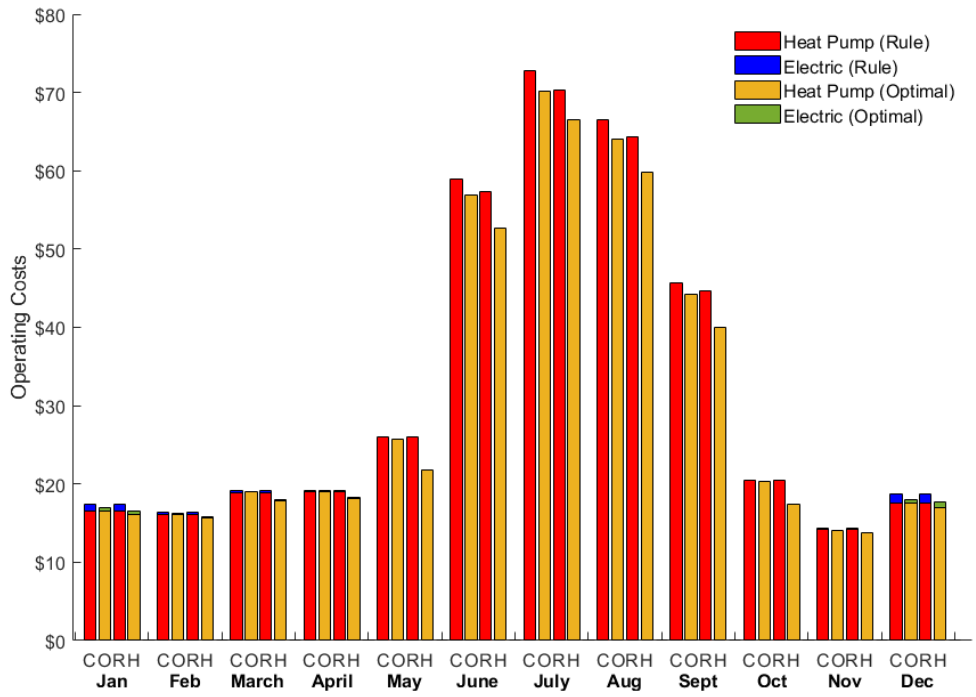

Figure 8-15. Monthly operating costs in Phoenix, AZ for different dynamic-tuning cases for high-incentive utility rates with no demand charge and a SAEWME on-peak period. Four cases are compared: (1) constant (C) PCTs for heating and cooling, (2) optimal PCTs for each operating mode (O) – charge and discharge, (3) PCTs for charge and discharge set by the rules-based controller (R), and (4) optimal PCTs for charge and discharge where the tank is charged with the house outlet flow (H).

Monthly operating costs for the SAEWME on-peak period are shown in Figure 8-15. These results differ from all other cases in that here the cooling loads, particularly in July and August, are large enough that significant cost savings can be achieved by the rules-based controller in cooling mode. Even with a maximally-sized storage system, there are still large enough heat pump loads during the on-peak period that savings of around $7/year can be obtained by using the rules-based controller. As a result, the rules-based controller here obtains 67.6% of the cost savings from dynamic tuning that optimal PCT values for charge and discharge achieve. This higher effectiveness is achieved because the increased number of times at which lowering the PCT to optimize the discharge flow rate is viable means that the optimizer uses this approach more often

and load-shifting through sensible heating less. While the effect of the longer on-peak period is most pronounced for the rules-based case, it does also increase the cost savings from charging with the house outlet flow to around $37/year, the highest value for any case without an on-peak demand charge.

The total operating costs for the SAEWME case are compared to the case with the same on-peak period and a demand charge in Table 8-13. Cost savings are slightly larger for the case with an on-peak demand charge, but the difference between the two cases is much smaller than it is for Kansas City. The rules-based controller is almost exactly as effective (67.5%) as it is for rates without a demand charge. This consistency is likely because the noticeable differences in how it performed in other cases had to do with optimizing the mass flow rate for heating, which can have a large effect on demand charges, but here almost all the cost savings are in cooling mode, where its performance is more consistent. Overall, the results for this on-peak period show that the strategy used by the rules-based controller for cooling can sometimes achieve cost savings, but that even in such cases they are still very limited- less than $10/year in this case.

Table 8-13. Comparison of annual operating costs for the SAEWME case in Phoenix, AZ for rates with and without an on-peak demand charge.

		Annual Operating Costs				
Case	**Demand?**	**Heat Pump**	**Auxiliary**	**Non-HVAC**	**Demand**	**Total**
Constant PCT	No	$392.83	$2.61	$1012.02	$0.00	$1407.46
Rules-Based	No	$385.70	$2.61	$1012.02	$0.00	$1400.32
Op-Mode Temps	No	$383.60	$1.30	$1012.02	$0.00	$1396.91
House Outlet Charge	No	$356.87	$1.61	$1012.02	$0.00	$1370.49
Constant PCT	Yes	$322.76	$2.61	$632.41	$491.91	$1449.70
Rules-Based	Yes	$320.68	$2.61	$632.41	$484.91	$1440.61
Op-Mode Temps	Yes	$320.00	$1.29	$632.41	$482.54	$1436.24
House Outlet Charge	Yes	$292.52	$1.62	$632.41	$482.54	$1409.10

8.2.5 Summary

Results from all three locations studied (Elizabeth City, NC; Kansas City, MO; and Phoenix, AZ) show that cost savings from dynamic tuning are reduced substantially by the larger

storage tank sizes used if the system is optimally sized. This is because a large portion of the cost savings come from optimizing the mass flow rate in discharge mode in order to improve heat pump performance. The gains from this strategy are greatly reduced if there are lower heat pump loads when discharging. While cost savings are consistently lower than those for a smaller storage tank, longer on-peak periods do result in higher cost savings from dynamic tuning for all locations studied, usually even higher if an on-peak demand charge is applied in this case. The rules-based controller is less effective compared to optimal charge and discharge temperatures for the cases studied in this section, in large part because the heat pump loads in cooling are often not large enough to justify lowering the PCT to optimize the mass flow rate. Instead, the optimizer usually achieves what cost savings it can in cooling mode by shifting charging loads from after the on-peak period to before, which the rules-based controller does not do.

The largest cost savings obtained for optimally-sized systems come from charging with the house outlet flow, which does not have reduced cost savings for a large tank size since it primarily reduces operating costs in charging mode rather than discharge mode. The highest cost savings obtained in this case for any of the rates and locations studied are around $42/year. All of these cost savings are neglecting any cost for changing the PCT; given the limited savings for all cases except charging with house outlet flow, and the higher costs for changing the PCT in that case (as discussed in Section 7.1.6), achieving any cost savings for these cases would require a very low cost for changing the PCT.

9. CONCLUSIONS

9.1 Summary

This dissertation examined the potential of variable-temperature thermal energy storage by examining the viability of metal hydrides as a material for this purpose and by determining the potential cost savings from an idealized variable-temperature system. A system architecture for integrating metal hydride storage into a building HVAC system was determined. A two-reactor system was used since a one-reactor system would require high-pressure hydrogen storage; however, this decision negated the significant potential advantage of reducing initial costs with variable-temperature storage by only requiring one storage tank. To model this system architecture, a dynamic model of a metal hydride storage system and a static model of a building HVAC system were developed and integrated with each other.

The performance of metal-hydride energy storage for a residential building in Elizabeth City, NC was examined for a range of utility rate structures. Metal hydride storage was found to achieve cost savings for favorable rate structures, but these savings were greatly reduced by the cost of running the compressor to move hydrogen between the hydride reactors. Even for the most favorable rate structures, the payback period was still very high due to the high initial cost of the metal hydrides. These results show that metal hydride energy storage will not be viable for this application unless there is a large reduction in the material cost of room-temperature metal hydrides. Two trends visible in the metal hydride results that were of interest for the study of other forms of TES were (1) that residential cost savings were larger in winter than in summer, due to the increased savings from reducing on-peak use of auxiliary heating, and (2) that rates with on-peak demand charges resulted in larger cost savings than rates with high on-peak rates. All the results described here were found to hold true for residential buildings with and without solar PV. The reduced savings from running the compressor and high initial cost were also found to hold true for commercial buildings; however, the use of auxiliary heating was a less significant factor here due to differences in the building load profiles.

To analyze the potential cost savings from dynamic tuning, a model of an idealized variable-temperature storage system was developed. A more detailed heat pump model was used to derive correlations for COP and capacity than was used with the metal hydride model, so that

these correlations would include the effect of the water glycol mass flow rate on heat pump performance. This allowed for the study of the effects of dynamic tuning to examine its effect on performance through its effects on both the heat pump inlet temperature and the water glycol mass flow rate. A modification to the system design that was made possible by variable-temperature storage, where the storage tank was charged using with the outlet flow from the house, was also studied. Control logic to set two operating temperatures each day, one for charging and one for discharging, was developed, both for the original and the modified system design, and optimal values for this case were compared to those for cases with a fixed time step. A rules-based controller was developed for setting these charge and discharge PCT values, which was capable of achieving significant cost savings relative to a fixed temperature in heating mode and of achieving cost savings essentially identical to the optimal case for cooling mode.

Short-term analysis of dynamic tuning showed that it can lead to cost savings, although these are usually limited. One effective strategy was to use the PCT closest to room temperature to charge the system in order to optimize the heat pump inlet temperature, while discharging at a PCT further from room temperature which results in an optimal mass flow rate. This strategy is based on charging being generally constrained by the storage tank outlet temperature, while discharging is constrained by the house outlet temperature; however, the system often discharges at an above-optimal mass flow rate in heating mode because there the lower optimal value is often less than the flow rate required by the storage tank. This strategy was found to achieve significant cost savings. Larger cost savings were obtained by charging with the house outlet flow, allowing for operating at higher PCT values when charging. Using a PCM with a high ratio of latent heat to specific heat can increase the cost savings when charging with house outlet flow but has only a small effect on cost savings otherwise. More frequent changes to the PCT were found to significantly improve performance in heating mode by allowing for operation at more favorable mass flow rates. Other changes to the PCT could also achieve cost savings in cooling mode by using sensible heating to shift charging of the system to times when the system can operate more efficiently.

All strategies for dynamic tuning were found to require a very low energy cost for changing the PCT to achieve cost savings. An examination of alternate utility rate structures and locations found that dynamic tuning achieves higher cost savings for higher on-peak heat pump loads, except in heating mode if the loads get high enough that some of the load must be met by electric heating.

This raised the question of whether these larger cost savings were only because the storage tank was not re-sized for the larger loads, or if higher cost savings could still be achieved for an optimally-sized system. The rules-based controller was found to be less effective, relative to optimal results, for rates with on-peak demand charges, especially in heating mode.

A comparison of the optimal sizing and resulting payback periods between a 2-PCM and a 1-PCM variable-temperature storage system showed that the variable-temperature system can reduce the payback period significantly if its initial cost is less than the combined cost of two fixed-temperature storage tanks, even if it is significantly higher than that of a single such tank. This was true even for locations where heating loads are significantly higher than cooling loads, or vice versa. In addition, the minimum payback period from variable-temperature storage tends to come from using a smaller heat pump than for a 2-PCM system.

Examining the effect of dynamic tuning for optimally-sized variable-temperature system showed that cost savings from this tended to be much lower than in the short-term results. This was primarily due to the large storage tank size used, which meant that heat pump loads were lower during the on-peak period and so there was less opportunity for cost savings from improving heat pump efficiency when discharging. In particular, for most cases cost savings could not be obtained in cooling mode by lowering the PCT in discharge mode to optimize the mass flow rate. Instead, what cost savings could be obtained in cooling mode were obtained by using sensible heating to shift when the system was charged to more efficient times. Because of this, the rules-based controller achieved much lower cost savings relative to optimal charge and discharge temperatures than it did for short-term cases. While cost savings from dynamic tuning were lower for all cases, they did tend to be higher for cases with longer on-peak periods. However, optimal charge and discharge temperatures only achieved limited cost savings, exceeding $15/year for only one of twelve cases studied. Cost savings were higher for the case where the tank is charged with the house outlet flow, since this case relies on reducing operating costs in charging mode, ranging from around $10-$45/year.

9.2 Directions for Future Research

This work has examined the potential of variable-temperature TES for building HVAC systems, looking at metal hydrides in particular as a material for this purpose. The results obtained

here suggest multiple future areas of inquiry for metal hydride storage in buildings and variable-temperature storage in general, as well as for PCM storage in residential buildings.

For metal hydrides, the primary obstacle to their viability for this application is their high initial cost. Without a significant change in the price of rare-earth metals, this means that any future research must involve looking for room-temperature metal hydrides that are not rare-earth metal alloys. The initial cost could also be reduced by using a system with a single hydride reactor and a hydrogen storage tank. Such a design would likely not be suitable for residential use due to safety concerns but might be more viable for energy storage in industrial applications. Another major area for improvement is the loss of cost savings to compressor work. For a two-reactor system, reducing compressor costs would mean selecting materials and operating temperatures so as to make the reactions in the system as temperature-driven as possible. For a one-reactor system, it would mean operating the hydride reactor at a high pressure to reduce the compression work required to send hydrogen back to the storage tank.

However, given the high initial cost of metal hydrides, a more fruitful line of inquiry might be to examine other forms of thermochemical energy storage that have seen some use in buildings to see how they might be modified to allow for year-round energy storage. This would mean determining the operating conditions that would allow for the same thermochemical storage system to both store and release heat at temperatures below and above room temperature. In any such for future work on year-round storage, the results shown here for dynamic tuning of a variable-temperature storage system should also be taken into account in determining the operating temperatures of the system.

Applying the strategies developed for dynamic tuning to real systems is one major avenue for future research on variable-temperature storage. This would primarily mean thermochemical storage systems, but could also include studying how the dual-ion battery TES system proposed by Lau et al. [29] would work when used for TES with a building HVAC system. In addition, for both the idealized system and real systems, another major area of research would be examining dynamic tuning for storage in commercial buildings. This study focused on residential buildings due to their proportionally higher heating loads, which create a higher incentive for year-round storage. However, cold storage is more commonly used in commercial buildings due to the larger scale of the cooling loads, so an examination of whether this increase in scale would also result in larger cost savings from dynamic tuning would be valuable. In addition, since this study primarily

focused on operating costs as the metric for system performance, further studies could consider variable-temperature storage from an exergetic or environmental standpoint to see how the optimal strategies would change if the system was analyzed from that perspective and what the potential benefits from dynamic tuning would be.

Another area for future study is improving the rules-based controller for setting the PCT. One way this could be done is by adding control logic for cooling mode to allow for shifting charging loads through sensible heating and cooling, since this method was found to still achieve cost savings for larger storage tank sizes where the method currently used by the controller is less effective. In addition, the control logic in heating could be improved since several checkpoints used in it depend on a comparison of the heat pump load to tank and house loads that change over the course of the off-peak or on-peak period. A more detailed study of which values from the period (average, minimum, etc.) should be used in the control logic could result in improved performance. Furthermore, a modified version of the controller for the case where the system is charged with the house outlet flow could also be developed.

As discussed in Section 7.4, particular features of this system, such as the compressor and heat exchanger used in the heat pump, the algorithm for the secondary loop setpoint temperatures, and the load-shifting control logic used for heating and cooling, play a role in determining the control logic for setting the PCT. Therefore, an important area of research would be examining dynamic tuning with different heat pumps and control strategies to see what modifications to the rules-based controller would be needed to account for these.

Finally, a comparison of the results for heat storage and cold storage for both systems studied indicates that there is a potential for significant cost savings from residential heat storage systems. This is particularly the case for buildings using a heat pump with auxiliary electric heating if there are still significant heating loads in their location; the optimal locations for heat storage would be the coldest climates in which such a heating system is still economically viable. The results for sizing a 2-PCM storage system indicate that combined heat storage and cold storage for residential buildings may be more economic than either system in isolation, since a large fraction of the initial cost for storage is the cost of a secondary loop, which can be used by both storage systems. Payback periods studied here were generally still greater than 10 years but might be lower for other locations or for larger residential buildings.

REFERENCES

[1] Department of Energy, 2015, *Quadrennial Technology Review: An Assesment of Energy Technologies and Research Opportunities*.

[2] Odukomaiya, A., Woods, J., James, N., Kaur, S., Gluesenkamp, K. R., Kumar, N., Mumme, S., Jackson, R., and Prasher, R., 2021, "Addressing Energy Storage Needs at Lower Cost via On-Site Thermal Energy Storage in Buildings," Energy Environ. Sci., **14**(10), pp. 5315–5329.

[3] Sanaye, S., and Shirazi, A., 2013, "Thermo-Economic Optimization of an Ice Thermal Energy Storage System for Air-Conditioning Applications," Energy Build., **60**, pp. 100–109.

[4] Akeiber, H., Nejat, P., Majid, M. Z. A., Wahid, M. A., Jomehzadeh, F., Zeynali Famileh, I., Calautit, J. K., Hughes, B. R., and Zaki, S. A., 2016, "A Review on Phase Change Material (PCM) for Sustainable Passive Cooling in Building Envelopes," Renew. Sustain. Energy Rev., **60**, pp. 1470–1497.

[5] MacCracken, M., 2004, "Thermal Energy Storage in Sustainable Buildings," ASHRAE J., **46**(9).

[6] Finn, P., and Fitzpatrick, C., 2014, "Demand Side Management of Industrial Electricity Consumption: Promoting the Use of Renewable Energy through Real-Time Pricing," Appl. Energy, **113**(2014), pp. 11–21.

[7] Potter, R. A., King, D. J., Weitzel, D. P., and Boettner, D. D., 1995, "Study of Operational Experience with Thermal Storage Systems," *ASHRAE Transactions*, pp. 549–557.

[8] Braun, J. E., 1992, "Comparison of Chiller-Priority Storage-Priority, and Optimal Control of an Ice-Storage System," ASHRAE Trans., **98**(pt 1), pp. 893–902.

[9] Sadineni, S. B., and Boehm, R. F., 2012, "Measurements and Simulations for Peak Electrical Load Reduction in Cooling Dominated Climate," Energy, **37**(1), pp. 689–697.

[10] Leger, A. S., Sobiesk, E., Farmer, A., and Rulison, B., 2014, "Demand Response with Photovoltaic Energy Source and Time-of-Use Pricing," Proc. IEEE Power Eng. Soc. Transm. Distrib. Conf., pp. 1–5.

[11] Tam, A., Ziviani, D., Braun, J. E., and Jain, N., 2019, "Development and Evaluation of a Generalized Rule-Based Control Strategy for Residential Ice Storage Systems," Energy Build., **197**, pp. 99–111.

[12] Nassif, N., Tesiero, R. C., and Singh, H., 2013, "Impact of Ice Thermal Storage on Cooling Energy Cost for Commercial HVAC Systems," ASHRAE Trans., **119**.

[13] Dincer, I., 2002, "On Thermal Energy Storage Systems and Applications in Buildings," Energy Build., **34**(4), pp. 377–388.

[14] Drees, K. H., and Braun, J. E., 1996, "Development and Evaluation of a Rule-Based Control Strategy for Ice Storage Systems," HVAC&R Res., **2**(4), pp. 312–334.

[15] Silvetti, B., 2002, "Application Fundamentals of Ice-Based Thermal Storage," ASHRAE J., **44**(2), pp. 30–35.

[16] Rawlings, L. K., 1985, "Ice Storage System Optimization and Control Strategies.," ASHRAE Trans., **91**(pt 1B), pp. 12–23.

[17] Krese, G., Koželj, R., Butala, V., and Stritih, U., 2018, "Thermochemical Seasonal Solar Energy Storage for Heating and Cooling of Buildings," Energy Build., **164**, pp. 239–253.

[18] Lee, K. H., Joo, M. C., and Baek, N. C., 2015, "Experimental Evaluation of Simple Thermal Storage Control Strategies in Low-Energy Solar Houses to Reduce Electricity Consumption during Grid on-Peak Periods," Energies, **8**(9), pp. 9344–9364.

[19] Abji, N., Tizghadam, A., and Leon-Garcia, A., 2015, "Energy Storage Management in Core Networks with Renewable Energy in Time-of-Use Pricing Environments," IEEE Int. Conf. Commun., **2015-Septe**, pp. 135–141.

[20] U.S. DOE, 2020, *Energy Storage Grand Challenge: Energy Storage Market Report*.

[21] Hasnain, S. M., 1998, "Review on Sustainable Thermal Energy Storage Technologies, Part II: Cool Thermal Storage," Energy Convers. Manag., **39**(11), pp. 1139–1153.

[22] Hasnain, S. M., 1998, "Review on Sustainable Thermal Energy Storage Technologies, Part I: Heat Storage Materials and Techniques," Energy Convers. Manag., **39**(11), pp. 1139–1153.

[23] Kung, F., Deru, M., and Bonnema, E., 2013, "Evaluation Framework and Analyses for Thermal Energy Storage Integrated with Packaged Air Conditioning," Natl. Renew. Energy Lab., (October).

[24] Tam, A., Braun, J. E., Ziviani, D., and Jain, N., 2018, "An Overall Assessment of Ice Storage Systems for Residential Buildings," 5th Int. High Perform. Build. Conf. Purdue, (July).

[25] Al-Hallaj, S., Khateeb, S., Aljehani, A., and Pintar, M., 2018, "Thermal Energy Storage for Smart Grid Applications," AIP Conf. Proc., **1924**.

[26] Agyenim, F., and Hewitt, N., 2010, "The Development of a Finned Phase Change Material (PCM) Storage System to Take Advantage of off-Peak Electricity Tariff for Improvement in Cost of Heat Pump Operation," Energy Build., **42**(9), pp. 1552–1560.

[27] Hamada, Y., and Fukai, J., 2005, "Latent Heat Thermal Energy Storage Tanks for Space Heating of Buildings: Comparison between Calculations and Experiments," Energy Convers. Manag., **46**(20), pp. 3221–3235.

[28] Desai, F., Sunku Prasad, J., Muthukumar, P., and Rahman, M. M., 2021, "Thermochemical Energy Storage System for Cooling and Process Heating Applications: A Review," Energy Convers. Manag., **229**(July 2020), p. 113617.

[29] Lau, J., Papp, J. K., Lilley, D., Khomein, P., Kaur, S., Dames, C., Liu, G., and Prasher, R., 2021, "Dynamic Tunability of Phase-Change Material Transition Temperatures Using Ions for Thermal Energy Storage," Cell Reports Phys. Sci., **2**(10), p. 100613.

[30] Han, G. G. D., Li, H., and Grossman, J. C., 2017, "Optically-Controlled Long-Term Storage and Release of Thermal Energy in Phase-Change Materials," Nat. Commun., **8**(1).

[31] Hauer, A., 2007, "Adsorption Systems for TES- Design and Demonstration Projects," *Thermal Energy Storage for Sustainable Energy Consumption*, Halime O. Paksoy, ed., Springer, Dordrecht, pp. 409–427.

[32] Sheppard, D. A., Paskevicius, M., Humphries, T. D., Felderhoff, M., Capurso, G., Bellosta von Colbe, J., Dornheim, M., Klassen, T., Ward, P. A., Teprovich, J. A., Corgnale, C., Zidan, R., Grant, D. M., and Buckley, C. E., 2016, "Metal Hydrides for Concentrating Solar Thermal Power Energy Storage," Appl. Phys. A Mater. Sci. Process., **122**(4).

[33] Corgnale, C., Hardy, B., Motyka, T., and Zidan, R., 2016, "Metal Hydride Based Thermal Energy Storage System Requirements for High Performance Concentrating Solar Power Plants," Int. J. Hydrogen Energy, **41**(44), pp. 20217–20230.

[34] Satya Sekhar, B., Muthukumar, P., and Saikia, R., 2012, "Tests on a Metal Hydride Based Thermal Energy Storage System," Int. J. Hydrogen Energy, **37**(4), pp. 3818–3824.

[35] Feng, P., Zhu, L., Zhang, Y., Yang, F., Wu, Z., and Zhang, Z., 2018, "Optimum Output Temperature Setting and an Improved Bed Structure of Metal Hydride Hydrogen Storage Reactor for Thermal Energy Storage," Int. J. Hydrogen Energy, pp. 1–13.

[36] Voskuilen, T. G., Waters, E. L., and Pourpoint, T. L., 2014, "A Comprehensive Approach for Alloy Selection in Metal Hydride Thermal Systems," Int. J. Hydrogen Energy, **39**(25), pp. 13240–13254.

[37] Crandall, B., 2017, "Trane Acquires CALMAC," FMLink [Online]. Available: https://www.fmlink.com/articles/trane-acquires-calmac-ice-storage-tanks/.

[38] MacCracken, M., and Heine, K., 2018, "Thermal Energy Storage, the Lowest Cost Storage," *NREL Space Conditioning Tech Team Webinar*.

[39] DOE Federal Energy Management Program, 2000, *Thermal Energy Storage for Space Cooling*.

[40] Henze, G. P., 2003, "An Overview of Optimal Control for Central Cooling Plants with Ice Thermal Energy Storage," J. Sol. Energy Eng., **125**(3), pp. 302–309.

[41] Drees, K. H., and Braun, J. E., 1995, "Modeling of Area-Constrained Ice Storage Tanks," HVAC R Res., **1**(2), pp. 143–158.

[42] Sehar, F., Rahman, S., and Pipattanasomporn, M., 2012, "Impacts of Ice Storage on Electrical Energy Consumptions in Office Buildings," Energy Build., **51**, pp. 255–262.

[43] Gansler, R. A., Reindl, D. T., and Jekel, T. B., 2001, "Simulation of Source Energy Utilization and Emissions for HVAC Systems," ASHRAE Winter Meet. CD, Tech. Symp. Pap., pp. 51–63.

[44] Mammoli, A., and Robinson, M., 2018, "Numerical Analysis of Heat Transfer Processes in a Low-Cost, High-Performance Ice Storage Device for Residential Applications," Appl. Therm. Eng., **128**, pp. 453–463.

[45] Fiorino, D. P., 1999, "Achieving High Chilled-Water Delta Ts," ASHRAE J., **41**(11), pp. 24–30.

[46] Rosiek, S., and Batlles Garrido, F. J., 2012, "Performance Evaluation of Solar-Assisted Air-Conditioning System with Chilled Water Storage (CIESOL Building)," Energy Convers. Manag., **55**(October 2006), pp. 81–92.

[47] Osman, K., Al Khaireed, S. M. N., Ariffin, M. K., and Senawi, M. Y., 2008, "Dynamic Modeling of Stratification for Chilled Water Storage Tank," Energy Convers. Manag., **49**(11), pp. 3270–3273.

[48] Krane, R. J., and Krane, M. J. M., 1992, "The Optimum Design of Stratified Thermal Energy Storage Systems — Part II : Completion of the Analytical Model , Presentation and Interpretation of the Results," **114**(3), pp. 204–208.

[49] Boonnasa, S., and Namprakai, P., 2010, "The Chilled Water Storage Analysis for a University Building Cooling System," Appl. Therm. Eng., **30**(11–12), pp. 1396–1408.

[50] Oró, E., Gracia, A. De, Castell, A., Farid, M. M., and Cabeza, L. F., 2012, "Review on Phase Change Materials (PCMs) for Cold Thermal Energy Storage Applications," Appl. Energy, **99**, pp. 513–533.

[51] Sun, Y., Wang, S., Xiao, F., and Gao, D., 2013, "Peak Load Shifting Control Using Different Cold Thermal Energy Storage Facilities in Commercial Buildings: A Review," Energy Convers. Manag., **71**, pp. 101–114.

[52] Moreno, P., Solé, C., Castell, A., and Cabeza, L. F., 2014, "The Use of Phase Change Materials in Domestic Heat Pump and Air-Conditioning Systems for Short Term Storage: A Review," Renew. Sustain. Energy Rev., **39**, pp. 1–13.

[53] Baker, J., 2008, "New Technology and Possible Advances in Energy Storage," Energy Policy, **36**(12), pp. 4368–4373.

[54] Caliskan, H., Dincer, I., and Hepbasli, A., 2012, "Energy and Exergy Analyses of Combined Thermochemical and Sensible Thermal Energy Storage Systems for Building Heating Applications," Energy Build., **48**, pp. 103–111.

[55] Finck, C., Li, R., Kramer, R., and Zeiler, W., 2018, "Quantifying Demand Flexibility of Power-to-Heat and Thermal Energy Storage in the Control of Building Heating Systems," Appl. Energy, **209**(November 2017), pp. 409–425.

[56] Helmns, D., Blum, D., Casillas, A., Prakash, A., Wolley, J., Vernon, D., Mande, C., Woodcox, M., and Dutton, S., 2021, "Towards a Techno-Economic Analysis of PCM-Integrated Hybrid HVAC Systems," *International High Performance Buildings Conference*, pp. 1–10.

[57] Yin, Z., Xin, W., and Yinping, Z., 2019, “Optimal Phase Change Temperature for BCHP System with PCM-TES Based on Energy Storage Effectiveness,” Therm. Sci., **23**(2B), pp. 1085–1093.

[58] Zhang, Y., Wang, X., Zhang, Y., and Zhuo, S., 2016, “A Simplified Model to Study the Location Impact of Latent Thermal Energy Storage in Building Cooling Heating and Power System,” Energy, **114**, pp. 885–894.

[59] Aydin, D., Casey, S. P., Chen, X., and Riffat, S., 2016, “Novel ‘Open-Sorption Pipe’ Reactor for Solar Thermal Energy Storage,” Energy Convers. Manag., **121**, pp. 321–334.

[60] Mette, B., Kerskes, H., and Drück, H., 2012, “Concepts of Long-Term Thermochemical Energy Storage for Solar Thermal Applications - Selected Examples,” Energy Procedia, **30**, pp. 321–330.

[61] Bertsch, F., Jaehnig, D., Asenbeck, S., Kerskes, H., Drueck, H., Wagner, W., and Weiss, W., 2014, “Comparison of the Thermal Performance of a Solar Heating System with Open and Closed Solid Sorption Storage,” Energy Procedia, **48**, pp. 280–289.

[62] Jähnig, D., Hausner, R., Wagner, W., and Isaksson, C., 2006, “Thermo-Chemical Storage for Solar Space Heating in a Single-Family House,” AEE – INTEC (Austria), Ecostock Conf. New Jersey; 31 May - 02 June, pp. 1–7.

[63] Tokoro, H., Yoshikiyo, M., Imoto, K., Namai, A., Nasu, T., Nakagawa, K., Ozaki, N., Hakoe, F., Tanaka, K., Chiba, K., Makiura, R., Prassides, K., and Ohkoshi, S. I., 2015, “External Stimulation-Controllable Heat-Storage Ceramics,” Nat. Commun., **6**(May), pp. 4–8.

[64] Li, B., Kawakita, Y., Ohira-Kawamura, S., Sugahara, T., Wang, H., Wang, J., Chen, Y., Kawaguchi, S. I., Kawaguchi, S., Ohara, K., Li, K., Yu, D., Mole, R., Hattori, T., Kikuchi, T., Yano, S. ichiro, Zhang, Z., Zhang, Z., Ren, W., Lin, S., Sakata, O., Nakajima, K., and Zhang, Z., 2019, “Colossal Barocaloric Effects in Plastic Crystals,” Nature, **567**(7749), pp. 506–510.

[65] Luo, S., Luo, W., Clewley, J. D., Flanagan, T. B., and Wade, L. A., 1995, “Thermodynamic Studies of the LaNi5-XSnx-H System from x = 0 to 0.5,” J. Alloys Compd., **231**(1–2), pp. 467–472.

[66] Tange, M., Maeda, T., Nakano, A., Ito, H., Kawakami, Y., Masuda, M., and Takahashi, T., 2011, "Experimental Study of Hydrogen Storage with Reaction Heat Recovery Using Metal Hydride in a Totalized Hydrogen Energy Utilization System," Int. J. Hydrogen Energy, **36**(18), pp. 11767–11776.

[67] Khayrullina, A., Blinov, D., and Borzenko, V., 2018, "Air Heated Metal Hydride Energy Storage System Design and Experiments for Microgrid Applications," Int. J. Hydrogen Energy, pp. 1–9.

[68] Aruna, R., and Jaya Christa, S. T., 2020, "Modeling, System Identification and Design of Fuzzy PID Controller for Discharge Dynamics of Metal Hydride Hydrogen Storage Bed," Int. J. Hydrogen Energy, **45**(7), pp. 4703–4719.

[69] Cho, J. H., Yu, S. S., Kim, M. Y., Kang, S. G., Lee, Y. D., Ahn, K. Y., and Ji, H. J., 2013, "Dynamic Modeling and Simulation of Hydrogen Supply Capacity from a Metal Hydride Tank," Int. J. Hydrogen Energy, **38**(21), pp. 8813–8828.

[70] Panos, C., Kouramas, K. I., Georgiadis, M. C., and Pistikopoulos, E. N., 2010, "Dynamic Optimization and Robust Explicit Model Predictive Control of Hydrogen Storage Tank," Comput. Chem. Eng., **34**(9), pp. 1341–1347.

[71] Georgiadis, M. C., Kikkinides, E. S., Makridis, S. S., Kouramas, K., and Pistikopoulos, E. N., 2009, "Design and Optimization of Advanced Materials and Processes for Efficient Hydrogen Storage," Comput. Chem. Eng., **33**(5), pp. 1077–1090.

[72] Chabane, D., Iqbal, M., Harel, F., Djerdir, A., Candusso, D., Elkedim, O., and Fenineche, N. eddin, 2021, "Coupling a Metal Hydride Tank with a PEMFC for Vehicular Applications: A Simulations Framework," Int. J. Energy Res., **45**(11), pp. 16511–16523.

[73] Nyamsi, S. N., Lototskyy, M., and Tolj, I., 2018, "Selection of Metal Hydrides-Based Thermal Energy Storage: Energy Storage Efficiency and Density Targets," Int. J. Hydrogen Energy, **43**(50), pp. 22568–22583.

[74] Corgnale, C., Hardy, B., Motyka, T., Zidan, R., Teprovich, J., and Peters, B., 2014, "Screening Analysis of Metal Hydride Based Thermal Energy Storage Systems for Concentrating Solar Power Plants," Renew. Sustain. Energy Rev., **38**, pp. 821–833.

[75] Ward, P. A., Corgnale, C., Teprovich, J. A., Motyka, T., Hardy, B., Sheppard, D., Buckley, C., and Zidan, R., 2016, "Technical Challenges and Future Direction for High-Efficiency Metal Hydride Thermal Energy Storage Systems," Appl. Phys. A Mater. Sci. Process., **122**(4).

[76] Manickam, K., Mistry, P., Walker, G., Grant, D., Buckley, C. E., Humphries, T. D., Paskevicius, M., Jensen, T., Albert, R., Peinecke, K., and Felderhoff, M., 2019, "Future Perspectives of Thermal Energy Storage with Metal Hydrides," Int. J. Hydrogen Energy, **44**(15), pp. 7738–7745.

[77] Bhogilla, S. S., 2021, "Numerical Simulation of Metal Hydride Based Thermal Energy Storage System for Concentrating Solar Power Plants," Renew. Energy, **172**, pp. 1013–1020.

[78] Yao, J., Zhu, P., Guo, L., Yang, F., Zhang, Z., Ren, J., and Wu, Z., 2021, "Study of a Metal Hydride Based Thermal Energy Storage System Using Multi-Phase Heat Exchange for the Application of Concentrated Solar Power System," Int. J. Hydrogen Energy, **46**(57), pp. 29332–29347.

[79] Kang, B. H. A. K., 1995, "Thermal Modelling and Analysis of a Metal Hydride Chiller for Air Conditioning," Int. J. Hydrog. Energy, **20**(8).

[80] Muthukumar, P., and Groll, M., 2010, "Metal Hydride Based Heating and Cooling Systems: A Review," Int. J. Hydrogen Energy, **35**(8), pp. 3817–3831.

[81] Nagel, M., Komazaki, Y., Uchida, M., and Suda, S., 1984, "Operating Characteristics of a Metal Hydride Heat Pump for Generating Cooled Air," J. Less-Common Met., **104**, pp. 307–318.

[82] Magnetto, D., and Mola, S., 2006, "A Metal Hydride Mobile Air Conditioning System," J. Chem. Inf. Model., **53**(9), pp. 1689–1699.

[83] Satheesh, A., and Muthukumar, P., 2010, "Performance Investigations of a Single-Stage Metal Hydride Heat Pump," Int. J. Hydrogen Energy, **35**(13), pp. 6950–6958.

[84] Satheesh, A., and Muthukumar, P., 2010, "Simulation of Double-Stage Double-Effect Metal Hydride Heat Pump," Int. J. Hydrogen Energy, **35**(3), pp. 1474–1484.

[85] Nie, X., Lv, Y., Gong, Y., Zhang, W., and Li, F., 2011, "Metal Hydride Air Conditioning of the Waste Heat of Automobile Engine Coolant Driving," 2011 IEEE Int. Conf. Cyber Technol. Autom. Control. Intell. Syst. CYBER 2011, pp. 97–101.

[86] Manickam, K., Mistry, P., Walker, G., Grant, D., Buckley, C. E., Humphries, T. D., Paskevicius, M., Jensen, T., Albert, R., Peinecke, K., and Felderhoff, M., 2019, "Future Perspectives of Thermal Energy Storage with Metal Hydrides," Int. J. Hydrogen Energy, **44**(15), pp. 7738–7745.

[87] Ni, J., and Liu, H., 2007, "Experimental Research on Refrigeration Characteristics of a Metal Hydride Heat Pump in Auto Air-Conditioning," Int. J. Hydrogen Energy, **32**(13), pp. 2567–2572.

[88] Choi, H., and Mills, A. F., 1990, "Heat and Mass Transfer in Metal Hydride Beds for Heat Pump Applications," Int. J. Heat Mass Transf., **33**(6), pp. 1281–1288.

[89] Abdin, Z., Webb, C. J., and Gray, E. M. A., 2018, "One-Dimensional Metal-Hydride Tank Model and Simulation in Matlab–Simulink," Int. J. Hydrogen Energy, **43**(10), pp. 5048–5067.

[90] Nakagawa, T., Inomata, A., Aoki, H., and Miura, T., 2000, "Numerical Analysis of Heat and Mass Transfer Characteristics in the Metal Hydride Bed," Int. J. Hydrogen Energy, **25**, pp. 339–350.

[91] Sunku Prasad, J., and Muthukumar, P., 2022, "Design and Performance Analysis of an Annular Metal Hydride Reactor for Large-Scale Hydrogen Storage Applications," Renew. Energy, **181**, pp. 1155–1166.

[92] Brown, T. M., Brouwer, J., Samuelsen, G. S., Holcomb, F. H., and King, J., 2008, "Accurate Simplified Dynamic Model of a Metal Hydride Tank," Int. J. Hydrogen Energy, **33**(20), pp. 5596–5605.

[93] Jemni, A., Nasrallah, S. Ben, and Lamloumi, J., 1999, "Experimental and Theoretical Study of a Metal-Hydrogen Reactor," Int. J. Hydrogen Energy, **24**, pp. 631–644.

[94] Aldas, K., Mat, M. D., and Kaplan, Y., 2002, "A Three-Dimensional Mathematical Model for Absorption in a Metal Hydride Bed," Int. J. Hydrogen Energy, **27**, pp. 1049–1056.

[95] Liu, Y., Wang, H., Ayub, I., Yang, F., Wu, Z., and Zhang, Z., 2021, "A Variable Cross-Section Annular Fins Type Metal Hydride Reactor for Improving the Phenomenon of Inhomogeneous Reaction in the Thermal Energy Storage Processes," Appl. Energy, **295**(April), p. 117073.

[96] Askri, F., Ben Salah, M., Jemni, A., and Ben Nasrallah, S., 2009, "Heat and Mass Transfer Studies on Metal-Hydrogen Reactor Filled with MmNi4.6Fe0.4," Int. J. Hydrogen Energy, **34**, pp. 6705–6711.

[97] Bhouri, M., and Bürger, I., 2017, "Numerical Investigation of H2 Absorption in an Adiabatic High-Temperature Metal Hydride Reactor Based on Thermochemical Heat Storage: MgH2 and Mg(OH)2 as Reference Materials," Int. J. Hydrogen Energy, **42**(26), pp. 16632–16644.

[98] Dunikov, D. O., Borzenko, V. I., Blinov, D. V, Kazakov, A. N., Romanov, I. A., and Leontiev, A. I., 2021, "Heat and Mass Transfer in a Metal Hydride Reactor: Combining Experiments and Mathematical Modelling," J. Phys. Conf. Ser., **2057**(1), p. 012122.

[99] Nuchkrua, T., and Leephakpreeda, T., 2013, "Neuro-Fuzzy Adaptive PID Control of Thermoelectric Module for Metal Hydride Reactor," Defect Diffus. Forum, **334**–**335**, pp. 182–187.

[100] VanGeet, O., Brown, E., Blair, T., and McAllister, A., 2008, "Solar San Diego: The Impact of Binomial Rate Structures on Real PV-Systems," Am. Sol. Energy Soc. - Sol. 2008, Incl. Proc. 37th ASES Annu. Conf., 33rd Natl. Passiv. Sol. Conf., 3rd Renew. Energy Policy Mark. Conf. Catch Clean Energy Wave, **6**, pp. 3819–3844.

[101] Janko, S. A., Arnold, M. R., and Johnson, N. G., 2016, "Implications of High-Penetration Renewables for Ratepayers and Utilities in the Residential Solar Photovoltaic (PV) Market," Appl. Energy, **180**, pp. 37–51.

[102] Myers, K. S., Klein, S. A., and Reindl, D. T., 2010, "Assessment of High Penetration of Solar Photovoltaics in Wisconsin," Energy Policy, **38**(11), pp. 7338–7345.

[103] Incropera, F., DeWitt, D., Bergman, T., and Lavine, A., 2011, *Fundamentals of Heat and Mass Transfer, 7th Edition*, John Wiley & Sons.

[104] Lexcellent, C., and Gondor, G., 2007, "Analysis of Hydride Formation for Hydrogen Storage: Pressure-Composition Isotherm Curves Modeling," Intermetallics, **15**(7), pp. 934–944.

[105] 2009, *2009 ASHRAE Handbook: Fundementals*, American Society of Heating, Refrigerating and Air-Conditioning Engineers.

[106] Office of Energy Efficiency and Renewable Energy, “Commercial and Residential Hourly Load Profiles for All TMY3 Locations in the United States,” OpenEI [Online]. Available: https://openei.org/doe-opendata/dataset/commercial-and-residential-hourly-load-profiles-for-all-tmy3-locations-in-the-united-states.

[107] Department of Energy, and Pacific Northwest National Laboratory, 2020, “Commercial Prototype Building Models: Medium Office.”

[108] Tina, G., Gagliano, S., and Raiti, S., 2006, “Hybrid Solar/Wind Power System Probabilistic Modelling for Long-Term Performance Assessment,” Sol. Energy, **80**(5), pp. 578–588.

[109] Duffie, J. A., Beckman, W. A., and McGowan, J., 2013, *Solar Engineering of Thermal Processes*, John Wiley & Sons.

[110] Energy Efficiency and Renewable Energy Office, 2016, “Technical Support Document: Energy Efficiency Program for Consumer Products: Residential Central Air Conditioners, Heat Pumps, and Furnaces,” US Dep. Energy, (December).

[111] 2017, “Argus Rare Earths Monthly Outlook,” Arg. Consult. Serv., (17–9).

[112] Comstock, O., 2014, “Everywhere but Northeast, Fewer Homes Choose Natural Gas as Heating Fuel,” Today in Energy [Online]. Available: https://www.eia.gov/todayinenergy/detail.php?id=18131.

[113] National Renewable Energy Laboratory, “1991-2005 Update: Typical Meteorlogican Year 3,” Natl. Sol. Radiat. Database [Online]. Available: https://rredc.nrel.gov/solar/old_data/nsrdb/1991-2005/tmy3/.

[114] National Renewable Energy Laboratory, “Utility Rate Database,” OpenEI [Online]. Available: https://openei.org/wiki/Utility_Rate_Database.

[115] Department of Energy, and Pacific Northwest National Laboratory, 2021, “Residential Prototype Building Models: 2021 IECC.”

[116] West, J., and Braun, J. E., 1999, “Modeling Partial Charging and Discharging of Area-Constrained Ice Storage Tanks,” HVAC R Res., **5**(3), pp. 209–228.

[117] Emerson, 2019, “YH-Series Compressor Data.”

[118] Wright, A., and Heggs, P., 2002, “Rating Calculation for Plate Heat Exchanger Effectiveness and Pressure Drop Using Existing Performance Data,” Chem. Eng. Res. Des.

[119] Ayub, Z. H., 2003, “Plate Heat Exchanger Literature Survey and New Heat Transfer and Pressure Drop Correlations for Refrigerant Evaporators,” Heat Transf. Eng., **24**(5), pp. 3–16.

[120] Yan, Y.-Y., Lio, H.-C., and Lin, T.-F., 1999, “Condensation Heat Transfer and Pressure Drop of Refrigerant R-134a in a Plate Heat Exchanger,” Int. J. Heat Mass Transf., **42**, pp. 993–1006.

[121] Hirschey, J., Kumar, N., Turnaoglu, T., Gluesenkamp, K. R., and Graham, S., 2021, “Review of Low-Cost Organic and Inorganic Phase Change Materials with Phase Change Temperature between 0°C and 65°C,” *International High Performance Buildings Conference*.

[122] Rao, Z., Xu, T., Liu, C., Zheng, Z., Liang, L., and Hong, K., 2018, “Experimental Study on Thermal Properties and Thermal Performance of Eutectic Hydrated Salts/Expanded Perlite Form-Stable Phase Change Materials for Passive Solar Energy Utilization,” Sol. Energy Mater. Sol. Cells, **188**(May), pp. 6–17.

[123] Guion, J., Sauzade, J. D., and Laügt, M., 1983, “Critical Examination and Experimental Determination of Melting Enthalpies and Entropies of Salt Hydrates,” Thermochim. Acta, **67**, pp. 167–179.

[124] Krane, P., Nash, A. L., Ziviani, D., Braun, J. E., Marconnet, A. M., and Jain, N., 2021, “Dynamic Modeling and Control of a Two-Reactor Metal Hydride Energy Storage System,” Submitt. to Appl. Energy.

[125] Krane, P., Ziviani, D., Braun, J. E., and Marconnet, A., 2021, “Assessment of Metal-Hydride Energy Storage Coupled with Heat Pumps and Solar PV for Residential Cooling and Heating,” *International High Performance Buildings Conference*.

[126] Krane, P., Ziviani, D., Braun, J. E., Jain, N., and Marconnet, A., 2022, “Techno-Economic Analysis of Metal-Hydride Energy Storage to Enable Year-Round Load-Shifting for Residential Heat Pumps,” Energy Build., **256**, p. 111700.